Technische Universität München

Max-Planck-Institut für Quantenoptik

QUANTUM COMPUTATION WITH NUCLEAR SPINS IN QUANTUM DOTS

Henning Christ

Vollständiger Abdruck der von der Fakultät für Physik
der Technischen Universität München
zur Erlangung des akademischen Grades eines

Doktors der Naturwissenschaften (Dr. rer. nat.)

genehmigten Dissertation.

Vorsitzender : Univ.-Prof. Dr. R. Gross

Prüfer der Dissertation : 1. Hon.-Prof. I. Cirac, Ph. D.
2. Univ.-Prof. J. J. Finley, Ph. D.

Die Dissertation wurde am 17.12.2007 bei der
Technischen Universität München eingereicht und
durch die Fakultät für Physik am 24.01.2008 angenommen.

Abstract

The role of nuclear spins for quantum information processing in quantum dots is theoretically investigated in this thesis. Building on the established fact that the most strongly coupled environment for the potential electron spin quantum bit are the surrounding lattice nuclear spins interacting via the hyperfine interaction, we turn this vice into a virtue by designing schemes for harnessing this strong coupling. In this perspective, the ensemble of nuclear spins can be considered an asset, suitable for an active role in quantum information processing due to its intrinsic long coherence times.

We present experimentally feasible protocols for the polarization, i.e. initialization, of the nuclear spins and a quantitative solution to our derived master equation. The polarization limiting destructive interference effects, caused by the collective nature of the nuclear coupling to the electron spin, are studied in detail. Efficient ways of mitigating these constraints are presented, demonstrating that highly polarized nuclear ensembles in quantum dots are feasible.

At high, but not perfect, polarization of the nuclei the evolution of an electron spin in contact with the spin bath can be efficiently studied by means of a truncation of the Hilbert space. It is shown that the electron spin can function as a mediator of universal quantum gates for collective nuclear spin qubits, yielding a promising architecture for quantum information processing. Furthermore, we show that at high polarization the hyperfine interaction of electron and nuclear spins resembles the celebrated Jaynes-Cummings model of quantum optics. This result opens the door for transfer of knowledge from the mature field of quantum computation with atoms and photons. Additionally, tailored specifically for the quantum dot environment, we propose a novel scheme for the generation of highly squeezed collective nuclear states.

Finally we demonstrate that even an unprepared completely mixed nuclear spin ensemble can be utilized for the important task of sequentially generating entanglement between electrons. This is true despite the fact that electrons and nuclei become only very weakly entangled through the hyperfine interaction. Straightforward experimentally feasible protocols for the generation of multipartite entangled (GHZ- and W-)states are presented.

Contents

Chapter 1

Introduction

A computing device properly harnessing the laws of quantum mechanics can solve certain problems that are intractable, i.e. computationally hard, for machines based on classical logic [1, 2, 3, 4]. Even more, quantum mechanics guarantees provably secure communication between two parties [5]. Based on these deep results, quantum information processing and quantum cryptography have quickly grown into a vibrant, very active, large and interdisciplinary field of physics [4]. Ranging from fundamental insights into the structure of quantum mechanics and reality [6] over ground breaking results in materials science [7, 8] to first commercially available products [9], the achievements are deeply impressive.

The challenges, however, are quite as remarkable: The quantum computer (QC) has to be very well shielded from its environment in order to avoid unwanted interruption of its coherent evolution, a phenomenon called decoherence. At the same time the constituents (quantum bits, or qubits) of the very same system typically need to be actively manipulated and finally read out. Thus one arrives at the contradictory requirements, that on the one hand isolation from the surrounding and on the other hand strong coupling to some classical interface is needed. The quest for suitable physical systems is still on, and has lead to a plethora of possible candidates for the realization of quantum information processing (QIP), spanning a fascinating range of systems [10, 11] from elementary (quasi-)two level systems, such as hyperfine levels in ions [12] and electron spins [13], to complex macroscopic structures like superconducting devices [14].

Since the early days of the field *spins* have been in the focus of both experimental and theoretical research, as they are natural qubits and very generally speaking possess long coherence times. The latter is particularly true for nuclear spins [15]. Some of our fundamental understanding of QIP has been triggered by liquid state nuclear magnetic resonance (NMR) exper-

iments [16, 17, 18] (which are listed in the Guiness book of world records as the largest running quantum computer). However, the two most prominent approaches to nuclear spin based QIP suffer from serious disadvantages. Liquid state NMR, relying on the nuclear spins of molecules in solution, is intrinsically unscalable, which has caused this line of research to fade. The Kane proposal [19, 20], with the qubits defined as (phosphorous) donor spins (in a silicon matrix), is based on electronically mediated gates, but due to the large extent of the electronic wave function, the clock cycle is rather low. In addition, the required sub-lattice-site precision placement is a daunting challenge [21], at the very least.

After these humbling insights, nuclear spins received considerable attention from a different point of view. Single electron spins in single quantum dots (QDs) are considered a highly promising route to QIP [13], with all basic (DiVincenzo-)requirements [22] experimentally demonstrated [23, 24, 25, 26]. Additionally, measured decay times of up to 20 milliseconds [27, 28], which should be compared to the two-qubit gate time of 180 picoseconds [23], indicate a bright future for the field. However, it was realized that the Fermi contact hyperfine interaction of the electron spin and the nuclear spins of the surrounding lattice is a very strong source of decoherence. The mechanism was thoroughly analyzed in experiment [23, 29, 30] and theory [31, 32, 33], and it turned out that the induced dephasing happens on a short timescale (10 nanoseconds in GaAs/AlGaAs QDs [23]). The reason for this remarkably strong process is ensemble averaging over many different nuclear spins states, which again is due to the small magnetic moment of the nuclei, which even for the strongest magnetic fields available in the labs does not allow for alignment of the spins. However, a most interesting property of this environment follows from what has been stated above: The long nuclear spin coherence times lead to a *static* environment. This has lead to a variety of ideas for boosting the electron spin coherence including spin echoes [23], more sophisticated control theories [34, 35], measurement of the nuclear spin state [36, 37, 38] and polarization of the nuclei [31].

The latter idea is not only interesting from the perspective of enhancing the electron spin coherence time. Highly polarized nuclear spins are a very attractive system for QIP, because collective excitations of polarized ensembles of two level systems have been proven to be very well suited for quantum information tasks. For example, the collective electronic excitation in a cloud of atoms, has been used successfully for storage of photonic ("flying") quantum information, and teleportation [39, 40]. In recent work, also the nuclear spin ensembles in QDs have been considered as a memory for the quantum information held by the electron spin [41, 42].

In this thesis a broad range of the benefits of actively using nuclear en-

sembles for quantum information processing is explored. The focus lies on the active role of nuclear spin ensembles for QIP, but the results bear relevance for electron spin QC in QDs, and more generally collective interactions. Before going into a detailed summary, we briefly review the most important concepts of QC in QDs.

1.1 Quantum Computation in Quantum Dots

A quantum dot is a small region of a semiconductor where the electron's motion is confined in all three spatial directions. The localized electron wave function and the resulting discrete energy spectrum are the defining characteristics of quantum dots. Depending on the fabrication technique, the most prominent ones being self-assembly [43] and top gates on two dimensional electron systems (2DES) [44], typical quantum dot sizes range between 1 μm and 1 nm. Despite the obvious complexity and physical richness of these structures [45], the commonly used descriptions "artificial atoms" and "particle in a box" have some justification: The confinement induced energy discretization allows to a large extent for rather simple explanations, such as the constant-interaction-model [46], and even elementary single particle intuition can be useful– in particular in situations where the number of electrons trapped in a quantum dot is small.

Charge control on the single electron level was achieved already in 1996 by Tarucha and coworkers [47]. In particular so-called "lateral" QD setups have since refined charge control to increasingly amazing levels, by going beyond single dots. In brief, these QDs are defined by starting out with a high-mobility 2DES, as can be realized by a GaAs/AlGaAs heterostructure [44, 48] (which is indeed used in most advanced quantum dot experiments). The QD is formed by applying voltages to lithographically defined (Schottky-)contacts on top of the heterostructure. The static electric field penetrating the structure creates the confinement potential, and therefore the quantum dot, within the 2DES by depletion of conduction band electrons. By ever more sophisticated control and design of the top gates precise charge control on a nanosecond timescale was experimentally demonstrated in double [23, 25, 49] and triple dots [50].

The charge degrees of freedom of electrons in QDs have been considered as a quantum bit [51], but strong electrical field noise is generally believed to be too large an obstacle for quantum coherence in this setup. Loss and DiVincenzo were the first to propose the *spin* of a single electron in a lateral QD as a qubit [13][1]. The spin is to first order insensitive to voltage fluctuations

[1] Subsequently Imamoglu *et al.* introduced a spin QC architecture for self-assembled

(for a discussion of spin-orbit coupling see below). This potentially combines the advanced fabrication techniques of established modern day semiconductor industry for large scale production with the favorable coherence times of quantum spins. A fundamental ingredient of this proposal is that the tunnelling of electrons between adjacent quantum dots gives rise to an exchange interaction, which in turn provides a universal two-qubit gate on a very short timescale. Single qubit gates can be effected by locally controllable magnetic fields, and furthermore it has been shown that by means of encoding one logical qubit into several electron spins the exchange (Heisenberg-)interaction alone suffices for universal quantum computation [53]. As a side note we mention that the symmetry induced exchange "interaction" proposed originally for QDs is now being successfully employed for QIP in other physical systems, like neutral atoms in optical lattices [54].

Every experimental setup aiming for QD QC is vulnerable to noise, such as fluctuating magnetic fields and voltages. Nevertheless, these extrinsic sources of noise are artifacts of a given experiment, and can be mitigated with improved electronics. However, there are also intrinsic noise sources, the dominant ones being the spin-orbit coupling and the hyperfine (HF) interaction, which are fundamental and thus require in-depth analysis.

Spin-orbit (SO) interactions are typically introduced by considering an electron moving in a frame with a stationary electric field in absence of a magnetic field. In the frame moving with the electron the magnetic field is non-zero, due to the properties of the Lorentz transformation. For electrons in bulk material this effect is present, but becomes strongly dependent on material and in particular symmetry. The SO interaction thus causes decoherence of the electron spin (coupling it for example to lattice phonons). Various studies have shown that the resulting relaxation-(T_1) and dephasing-(T_2) times are of the same order, very long and strongly suppressed with decreasing magnetic field, see e.g. [55, 56, 57]. The remarkable experimental demonstration of resulting long coherence times (up to 20 ms as measured for example by Kroutvar *et al.* [27]), turned the focus of the community to hyperfine interactions as the main remaining intrinsic source of noise.

1.2 Hyperfine Interaction in Quantum Dots

The HF interaction is the coupling of the nuclear magnetic moment to the magnetic field generated by the electron. Fermi calculated the corresponding Hamiltonian as early as 1930 [58]. In the semiconductor materials of our interest, i.e. the technologically most advanced ones, all stable isotopes carry

quantum dots, allowing for the optical realization of gates [52].

nuclear spin (e.g. $I_{\mathrm{Ga}} = I_{\mathrm{As}} = 3/2$) and thus inevitably one has to deal with HF couplings [59][2].

In materials in which the conduction band has predominantly s-orbital character [59, 61], as is the case for the QDs studied in this thesis, the hyperfine interaction reduces to good approximation to the Fermi contact interaction ($\hbar = 1$ henceforth)

$$H_{\mathrm{HF}} = \mathbf{S} \sum_{i=1}^{N} A_i \cdot \mathbf{I}_i, \tag{1.1}$$

where $\mathbf{S}$ is the electron spin, $\{\mathbf{I}_i\}$ are the (dimensionless) nuclear spin operators at lattice site i and

$$A_i = A|\Psi_e(\mathbf{r}_i)|^2,$$

is the coupling constant of the electron to the nucleus located at site i. It is proportional to the probability of the electron being at the location of the nucleus of site i $|\Psi_e(\mathbf{r}_i)|^2$. Typically $N = 10^4 - 10^6$ nuclear spins are coupled to the electron. The hyperfine coupling constant A can be expressed as

$$A = \frac{4\mu_0}{3I}\mu_B\mu_I\eta n_0,$$

where $\mu_B = 9.27 \times 10^{-24}$ J/T is the Bohr magneton, μ_I is the nuclear magnetic moment, $\mu_0 = 4 \times 10^{-7}$ N/A^2 the magnetic constant, and η is the absolute value squared of the Bloch wave function at the location of the nucleus. This parameter has been measured for several materials [59]. For later convenience we write the nuclear magnetic moment as $\mu_I = \mu_N g_I$, where $\mu_N = e\hbar/2m_{\mathrm{proton}} = 5.05 \times 10^{-27}$ J/T is the nuclear magneton and g_I the nuclear g-factor. As all nuclear parameters are species dependent, so is the coupling constant A. The relevant interaction strength is $A^{-1} \approx 40$ ps, see [59]. Of particular importance is the fluctuation of the combined nuclear field around its zero expectation value for a completely unpolarized state, which is of order

$$A/\sqrt{N},$$

and it is exactly this value that has been measured in state of the art dephasing experiments to be $\sim 1/(10\ \mathrm{ns})$. It is noteworthy that even the slowest relevant timescale connected to the Fermi contact interaction, the Knight shift felt by the nuclear spins $E_{\mathrm{Knight}} \approx N/A$, is larger than direct dipole-dipole couplings between nuclear spins, which thus can be neglected in most situations (cf. Table 1.1 and Refs. [61, 62, 63]).

[2]Note that very recently, there has been progress in controlling the charge degrees of freedom in a nuclear spin-free Si/Ge double quantum dot [60]. However, control over the spin degree of freedom remains to be demonstrated to date.

Interaction	Symbol	Typical Energy [meV]
Orbital level spacing	E_c	10^0
Electron spin exchange	J	10^{-1}
Hyperfine (full polarization)	A	10^{-1}
Hyperfine (random polarization)	$A/\sqrt{N}$	10^{-4}
Knight shift	A/N	10^{-6}
Electron-nuclear dipolar coupling	–	10^{-7}
Nuclear-nuclear dipolar coupling	–	10^{-8}
Electron Larmor precession	$g^*\mu_B$	$10^{-2}/T$
Nuclear Larmor precession	$g_I\mu_N$	$10^{-5}/T$

Table 1.1: Relevant energies scales for electron and nuclear spins in typical laterally defined GaAs quantum dots [61].

As indicated in the beginning of this section, there are anisotropic corrections to the Fermi contact interaction $H_a \propto \sum_i \frac{\mu_0\mu_B\mu_I}{Ir^3}\left(\frac{3(\mathbf{I}\cdot\mathbf{r})(\mathbf{S}\cdot\mathbf{r})}{r^2} - \mathbf{I}\cdot\mathbf{S}\right)$. This interaction has been estimated to be a very weak effect in comparison to the contact term [61] (good experimental agreement with prediction from the contact term has been shown, see e.g. [23, 29, 30]). A detailed derivation of the presented Hamiltonians is found in the textbook by Stoneham [64] (in particular Chapter 13.5).

As a side note we remark that Hamiltonian (1.1) is applicable to the Kane QC proposal [19], where the nuclear spins of the phosphorus donor and the surrounding lattice ^{29}Si are interacting with the donor electron.

The study of the electron evolution under the Hamiltonian from equation (1.1) has generated a tremendous amount of research output– both theoretical and experimental. First calculations of spin flip rates in perturbation theory [31, 33] were followed by an exact quantum solution for the case of full polarization [65] and an extensive semi-classical study of the free induction decay of the electron spin in the presence of a completely mixed nuclear state [66]. The results of the latter study have elaborated on the simple observation of the $\sqrt{N}/A$-scaling of the dephasing (T_2^*) time, and found successful application to numerous experiments. It turned out that the nuclear spin bath does not generate simple exponential decay, but rather Gaussian or polynomial behavior; which also means that the conventional $T_{1,2}$ times have to be taken with a grain of salt. In recent years the methods for calculating the electron spin evolution have become more sophisticated, ranging from a generalized master equation [67] to in-depth analysis with cluster expansion approaches [68, 69, 70]. We do not go into more details regarding HF induced electron spin decoherence here, because there exist extensive reviews

on the topic [59, 61], and because it diverts from the major perspective that is pursued and advocated in this thesis: The nuclear spins are an asset.

In contrast to most of the literature on the HF dynamics of electron and nuclei in QDs, we will study active manipulation of the nuclear spins via the HF interaction. The electron spin can be well manipulated by various means, e.g. magnetic or optical fields [11]. However, its strong coupling to the nuclear spins darkens its perspectives as the elementary unit of a future quantum computer. Nuclei on the other hand have demonstrated long coherence times. It is thus natural to combine the advantages of electrons (accessability) with those of nuclei (coherence). Clearly, one can not just gather all benefits of both systems without any drawbacks. One might be tempted to think that if the electron is decohered by the nuclei, the reverse effect is just as bad for the nuclei. However, as the electron can be very easily removed from the nuclear ensemble under study, the roles of electron and nuclei are not symmetric and this expectation is not true– a net benefit for the nuclei remains and thus a further valuable degree of freedom is introduced[3]. The means of connecting the advantages of electron and nuclei is the strong hyperfine interaction introduced in this section. It turns out that pursuing this idea, there is a lot of interesting physics to be found, as it is summarized and outlined in the next section.

1.3 Outline of this Thesis

The various chapters of this thesis are topically strongly interconnected, but are written to some extent in a self-contained style that allows the interested reader to study isolated individual chapters. The general context of the presented work has been established in this introductory chapter, and additionally at the beginning of each chapter some further details on the implications and interrelations of the specific content is given, supplemented by some concluding remarks and outlooks at the end of each chapter.

In Chapter 2 we study theoretically the cooling of an ensemble of nuclear spins coupled to the spin of a localized electron in a quantum dot. This corresponds to an initialization of the nuclear spin ensemble, similar to optical pumping or laser cooling for atoms. We obtain a master equation for the state of the nuclear spins interacting with a sequence of polarized elec-

[3] Another physical system exhibiting electron-nuclear HF spin interactions has entered the focus of QIP research: ^{13}C nuclear spins near nitrogen vacancy (NV) centers have been shown to be well controllable via optical excitation and to posses very long coherence times (1 ms) up to room temperature [71, 72, 73]. Hyperfine interaction functions here as the coherent coupling mechanism between the optically active NV-center and the carbon nuclear spin qubit.

trons that allows us to study quantitatively the cooling process including the effect of nuclear spin coherences, which can lead to "dark states" of the nuclear system in which further cooling is inhibited. We show that the inhomogeneous Knight field mitigates this effect strongly and that the remaining dark-state limitations can be overcome by very few shifts of the electron wave function, allowing for cooling far beyond the dark-state limit. Numerical integration of the master equation indicates that polarizations larger than 90% can be achieved within a millisecond time scale. Limitations due to dipolar interactions, for which we find a novel quantitative efficient description, are discussed and shown to be small. Two proposals based on double quantum dots for the experimental realization of our schemes are presented.

Cooling in the limit of homogeneous couplings, i.e., a flat electronic wave function, is analyzed in detail in Chapter 3. Approximate analytical solutions are shown to provide accurate results, allowing for the determination of cooling potential and rates, both of which reflect the effect of polarization-limiting dark states. We further provide a microscopic description of these states, that proves useful for the analysis of the effect of electron wave function changes during the cooling procedure.

The quantum dynamics of a single mode/particle interacting inhomogeneously with a large number of particles is studied in Chapter 4 in a slightly more general context. We introduce an effective approach to find the "accessible Hilbert space" where the dynamics takes place. This allows for efficient numerical treatment of the problem. Two relevant examples are given: the inhomogeneous Tavis-Cummings model (e.g. N atomic qubits coupled to a single cavity mode, or to a motional mode in trapped ions) and the inhomogeneous coupling of an electron spin to N nuclear spins in a quantum dot. In the latter case the performance of a quantum memory proposal in the presence of "defect" excitations in the nuclear spin ensemble is investigated.

Chapter 5 describes a technique for QIP based on localized ensembles of nuclear spins. A qubit is identified as the presence or absence of a collective excitation of a mesoscopic ensemble of nuclear spins surrounding a single quantum dot. All single- and two-qubit operations can be effected using hyperfine interactions and single-electron spin rotations, hence the proposed scheme avoids gate errors arising from entanglement between spin and orbital degrees of freedom. Long-range qubit coupling can be implemented by pregenerated entanglement as a resource or by electron spin transport. The scheme is particularly well suited for applications where long lived memory is essential.

By considering multiple excitations in Chapter 6, we enlarge the potential applications of the nuclear spin ensemble. We develop an "à la quantum optics theory" to describe the inhomogeneous coupling of a single electron

to the nuclear spin environment in a quantum dot in terms of a collection of bosonic modes interacting with a two level system. When the nuclear spins are highly polarized, the electron couples predominantly to one mode, giving rise to an interaction which closely resembles the Jaynes-Cummings model of quantum optics. Thus knowledge and experience already acquired for quantum optical systems can be transferred to the domain of semiconductor quantum dots. In the case of finite polarization, taking into account corrections to the ideal Jaynes-Cummings model through the weakly interacting bath modes, our model allows the derivation of analytic expressions for the electron spin evolution. We present further demonstration for the usefulness of our approach by designing a deterministic scheme for generating highly squeezed nuclear spin states.

In Chapter 7 we show that qubits coupled sequentially to a mesoscopic static infinite-temperature spin bath via the Heisenberg interaction can become highly entangled, with neither direct qubit-qubit interaction nor simultaneous interaction with the bath. Protocols for the generation of multipartite entangled (GHZ- and W-)states are presented. Arbitrary gates between the highly mixed nuclear system and the electron spin can be performed, when only one bit of information about the state of the nuclear ensemble is gained through a straightforward measurement in the beginning of the protocol. We show the feasibility of an experimental realization in a QD by the hyperfine interaction of an electron with the surrounding nuclear spins.

The author of this thesis has published several articles during the course of his Ph.D. The material presented here has partially been covered in Refs. [74], [75], [76], [77] and [78]; not presented are the results of a collaboration in the field of superconducting qubits [79, 80] and a general audience review article [81].

Chapter 2

Nuclear Spin Cooling in a Quantum Dot

In Section 1.2 we saw that the localized ensemble of nuclear spins in a QD has received special attention in the context of QIP with electron spins in QDs: the nuclei couple via a Fermi contact interaction to the electron spin [59] and, as predicted by theory [31, 33, 65, 66, 67], have been shown in recent experiments to constitute the major source of decoherence of electron spin qubits in some of the most promising QD-based implementations [23, 30]. The vice of this strong coupling can be turned into a virtue when the electron is used to initialize and manipulate the state of the nuclear ensemble. This has long been exploited in dynamical nuclear polarization (DNP) [82, 83, 84, 85] in bulk systems and afforded many insights in the spin dynamics in solids [62, 84].

DNP *in quantum dots* has come into focus more recently in the context of QIP, since strongly polarized nuclei could lead to much longer electron spin dephasing times [67], provide strong local magnetic field gradients required in quantum information proposals [86, 87], and even allow to utilize the nuclear spins themselves as long-lived quantum memory [42, 76]. More generally, a highly polarized nuclear spin ensemble in a QD provides, together with the electron spin, a strongly coupled, well isolated mesoscopic quantum system with close similarities to the Jaynes-Cummings model in quantum optics as we will detail in Chapter 6, with the fully polarized state corresponding to the vacuum in all cavity modes. Thus ultra-high DNP in QDs may open the door to realize cavity-QED in quantum dots and implement tasks such as state engineering.

Experimentally, significant nuclear polarization in self-assembled QDs has been achieved [88, 89, 90, 91]. However, the degree of polarization in these experiments was still too low to improve electron spin coherence times con-

siderably and still far from the ground state.

Theoretically, cooling dynamics has mostly been considered in the spin temperature approximation [84, 92, 93, 94], in which coherences among the nuclear spins are neglected. This is appropriate if, as in bulk or quantum well systems, there is no fixed electron wave function and many motional states are involved, or if the nuclear dephasing rate is large. In quantum dots, however, the nuclei interact collectively with an electron in the motional ground state of the QD and the higher motional levels are far detuned. Therefore the coupling strength of each nucleus is fixed, and well defined phase relationships between the nuclear spins can build up, necessitating a quantum treatment of the process, which was first pointed out by Imamoğlu *et al.* [95], who showed that the cooling process can be inhibited by so-called dark states, which trap excitations and potentially result in serious constraints on the achievable polarizations. While it was pointed out in [95] that inhomogeneities (either inherent in the system or introduced actively by modulating the wave function of the electron) can mitigate this problem, these ideas were put to numerical test only in very small 1D systems of 10 nuclear spins. However, the effect of inhomogeneities is expected to be reduced for realistic larger systems [42], and thus limitations due to dark states are more severe. For example, in a fully homogeneous system only a fraction of $\mathcal{O}(1/\sqrt{N})$ spins can be cooled before the system is trapped in dark states.

We consider the cooling of N nuclear spins in a QD through interaction with polarized electrons. One cooling cycle consists of (a) initialization of the electron spin in a well-defined direction, and (b) evolution of the combined system for a "short" time, see Fig. 2.1. In this way the electron spin acts effectively as a $T = 0$-reservoir for the nuclear spin bath, and pumps excitation out of it.

We derive in a consistent manner a full quantum model of this process, which allows us to numerically study particle numbers of up to $N \sim 10^3$. We show that a sufficient inhomogeneity of the couplings leads to a dephasing of nuclear spin states and thus limitations due to dark states are partially lifted. We demonstrate that enhanced cooling protocols involving only a few (< 10) modulations of the electron wave function, allow to fully overcome these limitations, indicating that Overhauser fields above 90% of the maximal value can be created within the nuclear spin diffusion time.

This chapter is organized as follows: In Sec. 2.1 we present the generic cooling protocol and analyze its performance in Sec. 2.2; the applicability of the scheme to some specific physical systems is studied in Sec. 2.3. A method for the quantitative treatment of nuclear dipolar interactions is introduced and applied in Section 2.4.

2.1 The Cooling Scheme

Interaction

As introduced in Section 1.2 the Fermi contact interaction between an (s-type conduction band) electron spin $\mathbf{S}$ and the spins $\mathbf{I}_i$ of the lattice nuclei leads to a Heisenberg like coupling $A\alpha_i \mathbf{I}_i \cdot \mathbf{S}$ to the nuclear spin at lattice site i, where A sets the overall strength of the hyperfine interaction and the factor $0 < \alpha_i < 1$ is determined by the probability to find the electron at site i and the gyromagnetic ratio of the ith nucleus. In the presence of an external magnetic field B_{ext} we write the Hamiltonian of the spin system with the collective nuclear spin operators $A^\mu = \sum_i g_i I_i^\mu$ ($\mu = \pm, z$) as

$$\begin{aligned} H &= \frac{g}{2}\left(A^+ S^- + S^+ A^-\right) + g A^z S^z + g^* \mu_B B_{\text{ext}} S^z, \\ &= H_{\text{ff}} + H_z + g^* \mu_B B_{\text{ext}} S^z \end{aligned} \tag{2.1}$$

where we have defined $g = A\sqrt{\sum_i \alpha_i^2}$ and $g_i = \alpha_i / \sqrt{\sum_i \alpha_i^2}$, such that $\sum_i g_i^2 = 1$, and denoted the electron g-factor by g^* and the Bohr magneton by μ_B.

We do not consider the Zeeman energy of the nuclear spins, because for typical QDs it is much (10^3 times) smaller than the electron's Zeeman energy [59], and similarly we neglect the even smaller dipolar interaction between the nuclei. Finally, we restrict the analysis to nuclear spins $I = 1/2$ and one nuclear species only. The resulting effects of these phenomena are discussed in Sec. 2.2.5 and in the case of dipolar interactions quantitatively considered in Sec. 2.4.

The first part of the above Hamiltonian H_{ff} exchanges spin excitation between the electron and the nuclei, and it is this mechanism that is used to create polarization. The second part of the Hamiltonian H_z constitutes a "quantum" magnetic field, the Overhauser field, for the electron spin generated by the nuclei.

The Cooling Scheme

We assume initially the electron spin to be pointing in the $-z$-direction $|\psi_e\text{-}\rangle = |\downarrow\rangle$. In the absence of a magnetic field this initial state defines the axis of quantization. The cooling cycle we consider is an iteration between evolution with Hamiltonian Eq. (2.1), and reinitialization of the electron to $|\downarrow\rangle$. The nuclei effectively "see" a large cold reservoir of electron spins and the concatenated evolution of the nuclear spin density matrix becomes

$$\rho \to \ldots U_t \text{tr}_e \left[U_t \Big(\rho \otimes |\downarrow\rangle\langle\downarrow| \Big) U_t^\dagger \right] \otimes |\downarrow\rangle\langle\downarrow| U_t^\dagger \ldots \quad . \tag{2.2}$$

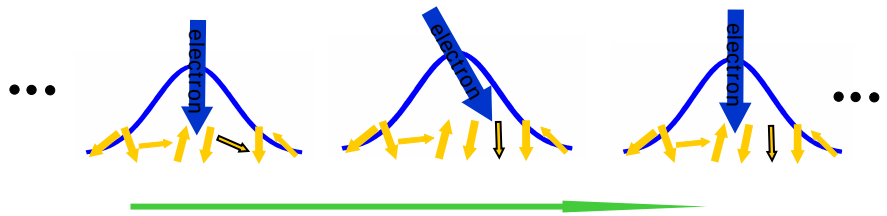

Figure 2.1: Sketch of the cooling scheme. The Gaussian-shaped electron wave function extends over many nuclear spins. The three depicted steps are initialization, interaction, and reinitialization. One nuclear spin is singled out to illustrate the progression of the protocol.

Here $U_t = \exp(-iHt)$ is the time evolution operator, tr_e denotes the trace over the electron, and here and in the following ρ will denote the state of the nuclear spin system only. Spin polarized currents or optical pumping with polarized light give rise to a polarized electron bath, but also the fast electrical control available in double QDs [23] allows for the creation of nuclear spin polarization without the need for pre-prepared electrons, as we will detail in the last section of this chapter.

Considering small times for the evolution in each individual step of the cooling protocol, we expand the time evolution operators in Eq. (2.2) to second order. The standard deviation of the $A^{\pm,z}$-terms scales as $A\sqrt{\sum_i \alpha_i^2} = g \sim \mathcal{O}(A/\sqrt{N})$ for the initially totally mixed nuclear spin state, and thus for $\Delta t \ll g^{-1} \sim \sqrt{N}/A$ we neglect higher orders. The readily obtained master equation

$$\begin{aligned}\rho_{t+\Delta t} - \rho_t = i\frac{g\Delta t}{2}[A^z, \rho_t] - \frac{g^2(\Delta t)^2}{8}[A^z, [A^z, \rho_t]] \\ - \frac{g^2(\Delta t)^2}{8}\left(A^+A^-\rho_t + \rho_t A^+A^- - 2A^-\rho_t A^+\right),\end{aligned} \tag{2.3}$$

contains a Hamiltonian part arising from the Overhauser field and a contribution in Lindblad form. The latter generates the nuclear spin polarization, and has been studied in the limit of homogeneous coupling constants in the context of superradiance [96, 97, 98].

As polarization builds up and $g\langle A^z\rangle \gg A/\sqrt{N}$ the Hamiltonian terms on the right hand side of Eq. (2.3) may become large (for fixed time step Δt). To preserve validity of the master equation one can either reduce the interaction time $\Delta t < A^{-1}$ or apply an external magnetic field that compensates the Overhauser field $\langle A^z\rangle$, so that $\langle gA^z - g^*\mu_B B_{\mathrm{ext}}\rangle\Delta t \ll 1$ for all times. In the

latter case Δt is short enough to ensure quasi-resonant hyperfine flips despite the random detunings stemming from the fluctuating Overhauser field and at the same time large enough to guarantee a fast cooling rate[1]. This is the situation we investigate in the following. Without retuning the system in this manner the polarization rate becomes dependent on the polarization itself and the emerging non-linearities give rise to the bistability effects observed in [99, 100, 101, 102, 103] and limit the final polarization, see also Section 2.4 and Appendix A.

Homogeneous Coupling

Before we discuss general inhomogeneous couplings, consider for a moment the homogeneous case, $\alpha_i \propto 1/N$, as a demonstration of some interesting features of the above master equation. For a more in depth discussion of these effects, the reader is referred to the next chapter. For homogeneous couplings, the operators $A^{\pm,z}$ appearing in Eq. (2.3) form a spin algebra $I^{\pm,z}$ and the collective angular momentum states (Dicke states) $|I, m_I, \beta\rangle$ provide an efficient description of the system dynamics [42, 104]. The permutation quantum number β accounts for the degeneracy of states with given I, m; with the number of degenerate states given by $D_I = \binom{N}{N/2-I} - \binom{N}{N/2-I-1}$. This can be seen by a simple argument: For a given m, $N/2 + m$ spins must be in state $|\uparrow\rangle$. There are $B_m = \binom{N}{N/2+m}$ configurations satisfying this requirement. The counting of states of given $\{I, m\}$ is now most conveniently done successively starting from $m = I/2 = I_{\max}$. In this case, the only possible state has $I = N/2$. Applying the lowering operator A^- to this state yields one state with $\{I = N/2, m = N/2 - 1\}$. Thus the remaining states with $m = N/2 - 1$ must have (the only other "compatible" angular momentum) $I = N/2 - 1$; implying $D_{N/2-1} = B_{N/2-1} - 1 = B_{N/2-1} - B_{N/2}$. This procedure is continued by applying A^- again, now to the states with $m = N/2 - 1$, yielding $B_{N/2-1}$ states with $m = N/2 - 2$ and $I > N/2 - 2$. Thus there are $D_{N/2-2} = B_{N/2-2} - B_{N/2-1}$ remaining $m = N/2 - 2$ states with $I = N/2 - 2$. By induction it follows that

$$D_{I,m} = D_I = B_I - B_{I+1}.$$

The total spin quantum number I is not changed by $A^{\pm,z}$ and the effect of Eq. (2.3) is simply to lower (at an (I, m_I)-dependent rate) the I_z quan-

[1] Ensuring the validity of Eq. (2.3) for all times by retuning B_{ext} assumes that the standard deviation of gA^z remains bounded by $\mathcal{O}(A/\sqrt{N})$ thus keeping the error in each cooling step small. Computing $\text{Var}A^z$ in each step and choosing Δt accordingly guarantees correctness. In general, the polarizing process is expected to *decrease* $\text{Var}A^z$ from the initial value in the maximally mixed state. This is confirmed by exact numerical calculations for small particle numbers. And we present further evidence for this in Sec. 2.2.2.

tum number. If $m_I = -I$ is reached, the system can not be cooled any further, even if (for $I \ll N/2$) it is far from being fully polarized. These dark states [42, 95] are a consequence of the collective interaction Eq. (2.1). Thus spin excitations are trapped and cooling to the ground state prevented. We evaluate the steady state polarization $\langle I^z \rangle_{\rm ss} = \langle \sum_i I_i^z / \sqrt{N} \rangle_{\rm ss}$ as

$$\frac{\langle I^z \rangle_{\rm ss}}{\langle I^z \rangle_0} = \frac{2}{2^N N} \sum_{I=0}^{N/2} I(2I+1) D_I = \sqrt{\frac{8}{\pi N}} + \mathcal{O}(1/N), \tag{2.4}$$

i.e. for a mesoscopic number of particles the obtained polarization is negligible. In the above equation $\langle I^z \rangle_0$ is the expectation value in the completely polarized state and the last equality has been obtained by employing the Stirling formula.

Evolving the nuclei according to Eq. (2.3), we find the exact time evolution of the polarization as shown in Fig. 2.2. In these and the following simulations $g\Delta t = 0.1$, i.e. $\Delta t = 0.1 g^{-1} \sim 0.1\sqrt{N}/A$. As expected the polarization decreases as $1/\sqrt{N}$ as N increases, which underlines the importance of the nuclear spin coherences. In particular this shows that an incoherent spin temperature description of the process would give even qualitatively wrong results. For more details regarding the homogeneous limit, including an approximate analytic solution for the time evolution of the polarization, see Chapter 3.

Inhomogeneous Coupling

Consider now an inhomogeneous wave function. The results for the exact evolution of the quantity of interest, $\langle A^z \rangle$, are shown in Fig. 2.2. The coupling constants g_j in this example are taken from a 1D Gaussian distribution with width $N/4$.[2] The most important and striking feature is that in this situation almost complete polarization is obtained.

The reason that this is possible here is *not* that there are no dark states in the case of inhomogeneous coupling constants. On the contrary it has been shown that there exists an one-to-one mapping [42] from the familiar homogeneous dark states ($|I, -I, \beta\rangle$ in the Dicke basis) to their inhomogeneous counterparts, defined by $A^-|D\rangle = 0$. The reason for obtaining high polarization beyond the homogeneous limit is the Hamiltonian part of the

[2] In the present chapter and for most of this thesis, we focus on Gaussian electron wave functions, which approximate experimental conditions well. For the coherent phenomena we discuss, the distribution of the groups of similarly coupled spins is of major importance. This property is generally mainly determined by the width and dimensionality of the wave function, and only to a smaller extent by its exact functional form.

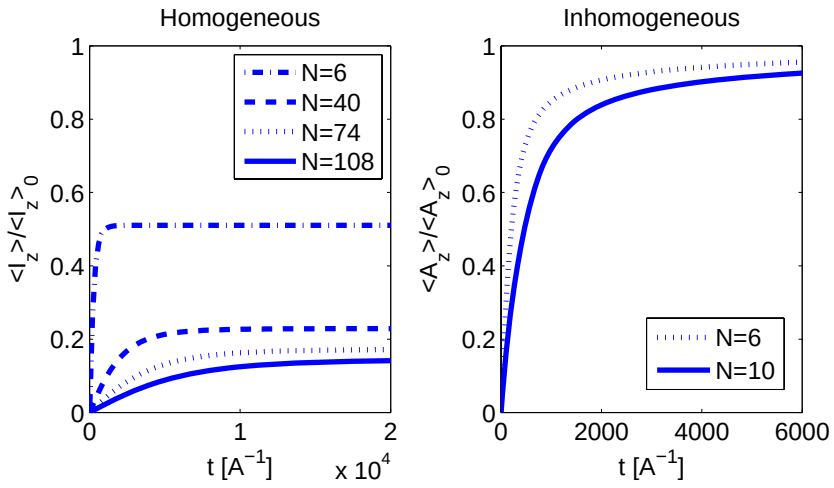

Figure 2.2: Exact polarization dynamics. Left: Homogeneous case, $g_j = 1/\sqrt{N}$. Right: In the inhomogeneous case, $g_j \propto \exp(-(j-N/2-1/4)^2/w^2)$. The term $1/4$ is added to account for asymmetry between electron wave function and the lattice and avoid symmetry effects for this small scale system.

master equation (2.3). To illustrate this point, consider two spins with coupling constants $g_1 \neq g_2$. Then the dark state $|\Psi_D\rangle \propto g_2|\uparrow\downarrow\rangle - g_1|\downarrow\uparrow\rangle$ evolves due to the A^z-term in Eq. (2.3) to $e^{i\delta_g t}g_2|\uparrow\downarrow\rangle - e^{-i\delta_g t}g_1|\downarrow\uparrow\rangle$, where δ_g is proportional to $g_1 - g_2$. Obviously this state will become "bright" again after a time $\propto 1/|g_i - g_j|$ and $A^-|D\rangle \neq 0$. This process is first order and, as we will detail later, "delivers" coolable excitations sufficiently fast to maintain a high cooling rate.

2.2 Polarization Dynamics

The polarization dynamics of the nuclear ensemble is governed by Eq. (2.3). While for homogeneous systems the collective angular momentum Dicke basis enables an efficient description of the problem, for realistically large and inhomogeneous systems more effort is required.

To study the evolution of the nuclear polarization, we are interested in the individual spin expectation values $\langle\sigma_i^+\sigma_i^-\rangle$. These depend, via Eq. (2.3) on all the elements of the covariance matrix

$$\gamma_{ij} = \langle\sigma_i^+\sigma_j^-\rangle,$$

which, in turn, depend on higher order correlations as seen from the equations

of motion

$$\frac{\Delta\gamma_{ij}}{\Delta t} = \xi_{ij}\gamma_{ij} - \kappa\sum_k g_k\Big(- g_i\langle\sigma_k^+[\sigma_i^+,\sigma_i^-]\sigma_j^-\rangle + g_j\langle\sigma_i^+[\sigma_j^-,\sigma_j^+]\sigma_k^-\rangle\Big), \quad (2.5)$$

where $\xi_{ij} = ig(g_j - g_i)/2 - g^2\Delta t(g_j - g_i)^2/8$ and $\kappa = g^2\Delta t/8$ and the σ_i^μ refer to the Pauli matrices at site i.

2.2.1 Approximation Schemes

The simultaneous solution of the ensuing hierarchy of equations is only feasible for very small particle numbers N and further approximations are needed to treat the large systems of interest. We introduce several ways, labelled (i) to (v), of closing this set of equations and discuss their validity and implications in detail below.

In the strongest approximation (i) all coherences between different spins are neglected yielding independent rate equations for each individual nuclear spin. This reproduces essentially the spin-temperature description commonly employed in the discussion of bulk DNP [84, 92] (each subset of spins with identical coupling strengths g_i is assigned its own effective temperature). This approach cannot reproduce the quantum effects we want to study, but it can serve as a benchmark for how strongly these are influencing the cooling process.

The simplest approximations that take quantum coherences between nuclear spins into account close the hierarchy of equations at the level of second order correlations. Our approximation (ii) is motivated by the generalized Holstein-Primakoff description [105], which in lowest order treats the nuclei as bosonic modes $\sigma_i^- \to a_i$. The bosonic commutations relations $[a_i, a_j^\dagger] = \delta_{ij}$ yield a closed set of equations for the elements of the covariance matrix γ. The bosonic description is known to be accurate for highly polarized and moderately inhomogeneous systems (Chapter 6) and allows to bring results and intuition from quantum optics to bear in the spin system discussed here. Dark states are included in the form of the vacuum of the collective mode $b_0 = \sum_i g_i a_i$ coupled to the electron in Eq. (2.1). For unpolarized systems (with on average 1/2 excitations per bosonic mode a_i), this description provides a lower bound on the performance of the cooling protocol, since in the absence of an inhomogeneous Knight field cooling is limited to $\mathcal{O}(1)$ excitations per mode rather than the $\mathcal{O}(\sqrt{N})$ coolable excitations expected at the beginning of the cooling process for spins, cf. Eq. (2.4). In the two limiting cases discussed so far, Eq. (2.5) simplifies to

$$\frac{\Delta\gamma_{ij}}{\Delta t} = \begin{cases} -2\kappa\delta_{ij}g_i^2\gamma_{ii} & (i)\ \text{Spin Temp.} \\ \xi_{ij}\gamma_{ij} - \kappa\sum_k g_k(g_i\gamma_{kj} + g_j\gamma_{ik}) & (ii)\ \text{Bosonic.} \end{cases}$$

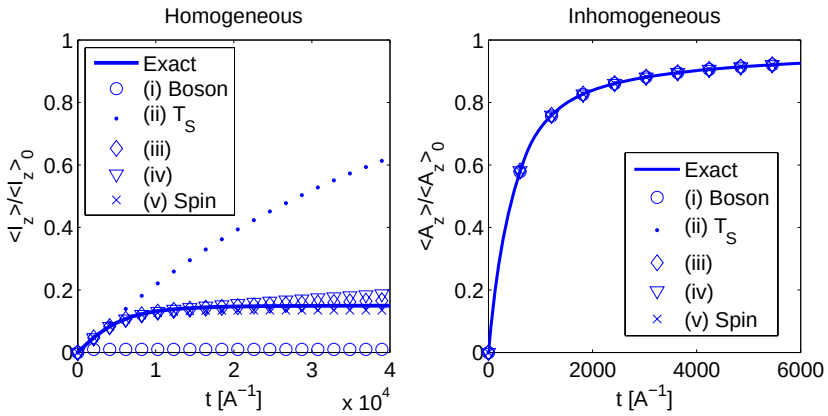

Figure 2.3: Comparison of different approximation schemes for the homogeneous situation with $N = 100$ (left) and the case of Gaussian couplings (as in Fig. 2.2) and $N = 10$ nuclear spins (right).

One can take into account more aspects of the spin algebra by replacing some higher order expectation values by lower orders using the properties of Pauli matrices $[\sigma_i^+, \sigma_i^-] = \sigma_i^z$ and $\sigma_i^z \sigma_i^\pm = \pm\sigma_i^\pm$, obtaining

$$\frac{\Delta\gamma_{ij}}{\Delta t} = \xi_{ij}\gamma_{ij} - \kappa\delta_{ij}\sum_k g_k(g_i\gamma_{kj} + g_j\gamma_{ik}) \qquad (2.6)$$
$$- \kappa(1-\delta_{ij})\Big(- \sum_{k\neq i} g_k g_i \langle \sigma_k^+ \sigma_i^z \sigma_j^- \rangle + g_i^2\gamma_{ij} - \sum_{k\neq j} g_k g_j \langle \sigma_i^+ \sigma_j^z \sigma_k^- \rangle + g_j^2\gamma_{ij}\Big).$$

The remaining higher order expectation values (now having distinct indices $i \neq j, j \neq k$) can be approximated in a Hartree-like way [106] (iii), or, having the bosonic limit in mind, by the Wick theorem (iv),

$$\frac{1}{2}\langle \sigma_k^+ \sigma_i^z \sigma_j^- \rangle = \begin{cases} (\gamma_{ii} - \frac{1}{2})\gamma_{kj} & (iii), \\ -\frac{1}{2}\gamma_{kj} + \gamma_{ki}\gamma_{ij} + \gamma_{kj}\gamma_{ii} & (iv). \end{cases}$$

The fifth and final approximation scheme we invoke has been introduced in the context of superradiance as a Wick-type factorization, that takes into account the partly bosonic, partly fermionic properties of spin-1/2 operators [98]. In contrast to the last two factorization schemes, it does not rely on distinction of cases. It is directly based on the exact Eq. (2.5), and approximates the three-operator-expectation values in the following way

$$\frac{1}{2}\langle \sigma_k^+ \sigma_i^z \sigma_j^- \rangle = -\frac{1}{2}\gamma_{kj} - \gamma_{ki}\gamma_{ij} + \gamma_{kj}\gamma_{ii} \qquad (v) \text{ “Spin”}.$$

Direct comparison of the approximation schemes (i)–(v) with the exact solution for both homogeneous and inhomogeneous couplings is shown in Fig. 2.3. In the homogeneous case the spin temperature description (i) is clearly qualitatively wrong, because it neglects correlations in the bath. The bosonic description (ii) captures the feature of dark states, but it overestimates their influence: Instead of $\sim \sqrt{N}$, only one excitation can be removed. The two schemes based on distinction of cases, (iii) and (iv), give very good results initially, until roughly $\sqrt{N}$ spins have been flipped. Then however, the polarization keeps increasing on a slow timescale and does not reach a steady state in the correct time. The (v)-"spin"-approximation gives very good results, and gets both the polarization timescale and the finally obtained value of the polarization right within a few percent.

The comparison of the different approaches to the exact solution for inhomogeneous couplings is restricted to small particle numbers (see Fig. 2.3). In this regime all introduced approximation schemes reproduce the exact dynamics correctly. The reason for the good correspondence is the strong dephasing of dark states and generally coherences between nuclear spins for small inhomogeneous systems.

Using these approximations we present the polarization dynamics for $N = 10^3$ spins coupled through a 2D Gaussian wave function in Fig. 2.4. The bosonic description displays the lowest final polarization and polarization rate (for the same reasons as in the homogeneous case) and is expected to give lower bounds on the performance on the polarization procedure. Of particular interest are the predictions of the (v)-"spin"-approximation scheme, because its good performance in the completely homogeneous situation gives confidence that also partial homogeneities are correctly accounted for. Achieved polarizations of $\sim 60\%$ in this setting show the importance of the intrinsic dephasing due to the inhomogeneity (homogeneous coupling would allow for $< 5\%$ polarization). However, the intrinsic inhomogeneity alone does not allow for ultra-high polarizations and we are thus lead to investigate more sophisticated cooling schemes. As shown later, in these enhanced protocols all approximation schemes lead to the same conclusions (in terms of cooling time and final polarization).

To gain a better understanding of the presented phenomena in the inhomogeneous situation, we go to an interaction picture $\rho_I = U_0 \rho U_0^\dagger$, with $U_0 = \exp(-iA^z t/2)$, which shows very clearly the oscillating coherences between spins with $g_i \neq g_j$

$$\frac{\Delta \rho_I}{\Delta t} = -\kappa \Big[\sum_{ij} g_i g_j e^{-ig(g_i - g_j)t/2} \sigma_i^+ \sigma_j^-, \rho_I \Big]_+ + 2\kappa \sum_{ij} g_i g_j e^{-ig(g_i - g_j)t/2} \sigma_j^- \rho_I \sigma_i^+ . \tag{2.7}$$

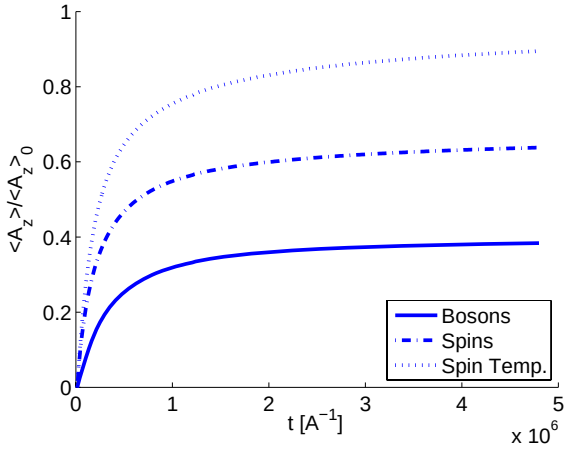

Figure 2.4: The polarization dynamics for $N = 1000$ spins coupled with a 2D Gaussian wave function, which is shifted from the origin by $1/3$ in x- and y-direction.

In the rotating wave approximation (RWA), the rotating terms ($g_i \neq g_j$) are neglected and in the absence of exact symmetries the above equation reduces to the spin temperature description.

More quantitatively, one can clearly see that the coherence between any two nuclear spins rotates at a frequency proportional to the difference in the two nuclei's individual coupling constants. The equations of motion for the coherences γ_{ij} can be formally integrated to yield

$$\gamma_{ij}(t) = e^{i\omega t}\gamma_{ij}(0) + \int_0^t dt' e^{-i\omega(t-t')} f(t'),$$

where $\omega = g(g_i - g_j)$ and the function f incorporates all the dynamics stemming from the polarizing parts of the master equation. This function does not need to be specified in more detail here, the property of relevance is that it varies slowly on the timescale of ω^{-1}. If the latter condition is fulfilled, then integral in the above equation is approximately zero, and as the spins are uncorrelated initially, also during the evolution correlations will not build up.

In order for the integral to vanish the condition

$$\frac{4|g_i - g_j|}{g\Delta t g_i g_j} \gg 1$$

has to be fulfilled. A *partial rotating wave approximation* neglects only the coherences between spins with considerably different coupling constants in

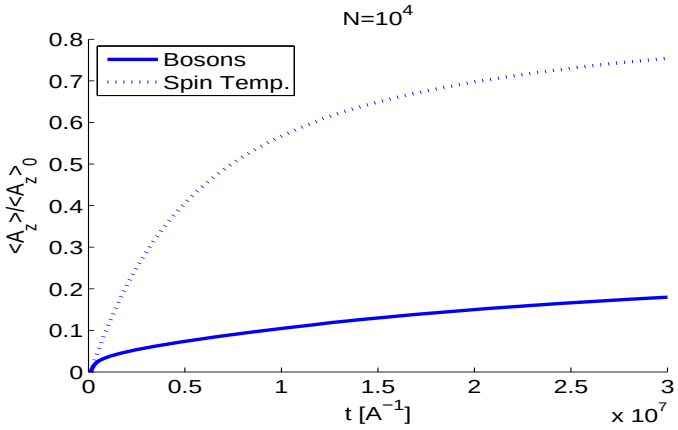

Figure 2.5: Development of the polarization for $N = 10^4$ nuclei in 2D with Gaussian couplings (the center is shifted again by $(1/3, 1/3)$. The numerical treatment is based on the partial rotation wave approximation (see text).

the sense of the above equation. In this case the Hamiltonian will become block diagonal, with the block defined by spins with similar couplings. This block diagonal structure simplifies numerical calculations considerably, allowing for an extension to particle numbers of up to 10^4, adding further to the practical relevance of the results. We present the evolution of the polarization for Gaussian couplings in 2D in Fig. 2.5. The numerical data shows that the phenomena observed for $N = 10^3$ are persistent for the larger particle number as well, giving further confidence that our approach is applicable to realistically large QDs.

2.2.2 The Bosonic Description

Before proceeding with an analysis of the polarization time, the steady states and enhanced protocols, we spend the next paragraphs on a more detailed analysis of the validity and usefulness of the bosonic approximation in the context of spin cooling; in Appendix B we elaborate further the "bosonic mode picture" of the cooling process.

Quantification of Differences between Spins and Bosons

The differences between the evolution with the correct spin operators and the evolution with the bosonic approximation are of course due to the fundamental difference in the commutation relations of the operators. As pointed out earlier this leads to the fact that for homogeneous couplings constants in

the bosonic limit only one excitation can be cooled– instead of $\sim \sqrt{N}$ excitations in the spin case. As inhomogeneous situations can be approximated by a sequence of homogeneous wave functions [107], we expect that the cooling potential for the bosons is a lower bound for the cooling potential for the spins. This expectation is confirmed by all our numerical calculations.

The cooling dynamics in the bosonic description can be thought of as consisting of the part of the process happening in the "physical subspace" (occupation of sites at most 1) and the "unphysical subspace" ($n \geq 2$). If evolution was restricted to the physical subspace, the bosonic and the spin formulation would yield identical results. However, the bosonic Hamiltonian leads to an occupation of the unphysical subspace, even when starting from a physical state initially. This can for example be seen by considering the action of second order terms of the expansion of the time evolution operator on states with initially two spins flipped (at sites $i \neq j$)

$$b_0^\dagger b_0 |\uparrow_i, \uparrow_j, \downarrow, \ldots, \downarrow\rangle = b_0^\dagger b_0 a_i^\dagger a_j^\dagger |0\rangle = g_i \sum_m g_m a_m^\dagger a_j^\dagger |0\rangle + g_j \sum_m g_m a_m^\dagger a_i^\dagger |0\rangle. \tag{2.8}$$

Thus with a certain amplitude the initially occupied sites i and j become occupied twice.

How does this occupation of unphysical states influence the cooling dynamics? Intuitively, the bosonic system starts out in the physical subspace, then, as cooling starts, the nuclear spins system is driven towards states with lower excitation number. Nevertheless, with a certain small probability, processes of the kind outlined in Eq. (2.8) will lead to occupation of unphysical states. However, as cooling proceeds also the unphysical states are driven back to higher polarizations. Thus, intuitively, the bosonic system makes a "detour" in the cooling process, which will lead to a reduction of the cooling rate. This behavior is indeed seen in all numerical calculation we have performed over a wide range of parameters.

After discussing cooling rate and final polarization qualitatively, we would like to find a more quantitative measure for the difference between spins and bosons in the cooling process. To this end we calculate the occupation in the states with 2 and more excitations in the bosonic limit. These states have no correspondence and are unphysical in a spin-1/2 system and thus give a figure of merit how far the bosonic system deviates from the spins. As indicated above, it is expected that occupation of the unphysical subspace reduces the cooling rate in comparison to the spins, so that the figure of merit calculated below should be seen as an indicator for the tightness of the bosonic bound on the cooling rate.

The populations of the Fock states with $n \geq 2$ of each of the localized

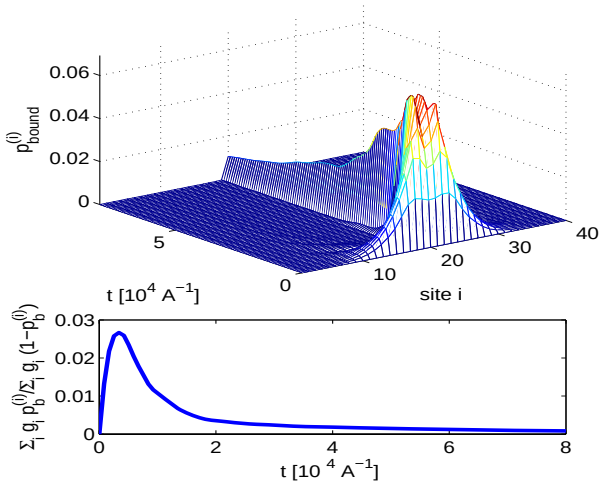

Figure 2.6: Upper plot: Numerical calculation of the evolution of the bound for the occupation of the higher ($n \geq 2$) lying states on each site. $N = 40$, the wave function is a 1D Gaussian shifted from the center by 1/3. Lower plot: Figure of merit for the ratio of the occupation of the unphysical subspace to the occupation to the physical subspace.

modes a_i are bounded by

$$p^{(i)}_{>2} = \sum_{n=2}^{\infty} p^{(i)}_n \leq \sum_{n=0}^{\infty} \frac{1}{2} n(n-1) p^{(i)}_n = \frac{1}{2}(\langle n_i^2 \rangle - \langle n_i \rangle) =: p^{(i)}_{\text{bound}}, \tag{2.9}$$

where $n_i = a_i^\dagger a_i$ is the number operator at site i and $p^{(i)}_n$ is the probability to find the mode at site i in the Fock state $|n\rangle$.

In order to compute the above expression we need to calculate 4-operator expectation values. We define

$$\theta_{ijkl} = \langle a_i^\dagger a_j a_k^\dagger a_l \rangle, \tag{2.10}$$

and the equations of motion for the elements of the tensor θ are readily found to be

$$\begin{aligned} \frac{\Delta \theta_{ijkl}}{\Delta t} &= \xi_{ijkl} \theta_{ijkl} \\ &\quad - \kappa \sum_m g_m \Big(g_k \big(\theta_{mjil} - \delta_{ij} \gamma_{ml} \big) + g_i \theta_{mjkl} + g_l \theta_{ijkm} + g_j \big(\theta_{ilkm} - \delta_{kl} \gamma_{im} \big) \Big), \end{aligned} \tag{2.11}$$

with $\xi_{ijkl} = ig(g_k + g_i - g_j - g_l)/2 - g^2 \Delta t (g_k + g_i - g_j - g_l)^2/8$, and $\kappa = g^2 \Delta t/8$. Together with the equation of motion for γ the Eqs. (2.11) form a closed

set. The size of this system of coupled differential equations is N^4, which restricts numerical solutions to small particle numbers. In Fig. 2.6 we show the evolution of the bounds for the occupation of the unphysical states $p^{(i)}_{\text{bound}}$ for $N = 40$ spins. Initially the higher lying states become occupied, primarily in the center of the dot. However, the occupation stays below 6 % for all times and states, serving as further indication that the bosonic approximation is good. In the long time limit the occupation of the unphysical states tends to zero, as expected for a system approaching the vacuum state. In order to estimate the effect on the Overhauser field we consider the weighted average of the probabilities for being in the physical and the unphysical subspaces

$$\frac{\sum_i g_i p^{(i)}_{\text{bound}}}{\sum_i g_i (1 - p^{(i)}_{\text{bound}})}. \tag{2.12}$$

As shown in Fig. 2.6 this ratio stays below 0.03 which confirms our expectation that the spin cooling rate should be well approximated by the bosonic description.

In summary we have quantified in this subsection differences between spin- and bosonic- cooling. The cooling potential in the bosonic system is smaller than in the spin case and we have presented evidence that the cooling rate for the spins system is lower bounded by the cooling rate in the bosonic system. The figure of merit quantifying the difference between the two approaches remains small, such that the (initial) spin-cooling rate can be rather tightly bounded with the bosonic description.

Evolution of the Overhauser field variance –Justification for the expansion of the time evolution operators

For completeness we use the presented Eqs. (2.11), to calculate the variance of the A_z-operator, which we have argued and required to be small in Sec. 2.1. It is clear that in the final stages of the cooling protocol $\text{Var}(A^z)$ will obey that limit, because the system is driven into an A^z-eigenstate. Starting from a totally mixed state and ending (ideally) in a pure eigenstate, it is to be expected that *during* the cooling protocol the variance of the collective spin operators is reduced monotonically. We confirmed this for small systems (allowing for numerical simulation) as exemplarily shown in Fig. 2.7. We are confident that this holds for large N, too, since the generic states exhibit standard deviation $\leq \mathcal{O}(A/\sqrt{N})$ (as evidenced by the variance of the maximally mixed state). Moreover, the standard deviation in the maximal entropy state of total polarization P is $\mathcal{O}((1-P^2)A/\sqrt{N})$ for all P. Similar reasoning holds for the x- and y-directions.

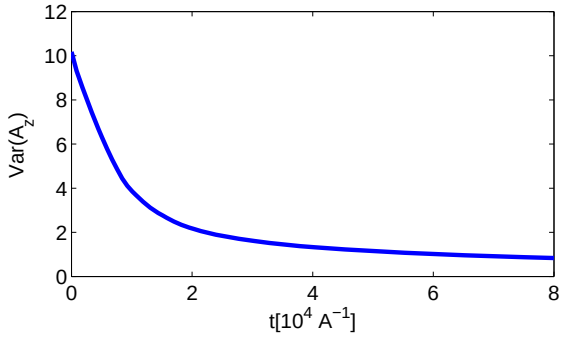

Figure 2.7: Evolution of $\mathrm{Var}(A^z)$ during the cooling protocol for $N = 40$, and a 1D Gaussian electron wave function (shifted by 1/3 from center).

2.2.3 Polarization Time

In the RWA we evaluate the build-up time τ_p for the polarization as the inverse of the weighted average of the individual spin decay times $\kappa_i = 2g_i^2\kappa$ [cf. (i)]

$$\tau_p = \left(\frac{\sum_i g_i\kappa_i}{\sum_i g_i}\right)^{-1} = \frac{4\sum_i g_i}{g(g\Delta t)\sum_i g_i^3} = \mathcal{O}\left(\frac{4N^{3/2}}{A(g\Delta t)}\right), \tag{2.13}$$

and find good agreement with the numerically obtained timescale to reach the steady state in all discussed schemes. For example, for the data presented in Fig. 2.4 we find times of 3.4×10^5 (Spin Temp.), 4.6×10^5 (Bosonic), and 3.3×10^5 ("Spin") in units of A^{-1} to reach $(1 - e^{-1}) \approx 0.63$ of the quasi steady state Overhauser-field. This agrees well with the analytical estimate $\tau_p \approx 2.4 \times 10^5/A$; despite the differences in the final polarizations obtained in the different approximation schemes. This correspondence between the RWA-based estimate and the numerically obtained polarization times for the coherent evolution indicates that the inhomogeneous Knight field provides coolable excitations at a rate larger than the polarization rate, thus not slowing down the process.

For completeness we present here a further comparison of numerically obtained polarization times and our analytical estimate. As shown in Fig. 2.8, over a rather wide range of particle numbers N the estimate agrees well.

When the inhomogeneity of the coupling is large enough to justify the rotating wave approximation, each spin evolves with its own Liouvillian and the nuclei remain in a product state during the whole evolution. To keep the errors in the derivation of the master equation [due to higher order terms in the expansion of the time evolution operators in Eq. (2.2)] small, it is sufficient to do so for each spin individually in this case. This allows a larger

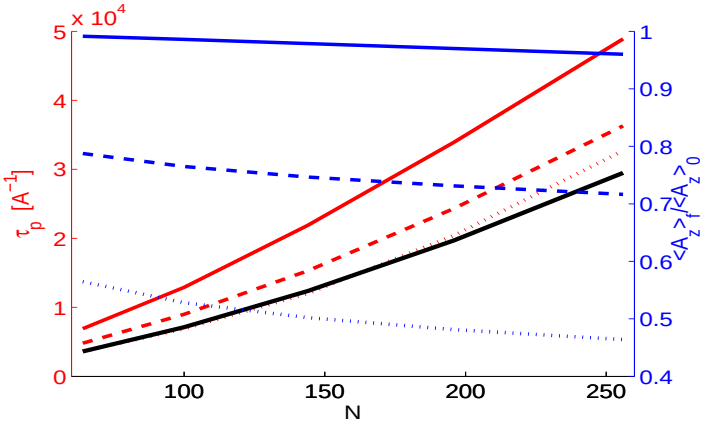

Figure 2.8: The polarization time (left axis, red) and total achieved polarization (right axis, blue) as a function of particle number N. Solid curves: spin temperature description, dashed curves: "Spin", dotted curves: bosonic approximation. The thick black line is the polarization time τ_p according to the estimate given in the text.

time step $\Delta t \ll (A\alpha_{\max})^{-1} = \mathcal{O}(N/A)$ in each cycle and therefore the cooling rate can be significantly enhanced. The cooling time effectively scales only linearly in the particle number

$$\tilde{\tau}_p = \mathcal{O}\left(\frac{4N}{A(A/N\Delta t)}\right). \tag{2.14}$$

Taking $A = 100\mu\text{eV} \sim 40\text{ps}$, a value typical for GaAs QDs, and 0.1 as the value for the terms $g\Delta t$ and $A/N\Delta t$ in the denominators of Eqs. (2.13) and (2.14) respectively, we find that approximately 4×10^3 and 3×10^5 spins can be cooled to more than 90% of the steady state value $\langle A^z \rangle_{\text{ss}}$ within a millisecond.

2.2.4 Enhanced Protocols

We now study enhanced cooling protocols that lift the dark-state limitations and which rely solely on the ability to shift the center of the electron wave function. These shifts can be effected by applying dc gate voltages to the QD. After such a shift only very few spins will have the same coupling constants for *both* wave functions and therefore singlet-like coherences are broken up. We confirm this expectation numerically as shown in Fig. 2.9 for some exemplarily chosen shifts of the electron wave function. The shifts range from a few lattice sites to roughly the width of the electron wave function. In

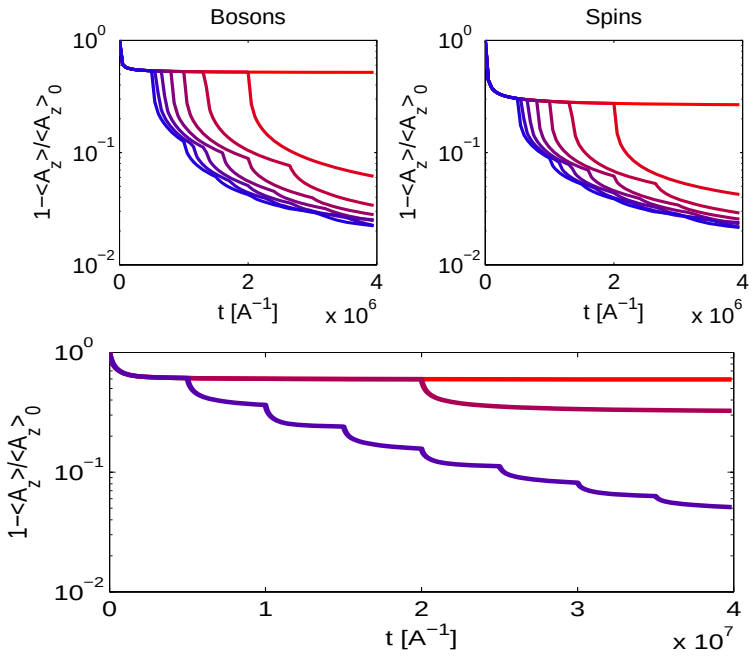

Figure 2.9: Polarization dynamics in the enhanced cooling protocol for $N = 196$ (upper plots) and $N = 1000$ (lower plot). In the upper plots approximation schemes (ii) (left) and (v) (right) have been invoked, the lower plot is based on (v) and the partial rotating wave approximation. In all plots the different lines are representing cooling procedures with different numbers of mode changes. Upper plots are based on randomly chose Gaussian modes (fixed width) and lower plots on iteration of two modes (see text).

the upper plots of Fig. 2.9 the randomly chosen Gaussian modes with width $w = N/4$ are defined by the centers $\{(1/3, 1/3), (1.35, -0.81), (0.32, -0.04), (1.17, 0.79), (-0.13, -1.44), (0.96, -0.17), (0.35, 0.88), (1.27, 0.71)\}$. In the lower plot two modes with centers $\{(1/3, 1/3), (-3.15, -1.5)\}$ have been iterated.

Regarding the approximation schemes, we have found that all schemes taking into account coherences, (ii)-(v), predict the same behavior, and the spin-based factorization (v) offers the quantitatively best description. It is important to note that all these descriptions coincide at the end of the cooling protocol [shown in Fig. 2.9 only for (ii) and (v)]. In particular the limiting bosonic model predicts the same high ($\geq 95\%$) polarizations and cooling rates as the other schemes, which leads us to conclude that $\mathcal{O}(10)$ mode changes are sufficient to achieve near-ground state cooling for realistically large numbers of nuclei in QDs.

Despite being a radical approximation at low polarization, the bosonic scheme (*ii*) captures the cooling dynamics qualitatively and we remark that it can be generalized to provide an accurate and conceptually simple description of the electron-nuclear spin dynamics at high polarizations (cf. Chapter 6).

The cooling schemes we have presented are governed by the optimal timescale set by the hyperfine interaction constant A, but the schemes themselves leave room for optimization: The cooling rate can be tuned by choosing Δt adaptively during the cooling process. The mode changes can be optimized by a careful choice of the size and the timing of the shifts, and through more sophisticated deformations of the electron wave function. These and further modifications are implementation-dependent and will be the topic of future work.

Intuitive Picture for Break-up of Dark State Coherences

We give here an intuitive picture of the physical processes that lead to the enhanced cooling when the cooling mode is changed. We focus on the spatial structure of the spin excitations in the nuclear spin ensemble, for an examination of the same phenomenon in terms of the bosonic picture see Appendix B.

Consider a 2D Gaussian distribution of coupling constants as depicted in Fig. 2.10, for clarity. The inhomogeneous Knight shifts do not decorrelate spins which have the same or very similar coupling constants, indicated by the black circles in Fig. 2.10. In an ideal partial RWA the spins within these circles would become highly correlated, or remain so, in the course of the cooling procedure, whereas correlation between spins in different circles would decay[3].

What happens to these correlations when the mode is changed? This is most easily illustrated by considering the effect of the hyperfine z-interaction on a singlet of the two spins which have the same coupling before, but not after the mode change

$$e^{iA_z t}(|\uparrow\downarrow\rangle - |\downarrow\uparrow\rangle) = (e^{-i\delta_{ij}t}|\uparrow\downarrow\rangle - e^{i\delta_{ij}t}|\downarrow\uparrow\rangle) \rightarrow (|\uparrow\downarrow\rangle + |\downarrow\uparrow\rangle),$$

with $\delta_{ij} \propto (g_i - g_j)$.

However, even with mode changes dark states continue to play a role:

- Two spins can have the same coupling before and after the mode change (more precisely: the first mode couples both spins with a constant g_A and the second mode with a constant g_B, which do not necessarily fulfill $g_A = g_B$). Note that each spins has a certain "partner" with

[3] Clearly, the role of the circles in 2D would be played by points in 1D and shells in 3D.

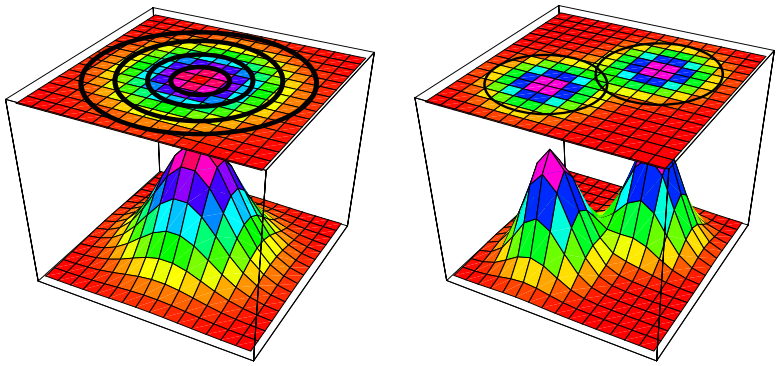

Figure 2.10: Schematic representation of dark states. Plotted is the electron probability density. Left plot: The black circles on the top plane indicate the "shells" of spins with similar coupling, where a dephasing of dark states due to the inhomogeneous Knight field is not possible. Right plot: Schematic representation the evolution of dark state correlations during a mode change. Plotted is the coupling strength due to the two electron wave functions.

which it retains its correlations after the mode change. Note also that the retainment is the exception, and most correlations are destroyed.

The situation discussed is illustrated by the intersections of the two black circles in Fig. 2.10.

- Two spins have different couplings before the mode change, but both of them cannot be fully cooled, as of each them participates in a shell which traps excitation. After the mode change they have the same coupling constants and generally not all remaining excitations can be cooled.

Breaking up of dark state correlations of the first kind requires more than two modes, the 2nd kind of correlations can be overcome by iterating two modes. Later in this subsection, we will see both effects in a more quantitative study.

Steady State Characterization

We present here a semi-analytical calculation of the final polarization of the nuclear spin ensemble that can be obtained and the timescale needed to achieve this high polarization, taking into account inhomogeneous coupling constants *and* the mode changes proposed for the enhanced cooling proto-

cols[4]. The direct numerical integration of the master equation we have presented is currently limited to particle numbers $N \sim 10^3 - 10^4$, corresponding to small QDs. The tools we develop in this subsection allow for treatment of large particle numbers $N \sim 10^5 - 10^6$, which cover practically all currently experimentally relevant setups for QIP.

We obtain the final polarization reachable in a cooling experiment as follows: For the first mode we determine the groups of spins that have "nearly degenerate" coupling constants according to the relation

$$4|g_i - g_j|/(g\Delta t g_i g_j) < 1. \tag{2.15}$$

This yields a partition of the coupling constants g_i into groups $\{g_i\}_{i\in\alpha_m^{(1)}}$, where the $\alpha_m^{(1)}$ are sets of indices fulfilling the above condition[5]. Each set of indices has $M_m^{(1)}$ entries (such that $\sum_m M_m^{(1)} = N$). From this we directly estimate the cooling potential for this mode: In the bosonic limit one expects that at most one excitation can be cooled for each group of particles and for the spins $\sqrt{M_m^{(1)}}$ particles can be cooled (given that enough time is allowed to reach quasi steady state for all groups of spins).

Considering the second mode, we split each of the sets of indices introduced above into smaller subsets, which fulfill Eq. (2.15) for the second mode. This will lead to smaller sets of coupling constants, characterized by sets of indices $\alpha_m^{(2)}$. Then one proceeds in finding the cooling potential in the same way as outlined above for the first mode. Note that the final polarization calculated in that way would be obtained in actual experiment only when all groups of particles reach quasi steady state, and the modes are iterated often enough, cf. Sec. 2.2.4.

In Fig. 2.11 the dotted lines have been computed in the way outlined above. The presented data indicates that for particle numbers $N \sim 10^3 - 10^5$ two modes are sufficient to overcome most dark state effects and reach polarization in the 99% regime[6].

A more accurate estimate of the final polarization can be obtained by considering a simple model for the temporal evolution in each of the subspaces of spins, given by the $\alpha_m^{(1,2)}$. These partitions are obtained in the same way

[4]Recall that our previous estimate for the cooling timescale Eq. (2.13) was valid for the cooling with one mode and didn't make a prediction of the reachable final polarization.

[5]For explicit quantitative calculations, these sets are determined by starting at a random location in the lattice, and constructing the group according to relation Eq. (2.15). Then the next random location is chosen and the procedure iterated. In this manner *disjoint* sets are constructed, for which we have verified that the starting point of the procedure does not change the results we obtain.

[6]Numerical checks indicate that on the order of 10 mode changes are sufficient to reach that regime.

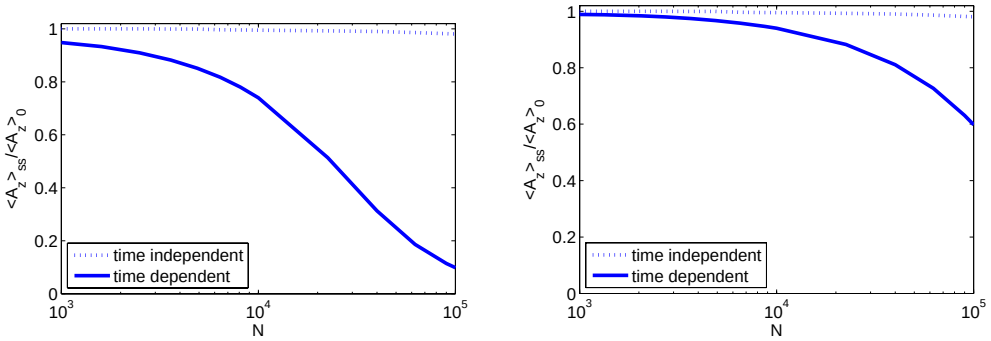

Figure 2.11: Estimates of the possible final Overhauser field. The total time for the cooling is $4 \times 10^7 A^{-1}$ (left plot) and $4 \times 10^8 A^{-1}$ (right plot). The electron wave function is a 2D Gaussian of width $N/4$. Two modes with centers (1/3,1/3) and $-(3.15, 1.5)$ have been used.

as before and now we assume a simple exponential decay in each of the subgroups of spins. The time constant is given by the coupling constant in the respective subgroup and final value of the decay determined in the above way. Some exemplary results of these calculations are presented in Fig. 2.11 by the solid lines. One can see that the time for these plots is chosen such that it is a more limiting factor than the dark state coherences. Note that the left plot can be compared to the results of the full evolution of the master equation given in the lower plot of Fig. 2.9 (in this plot numerical data on the bosonic scheme has been presented but, as argued earlier, for the enhanced cooling protocols they coincide). The final polarization by the methods outline in this subsection agrees well with the full numerical propagation, thus giving further evidence for the validity of the predictions made for very large particle numbers.

So far we have considered the final polarization as a function of the particle number N, and now turn to the dependency on the total polarization time of the cooling process, T_{final}, for a given particle number $N = 10^5$. We investigate this situation given that 2 or 3 Gaussian modes are iterated.

In Fig. 2.12 one can clearly see that (a) longer cooling times directly translate into higher final polarizations, (b) dark state limitations are largely overcome by using two or three modes, thus preventing rapid slow down of the cooling process at low polarizations, and (c) employing 3 instead of 2 modes increases the final polarization approximately 4% in the given example. Regarding the long total cooling time, one should keep in mind that the presented example serves to illustrate the power of our approach and is not

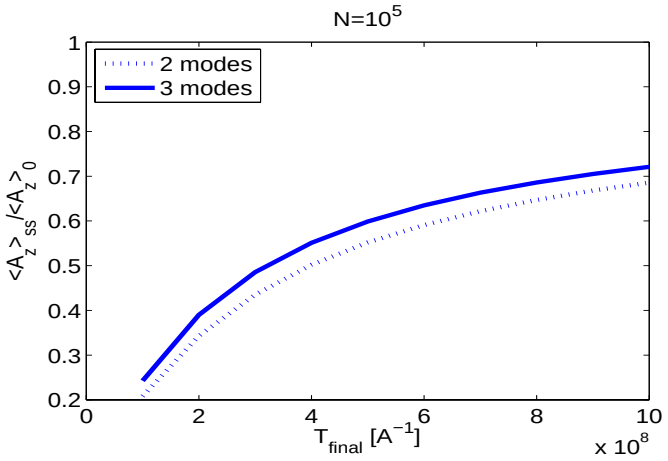

Figure 2.12: Estimates of the possible final Overhauser field for $N = 10^5$ and a 2D Gaussian wave function as a function of total cooling time. The modes are centered at (1/3,1/3), $-(3.15, 1.5)$, and $(0.6, -0.2)$.

optimized (see also next section) to obtain high efficiency cooling.

2.2.5 Imperfections

In using the Hamiltonian Eq. (2.1) we have neglected a number of weak interactions that are present in actual systems and, while being much smaller than the dominant hyperfine term, may become important on the long time-scales required to reach high polarization. We argue in the following that these terms do not affect the quantitative conclusions obtained. While nuclear Zeeman energies are large enough to cause additional dephasing between the nuclear spins, similar to the inhomogeneous Knight fields, this will only be effective between nuclei of *different* Zeeman energy, i.e., belonging to different nuclear species. This leads to 2 to 3 mutually decohered subsystems (in a partial rotating wave approximation) each of which is described by our model.

The nuclear dipole-dipole interaction [108] can lead to both diffusion and dephasing processes, both of which are of minor importance as shown below. Dipolar processes that change A^z are off-resonant and hence expected to be slow, as indicated by the nuclear spin diffusion rates measured, e.g., in [63, 109] and should not significantly affect the polarizations reached. Resonant processes such as terms $\propto I_i^z I_j^z$ affect the cooling process only insofar as they can cause dephasing of dark states similar to the inhomogeneous Knight shift. The rate at which coolable excitations are provided is set by

the energy difference for two nuclear spins in a dark pair. The interaction energy for two neighboring spins is about $\sim 10^{-5}\mu$eV [59], hence a singlet of neighboring spins can dephase in $\sim 100\mu$s (or slower if all surrounding spins are polarized). Even widely separated spins interacting with differently polarized environments dephase only up to a few ten times faster than this (depending on the geometry). Thus we see that the dipolar dephasing is considerably slower than that caused by the inhomogeneous Knight field and only if the latter becomes inefficient due to homogeneities (towards the end of cooling a given mode) the dipolar dephasing can contribute coolable excitations, but at a much slower rate than what can be achieved by changing the electron wave function and the ensuing return to a situation of strong Knight inhomogeneity. Thus, one does not expect the cooling process to be affected except for a slight additional dephasing. However, on much longer timescales of tens of ms the dipole-dipole interaction provides depolarizing mechanism (affecting mainly nuclei with a weak hyperfine interaction) that needs to be considered, e.g., when cooling much beyond 90% polarization is studied (see also Sec. 2.4).

Clearly a polarization $< 100\%$ of the electron "reservoir" directly translates into limitations on the final polarization of the nuclei. A quantification of this necessarily needs to refer to the details a concrete physical realization of our model, which is not the topic here. The limitations can be minute, e.g. in the case of the double dot setup presented in the next section.

2.3 Adapting the Model to Concrete Physical Settings

The generic model of a single spin-1/2 particle coupled inhomogeneously to an ensemble of N nuclear spins can readily be adapted to various experimental settings.

If a source of spin polarized electrons is available, single electron tunnelling into the QD provides the initialization. Controlled tunnelling into and out of the QD with rates $> 10\,\mathrm{ns}^{-1}$ appears feasible [110, 111], justifying the description of the dynamics by an interaction suddenly switched on and off.

For self-assembled QDs, optical pumping with polarized light has been shown to provide a spin polarized bath of electrons that cools the nuclei [88, 89, 90, 91, 112]. However, in this setup the average dwell time of a single polarized electron in the dot is large, making Eq. (2.3) not directly applicable. Moreover, the detuning due to the z-component of the Overhauser field leads to instabilities [101, 102, 103] in the nuclear polarization which are avoided

in our scheme.

In double QDs in the two-electron regime [113, 114] the role of the states $|\downarrow\rangle, |\uparrow\rangle$ is played by the two-electron singlet $|\tilde{S}\rangle$ and one of the triplet states; in the following we consider $|T_+\rangle = |\uparrow\rangle|\uparrow\rangle$. Tunnel coupling between the two dots and the external magnetic field are chosen such that the other triplet states are off-resonant and cause only small corrections to the dynamics sketched here.

As discussed in more detail in [113, 114] the hyperfine interaction in this system is described by the Hamiltonian $\sum_l \mathbf{S}_l \cdot \mathbf{A}_l$, where $l = L, R$ refers to the orbital state of the electron. Coupling between $|\tilde{S}\rangle$ and $|T_+\rangle$ is mediated by the *difference* $\delta A^{\pm} = (A_L^{\pm} - A_R^{\pm})/2$ of the collective nuclear spin operators of the two dots L, R, while the effective Overhauser field is given by the sum $(A_L^z + A_R^z)/2$. Thus we have that the analysis of the previous sections applies to the double dot case in this regime (to zeroth order, cf. [87]) with the replacements

$$|\downarrow\rangle \to |\tilde{S}\rangle, \quad |\uparrow\rangle \to |T_+\rangle,$$
$$A^{\pm} \to -\sqrt{2}(\cos\theta)\delta A^{\pm}, \; A^z \to \frac{1}{2}(A_L^z + A_R^z).$$

The adiabatic singlet has contributions from both the delocalized $(1,1)$ and the localized $(0,2)$ charge states, and with $\cos\theta$ we denote the amplitude of the $(1,1)$ contribution [114] (with (m,n) we denote a state with m electrons on the left and n electrons on the right dot). The effect of higher-order terms (e.g., of the nuclear spin components $\delta A^z, A_L^{\pm} + A_R^{\pm}$) merits more detailed analysis.

Gate Controlled Double Dot Setup

This system is of particular interest since fast electrical control of gate voltages can provide a highly spin polarized electron system through near unit fidelity initialization of a singlet in the right hand dot $|S(0,2)\rangle$ [25, 23]. Starting from this singlet, rapid adiabatic passage (1 ns [23]) by means of tuning the asymmetry parameter ϵ between the dots, initializes the electrons to the adiabatic singlet $|\tilde{S}\rangle$ and brings the system to the $S - T_+$ resonance.

The transitions from the singlet to the other two triplets $T_{0,-}$ are detuned by an external magnetic field (of order 100 mT in the experiments of Ref. [23]). After a time Δt the system is ramped back to the (0,2) charge region and the electrons relax to the singlet ground state, completing one cooling cycle. If relaxation to the state $S(0,2)$ is fast, the limiting timescale for this cycle is given by the hyperfine coupling constant A, showing that here the polarization rate is governed by the natural and optimal timescale

(and not other, slower timescales, like e.g. cotunnelling in Refs. [94, 99] (note Ref. [115] though)).

In the GaAs double dot setup the sudden approximation is justified for typical tunnel couplings $\sim 10\mu$eV, which have to be compared to the typical timescale for a hyperfine flip $\leq 0.1\mu$eV and the fact that additionally all spin flip transitions are off-resonant during the adiabatic ramp. At the $S - T_+$ resonance selecting a suitable combination of external magnetic field and time step Δt detunes the unwanted transitions and at the same time ensures resonance for the polarizing transition. Note also that the Overhauser field increases the external magnetic field in materials with negative electron g-factor, like GaAs ($g^* \approx -0.44$), when the $S - T_-$ transition is used, thus further suppressing unwanted transitions and requiring retuning of the end-point of the adiabatic ramp. Given the availability of fast (100 ps) voltage pulses, the reinitialization of $|S(0,2)\rangle$ via a $(0,1)$ charge state is likely to be limited by the tunnelling rate from the reservoir to the QD. For optimal cooling efficiency this rate should and could be made large $\gtrsim 10A/\sqrt{N}$ [110, 111].

Since in the gate controlled double dot setup the "polarized" state is a spin singlet, there is no inhomogeneous Knight field to dephase the dark states and DNP will be severely limited. However there are many ways of providing it, for example by extending the cooling cycle to include a third step in which a single-electron state of the double dot is realized or by increasing the time spent at the $S-T_+$ resonance in each cooling cycle (the latter would require a reformulation of the master equation (2.3) not presented here). At the same time it would be interesting to find evidence for quantum coherence between nuclear spins in QDs by comparison of the obtained Overhauser field in the case of strong and weak inhomogeneous Knight fields[7].

Spin Blockade Regime

In the presence of an applied source-drain voltage the current through a double quantum dot (DQD) can be blocked when the electron tunnelling into the DQD has the same spin orientation as the one already present (we consider here the regime of one or two electron in the dot exclusively). The HF field of the nuclear spins can rotate this blockaded triplet at a rate of $A/\sqrt{N} \sim 1/(10$ ns) (GaAs) [30, 99, 115]. Careful tuning of the DQD parameters and external magnetic field can create the situation in which only one triplet state, say $|T_+\rangle$, is resonant with the singlet $|S_{1,1}\rangle$, see. Fig. 2.13. As the HF interaction preserves the total spin, repeated $T_+ \rightarrow S_{1,1}$ transitions drive the nuclear

[7] Subradiance is not easily demonstrated in quantum optical systems; it was experimentally observed many years after superradiance, see Ref. [116].

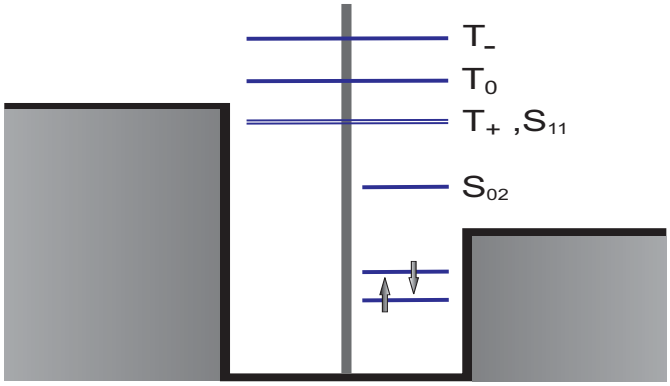

Figure 2.13: Sketch of the relevant energy levels for current-based nuclear spin cooling setup. The key process is the hyperfine-mediated lifting of the spin blockade via transitions between the degenerate triplet and singlet state $T_+ \to S_{1,1}$.

spin system into a polarized state (without a source of polarization or active in situ control needed as mentioned in the beginning). The resulting spin dynamics is likely to be even richer than in the gate controlled setup (polarization bistabilities, feedback, and current oscillations are examples of the phenomena to be expected). We show in the next paragraphs that the tools we developed in the previous section provide an efficient description also of this setup.

Model– For the setup we have in mind, Fig. 2.13, the T_- and T_0 states do not play a role since they are high in energy and cannot be populated by electrons tunnelling from the lead. Thus we consider only the effective Hamiltonian H_{eff} for the remaining states, which contains the Hermitian part H_0 and the non-Hermitian part H_1

$$\begin{aligned} H_0 &= E_{S_{0,2}} |S_{0,2}\rangle \langle S_{0,2}| + E_\downarrow |\downarrow\rangle\langle\downarrow| + E_\uparrow |\uparrow\rangle\langle\uparrow| + t(|S_{0,2}\rangle\langle S_{1,1}| + \text{H.c.}) + \\ &\quad + g\left(|S_{1,1}\rangle\langle T_+|L_+ + \text{H.c.}\right) + (g^*\mu_B B_z + gL_z)\,|T_+\rangle\langle T_+|\,, \\ H_1 &= -i\Gamma_{S_{0,2}} |S_{0,2}\rangle \langle S_{0,2}| - i\sum_{\sigma=\uparrow,\downarrow} \Gamma_\sigma |\sigma\rangle\langle\sigma|\,. \end{aligned} \tag{2.16}$$

Pairs of numbers (m, n) denote the number of electrons on the left and right QD and $|\uparrow\rangle, |\downarrow\rangle$ are single particle states on the right dot. The non-Hermitian H_1 incorporates the relaxation from the localized singlet state $|S_{0,2}\rangle$ to $|\uparrow\rangle, |\downarrow\rangle$ (at rate $\Gamma_{S_{0,2}}$) and from $|\uparrow\rangle, |\downarrow\rangle$ to both $|S_{1,1}\rangle$ and $|T_+\rangle$, i.e. $\Gamma_{\uparrow,\downarrow}$ are the rates for the double dot to be filled with a second electron after only one electron occupies the right dot. Besides the energies $E_{\uparrow,\downarrow,S_{0,2}}$ of the states, H_0 contains the HF coupling in the $S - T_+$ subspace and the external magnetic field. We

have introduced the abbreviation $L_- = A_-^{(\text{left})} - A_-^{(\text{right})} = \delta A_-$, $L_+ = L_-^\dagger$ and $L_z = A_z^{(\text{left})} + A_z^{(\text{right})}$, where the A are the usual collective spin operators. Note that the L-operators do fulfill angular momentum commutation relations in the homogeneous limit. The full Liouvillian is thus written as

$$\begin{aligned}\mathcal{L}\rho = &- i(H_{\text{eff}}\rho - \rho H_{\text{eff}}^\dagger) \\ &+ 2\Gamma_{S_{0,2}} \sum_{\sigma=\uparrow,\downarrow} |\sigma\rangle\langle S_{0,2}|\rho|S_{0,2}\rangle\langle\sigma| + \sum_{\sigma=\uparrow,\downarrow} \Gamma_\sigma \Big(\sum_{x=T_+,S_{1,1}} |x\rangle\langle\sigma|\rho|\sigma\rangle\langle x| \Big).\end{aligned}$$

The HF transition rate $\sim A/\sqrt{N}$ is now the slowest timescale in the system[8]. Typical experimental numbers are [117]

- HF-rate: $A/\sqrt{N} \sim (10\text{ ns})^{-1}$=100 MHz
- tunneling dot↔lead (i.e. $\Gamma_{\uparrow,\downarrow,S_{0,2}}$): ≤ 100 GHz
- coherent tunneling rate t: typically $1-10$ GHz, possibly 1 MHz−100 GHz

Eliminating the single particle states and the localized singlet state $S_{0,2}$ [118, 119] yields the Liouvillian

$$\mathcal{L}\rho = -i(H_{\text{eff}}\rho - \rho H_{\text{eff}}^\dagger) + 2\Gamma \sum_{x=T_+,S_{1,1}} |x\rangle\langle S_{1,1}|\rho|S_{1,1}\rangle\langle x|, \tag{2.17}$$

$$H_{\text{eff}} = g\left(|S_{1,1}\rangle\langle T_+|L_+ + \text{H.c.}\right) + \left(g^*\mu_B B_z + gL_z\right)|T_+\rangle\langle T_+| + (\delta - i\Gamma)|S_{1,1}\rangle\langle S_{1,1}|,$$

where Γ is now the effective decay rate of the delocalized singlet and δ is an ac-stark shift. We are thus left with only two electronic states, namely T_+ and $S_{1,1}$, which yields a simplified picture of the cooling process (Fig. 2.14).

Master equation for nuclei– Starting from the simplified Liouvillian from the last section, Eq.(2.17), we now eliminate the electronic levels altogether. We do so by first defining projectors onto subspaces

$$\begin{aligned}\mathcal{P}\rho &= P\rho P, \quad \text{with } P = |T_+\rangle\langle T_+| \otimes \mathbb{1}_{\text{nuc}}, \\ \mathcal{Q} &= 1 - \mathcal{P},\end{aligned} \tag{2.18}$$

[8]Note that we did not include co-tunnelling, because this is only important when the blocked T_0, T_- states are occupied. It could be included through

$$\mathcal{L}_{\text{cot}}\rho/\Gamma_{\text{cot}} = \sum_y |y\rangle \left(\sum_x \langle x|\rho|x\rangle \right) \langle y| - \sum_x |x\rangle\langle x|\,\rho - \rho \sum_x |x\rangle\langle x|\,,$$

with $x, y = S_{1,1}, T_+$.

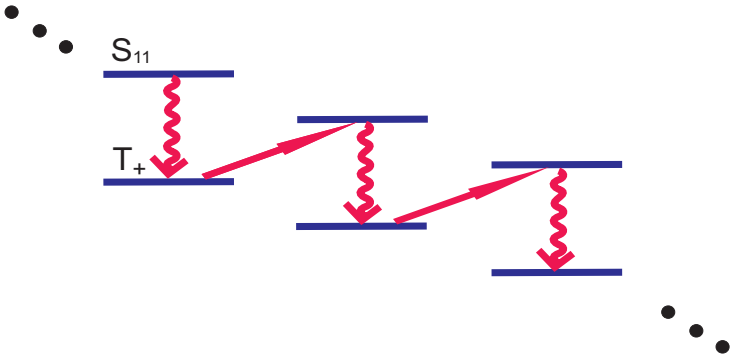

Figure 2.14: Schematic view of the simplified cooling process. The straight arrows indicate HF induced spin flips from the polarized triplet to the singlet, from which in turn the triplet is reloaded. During each such cycle the nuclear spins loose energy/spin excitation. The singlet does not exclusively relax to the triplet T_+, but can also *itself* be the result of the cascaded tunnelling process described in the main text. This, however, does neither change the nuclear spin state, nor lead to a slowdown of the whole procedure and thus this case is not relevant, and consequently not plotted in this sketch.

where $\mathcal{P}\rho$ contains the "slow" and $\mathcal{Q}\rho$ the "fast" dynamics. Similarly the Liouvillian is separated into a slow part $\mathcal{L}_1$ and a fast part $\mathcal{L}_0$, which has the property $\mathcal{L}_0\mathcal{P}\rho = 0$.

We now formally consider the polarization process split into time intervals t_i, such that $< \mathcal{O}(\sqrt{N})$ spins are flipped within one such interval. Within each of these intervals the Overhauser field does not vary by more than $\mathcal{O}(A/\sqrt{N})$. For each of these intervals we derive a master equation that is in the end brought to a form valid for all times.

For the situation at hand we define $\mathcal{L}_0 = \mathcal{L}_\Delta + \mathcal{L}_\Gamma$ and $\mathcal{L}_1 = \mathcal{L}_{ff} + \mathcal{L}_z$, such that $\mathcal{L}_1$ contains the hyperfine interactions

$$\begin{aligned} \mathcal{L}_{ff} &= g\left(|S_{1,1}\rangle\langle T_+|L_+ + |T_+\rangle\langle S_{1,1}|L_-\right), \\ \mathcal{L}_z &= g\,|T_+\rangle\,\langle T_+|\,(L_z - \langle L_z\rangle_0), \end{aligned} \tag{2.19}$$

and $\mathcal{L}_0$ the Lindblad-form decay from the singlet (see Eq. (2.17)) and the extra energy of the singlet state $\mathcal{L}_\Delta \to H = \Delta\,|S_{1,1}\rangle\,\langle S_{1,1}|$, with Δ denoting the energy difference between the singlet and the triplet state $\Delta = \delta + g^*\mu_B B$. We define here $B = B_z + g\langle L_z\rangle_0/(g^*\mu_B)$, i.e. as the sum over the internal Overhauser field and the external field, and $\langle L_z\rangle_0$ is the expectation value at the beginning of a time interval.

We now rewrite $gL_z = g\langle L_z\rangle_0 + \varepsilon_t$, where $\|\varepsilon_t\|_{\text{typ}} < \mathcal{O}(A/\sqrt{N})$. The norm is to be understood as the norm of the state projected onto the subspace of

A^z values, i.e. the developed description is only valid for those typical fields. This is a reasonable and not restrictive approach as the distribution of fields is narrow (of width $\mathcal{O}(\sqrt{N})$) initially and does not grow during the cooling process (cf. Sec. 2.2.2). We perform now the adiabatic elimination for one (arbitrary) time segment; we have [120]

$$\frac{d}{dt}\mathcal{P}\rho = \mathcal{P}\mathcal{L}\mathcal{P}\rho + \underbrace{\int_0^t dt' \mathcal{P}\mathcal{L}e^{\mathcal{Q}\mathcal{L}(t'-t)}\mathcal{Q}\mathcal{L}\mathcal{P}\rho(t')}_{=\mathcal{I}}, \tag{2.20}$$

which is exact and approximationless (Nakajima-Zwanzig equation). Integrating by parts we have

$$\begin{aligned}\mathcal{I} &= \mathcal{P}\mathcal{L}\frac{1}{\mathcal{Q}\mathcal{L}}\left(1 - e^{-\mathcal{Q}\mathcal{L}t}\right)\mathcal{Q}\mathcal{L}\mathcal{P}\rho - \int_0^t dt' \mathcal{P}\mathcal{L}\frac{1}{\mathcal{Q}\mathcal{L}}\, e^{\mathcal{Q}\mathcal{L}(t'-t)}\mathcal{Q}\mathcal{L}\mathcal{P}\dot{\rho}(t') \\ &\approx \mathcal{P}\mathcal{L}\frac{1}{\mathcal{Q}\mathcal{L}}\mathcal{Q}\mathcal{L}\mathcal{P}\rho - \int_0^t dt' \mathcal{P}\mathcal{L}\frac{1}{\mathcal{Q}\mathcal{L}}\, e^{\mathcal{Q}\mathcal{L}(t'-t)}\mathcal{Q}\mathcal{L}\mathcal{P}\dot{\rho}(t'),\end{aligned}$$

where we used the fact that $\exp(-\mathcal{Q}\mathcal{L}t)$ decays quickly [118]. Our goal is the derivation of a master equation to second order, i.e. g^2/Γ. The second term on the rhs of the above equation is $\mathcal{O}(\frac{g^2}{\Gamma}\frac{g}{\Gamma})$ and thus negligible.

Now the operator $(\mathcal{Q}(\mathcal{L}_0 + \mathcal{L}_1)\mathcal{Q})^{-1}$ is approximated by expansion in $\mathcal{L}_1/\mathcal{L}_0$, which is justified as $\mathcal{L}_1/\mathcal{L}_0 \sim (A/\sqrt{N})/\Gamma$ is the small parameter of our problem. To the relevant order we have

$$(\mathcal{Q}(\mathcal{L}_0 + \mathcal{L}_1)\mathcal{Q})^{-1} \approx \mathcal{L}_{0q}^{-1} - \mathcal{L}_{0q}^{-1}\mathcal{L}_{1q}\mathcal{L}_{0q}^{-1}, \tag{2.21}$$

where we have defined $\mathcal{L}_{iq} = \mathcal{Q}\mathcal{L}_i\mathcal{Q}$, $i = 0, 1$. Thus we get

$$\frac{d}{dt}\mathcal{P}\rho = \underbrace{\mathcal{P}\mathcal{L}_1\mathcal{P}\rho}_{A} - \mathcal{P}(\mathcal{L}_0 + \mathcal{L}_1)\left(\underbrace{\mathcal{L}_{0q}^{-1}}_{B} - \underbrace{\mathcal{L}_{0q}^{-1}\mathcal{L}_{1q}\mathcal{L}_{0q}^{-1}}_{C}\right)\mathcal{Q}\mathcal{L}_1\mathcal{P}\rho, \tag{2.22}$$

which is the equation we desired[9].

Term A– $\mathcal{P}\mathcal{L}_1\mathcal{P}\rho$ is given through the Hamiltonian $H_A = gL_z$.

Term B– is found to be

$$-g^2\left(\frac{L_-L_+\rho_{\text{nuc}}}{\Gamma - i\Delta} + \frac{\rho_{\text{nuc}}L_-L_+}{\Gamma + i\Delta}\right) \otimes |T_+\rangle\langle T_+|\,.$$

Term C– is $2g^2\frac{\Gamma}{\Gamma^2+\Delta^2}L_+\rho_{\text{nuc}}L_-\,|T_+\rangle\langle T_+|$ (in relevant order).

[9] The same equation is obtained by assuming $d/dt(\mathcal{Q}\rho) = 0$ (fast relaxation leads to steady state after short time initial transients, cf. Refs. [118, 119]).

Grouping these terms together yields the master equation for the nuclei

$$\frac{d}{dt}\rho = -ig[L_z,\rho] + ig^2\frac{\Delta}{\Gamma^2+\Delta^2}[L_-L_+,\rho] - g^2\frac{\Gamma}{\Gamma^2+\Delta^2}\left(L_-L_+\rho + \rho L_-L_+ - 2L_+\rho L_-\right), \tag{2.23}$$

for one time interval.

Now all these equations can be written in a short form that is valid over the whole polarization time, because in each time interval the equation has the same form. Indeed, one merely needs to reinterpret the detuning as an instantaneous one, $\Delta = \Delta(t) = \delta + g^*\mu_B(B_z + g\langle L_z\rangle(t)/(g^*\mu_B))$, and the above equation is the globally valid.

Eq. (2.23) resembles very much the one we have studied in the previous cooling scheme (which was based on short time expansion in a different setup). So the tools we developed there, are applicable here. In terms of described physical effects the equation is important because it incorporates the dependence of the cooling rate on the already achieved polarization which can lead to interesting effects, see. e.g. [102]. We have numerically simulated the equation extending it to additionally include dipolar effects, as is detailed in the next section. This treatment will be further detailed and developed in future work– we present here the results that are relevant for showing that the experimental realizations we have proposed are indeed suitable and that the polarization scheme is not crucially affected by nuclear dipole-dipole interactions.

2.4 Quantitative Treatment of Dipolar Interactions

Nuclear dipolar interactions are likely to become important on very long timescales which are probably necessary for close-to-ground state cooling. We show here that they can be treated with the same covariance matrix approach that proved successful for the treatment of hyperfine interactions. The nuclear dipolar Hamiltonian is [59, 108]

$$H_{\mathrm{dd}} = \sum_{m\neq n}\frac{\mu_0 g_{I,m} g_{I,n}\mu_N^2}{8\pi r_{nm}^3}\left(\mathbf{I}_n\cdot\mathbf{I}_m - \frac{3(\mathbf{I}_n\cdot\mathbf{r}_{nm})(\mathbf{I}_m\cdot\mathbf{r}_{nm})}{r_{nm}^2}\right), \tag{2.24}$$

where $\mathbf{r}_{nm}$ is the vector connecting spins n and m, $\mu_N = e\hbar/(2m_{\mathrm{proton}}) \approx 5.05\times10^{-27}$ J/T is the nuclear magneton, $g_{I,n}$ the g-factors and $\mu_0 = 4\times10^{-7}$ N/A^2 the magnetic constant. (Note that here as well as previously, the spin

operators have been taken to be dimensionless.) Anisotropic contributions to the hyperfine interaction (cf. Chapter 1 and Table 1.1) could be comparable in strength to the nuclear dipole-dipole interactions. However, they would still constitute a minor correction to the dominant contact term of the HF interaction, whereas the dipolar coupling actually couples the nuclear ensemble to an external bath. This coupling leads to spin diffusion and therefore decay of the nuclear polarization, i.e. the phenomenon under study here. Furthermore, as it will turn out in the course of this section, the nuclear dipole-dipole interaction is weak in comparison to other phenomena occurring in realistic setups, such as detuning due to the built-up Overhauser field and species inhomogeneity.

Due to energy conservation the terms changing the total magnetic Zeeman energy of the nuclei can be neglected in the present setup, which requires a large magnetic field[10]. From the most simple golden rule estimation for nearest neighbor coupling one gets the rate $\gamma_{\mathrm{dip}}^2/B \sim (10^{-5}\mu\mathrm{eV})^2/25\mu\mathrm{eV}/T$, which is using μeV ~ 4 ns approximately 1000 s/T for these processes. Thus the non-secular terms are neglected, yielding

$$\begin{aligned} H_{\mathrm{dd}} &= \sum_{m\neq n} \frac{\mu_0 g_{I,m} g_{I,n} \mu_N^2}{16\pi r_{nm}^3} (1-\cos^2(\theta_{nm})) \left(I_n^+ I_m^- - 2I_n^z I_m^z\right) = \\ &= \sum_{m\neq n} d_{nm} \left(I_n^+ I_m^- - 2I_n^z I_m^z\right). \end{aligned} \tag{2.25}$$

Here θ_{nm} is the angle between $\mathbf{r}_{nm}$ and the z axis (which is also the direction of the magnetic field). This approximation is standard in the literature; see e.g. Ref. [70], and references therein.

For the evolution of the covariance matrix $\gamma_{ij} = \langle \sigma_i^+ \sigma_j^- \rangle$ we thus have

$$\begin{aligned} \frac{d\gamma_{ij}}{dt} &= i \sum_{k,l} d_{kl} \left(\langle \sigma_i^+ \sigma_k^z \sigma_j^- \rangle (\delta_{li} - \delta_{lj}) + \langle \sigma_i^+ \sigma_l^z \sigma_j^- \rangle (\delta_{ki} - \delta_{kj}) + \gamma_{ij} (\delta_{ki}\delta_{li} - \delta_{kj}\delta_{lj}) \right) \\ &\quad + 4i \sum_k \left(d_{ki} \langle \sigma_k^+ \sigma_i^z \sigma_j^- \rangle - d_{kj} \langle \sigma_i^+ \sigma_j^z \sigma_k^- \rangle \right) \\ &= 2i \sum_k \left((d_{ki} - d_{kj}) \langle \sigma_i^+ \sigma_k^z \sigma_j^- \rangle + 2 d_{ki} \langle \sigma_k^+ \sigma_i^z \sigma_j^- \rangle - 2 d_{kj} \langle \sigma_i^+ \sigma_j^z \sigma_k^- \rangle \right) \\ &= 2i \sum_k (d_{ki} - d_{kj}) \left(-\gamma_{ij} - 2\gamma_{ik}\gamma_{kj} + 2\gamma_{ij}\gamma_{kk} \right) + \ldots, \end{aligned} \tag{2.26}$$

where we used $d_{kl} = d_{lk} = \frac{\mu_0 g_{I,k} g_{I,l} \mu_N^2}{16\pi r_{kl}^3}(1-\cos^2(\theta_{kl}))$ and defined $d_{kk} = 0$. The higher order expectation value has been factorized according to the (v) "spin"

[10] Indeed, even fields of order 0.1 T are sufficient for the approximation we make [70].

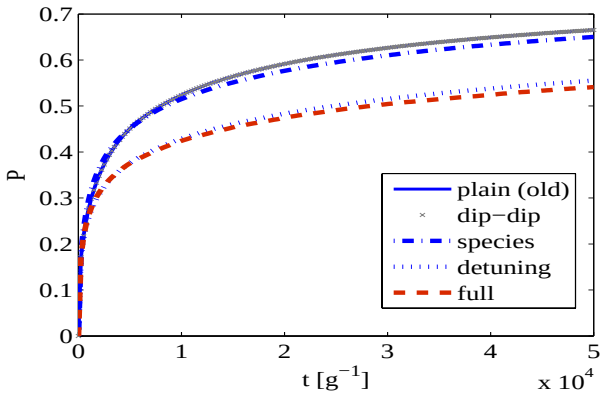

Figure 2.15: Simulation of the cooling process in the spin-blockade configuration. For clarity we have separated out the various contributions of the master equation according to Eq. (2.23). The strongest influence is the detuning caused by the build-up of the Overhauser field. These simulation comprised a total of $N = 288$ Ga- and As-spins. $\Gamma = A/4 = 1/(10\text{ps})$ and $B = 1$ T. (Note that the 'crosses' lie on top of the 'plain' curve.)

factorization scheme in the same way as the hyperfine terms, and can thus be treated straightforwardly with the numerical methods developed earlier.

For completeness we give here also explicitly the contribution of the nuclear Zeeman energies to the equation of motion for the covariance matrix

$$\dot{\gamma}_{ij} = iB\gamma_{ij}\mu_I(g_{I,i} - g_{I,j}),$$

and write out the middle term of Eq. (2.23), which of course also needs to be included in the numerical computations for consistency

$$\dot{\gamma}_{ij} = 2ig^2\frac{\Delta}{\Gamma^2+\Delta^2}\sum_k g_k\left(g_i\langle\sigma_k^+\sigma_i^z\sigma_j^-\rangle - g_j\langle\sigma_i^+\sigma_j^z\sigma_k^-\rangle\right).$$

For the simulations we consider two species of nuclei, ^{75}As and ^{69}Ga, with nuclear moments $1.44\mu_I$ and $2.02\mu_I$, respectively, placed on a Zincblende lattice. In Fig. 2.15 one can see clearly that the dipole interaction leads indeed to a very small reduction of the total polarization. More important is the effect of the Overhauser field that is built up over time and detunes the initially resonant transition. However, as discussed earlier, this effect can be compensated by adjusting the external field. Not shown here, we have explicitly verified that the different nuclear Zeeman energies of Ga and As lead to a slightly enhanced cooling performance due to extra dephasing of dark state coherences.

Summarizing these quantitative considerations of dipolar interactions, we can put to record that we have designed an efficient way of describing the interaction and shown that our previous analytic estimates indeed hold well. This indicates that high polarizations are in fact achievable realistically. Future work will explore further open questions regarding dipolar interaction in QDs that have become now quantitatively treatable– most noticeable the lifetime of collective nuclear spin states.

2.5 Conclusions

In summary we have presented in this chapter a quantum treatment of a dynamical nuclear spin polarization scheme in few-electron quantum dots that takes into account quantum coherences between nuclei and allows numerical study of the cooling dynamics for thousands of spins. We have quantified limitations due to dark states and shown that these limits are overcome by the inhomogeneous Knight shift and active mode changes. From this we conclude that cooling to more than 90% (of the maximal Overhauser field) is feasible faster than typical nuclear spin diffusion processes. Setups for the experimental realization of our scheme have been proposed.

In order to go beyond the presented results to polarizations larger than 99%, which would bring the system of coupled nuclei close to a pure state and significantly reduce electron spin decoherence, the presented scheme can be optimized, both in terms of timing (length of the individual cooling step and wave function changes) and in terms of the electron wave functions chosen. A further enhancement may be achieved by combining the polarization scheme with A^z-measurements [37, 38, 36] to reduce the A^z variance and to tailor the interaction times and the external field to the measured A^z value. Dipolar interaction and other depolarizing processes will become more important in later stages of the cooling and need to be considered carefully in the development of ground-state cooling techniques. More detailed studies of these processes may, in addition, lead to schemes to monitor the intrinsic (dipolar) nuclear dynamics via the hyperfine interaction.

The combination of high polarization and long coherence times make the nuclear spin ensemble itself a candidate for an active role in quantum computation. Like the actively explored single-nucleus-spin qubits [19], collective excitations of a polarized ensemble of spins could also be used for quantum information purposes (cf. Chapters 5 and 6). Similar to their atomic counterparts [39, 121], the ensembles might become more suited than their isolated constituents for certain quantum information tasks.

Chapter 3

Nuclear Spin Cooling – The Homogeneous Limit

We present here further evidence for the importance of dark state effects in nuclear spins cooling (as introduced in Chapter 2) by considering the limit of a spatially homogeneous electron wave function, which is commonly assumed in studies of electron spin decoherence. Naturally our theory is directly applicable to QD potentials and shapes producing a quasi-homogeneous electron distribution. Furthermore, as an inhomogeneous wave function can be approximated by a step function and our results bear relevance for the dynamics in each of the steps, the results presented here can be transferred to more general situations (cf. e.g. Ref. [107]).

In Sections 3.1 and 3.2 approximate analytical solutions are shown to provide accurate results, allowing for the determination of cooling potential and rates, both of which reflect the effect of polarization-limiting dark states. In particular it is shown that the time evolution of the polarization follows very closely a hyperbolic tangent shape. By generalizing the two-particle singlet picture to the many body case, we provide a handy and detailed microscopic description of dark states, which proves useful for the analysis of the effect of electron wave function changes during the cooling procedure (Sections 3.3 and 3.4). Finally we investigate the effect of *trapping states* in the cooling procedure in Section 3.5 and end this chapter with concluding remarks.

We consider, as in the previous chapter, the cooling of N nuclear spins in a QD through interaction with polarized electrons. One cooling cycle consists of (i) initialization of the electron spin in a well-defined direction $|\uparrow\rangle$, and (ii) evolution of the combined system for a "short" time Δt.

Using a slightly different normalization (to retain the angular momentum

structure) the HF interaction for homogeneous coupling constants reads

$$H = \frac{A}{2N}\left(I^+S^- + S^+I^-\right) + \frac{A}{N}I^zS^z + B_{ext}S^z. \tag{3.1}$$

$\mathbf{S}$ is the spin operator for the electron, A the HF coupling constant, and $I^\mu = \sum_i I_i^\mu$ are the three components of the homogeneous collective nuclear spin operators ($\mu = \pm, z$). The collective operators fulfill the angular momentum commutation relations

$$[I^+, I^z] = -I^+,$$
$$[I^+, I^-] = 2I^z.$$

We take $I = 1/2$ and neglect nuclear dipolar interactions, nuclear Zeeman energies and species inhomogeneities . If the relevant system dynamics happens on a time scale larger than Δt, as is the case in the present study, we arrive at the continuous version of the master equation Eq. (2.3) for the density matrix ρ of the nuclei

$$\frac{d}{dt}\rho = i\frac{A}{2N}[I^z,\rho] - \frac{A^2\Delta t}{8N^2}[I^z,[I^z,\rho]] - \frac{A^2\Delta t}{8N^2}\left(I^+I^-\rho + \rho I^+I^- - 2I^-\rho I^+\right). \tag{3.2}$$

Although we consider in our model the polarization process in a single dot, the results bear relevance for spin cooling in the recently investigated double QDs [115, 122]. There, the polarizing dynamics happens in the subspace of a two-electron singlet and a polarized triplet; coupling between the two is mediated by the *difference* $\delta I^\pm = (I_L^\pm - I_R^\pm)/2$ of the collective nuclear spin operators of the two dots L, R, while the effective Overhauser field is given by the sum $(I_L^z + I_R^z)/2$. In the homogeneous limit these operators obey the same algebra as the "bare" ones of our model, thus making our results directly applicable.

3.1 Achievable Polarization

Due to the collective nature of the coupling, singlet-like "dark states" can trap spin excitation and prevent cooling to the ground state. This effect is for homogeneous couplings most conveniently described in the Dicke basis [104], which is well-known for example from the literature on superradiance. The basis states are $|I, m, \beta\rangle$ where $I(I+1)$ is the eigenvalue of the collective angular momentum operator $\mathbf{I}^2$, and the eigenvalue of I^z is given by m. The possible values of I are $N/2, N/2-1, \ldots$, the smallest value being 0 if N is

even and 1/2 if N is odd; $|m| \leq I$. β is the permutation quantum number, which labels the different degenerate states with the same quantum numbers I and m. The degeneracy D of the states depends only on I and not on m, $D(I) = \binom{N}{N/2-I} - \binom{N}{N/2-I-1}$.

When acting on a state $|I, m, \beta\rangle$, the operator I^- decreases the quantum number m by one $I^-|I, m, \beta\rangle = \sqrt{I(I+1) - m(m-1)}|I, m-1, \beta\rangle$. For $m = -I$ the action of I^- yields zero, and thus the states $|I, -I, \beta\rangle$ can not be polarized further in a system evolving according to Eq. (3.2). The steady state of the cooling process described by the master equation (3.2) starting from a completely mixed state is thus

$$\rho_{\text{ss}} = 1/2^N \sum_I D(I)(2I+1)|I, -I\rangle\langle I, -I|, \tag{3.3}$$

where the trace over the permutation quantum number β has been performed.

We now evaluate the polarization of the steady state (3.3) normalized to the polarization of the ground state

$$\frac{\langle I^z\rangle_{\text{ss}}}{\langle I^z\rangle_0} = \frac{2}{2^N N} \sum_{I=0}^{N/2} I(2I+1)D(I). \tag{3.4}$$

For the explicit evaluation of this expression, we first note that the difference in the formula for the degeneracies of the $|I, m\rangle$ states makes the series for the steady state polarization Eq. (3.4) telescopic. In particular grouping the prefactors of the binomial coefficients with the same entries in the Ith and $I+1$st term gives $(I+1)(2(I+1)+1) - I(2I+1) = 4I+3$, thus transforming the sum of Eq. (3.4) into a sum of binomial coefficients having linear prefactors

$$\frac{\langle I^z\rangle_{\text{ss}}}{\langle I^z\rangle_0} = \frac{2}{2^N N} \sum_{I=1}^{N/2} (4I-1) \begin{pmatrix} N \\ N/2-I \end{pmatrix}.$$

Evaluation of this sum and regrouping of the terms leads to

$$\frac{\langle I^z\rangle_{\text{ss}}}{\langle I^z\rangle_0} = \frac{2}{2^N N} \left[\frac{4(N-1)!}{([(N-1)/2]!)^2} - \left(2^{N-1} - \frac{1}{2} \begin{pmatrix} N \\ N/2 \end{pmatrix} \right) \right]. \tag{3.5}$$

As an example this expression can applied to the case $N = 2$, where one finds a final polarization of 3/4. This is the expected result because one out of the four two-spin states can not be cooled (the singlet). In Fig. 3.1 it is shown that for increasing particle number the possible polarization quickly decreases from the 75% of the two-particle case. The negative indications for cooling purposes are obvious.

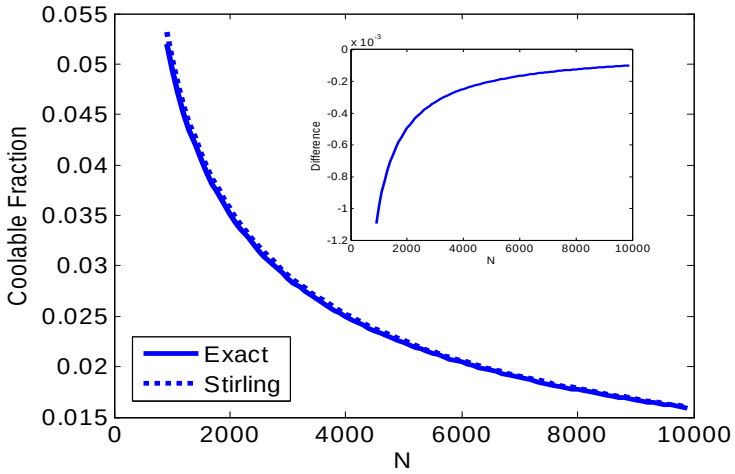

Figure 3.1: The fraction of the nuclei that can be polarized in the case of homogeneous coupling constants. Shown are both the exact and the approximate numbers; the inset shows the difference between the two.

Application of the Stirling formula $N! \approx \sqrt{2\pi} N^{N+1/2} e^{-N}$ gives the approximate result for $N \gg 1$

$$\frac{\langle I^z \rangle_{\rm ss}}{\langle I^z \rangle_0} = \sqrt{\frac{8}{\pi N}} + \mathcal{O}(1/N). \tag{3.6}$$

For the mesoscopic particle numbers of interest in the study of quantum dots, the obtainable polarization is thus negligible. In Fig. 3.1 it is shown that the approximate first order formula matches the exact value very well, as expected.

3.2 Time Evolution - Analytic Expressions

The study of the time evolution of the nuclear spin system under the master equation (3.2) is similar to the study of the evolution of the atomic population in superradiant light emission from an ensemble of atoms. The latter problem has received considerable attention in the quantum optics literature, see e.g. the textbook [98] and review [97]. The focus of these studies was slightly different than it is in the cooling protocol we are considering: In quantum optics an ensemble with all atoms excited is the most studied situation, because for this initial condition one has pronounced signatures in the emitted light pulses *and* it is experimentally accessible. Here on the other

hand, we are dealing with a completely mixed initial state. This complicates the situation because in this mixture super- as well as subradiant states occur. Nevertheless we extract and present here approximate explicit analytic expressions for the evolution of the nuclear spin polarization.

Instead of solving the dynamics of the density matrix of the nuclei, we concentrate on the evolution of the variable of our interest, $\langle I^z \rangle$. It obeys the equation of motion

$$\frac{d}{dt}\langle I^z \rangle = \mathrm{tr}(I^z \frac{d}{dt}\rho) = -2\kappa \langle I^+ I^- \rangle,$$

where we have introduced $\kappa = \frac{A^2 \Delta t}{8N^2}$. The equation for the polarization $\langle I^z \rangle$ does not close, but couples to the variable $\langle I^+ I^- \rangle$. The time evolution of this quantity depends on $\langle I^+ I^z I^- \rangle$. Continuing this procedure leads to a hierarchy of coupled equations. Following the quantum optics literature on superradiance we make a factorization assumption

$$\langle (I^z)^2 \rangle = \langle I^z \rangle^2, \tag{3.7}$$

which is equivalent to the assumption that $\langle I_i^z I_j^z \rangle = \langle I_i^z \rangle \langle I_j^z \rangle$. In the following we apply this factorization to obtain analytical results for the time evolution of the polarization and check its validity by comparison with the exact numerical solution.

Using this assumption the equation of motion for the polarization becomes

$$\frac{d}{dt}\langle I^z \rangle = -2\kappa \left(\langle \mathbf{I}^2 \rangle - \langle I^z \rangle^2 + \langle I^z \rangle \right), \tag{3.8}$$

where $\mathbf{I}^2 = (I^z)^2 + \frac{1}{2}(I^+ I^- + I^- I^+)$ was used. For each given initial state $|I, m, \beta\rangle$ this equation is solved by

$$\langle I^z(t) \rangle_{I,m} = 1/2 - \nu_I \tanh\left(\nu_I (2\kappa t - c_0)\right), \tag{3.9}$$

where $\nu_I = \sqrt{4I(I+1)+1}/2$ and the initial condition depends on the value of m and enters through the constant $c_0 = \mathrm{arctanh}\left[-2(m-1/2)/\nu_I\right]/(2\nu_I)$. In Fig. 3.2 we compare the evolution of the polarization averaged over all initial states

$$\langle I^z(t) \rangle_{\text{averaged}} = \sum_{I,m} D(I) \langle I^z(t) \rangle_{I,m} \tag{3.10}$$

with the exact numerical calculation. The curves show good agreement, which serves as an indication that the factorization assumption captures the correct physics of the polarization process.

To gain further insight to the evolution of the population, we consider the evolution of a pure initial state with total angular momentum and z-projection equal to the mean value of the totally mixed state, i.e. $m = 0$

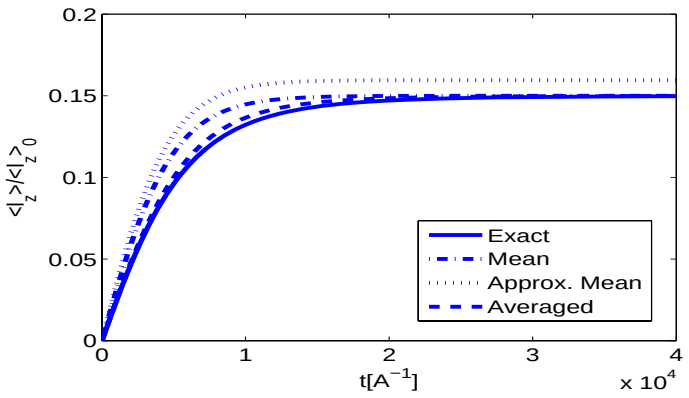

Figure 3.2: Comparison between the various (semi-)analytical solutions based on Eq. (3.7) and the exact numerical result for $N = 100$ particles. The "average" (dashed) line is averaged over all states in the initially totally mixed nuclear state, see Eq. (3.10). The two other curves are directly obtained from Eq. (3.9) by substituting one specific value for the angular momentum I: For the dashed-dotted line the average value of the total angular momentum I has been calculated exactly and for the dotted curve the approximate expression $I = \sqrt{2N/\pi}$ was used.

and $I_{\text{mean}} = \frac{1}{2^N}\sum_{I=0}^{N/2} I(2I+1)D(I)$. Using the same approximations as for the evaluation of the total obtainable polarizations (Eq. (3.6)) one gets $I_{\text{mean}} = \sqrt{\frac{2N}{\pi}} + \mathcal{O}(1)$. In this limit the polarization develops according to

$$\langle I^z(t)\rangle_{\text{mean}} = -\frac{1}{2}\sqrt{\frac{8N}{\pi}}\tanh\left(\sqrt{\frac{8N}{\pi}}\frac{A^2\Delta t}{8N^2}t\right), \tag{3.11}$$

where we used $\sqrt{N} \gg 1$. Fig. 3.2 shows the evolution in the "mean state" for both the exact and the approximate expression for the mean value of the average spin I_{mean}. Using the exact mean the results are very close to the actual evolution: Both the timescale and the final polarization are correctly predicted. When the approximate expression for the mean is employed, the timescale of the process is still correct. However, the predicted final polarization differs from the real polarization. This is to be expected, since the approximated mean value of I is only correct to order 1, which translates into a $\mathcal{O}(1/N)$ error for the polarization.

From Eq. (3.11) we can thus extract the timescale for reaching the steady

state of the polarization

$$\tau_{\text{hom}} = \frac{N}{A}\frac{\sqrt{8\pi}}{0.1}, \tag{3.12}$$

where we used $\Delta t = 0.1\sqrt{N}/A$, i.e. Δt is chosen such that the condition necessary for the expansion of the time evolution operator is fulfilled.

3.3 Microscopic Description of Dark States

In this section a new microscopic description of dark states is introduced, which, besides providing handy intuition, will serve in the following section as the basis for our estimations regarding ground state cooling in homogeneous situations. We prove that one can understand all dark states $I^- |I, -I, \beta\rangle = 0$ as a superposition of states describing $n = N/2 - I$ singlets and $2I = N - 2n$ polarized spins $|\downarrow\rangle$. Let us denote a singlet of spins i and j as $|S_{ij}\rangle$ and by $\left|S\left\{s_i\right\}_{i=1}^{2S}, \downarrow\right\rangle$ the state with S singlets $\left|S_{s_i s_{i+1}}\right\rangle$ and the remaining spins in state $|\downarrow\rangle$. Also we use the notation $P_{|x\rangle} = |x\rangle\langle x|$. The idea is to show that the statistical mixture of all permutations of $\left|S\left\{i\right\}_{i=1}^{2S}, \downarrow\right\rangle$

$$P_I = \frac{1}{N!}\sum_{\pi \in S_N} X(\pi) P_{|S\{1,\ldots,2S\},\downarrow\rangle} X(\pi)^\dagger$$

(where for a permutation $\pi \in S_N$ let $X(\pi)\left|S\left\{s_i\right\}, \downarrow\right\rangle = \left|S\left\{\pi(s_i)\right\}, \downarrow\right\rangle$) is equal to the projector on the $(I, -I)$-subspace:

$$P_I = \frac{1}{D(I)}\sum_{\beta} |I, -I, \beta\rangle \langle I, -I, \beta| .$$

To see this, we first observe (for $\pi \in S_N$) that $\pi \mapsto X_{(I,M)}(\pi) \in M_{2^N}$ with $X_{(I,M)}(\pi)$ acting (as above) on the space spanned by the vectors $|I, M; \beta\rangle$ with $\beta = 1, \ldots, D(I)$ a label for the eigenvalues of a set of permutation operators extending $\mathbf{I}^2$, and I^z to a complete commuting set (e.g., $P_{2i-1,2i}, i = 1, \ldots N/2$ cf. [104]) is a *representation* of the permutation group S_N. The representation must be *irreducible*, since if it were not, there would exist at least two sets of vectors in $\mathcal{H}_{(I,M)}$ that are *not* connected by S_N, hence the projector on one of those would be an operator commuting with $\{\mathbf{I}^2, I^z, P_{2i-1,2i}\}$, contradicting that this is a *complete* set of commuting observables on $(\mathbb{C}^2)^{\otimes N}$. Finally, we clearly have $X_{(I,-I)}(\pi) P_I X_{(I,-I)}(\pi)^\dagger = P_I$ and by Schur's Lemma (which states that any operator commuting with all elements of a irrep is proportional to the identity see, e.g., [123]) it follows that $P_I \propto \mathbb{1}_{I,-I}$. Counting the number of permutations resp. the degeneracy of the $(I, -I)$-subspace gives the normalization factor.

This shows that the projector on the (I, m)-subspace is given by the equal-weight mixture of all permutations of $N/2 - I$ singlets and the remaining $2I$ spins in the state $|I, m\rangle$.

3.4 Mode Changes

To cool beyond the dark state, one needs to break up singlets. One way of achieving this is changing the electron wave function as discussed in Chapter 2. When we talk about "mode changes" in the following, we do not consider the effects of active manipulations of the electron wave function and the induced inhomogeneous Knight fields (in contrast to Chapter 2). We want to keep the focus of this chapter on (quasi-)*homogeneous* effects. We do so by breaking up singlets through inducing local phase flips (as discussed below).

The number of modes that are needed to cool the nuclear spins to the ground state is in general not easily estimated due to the fact that orthogonal spin modes do not commute[1]. In order to get an estimate for the number of modes needed for cooling the spins, we use the simple Hadamard basis for the modes. The Hadamard matrices are recursively defined by $H_0 = 1$, and

$$H_{m+1} = \frac{1}{\sqrt{2}} \begin{pmatrix} H_m & H_m \\ H_m & -H_m \end{pmatrix}.$$

The size of the matrix is 2^m. Its columns are mutually orthogonal and represent the different modes we aim to address. This would be achieved by changing from the standard homogeneous coupling to the ith Hadamard mode by performing phase flips $|\downarrow\rangle_j \to -|\downarrow\rangle_j$ for all j with $(H_m)_{ji} = -1$.

When applied after cooling with the first mode, such a mode change has no effect on nuclei already in state $|\downarrow\rangle$, but singlets are transformed to triplets (with zero z-projection) if the phase of only one of the two spins is flipped, so that the state in the new mode is

$$\sum_n p(n) \sum_{\pi \in S_N} \sum_{u=0}^{n} q(n,u) X(\pi) P_{|S\{1,\ldots,2(n-u)\};\downarrow\rangle} X(\pi)^\dagger \otimes |T_0\rangle\langle T_0|^{\otimes u}$$

where $q(n, u)$ denotes the probability that u of the n singlets become a triplet after the mode change. We assume that changing from one Hadamard mode

[1] In the bosonic approximation the number of required modes is easily seen to be N, because the modes are mutually independent and initially all N modes are occupied and consequently have to be cooled one by one (not considering Knight shifts). It is unclear, if the scaling behavior of the number of required modes is the same for spins. One might think, for example, that one needs only $\mathcal{O}(\sqrt{N})$ modes in the spin case, because in the first mode $\sim \sqrt{N}$ excitations can be removed from the spin system.

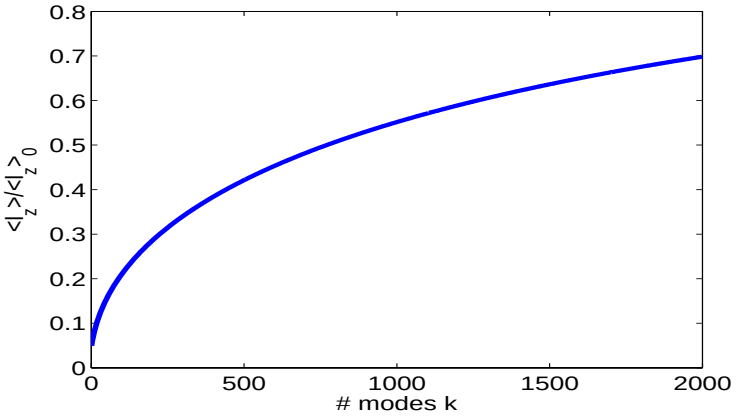

Figure 3.3: Estimate of the achieved cooling after a given number of (Hadamard-) mode changes for $N = 10^3$ nuclear spins.

to the next typically breaks up half the singlets in each of the terms in the mixture, i.e. $\bar{u} = n/2$.

We now calculate the average total angular momentum $\mathbf{I}^2$ of this state, by first noting that in each of the above terms in the mixture one can split the collective operators up into terms that act on spins which remained untransformed by the mode change, and the rest $\sum_{\text{all spins}} = (\sum_{\text{in some T}_0} + \sum_{\text{rest}})$. The mixed terms between the two sums are found to be 0. The terms involving the unchanged (rest) spins have the same total spin as before the mode change: Only singlets have been taken away. For the spins that have turned from singlets to triplets one can readily verify that their contribution to the new total angular momentum squared, $\langle \mathbf{I}^2 \rangle$, is $(N/2 - I_{\text{old}})/4$.

In a semiclassical treatment we now calculate in the way outlined above the average angular momentum after k mode changes and arrive at the recursive formula for the expectation values

$$I_{k+1}(I_{k+1} + 1) = I_k(I_k + 1) + (N/2 - I_k)/4, \tag{3.13}$$

where k is the index for the number of modes changes, and from which we extract the minimal compatible polarization, $I_k^z = -I_k$. The numerical solution of the above recursive formula presented in Fig. 3.3 indicates that order of $\mathcal{O}(N)$ modes are necessary to completely cool the nuclear spins. We have verified this scaling behavior for a wide range of particle numbers.

Note that a scheme employing Hadamard modes is not optimal: if one had complete freedom in the choice of modes, one could perform the phase flips one by one for the spins and cool everything to the perfect ground state

in N steps; which is better than the cooling procedure shown in Fig. 3.3.

We are thus lead to the conclusion that achieving high polarization for homogeneous couplings is hard: Sophisticated and undesirable control mechanisms are be needed. As seen in Chapter 2, a real *inhomogeneous coupling* significantly simplifies the cooling process.

3.5 Trapping States

Trapping states have first been discussed in the micromaser literature more than 20 years ago [124, 125]. The micromaser, or one-atom maser, is an experimental realization of the Jaynes-Cummings (JC) model: In a typical setup [126, 127] excited rubidium Rydberg atoms are injected into a high Q ($Q \sim 10^{10}$, lifetime ~ 0.1 s) superconducting microwave cavity, where they experience a JC interaction with a cavity mode. After the passage through the cavity the state of the atoms can be inferred by state selective ionization of the atoms. At low temperature ($\leq$ 100 mK), thermal photons in the cavity are greatly reduced and trapping states can begin to appear [125]. They occur when the product of the atom-field coupling strength g and the interaction time Δt (chosen via the velocity of the atoms) are such that the atoms undergo an integer number of Rabi oscillations

$$g\Delta t\sqrt{n_q+1} = 2\pi k, \tag{3.14}$$

where $k \in \mathbb{N}$, and n_q is the number of photons in the cavity. Thus, under trapping conditions the photon number in the cavity will be upper bounded by n_q, even though the cavity is pumped with excited atoms carrying excitation into the cavity. Trapping states are robust to photon decay from the cavity; as any loss of a photon leads to a non-trapped state, which can receive excitation from the passing atoms and consequently restores the trapping state. Trapping states have first been observed by Weidinger *et al.* [128] in 1999. A primary basis for the interest in trapping states has been their close connection to Fock state generation [126], and more generally non-classical field states [124, 129].

In the context of electron-nuclear spin interactions in QDs trapping states can appear in several forms: Clearly at high polarization, when the bosonic description of the HF interaction is valid, the results from the micromaser directly carry over to the QD setup. More importantly however, also at low polarizations trapping-related phenomena can be of importance, as we will elaborate in the remainder of this section for the limit of homogeneous

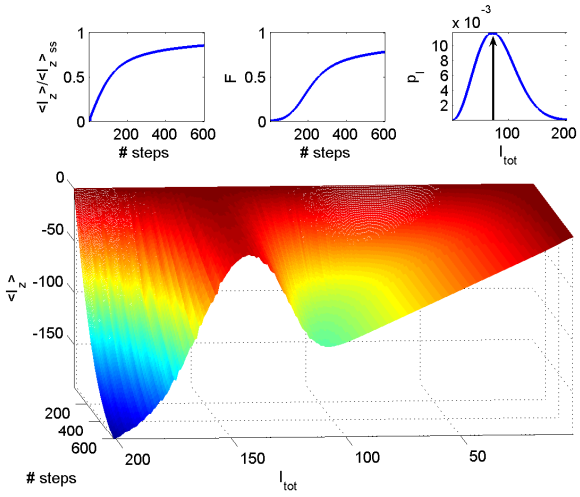

Figure 3.4: Trapping states in nuclear spin cooling ($N = 10^4$, homogeneous coupling). The maximum of the probability distribution p_I shown at the upper right lies at ≈ 75, implying the appearance of trapping state features visible in the lower plot at $I \approx 2 \times 75$. The upper left plot shows the reduced probability of being in a dark subspace, cf. Eq. (3.19). The arrow in the upper right plot indicates the choice of the resonant subspace (Eq. (3.17)).

coupling constants. Let us first write the HFI as

$$H = \frac{A}{2N} \begin{pmatrix} m & \xi_{I,m} \\ \xi_{I,m} & -(m+1) \end{pmatrix}_{|I,m,\uparrow\rangle,|I,m+1,\downarrow\rangle}, \tag{3.15}$$

with $\xi_{I,m} = \sqrt{I(I+1) - m(m+1)}$. The eigenfrequencies are given by

$$\nu_+^I = \frac{A}{2N} I/2, \qquad \nu_-^I = \frac{A}{2N}(-I/2 - 1/2). \tag{3.16}$$

Thus the frequencies of the quasi Rabi oscillations in these subspaces depend on the total angular momentum I and not on the z-quantum number m. As we have stated earlier, for a completely mixed initial state the probability of being in a certain I-subspace is peaked at $I = \mathcal{O}(\sqrt{N})$ and has a width of the same order. Thus, roughly, the frequencies $\nu_\pm^I$ will cover a range of $k \times \mathcal{O}(A/\sqrt{N})$, with $k \sim 1 - 10$.

In Chapter 2 we considered an iterative cooling protocol with a short evolution time step $\Delta t < \sqrt{N}/A$ for each cooling cycle. Certainly there are situations in which larger steps Δt yield a higher cooling rate and are favorable (this is the case in situations where detuning effects of the generated

Overhauser field are negligible, like in the experiments of Feng *et al.* [130]). For concreteness in the following we consider a natural choice for a longer interaction time

$$\nu_+^{\bar{I}} \Delta t = \pi, \tag{3.17}$$

where $\bar{I}$ denotes the peak of the probability distribution p_I for the occupancy of the I-subspaces, as indicated by the arrow in Fig. 3.4[2]. With the choice of Δt according to Eq. (3.17) a full electron spin flip occurs in the most highly occupied subspace, retrieving a large amount of excitation from the nuclear ensemble to be cooled in each step of the iteration. However for the subspace I' whose Rabi frequency obeys

$$\nu_+^{I'} \Delta t = 2\pi, \tag{3.18}$$

a trapping condition is fulfilled in the sense that the electron makes a full rotation, and is thus not polarizing the nuclei at all. From Eq. (3.16) we get

$$I' \approx 2\bar{I}.$$

Recalling that the width of the distribution p_I is $\mathcal{O}(\sqrt{N})$, just as the location of its peak, it directly follows that trapping states will play a role in the nuclear spin cooling setup we have been discussing in the past sections.

In Fig. 3.4 we present numerical calculations for $N = 10^4$ homogeneously coupled nuclear spins directly confirming the above observations: The subspace where $I' \approx 2\bar{I}$ is basically not cooled due to trapping states. This leads to a decrease in final polarization of about 20%. Also the probability to be in a dark subspace

$$F(t) = \sum_I c_{I,-I}(t), \tag{3.19}$$

is reduced by a similar amount (here we wrote the time-evolved state $\rho(t) = \sum_{I,m} c_{I,m}(t)|I,m\rangle\langle I,m|$) .

We have stochastically varied the interaction times from cooling cycle to cooling cycle by 10%, which is reflected in the small features in the lower plot of Fig. 3.4. The overall dark state properties are, however, not overshadowed by this (potential experimental) imperfection.

There are several ways of overcoming these trapping state limitations. The simplest one is to reduce the interaction time Δt. Just moving the resonance condition Eq. (3.17) rather slightly to larger angular momenta I, i.e. use slightly shorter times, solves the problem of trapping state limitations. We have verified this numerically for the same setup as above, but with the

[2] We consider here the frequency $\nu_+^{\bar{I}}$ for concreteness, but the results of the following discussion hold true for $\nu_-^{\bar{I}}$ as well.

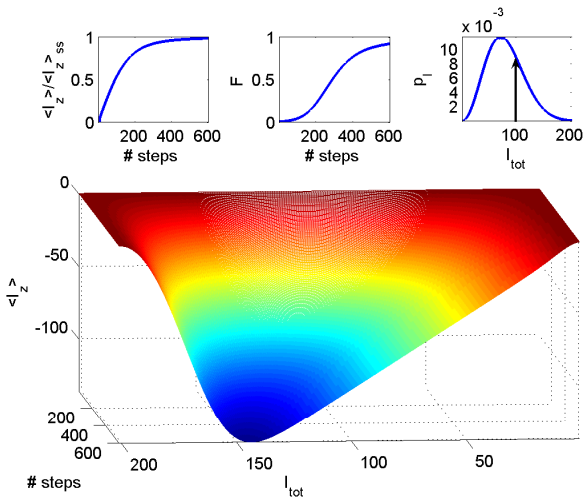

Figure 3.5: Mitigation of trapping state effects in nuclear spin cooling. Calculated quantities and parameters are the same as in preceding Fig. 3.4, but the interaction time has been changed as indicated by the arrow in the upper right plot. Trapping states appear only for subspaces with angular momenta that have negligible occupation for the (totally mixed) nuclear state we consider.

resonance at $I = 100$, instead of ≈ 75. The results are shown in Fig. 3.5, where trapping states appear, but now at $I \approx 200$. The subspace of this large angular momentum has negligible occupation (upper right plots of Figs. 3.4 and 3.5), such that the cooling process remains approximately unaffected.

The effect of inhomogeneous coupling constants on the trapping states is generally non-trivial to determine. However, one can develop an intuition by considering the picture we have introduced and motivated earlier: A set of "independent" shells is coupled to the same electron spin. Each of the shells contains homogeneously coupled spins, but has no or little correlations with the other shells (cf. Section 2.2.4). In this case there would be distinct trapping conditions for each shell, because each of them is coupled with a different overall strength. Thus one expects that only few shells have *simultaneous* trapping conditions, hence reducing the overall impact of them. Furthermore, for each homogeneously coupled shell the same simple presented strategies for overcoming trapping state limitations apply.

3.6 Conclusions

We have presented a study of nuclear spin cooling in quantum dots in the limit of a homogeneous electron wave function. We calculated exactly the cooling potential, presented analytical formulas for the time evolution of the polarization and, after introducing a handy intuition for the microscopic description of dark states, demonstrated the difficulties for cooling in quasi-homogeneous by considering Hadamard-modes. The results underline the importance of the inhomogeneous Knight shift in nuclear spin cooling, which mitigates these limitations so strongly, that polarizations above 90% are achievable in realistic setups (Chapter 2).

Furthermore, we have shown that trapping states can in principle hinder nuclear spin polarization in QDs and could be observed in the course of a cooling procedure (for example by measuring the finally obtained Overhauser field after cooling with different time steps Δt). However, their unwanted effect can be mitigated straightforwardly. As the original motivation for the study of trapping states in the micromaser was photonic state preparation, further research might explore the uses of trapping states with respect to nuclear spin state preparation. Novel spin measurement schemes [36] and the parity-dependent entanglement scheme presented in Chapter 7 pursue similar lines of thought and provide further evidence for the usefulness of ideas put forth here.

Chapter 4

Effective Dynamics of Inhomogeneously Coupled Systems

In this chapter we study the quantum dynamics of a single mode/particle interacting inhomogeneously with a large (mesoscopic) number of particles and introduce an effective approach to find the accessible Hilbert space where the dynamics takes place. The method is tailored for highly polarized samples, and we apply it to two relevant examples: the inhomogeneous Tavis-Cummings model (e.g., N atomic qubits coupled to a single cavity mode, or to a motional mode in trapped ions) and the inhomogeneous coupling of an electron spin to N nuclear spins in a quantum dot.

In quantum optics and condensed matter physics, a great effort has been oriented to the study of single quantum systems, or a few of them, and their experimental coherent control. This is the case for cavity QED [131], trapped ions [132], quantum dots [61], and circuit QED [133], among others. On the other hand, scaling up these highly isolated and controlled systems, many particle effects re-enter the stage and collective effects may play a central role.

The interaction of a single atom with a quantized electromagnetic mode, described by the Jaynes-Cummings (JC) model [134], has played a central role in quantum optics and other related physical systems. Among its many fundamental predictions, we can mention vacuum-field Rabi oscillations, collapses and revivals of atomic populations, and squeezing of the radiation field [135]. Atomic ensemble physics can be conveniently described by the Dicke model [136], when considering the interaction of atoms with light in free space, or by the Tavis-Cummings (TC) model [137], when the coupling takes place inside a cavity. In most treatments and applications of the TC

model, a constant coupling between the atoms and the radiation field is assumed, a simplification that greatly reduces the complexity of an analytical description [138, 139, 140]. Even in the case of many atoms, the homogeneous-coupling case profits from the $SU(2)$ group structure of the collective operators, allowing at least numerical solutions. However, the situation is drastically different when we consider the more realistic case of inhomogeneous coupling. In this case, there is no such straightforward way to access the Hilbert space in an efficient way, because all angular momenta representations are mixed through the dynamical evolution of the system and no analytical approach is known.

On the other hand, electron and nuclear spin dynamics in semiconductor nanostructures has become of central interest in recent years [61, 141], and several techniques for quantum information processing have been proposed [13, 19, 76, 142, 143, 144]. As described in the introduction of this thesis, the nuclear spins (when highly polarized) are likely to become an important asset in QD QIP. In the light of the results from Chapters 2 and 3, in which it was demonstrated that efficient cooling is possible, we turn now to the study of the dynamics generated by only *nearly* perfectly polarized samples.

In this chapter, we develop an effective approach to study the dynamics of a single mode/particle coupled inhomogeneously to a large number of particles, which are close to full polarization. In particular, we analyze in Sec. 4.1 the interaction of a collection of two-level atoms with a quantized field mode, that is, the inhomogeneous TC model. The main result is a successful identification of the states in Hilbert space that are relevant for the dynamics. We show that we are able to reproduce accurate results with a small number of states by comparison with exact numerical calculations. In Sec. 4.2 we consider the Fermi contact interaction of a single excess electron spin confined in a quantum dot with quasi-polarized nuclear spins. Using the formalism developed in Section 4.1, we study the transfer of quantum information between those systems in the presence of a single excitation in the nuclear spin system prior to the write-in procedure. The nature of the imperfections in polarization, i.e. coherent or incoherent excitation, plays a central role for the resulting dynamics. As coherent excitations can strongly populate the mode to be used for QIP, they are generally more harmful than incoherent ones; which typically have small effects (of order N^{-1}) on the important mode. We perform detailed calculations of the performance of the spin memory [41, 42] in the presence of imperfections, employing our developed formalism. In Sec. 4.3, we present our concluding remarks.

4.1 Inhomogeneous Tavis-Cummings model

The Hamiltonian describing the inhomogeneous coupling of N atoms with a quantized single field mode in the interaction picture and under resonant conditions, can be written as

$$H_{\mathrm{ITC}} = \sum_{i=1}^{N} g_i \left(\sigma_i^- a^\dagger + \sigma_i^+ a\right). \tag{4.1}$$

Here, $g_i = g(\mathbf{r}_i)$ is the (real) inhomogeneous coupling strength of atom i at position $\mathbf{r}_i$, σ_i^- (σ_i^+) is the lowering (raising) operator of atom i, and a ($a^\dagger$) is the annihilation (creation) operator of the field mode. We will refer to this model as the inhomogeneous Tavis-Cummings (ITC) model. In the homogeneous case, $g_i = g, \forall i$, one can define the angular momentum operator $J^+ \propto g\sum_{i=1}^{N}\sigma_i^+$, describing transitions between the common eigenvectors of J^z and $\mathbf{J}^2$, where $J^z = \sum_{i=1}^{N}\sigma_i^z$. This is not true for the inhomogeneous case, because $\tilde{J}^+ = \sum_{i=1}^{N} g_i\sigma_i^+$ does not satisfy the $SU(2)$ algebra anymore. However, we will show that this problem can still be addressed efficiently with certain restrictions. The strategy consists in following the Hilbert space that the system will visit along its evolution, and implementing a truncation to the significantly populated states.

Let us first consider the initial condition given by

$$|\Psi(0)\rangle = \sum_{n=0} c_n|n\rangle|\bar{\mathbf{0}}\rangle,$$

where $|n\rangle$ denotes a photonic Fock state and $|\bar{\mathbf{0}}\rangle$ denotes the collection of N atoms in the ground state. For each product state $|n\rangle|\bar{\mathbf{0}}\rangle$, we have a fixed number of excitations, which, even in the inhomogeneous case, is conserved by the dynamics determined by H_{ITC}. If the initial state is $|0\rangle|\bar{\mathbf{0}}\rangle$, the unitary evolution is trivial $|0\rangle|\bar{\mathbf{0}}\rangle \longrightarrow |0\rangle|\bar{\mathbf{0}}\rangle$.

Having in mind a series expansion of the time evolution operator, starting from initial state $|1\rangle|\bar{\mathbf{0}}\rangle$, H_{ITC} produces a nontrivial dynamics via the term $\tilde{J}^+ a$, so that

$$\tilde{J}^+ a|1\rangle|\bar{\mathbf{0}}\rangle = |0\rangle\sum_{i=1}^{N} g_i|\bar{\mathbf{1}}_i\rangle,$$

where $|\bar{\mathbf{1}}_i\rangle = \sigma_i^+|\bar{\mathbf{0}}\rangle$ represents a N-atom state with one excitation in the ith

atom. We define

$$|\bar{\mathbf{1}}\rangle = \frac{1}{N_0}\sum_{i=1}^{N} g_i|\bar{\mathbf{1}}_i\rangle,$$
$$N_0 = \sqrt{\sum_{i=1}^{N} g_i^2}, \tag{4.2}$$

such that $|\bar{\mathbf{1}}\rangle$ is a normalized state. Note that the system evolves in a closed two-dimensional subspace $\{|1\rangle|\bar{\mathbf{0}}\rangle, |0\rangle|\bar{\mathbf{1}}\rangle\}$ in which both states have the same fixed number of excitations.

If we start the dynamics with the two-excitation state $|2\rangle|\bar{\mathbf{0}}\rangle$, it evolves through

$$\tilde{J}^{+}a|2\rangle|\bar{\mathbf{0}}\rangle = \sqrt{2}|1\rangle\sum_{i=0}^{N} g_i|\bar{\mathbf{1}}_i\rangle = \sqrt{2}N_0|1\rangle|\bar{\mathbf{1}}\rangle.$$

The generated state $|1\rangle|\bar{\mathbf{1}}\rangle$ produces now

$$\tilde{J}^{+}a|1\rangle|\bar{\mathbf{1}}\rangle = \frac{1}{N_0}|0\rangle\sum_{i=1}^{N} g_i\sigma_i^{+}\sum_{j=1}^{N} g_j|\bar{\mathbf{1}}_j\rangle = \frac{N_1}{N_0}|0\rangle|\bar{\mathbf{2}}\rangle,$$

where $|\bar{\mathbf{2}}\rangle = \frac{2}{N_1}\sum_{i<j} g_i g_j|\bar{\mathbf{2}}_{ij}\rangle$ and $N_1 = \sqrt{4\sum_{i<j} g_i^2 g_j^2}$.

At the same time $\tilde{J}^{-}a^{\dagger}|1\rangle|\bar{\mathbf{1}}\rangle = \sqrt{2}N_0|2\rangle|\bar{\mathbf{0}}\rangle$ and the state $|0\rangle|\bar{\mathbf{2}}\rangle$ evolves according to

$$\tilde{J}^{-}a^{\dagger}|0\rangle|\bar{\mathbf{2}}\rangle = |1\rangle\frac{2}{N_1}\sum_{k}\sum_{i<j} g_k g_i g_j\sigma_k^{-}|\bar{\mathbf{2}}_{ij}\rangle = |1\rangle|\phi_1\rangle, \tag{4.3}$$

with

$$|\phi_1\rangle = \sum_i\Big(\sum_{j\neq i} c_{ij}g_j\Big)|\bar{\mathbf{1}}_i\rangle$$

and $c_{ij} = 2g_i g_j/N_1$. The result is a one-excitation state in the atomic system which is different from $|\bar{\mathbf{1}}\rangle$ defined in Eq. (4.2). The resulting state can be expressed conveniently as a linear combination of $|\bar{\mathbf{1}}\rangle$ and an orthogonal state $|\bar{\mathbf{1}}_p\rangle$,

$$|\bar{\mathbf{1}}_p\rangle = \frac{1}{\sqrt{\langle\phi_1|\phi_1\rangle - |\langle\bar{\mathbf{1}}|\phi_1\rangle|^2}}\big(|\phi_1\rangle - \langle\bar{\mathbf{1}}|\phi_1\rangle|\bar{\mathbf{1}}\rangle\big), \tag{4.4}$$

yielding

$$|1\rangle|\phi_1\rangle = \langle\bar{\mathbf{1}}|\phi_1\rangle|1\rangle|\bar{\mathbf{1}}\rangle + \sqrt{\langle\phi_1|\phi_1\rangle - |\langle\bar{\mathbf{1}}|\phi_1\rangle|^2}|1\rangle|\bar{\mathbf{1}}_p\rangle.$$

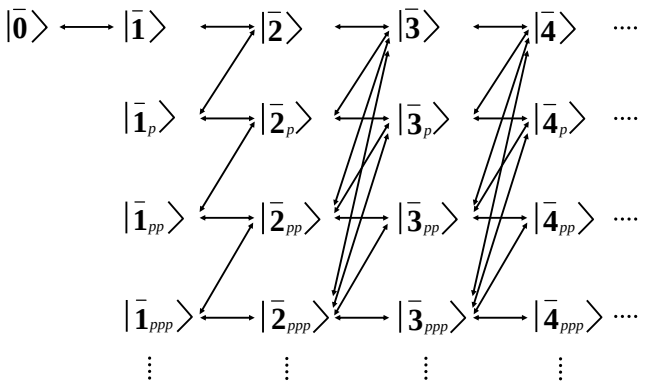

Figure 4.1: Schematic representation of the growth of the Hilbert space associated with the collective atomic states.

The state $|1\rangle|\bar{\mathbf{1}}_p\rangle$ is a new orthogonal state of the considered two-excitation Hilbert subspace. Via $\tilde{J}^- a^\dagger$, $|1\rangle|\bar{\mathbf{1}}_p\rangle$ goes back to $|2\rangle|\bar{\mathbf{0}}\rangle$, the latter being coupled only to the state $|1\rangle|\bar{\mathbf{1}}\rangle$. We observe also that, while $\tilde{J}^- a^\dagger|1\rangle|\bar{\mathbf{1}}_p\rangle = 0$, the associated Hilbert subspace grows according to

$$\tilde{J}^+ a|1\rangle|\bar{\mathbf{1}}_p\rangle = \alpha_2|0\rangle|\bar{\mathbf{2}}\rangle + \alpha_{2p}|0\rangle|\bar{\mathbf{2}}_p\rangle, \tag{4.5}$$

where we introduced $|\bar{\mathbf{2}}_p\rangle$ perpendicular to $|\bar{\mathbf{2}}\rangle$. The state $|\bar{\mathbf{2}}_p\rangle$ thus obtained is coupled via $\tilde{J}^-$ to states $|\bar{\mathbf{1}}_p\rangle$ and $|\bar{\mathbf{1}}_{pp}\rangle$, where $|\bar{\mathbf{1}}_{pp}\rangle$ is orthogonal to $|\bar{\mathbf{1}}_p\rangle$ and $|\bar{\mathbf{1}}\rangle$. In fact, applying $(\tilde{J}^+ a)^n$ on $|n\rangle|\bar{\mathbf{0}}\rangle$ yields the state

$$|0\rangle|\bar{\mathbf{n}}\rangle = (n!)^{3/2}\,|0\rangle \sum_{i_1<\ldots<i_n} g_{i_1} g_{i_2} \ldots g_{i_n} |\bar{\mathbf{n}}_{i_1 i_2 \ldots i_n}\rangle, \tag{4.6}$$

and the collective atomic states are coupled hierarchically as depicted schematically in Fig. 4.1.

Eventually and generally, all states of the accessible Hilbert space can be visited by an arbitrary system evolution but, within a given time window, only a restricted portion of the Hilbert space will be accessed with significant probability. In the example of Fig. 4.2 ($N = 6$), we observe that our approximation for the evolution of the collective atomic ground state is in good agreement with the exact result even for long times, reproducing accurately even population collapses and revivals. Surprisingly, to achieve this level of accuracy, it is enough to consider the first two rows displayed in Fig. 4.1. The number of columns that has to be considered is determined by the number of initial excitations in the system because the Hamiltonian

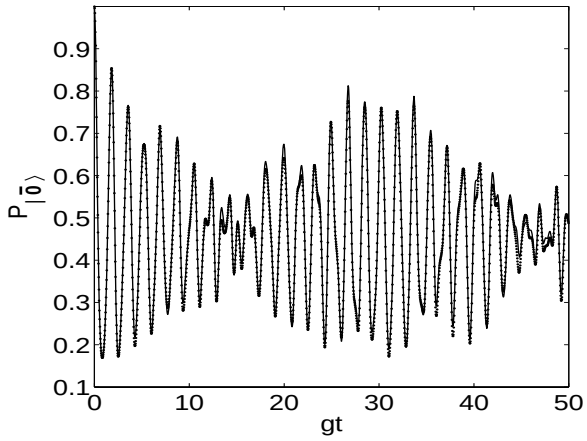

Figure 4.2: Evolution of the collective atomic ground state population, $P_{|\bar{\mathbf{0}}\rangle}$, in the case of inhomogeneous coupling $g_j = g \sin\left[j\pi/\left(N+1\right)\right]$, $j = 1, .., N$, with $N = 6$, an initial atomic state $|\bar{\mathbf{0}}\rangle$, and an initial coherent state in the field with $\bar{n} = 1.8$. Exact evolution (solid line) and approximated evolution (dotted line).

of Eq. (4.1) preserves this number. In consequence, the low mean photon number, $\bar{n} = 1.8$, suggests that the initially unpopulated atomic state may reach at most a similar mean value. Given that the number of atoms is larger, $N = 6$, it is expected that the normalized couplings between the few visited atomic states in the first row of Fig. 4.1 and the rows below are quite small.

In order to confirm the above intuition, we show in Fig. 4.3 how the population of the second and third rows of Fig. 4.1 decreases as the number of atoms N increases for the same parameters of Fig. 4.2. Clearly, also increasing inhomogeneity of the coupling causes increased leakage into higher order rows, see Eq. (4.4). The example of Fig. 4.2 shows a reduction of the Hilbert space dimension from $2^6 \times 7 = 448$, where 7 is the dimension of the truncated field space, to an effective size of 49. In general, to improve the accuracy, we only need to take into account more rows in the calculation.

We have proposed a method to follow the dynamics of a system with inhomogeneous coupling in a relatively simple manner. It is now interesting to see how strong the effects of inhomogeneity can be on the dynamics of relevant observables. For example, in Fig. 4.4, we compare the different predictions for the fluctuations of the field quadratures. For the homogeneous case, the relevant time scale corresponds to $\sqrt{N}g$, while for the inhomogeneous case the analogous would be $(\sum_j g_j^2)^{1/2}$. In this manner, to compare both cases, i.e. homogeneous and the inhomogeneous, we consider the homogeneous coupling case with coupling $g_j = 1/(\sqrt{N})(\sum_j g_j^2)^{1/2}$. In Fig. 4.4

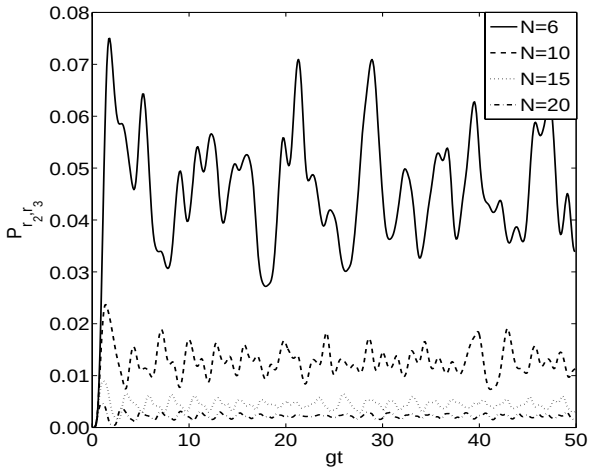

Figure 4.3: Evolution of the total population of the second and third rows (as depicted in Fig. 4.1), P_{r_2,r_3}, for different numbers N of atoms.

we observe that not only does the inhomogeneous situation differ from the homogeneous in the typical timescale of the dynamics, but also it shows additional effects, which, in the case we consider, are reflected in an increase of the quadrature fluctuations. Our method allows the study of these effects for particle numbers that are intractable for standard simulation methods.

4.2 Quantum Dots

We have already seen that inhomogeneous couplings appear naturally in the hyperfine interaction of single electron confined in a quantum dot with the surrounding nuclear spins. Neglecting dipolar interactions between nuclear spins, in the presence of a magnetic field B_0 along the z-axis we write the Hamiltonian introduced in Section 1.2 as

$$H_{\mathrm{QD}} = g^* \mu_B B_0 S^z + g_I \mu_I B_0 \sum_{i=1}^{N} I_i^z + H_{\mathrm{HF}}, \tag{4.7}$$

with the notation used before. Below, the nuclear Zeeman energies will be neglected, as their magnetic moment is much smaller than the one of the electron [59] and irrelevant for the short $(\sqrt{N}/A)$ timescales of our interest.

Here, we define for convenience the collective nuclear spin operators with a different normalization than before

$$\tilde{A}^{\pm,z} = \sum_i \alpha_i I_i^{\pm,z},$$

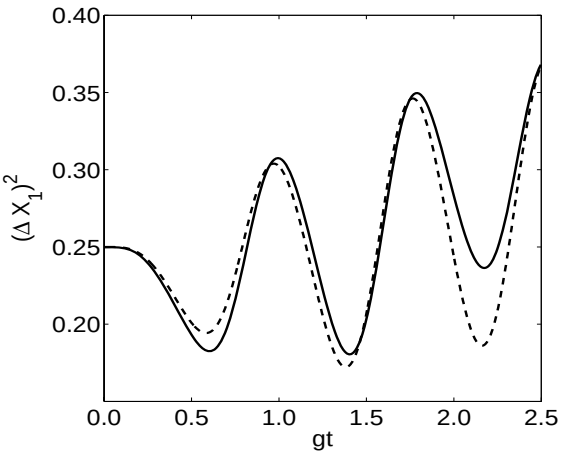

Figure 4.4: Evolution of the quadrature fluctuations $(\Delta X_1)^2 = \langle X_1^2 \rangle - \langle X_1 \rangle^2$ for $N = 8$, initial atomic ground state, and a coherent field with $\bar{n} = 1$. Solid line: inhomogeneous coupling $g_j = g \sin[j\pi/(N+1)]$, where j labels the position of the jth atom. Dashed line: homogeneous case with $g_j = \bar{g} = 1/(\sqrt{N})(\sum_i g_i^2)^{1/2}$. We remark that actually some squeezing is produced in the situation considered (the standard quantum limit is 1/4 in the present case), cf. Refs. [145, 146].

where $\alpha_i = A|\psi_e(\mathbf{r}_i)|^2$ (here and in the following we use α for local couplings of order $1/N$; the g_i used in previous chapters are of order $1/\sqrt{N}$). By applying an appropriate field B_0 one can allow the spin-exchange flip-flop terms of the HF Hamiltonian to dominate the dynamics. The Hamiltonian of Eq. (4.7) approximately reduces to $H_{\rm ff} = (1/2)(\tilde{A}^- S^+ + \tilde{A}^+ S^-)$. However, in general, the term $H_z = \tilde{A}^z S^z$ cannot be neglected. Even on resonance, where $B_0 = -(1/g^*\mu_B)\langle \tilde{A}^z \rangle$, one may have $\langle (\tilde{A}^z)^2 \rangle - \langle \tilde{A}^z \rangle^2 \neq 0$- indicating that the Overhauser field felt by the electron spin cannot be fully compensated. To include this effect we rewrite the zz-part of the interaction as $\tilde{A}^z = \bar{\alpha} J^z + \delta\tilde{A}^z = \bar{\alpha} \sum_{i=1}^N I_i^z + \sum_i (\alpha_i - \bar{\alpha}) I_i^z$, so that the on-resonance Hamiltonian becomes

$$\widetilde{H}_{\rm QD} = \frac{1}{2}\left(\tilde{A}^- S^+ + \tilde{A}^+ S^-\right) + \bar{\alpha} S^z (J^z - \langle J^z \rangle_0) + V_{zz}. \tag{4.8}$$

Here $\langle J^z \rangle_0$ is the expectation value with respect to the fully polarized state, $\bar{\alpha} = \sum_i \alpha_i / N$ is the average coupling constant (which equals A/N due to the normalization of the electron wave function), and $V_{zz} = S^z \delta\tilde{A}^z$. The latter term, i.e. the inhomogeneous contribution to the z-term of the interaction, can be treated perturbatively. As we show later, the homogeneous zz-term $S^z J^z$ is negligible with respect to the flip-flop term due to a small factor

$1/\sqrt{N}$. The term V_{zz} is even smaller and negligible, because it depends additionally on an inhomogeneity parameter, like the variance of the (smooth) electron wave function.

In this chapter we consider $I = 1/2$ nuclear spins in a spherical quantum dot, and

$$|\psi(\mathbf{r})|^2 \propto e^{-\frac{r^2}{r_0^2}}, \tag{4.9}$$

as the electron envelope function [59] of size r_0.

Electron and Nuclear Spin Dynamics

The inhomogeneous coupling of the electron spin to the nuclear spins does not allow for a general analytical solution of the dynamics. The assumption of a fully polarized initial nuclear spin state reduces the dimension of the relevant Hilbert space from 2^{N+1} to $N + 1$ and therefore the problem is readily analyzed [65]. On the other hand, a more general initial state of nuclear spins vastly increases the dimension of the Hilbert space that the system will visit along the evolution. Motivated by the proposals for quantum information storage via the hyperfine interaction [41], we will study situations of imperfect, but high, polarization. We analyze the case where the dynamics involves one excitation in the nuclear spin system, which we will refer to as "defect". We show, with methods similar to the ones developed in Sec. 4.1, that the relevant Hilbert space remains still small.

The most general pure state describing this "coherent" situation is

$$|\mathbf{1}\rangle = \sum_{j=1}^{N} a_j \, |\mathbf{1}_j\rangle \,, \tag{4.10}$$

with $\sum_{j=1}^{N} |a_j|^2 = 1$, and $|\mathbf{1}_j\rangle$ represents the state $|\downarrow\downarrow \ldots \uparrow_j \ldots \downarrow\downarrow\rangle$ with an inverted nuclear spin at position $\mathbf{r}_j$. In particular we consider the case of an uniformly distributed defect $a_j = 1/\sqrt{N}$ and a localized defect at position j_0,

$$a_j = C \, (\Gamma/2)^2 \, / \left[(j - j_0)^2 + (\Gamma/2)^2 \right], \tag{4.11}$$

where C is a normalization constant and Γ characterizes the width of the distribution.

Let us consider two possible initial states for the electron and the nuclear spins with a single imperfection,

$$|\downarrow \mathbf{1}\rangle \,, \tag{4.12}$$

$$|\uparrow \mathbf{1}\rangle \,. \tag{4.13}$$

In order to solve the dynamical evolution of the composite system, we employ the recipe of following the relevant Hilbert space, as described in Sec. 4.1. We observe that, under the action of the Hamiltonian of Eq. (4.8), the initial state $|\downarrow \mathbf{1}\rangle$ is coupled to the state $|\uparrow \mathbf{0}\rangle$ via $S^+\tilde{A}^- |\downarrow \mathbf{1}\rangle = \gamma |\uparrow \mathbf{0}\rangle$, with $|\mathbf{0}\rangle = |\downarrow\downarrow \ldots \downarrow\downarrow\rangle$ and

$$\gamma = \sum_i a_i \alpha_i. \tag{4.14}$$

The state $|\uparrow \mathbf{0}\rangle$ will be coupled through the term $S^-\tilde{A}^+$ to a state with one excitation, but different from $|\downarrow \mathbf{1}\rangle$. Similar to the formalism developed in Sec. 4.1, we can write $S^-\tilde{A}^+ |\uparrow \mathbf{0}\rangle = \gamma |\downarrow \mathbf{1}\rangle + \beta |\downarrow \mathbf{1}_\perp\rangle$, where

$$|\mathbf{1}_\perp\rangle = \frac{1}{\beta}\left(\sum_i \alpha_i |\mathbf{1}_i\rangle - \gamma |\mathbf{1}\rangle\right) \tag{4.15}$$

is orthogonal to state $|\mathbf{1}\rangle$, with $\beta = \sqrt{N_0^2 - \gamma^2}$ and $N_0 = \sqrt{\sum_i \alpha_i^2}$. Finally, we observe that $S^+\tilde{A}^- |\downarrow \mathbf{1}_\perp\rangle = \beta |\uparrow \mathbf{0}\rangle$. In summary, the exchange terms yield

$$\begin{aligned} S^+\tilde{A}^- |\downarrow \mathbf{1}\rangle &= \gamma |\uparrow \mathbf{0}\rangle, \\ S^-\tilde{A}^+ |\uparrow \mathbf{0}\rangle &= \gamma |\downarrow \mathbf{1}\rangle + \beta |\downarrow \mathbf{1}_\perp\rangle, \\ S^+\tilde{A}^- |\downarrow \mathbf{1}_\perp\rangle &= \beta |\uparrow \mathbf{0}\rangle. \end{aligned} \tag{4.16}$$

Furthermore, the zz-interaction yields matrix elements

$$\begin{aligned} \langle\downarrow \mathbf{1}| \bar{\alpha} S^z (J^z - \langle J^z\rangle_0) |\downarrow \mathbf{1}\rangle &= -\frac{\bar{\alpha}}{2}, \\ \langle\uparrow \mathbf{0}| \bar{\alpha} S^z (J^z - \langle J^z\rangle_0) |\uparrow \mathbf{0}\rangle &= 0, \\ \langle\downarrow \mathbf{1}_\perp| \bar{\alpha} S^z (J^z - \langle J^z\rangle_0) |\downarrow \mathbf{1}_\perp\rangle &= -\frac{\bar{\alpha}}{2}. \end{aligned} \tag{4.17}$$

Therefore, for the initial condition of Eq. (4.12) the system evolves only in the subspace spanned by $\{|\downarrow \mathbf{1}\rangle, |\uparrow \mathbf{0}\rangle, |\downarrow \mathbf{1}_\perp\rangle\}$. The temporal evolution in this subspace can be exactly solved, obtaining $|\Psi_{\downarrow,1}(t)\rangle_{e-n} = a_1(t) |\downarrow \mathbf{1}\rangle + b_1(t) |\uparrow \mathbf{0}\rangle + c_1(t) |\downarrow \mathbf{1}_\perp\rangle$, where the probability amplitudes are given by

$$\begin{aligned} a_1(t) &= 1 + \frac{\gamma^2 \exp(i\bar{\alpha}t/4)}{\Omega^2\delta}[\delta \cos(\delta t/2) + i\frac{\bar{\alpha}}{2}\sin(\delta t/2) - \delta \exp(-i\bar{\alpha}t/4)], \\ b_1(t) &= -i\frac{\gamma}{\delta}\exp(i\bar{\alpha}t/4)\sin(\delta t/2), \\ c_1(t) &= \frac{\gamma\beta \exp(i\bar{\alpha}t/4)}{\Omega^2\delta}[\delta \cos(\delta t/2) + i\frac{\bar{\alpha}}{2}\sin(\delta t/2) - \delta \exp(-i\bar{\alpha}t/4)] \end{aligned} \tag{4.18}$$

Here, $\Omega = \sqrt{\gamma^2 + \beta^2} = N_0$ and $\delta = \sqrt{(\bar{\alpha}/2)^2 + \Omega^2}$ plays the role of a generalized Rabi frequency for a process with detuning $\bar{\alpha}$. The zz-interaction thus leads to a small detuning for the exchange of excitation between electron and nuclear spins: We have that $\Omega = \sqrt{\gamma^2 + \beta^2} = N_0 = \sqrt{\sum_i \alpha_i^2}$. The α_i are $\mathcal{O}(1/N)$, such that $\sum_i \alpha_i^2 = \mathcal{O}(1/N)$. When $N \gg 1$, then $A/N = \bar{\alpha} \ll \Omega = \mathcal{O}(A/\sqrt{N})$. Obviously, the state $|\mathbf{0}\rangle\,|\downarrow\rangle_e$ is decoupled from the dynamics.

If the system is initially in the state $|\uparrow\rangle_e\,|\mathbf{1}\rangle$, the coupling through the Hamiltonian of Eq. (4.8) does not lead to a closed Hilbert space. Then, some approximations are necessary in order to obtain solutions for the evolution of the overall system dynamics. Starting from $|\uparrow \mathbf{1}\rangle$, we have

$$S^- \tilde{A}^+ |\uparrow \mathbf{1}\rangle = |\downarrow\rangle \sum_{i<j} b_{ij}\,|\mathbf{2}_{ij}\rangle\,, \tag{4.19}$$

where $b_{ij} = a_i\alpha_j + a_j\alpha_i$ and $|\mathbf{2}_{ij}\rangle = |\downarrow\downarrow \ldots \uparrow_i \ldots \uparrow_j \ldots \downarrow\downarrow\rangle$. Defining

$$|\mathbf{2}\rangle = \sum_{i<j} c_{ij}\,|\mathbf{2}_{ij}\rangle\,,$$

with $c_{ij} = b_{ij}/N_2$ and $N_2 = \sqrt{\sum_{i<j} b_{ij}^2}$, we observe that the state $|\downarrow \mathbf{2}\rangle$ is coupled only through

$$S^+ \tilde{A}^- |\downarrow \mathbf{2}\rangle = \sum_i (\sum_{j\neq i} c_{ij}\alpha_j)\,|\uparrow \mathbf{1}_i\rangle \equiv |\uparrow \phi_1\rangle\,.$$

Here, $|\phi_1\rangle$ can be seen as having one component along the state $|\mathbf{1}\rangle$ and one other component along orthogonal state $|\mathbf{1}_p\rangle$, such that

$$|\phi_1\rangle = \langle \mathbf{1}\,|\phi_1\rangle\,|\mathbf{1}\rangle + \sqrt{\langle\phi_1|\phi_1\rangle - |\langle \mathbf{1}|\phi_1\rangle|^2}|\mathbf{1}_p\rangle, \tag{4.20}$$

where $|\mathbf{1}_p\rangle = \left(1/N_{\mathbf{1}_p}\right)(|\phi_1\rangle - \langle \mathbf{1}|\phi_1\rangle|\mathbf{1}\rangle)$, with $N_{\mathbf{1}_P} = \sqrt{\langle\phi_1|\phi_1\rangle - |\langle \mathbf{1}|\phi_1\rangle|^2}$. Following this procedure, we have

$$S^- \tilde{A}^+ |\uparrow \mathbf{1}_p\rangle = |\downarrow \mathbf{2}\rangle + N_{\mathbf{2}_p}\,|\downarrow \mathbf{2}_p\rangle \equiv |\uparrow \phi_2\rangle\,, \tag{4.21}$$

where $|\mathbf{2}_p\rangle = (1/N_{\mathbf{2}_P})\,(|\phi_2\rangle - \langle \mathbf{2}\,|\phi_2\rangle\,|\mathbf{2}\rangle)$, with $|\phi_2\rangle = \tilde{A}^+\,|\mathbf{1}_p\rangle$ and $N_{\mathbf{2}_P} = \sqrt{\langle\phi_2\,|\phi_2\rangle - \langle \mathbf{2}\,|\phi_2\rangle^2}$. In order to implement a semi-analytical description for the overall system dynamics we have to truncate the Hilbert space. This can be accomplished by approximating the action of $S^+\tilde{A}^-$ over $|\mathbf{2}_p\rangle$ such that

$$\begin{aligned} S^+ \tilde{A}^- |\downarrow \mathbf{2}_p\rangle &= N_{\mathbf{2}_P}\,|\uparrow \mathbf{1}_p\rangle + N_{\mathbf{1}pp}\,|\uparrow \mathbf{1}_{pp}\rangle \\ &\simeq N_{\mathbf{2}_P}\,|\uparrow \mathbf{1}_p\rangle\,, \end{aligned} \tag{4.22}$$

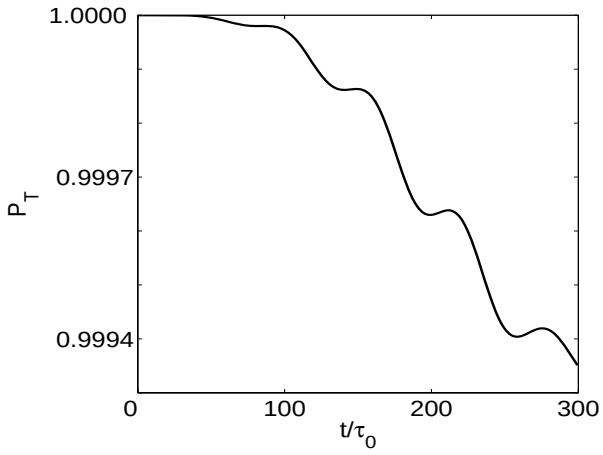

Figure 4.5: Total population P_{T} of the states $\{|\uparrow \mathbf{1}\rangle, |\downarrow \mathbf{2}\rangle, |\uparrow \mathbf{1}_p\rangle, |\downarrow \mathbf{2}_p\rangle\}$, with $N = 10^3$ and defect distribution $a_j = 1/\sqrt{N}$ ($\tau_0 = A^{-1}$)..

where the state $|\uparrow \mathbf{1}_{pp}\rangle$ is similarly defined in terms of $|\uparrow \mathbf{1}_p\rangle$. This approximation can be justified from Fig. 4.5 where we have plotted the total occupation probability of states within the subspace of first orthogonal states $|\uparrow \mathbf{1}\rangle, |\downarrow \mathbf{2}\rangle, |\uparrow \mathbf{1}_p\rangle, |\downarrow \mathbf{2}_p\rangle$. As all of them are eigenstates of the J^z term, its effect is again a small detuning. These results have been obtained by numerical calculation considering a 12-dimensional truncated Hilbert space up to $|\downarrow \mathbf{2}_{ppppp}\rangle$. However, if we use a Hilbert space truncated up to $|\downarrow \mathbf{2}_{pp}\rangle$, the total occupation probability of the mentioned subspace is practically the same as shown in Fig. 4.5.

We have seen before that the typical timescale for the exchange of an excitation between the electron and nuclei is given by the inverse of the generalized Rabi frequency

$$\tau = \pi/\Omega = \pi/N_0 = \mathcal{O}\left(\frac{\pi\sqrt{N}}{A}\right). \tag{4.23}$$

From Fig. 4.5 we deduce that the dynamics of the composite system is well described for times beyond τ, which is important for our subsequent analysis of the quantum memory. In particular, for the case $N = 10^3$, this time is approximately $\tau \approx 68\tau_0$, with $\tau_0 = 1/A$, and we are allowed to restrict the dynamics to the subspace spanned by $\{|\uparrow \mathbf{1}\rangle, |\downarrow \mathbf{2}\rangle, |\uparrow \mathbf{1}_p\rangle, |\downarrow \mathbf{2}_p\rangle\}$. This is an important feature of our method, since numerical calculations are significantly simplified.

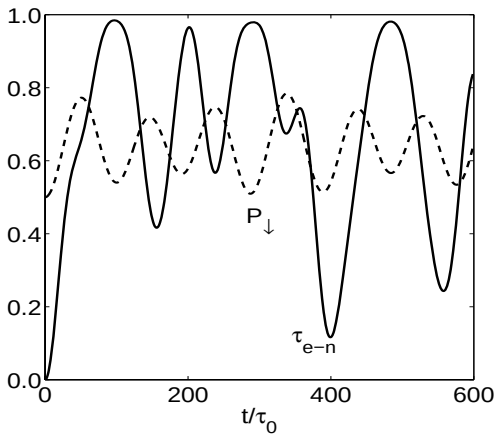

Figure 4.6: Evolution of the tangle τ_{e-n} (solid line) and population $P_\downarrow$ of $|\downarrow\rangle_e$ (dashed line) for a uniformly distributed defect. The initial state is $|\Psi\rangle = 1/\sqrt{2}\,(|\uparrow\rangle + |\downarrow\rangle)_e \otimes |\mathbf{1}\rangle$, $N = 10^3$, and $\tau \sim 68\tau_0$.

Quantum Information Storage

In Refs. [41, 42] a long-lived quantum memory based on the capability that an electronic spin state can be reversibly mapped into a fully polarized nuclei state was proposed. This dynamics can be expressed as

$$(u\,|\uparrow\rangle + v\,|\downarrow\rangle) \otimes |\mathbf{0}\rangle \rightarrow |\downarrow\rangle\,(v\,|\mathbf{1}\rangle + iu\,|\mathbf{0}\rangle) \tag{4.24}$$

where $|\mathbf{1}\rangle = (1/N_0)\sum_i \alpha_i\,|\mathbf{1}_i\rangle$. This coherent mapping is effected by pulsing the applied field from $g^*\mu_B B_{\text{eff}} \gg H_{\text{ff}}$ to $B_{\text{eff}} \approx 0$ for a time $\tau = \pi/N_0$. Here, we study this dynamics in the context of an initial distributed single defect in the nuclear spin state. For the transfer process to be successful it is necessary that the electronic state factorizes from the nuclear spin state, thus requiring that at some point of the evolution

$$(u\,|\uparrow\rangle + v\,|\downarrow\rangle) \otimes |\mathbf{1}\rangle \rightarrow \left\{ \begin{array}{c} |\downarrow\rangle_e \otimes \left|\psi^{\downarrow}_{u,v}\right\rangle \\ |\uparrow\rangle_e \otimes \left|\psi^{\uparrow}_{u,v}\right\rangle \end{array} \right. . \tag{4.25}$$

In order to verify if this is possible we analyze the populations of the electron spin and study the entanglement between the electron and the nuclear spins. Since the overall system is in a pure state we can use as an entanglement measure the tangle [147], $\tau_{AB}{=}2\nu_A\nu_B\,[1 - \text{tr}\,(\rho_A^2)]$, where ρ_A is the reduced density operator after tracing over subsystem B, and ν_A and ν_B are arbitrary scale factors set to $\nu_A = \nu_B = 1$.

We first consider the case of a uniformly distributed initial nuclear spin excitation. In Fig. 4.6 we show the electron spin population $p_\downarrow$ and the

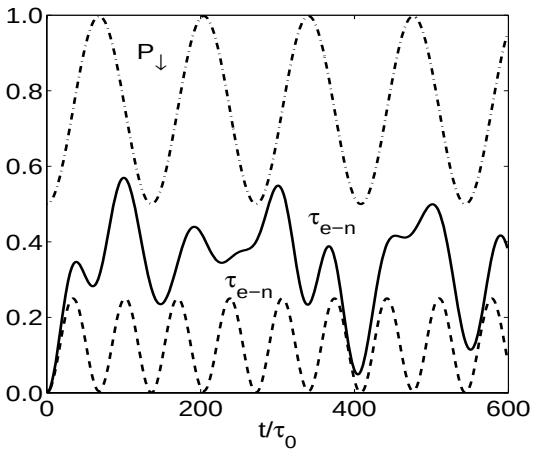

Figure 4.7: Evolution of the tangle τ_{e-n} for a defect distribution peaked at the edge of the quantum dot. Shown are the electron spin population $P_\downarrow$ (dot-dashed line) and the tangle (dashed line) for a defect distribution width $\Gamma = N/50$, and the tangle for the width $\Gamma = N$ (solid line) for $N = 10^3$ and the initial state $|\Psi\rangle = 1/\sqrt{2}\,(|\uparrow\rangle + |\downarrow\rangle)_e \otimes |\mathbf{1}\rangle$.

tangle between the electron and $N = 10^3$ nuclear spins. We observe that, for the case of a uniformly distributed defect, there is no time for which the composite state evolves to a factorized state as in Eq. (4.25). The electron spin population is never maximal or minimal (in both cases the tangle would vanish), meaning that there is no high-fidelity information transfer to the nuclei.

We study now the transfer process for the case of a localized defect as introduced in Eq. (4.11). When the defect is peaked in the center of the dot, information storage is seriously hindered. However, if the defect is located at a border of the QD, the coupling of the defect-spin to the electron is weak, and separability is reached even for rather broad defect distributions, as seen in Fig. 4.7. The necessary conditions for a successful transfer are fulfilled after a time $t \approx 68\tau_0$, which is very close to the transfer time for an initial fully polarized nuclear spin state given by Eq. (4.23).

The performance of the quantum information storage protocol is analyzed now in a more quantitative manner by simulating a complete cycle of write-in, storage and retrieval[1]. In the first step the electron spin in state $|\psi_i\rangle$ interacts with the nuclei and after a time τ the evolution is interrupted and the electron traced out. Then a fresh electron in state $|\downarrow\rangle$ interacts with the nuclei and

[1]Here we are not concerned with the degradation of the memory due to dynamics of the nuclear bath, see e.g. Ref. [148].

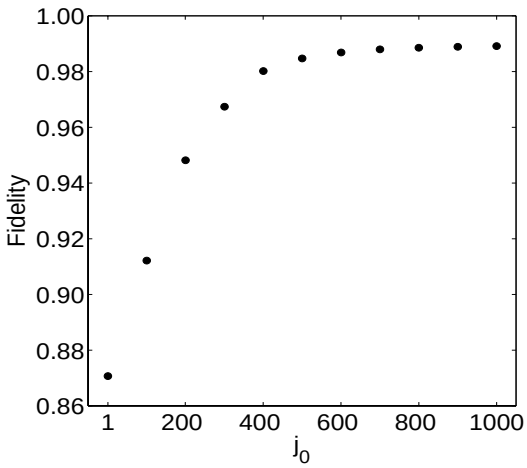

Figure 4.8: Fidelity of the quantum memory for $N = 10^3$ nuclear spins and different defect peak centers j_0, $1 \leq j_0 \leq N$ (left to right: center to edge of dot).

after another time τ the nuclei are traced out. The fidelity $F = \langle\psi_i|\rho_f|\psi_i\rangle$ between this final electron spin state ρ_f and the initial state is plotted in Fig. 4.8 for various defect distributions, where F has been calculated by averaging on the electron spin Bloch sphere.

A figure of merit for the obtained fidelities is the parameter γ from Eq. (4.14): It quantifies how well a given defect couples to the mode relevant for the quantum information storage. γ being the scalar product of the two vectors $\mathbf{a}$ and α, we confirm the intuitive picture that orthogonal modes do not interfere with each other.

Incoherent Nuclear Spin Excitation

Finally we consider the effect of incoherent excitations present in the nuclear ensemble prior to QIP applications. In Fig. 4.9 (left plot) the electron spin population evolution is displayed, with a mixed nuclear spin state of one excitation (see caption) as the starting condition. The figure shows that the electron spin performs very regular Rabi oscillations that deviate only slightly from the ideal situation with no defect present. In particular the performance is better than in the corresponding cases of coherently distributed defects. This is to be expected as the quantum information storage is sensitive to the coherences of the nuclear spins state, which are absent in this mixed state case.

Another possible physical scenario is that of an initial nuclear system at

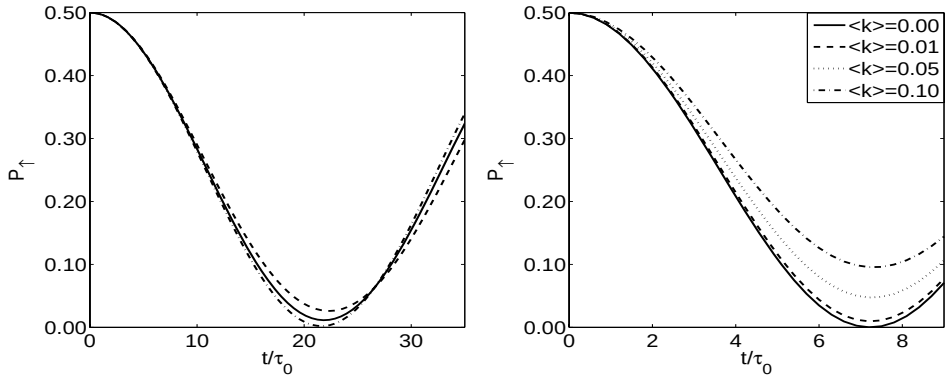

Figure 4.9: Left plot: Evolution of the population $P_\uparrow$ of the electronic spin state $|\uparrow\rangle_e$ for $N = 40$. The initial state for the electron spin is $|\Psi\rangle_e = 1/\sqrt{2}\,(|\uparrow\rangle + |\downarrow\rangle)_e$ and $\rho_N = \sum_{j=1}^{N} a_j \sigma_j^+ |\mathbf{0}\rangle\langle\mathbf{0}| \sigma_j^-$ for the nuclear spins. Solid line: $a_j = 1/N$; Dashed line: $a_j = [C\,(\Gamma/2)^2/((j-j_0)^2 + (\Gamma/2)^2)]^2$, with $\Gamma = N \quad j_0 = 1$, and C a normalization constant. Dot-dashed line: same as for dashed line but $j_0 = N$. Right plot: Evolution of population $P_\downarrow$ of electronic spin state $|\uparrow\rangle_e$ for an initial thermal distribution for each nuclear spin $N = 10$ and different $\langle k\rangle$. The initial electron spin state is $|\Psi\rangle = 1/\sqrt{2}\,(|\uparrow\rangle + |\downarrow\rangle)_e$. For this case, $\langle k\rangle = \exp(-\beta\hbar\omega)\,/\,(1+\exp(-\beta\hbar\omega))$.

finite temperature. Our method is not directly applicable to that situation because already the initial state covers a large part of the Hilbert space. Nevertheless, for the sake of completeness, we include a brief analysis of this case in the context of a quantum memory in the presence of defects. Consider a thermal state for each nuclear spin

$$\rho_{\mathrm{th}}^i = \frac{e^{-\hbar\omega\sigma_i^z\beta}}{\mathrm{tr}(e^{-\hbar\omega\sigma_i^z\beta})},$$

with $\beta = 1/k_B T$, where T is the associated temperature. The average population of each spin is $\langle k\rangle = \langle\sigma_i^z\rangle + 1/2$. As for the initial mixed state case on the left of Fig. 4.9, it is not possible to define collective states in the same way as for pure initial states. The results of our direct simulations taking into account the whole Hilbert space are shown in Fig. 4.9 (right plot), where we show the population of the electronic spin state $|\uparrow\rangle$. For nuclear polarizations above 95% the contrast of the Rabi oscillations of the electron spin deviate from the ideal situation by only a few percent. The scaling of the error with the particle number N is beyond the scope of the current treatment.

4.3 Conclusions

We have developed a technique, based on suitable inspection and truncation of the associated Hilbert space, that allows one to follow the quantum evolution of interacting systems with inhomogeneous coupling in an accurate and controlled manner. As a first general case, we illustrated the proposed method for the inhomogeneous Tavis-Cummings model and showed how the statistical properties may change appreciably depending on the spatial coupling distribution. As a second major example, we studied the dynamics of an electron spin interacting inhomogeneously with a system of polarized nuclear spins in a quantum dot, previously considered as a quantum memory candidate. We found that the reliability of the storage process depends strongly on the presence and position of a single distributed defect in the polarized nuclei state. The direct applicability of the model to general incoherent imperfection is not guaranteed (for example for a thermal state), but as will be shown in the next two chapters the idea of identifying the states relevant for the dynamics can be readily generalized to more complex situations.

Chapter 5

Quantum Computation with Nuclear Spin Ensembles

Nuclear spin degrees of freedom have attracted considerable attention as potential carriers of quantum information due to their exceptionally long coherence times. Early NMR work [16] has substantially enriched our understanding of the key features of quantum computation [18, 149]. The fundamental difficulties in scaling liquid state NMR to a large number of qubits motivated efforts to use single, individually addressable nuclear spins in semiconductors as qubits [19], where computation is primarily mediated by the hyperfine interaction between electron and nuclear spin. While possibly scalable, such a scheme is limited by the fact that the electron wave-function is spread over many lattice sites, reducing the strength of the hyperfine interaction. In addition, two-qubit operations in Ref. [19] rely upon exchange coupling, making them susceptible to fast orbital decoherence mechanisms.

A method for robust storage of quantum information in localized ensembles of nuclear spins was suggested by Taylor *et al.* [41, 42], who showed that the collective hyperfine coupling between nuclear and electron spin degrees of freedom provides a controllable mechanism for coherent storage and manipulation of quantum states. As a quantum memory, such nuclear ensembles are robust with respect to variations in dot characteristics, rely upon proven fabrication techniques, and provide high fidelity storage.

In this chapter, we describe a technique to efficiently process quantum information stored in localized nuclear spin ensembles. Specifically, these ensembles enable a robust, scalable implementation of quantum computation protocols, unencumbered by the difficulties faced by single spin impurity or bulk NMR approaches. The fundamental interaction that allows for spin manipulation in our scheme is hyperfine coupling: as a result, the orbital and spin degrees of freedom remain unentangled throughout the two-qubit

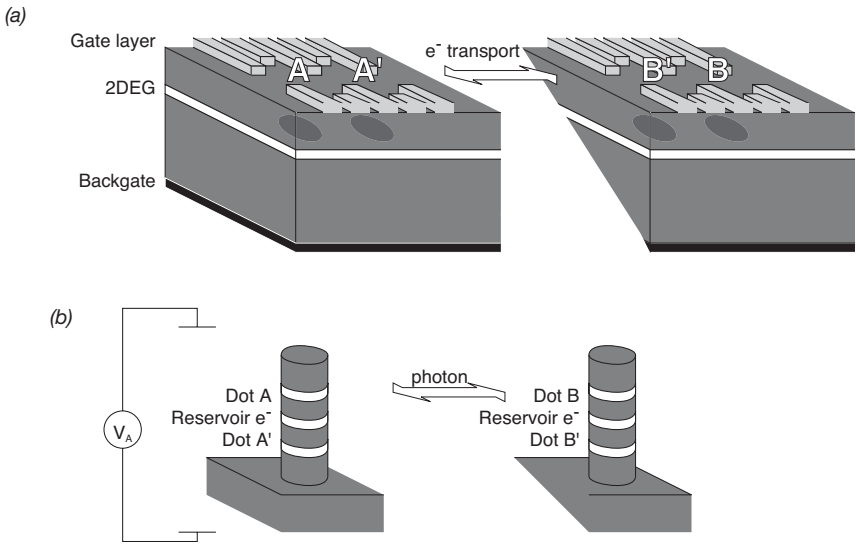

Figure 5.1: Quantum dot based approaches for nuclear ensemble-based computation. (a) Electrically defined (lateral) quantum dots connected by transport e.g. through a series of quantum dots. (b) Nanowhiskers [150] with several optically active dots. Tasks between A and A' are achieved through shuttling of an electron from the reservoir dot via a potential difference, V_A. Long distances tasks are performed through photon-based entanglement generation between A' and B' [151].

gate operations, mitigating the effects of orbital decoherence on gate fidelity. While collective enhancement of hyperfine interaction and fast operations on the electron allow for fast quantum gates, the ultra-long nuclear spin coherence times render the scheme particularly attractive for memory intensive quantum information processing tasks.

The scheme proposed here can be realized using either electrically [13] or optically [52] manipulated quantum dots, cf. Fig. 5.1.

5.1 Qubits and Gates

5.1.1 Electron Spin Manipulation

The qubits in the presented proposal are collective excitations of the lattice nuclei in QDs. The electron spin, however, needs to be well controlled, i.e. initialized, rotated and measured. The added benefit of using the nuclear qubit stems from the longer qubit lifetime in comparison to the electron [41].

Electron spin operations have been studied in detail in the literature, see e.g. [61], and references therein. Here, only a brief review of some major

concepts is presented.

A single electron spin in a quantum dot can be prepared in a known state by applying a large external magnetic field. For example, in electrically defined quantum dots, when the Zeeman energy splitting of the ground-state doublet is much larger than the thermal energy, turning on coupling to a nearby Fermi sea results in fast filling of the ground state of the dot, $|\uparrow\rangle$. On the other hand, appropriate tuning of the lead and QD potentials can lead to spin-selective ionization of the QD (only the excited state $|\downarrow\rangle$ tunnels out). Via spin-charge conversion the single electron spin can be measured, as has been done experimentally with a quantum point contact by Elzerman *et al.* [24]. The conceptually most straightforward implementation of single electron spin rotations are rotations in externally applied magnetic fields [13, 25]. As this turned out to be experimentally very challenging, there is a wealth of alternative proposals, including promising exchange based schemes [143, 152].

For self assembled optical QDs, a quantum computation architecture has been proposed by Imamoglu *et al.* [52]. The initialization of electron spins is achieved by combination of pumping with polarized light and static magnetic fields, and has been experimentally demonstrated with 99.8 % fidelity [153]. Similar techniques can be employed for optical single spin measurements; optical single qubit rotations can be affected by driving a Raman transition through a far-detuned trion state [52, 154].

5.1.2 Nuclear Qubit Gates

The Hamiltonian describing a single electron interacting with the nuclear spins in a quantum dot is, as introduced previously,

$$H = Bg^*\mu_B S_z + \mu_N B \sum_i g_{I,i} I_i^z + g\mathbf{S}\cdot\mathbf{A}. \tag{5.1}$$

Here $A^{\pm,z} = \sum_i g_i I_i^{\pm,z}$, with the g_i proportional to the probability density of the electron at the location of the corresponding nuclei normalized such that $\sum_i g_i^2 = 1$ and $g = \mathcal{O}(A/\sqrt{N})$. As discussed in Chapter 2, additional terms in the Hamiltonian, most notably the dipole-dipole interaction between nuclear spins, are typically smaller, and lead to non-negligible effects only on long timescales (of ms), that are beyond the range of our interest here.

The nuclear ensemble in each dot is prepared using polarized electron spins, see Ref. [74] and Chapter 2. We illustrate our technique by considering the fully polarized case (when the nuclear state is $|0\rangle = |-I,\ldots,-I\rangle$ for N spin-I nuclei), demonstrate how to perform single qubit and two-qubit gates, and then consider sources of error.

Excitations out of the fully polarized state due to the coupling to the nuclear spins produce collective nuclear spin states $|n\rangle = A_+^n|0\rangle/\sqrt{n!}$, where n is the number of excitations. The nuclear spins states with n spins flipped that can not be written in the above form, will be a source of leakage out of the computational states. However, as shown in Chapters 4 and 6 of this Thesis and Refs. [41, 75], this leakage is small (when n is). When an electron is confined in the dot, evolution over times much shorter than $1/(g/\sqrt{N})$ is restricted to subspaces spanned by $\{|n-1\rangle|\uparrow\rangle, |n\rangle|\downarrow\rangle\}$. Using Pauli matrices, the Hamiltonian for each subspace with a fixed excitation number n is $H^{(n)} = \delta_n\sigma_z^{(n)} + \Omega_n\sigma_x^{(n)}$, with

$$\Omega_n = g/2\sqrt{\langle n-1|A^-A^+|n-1\rangle}; \tag{5.2a}$$

$$\delta_n = g/4(\langle n|A^z|n\rangle + \langle n-1|A^z|n-1\rangle) + [\gamma_S - (\langle n|K^z|n\rangle - \langle n-1|K^z|n-1\rangle)]B/2, \tag{5.2b}$$

where $K^z = \sum_i g_{I,i}\mu_I I_i^z$ is a weighted sum over nuclear spin operators. When Overhauser shift and Zeeman energy sum to zero ($|\delta_n| \ll \Omega_n$), coherent flip-flop (Rabi) oscillations occur at rate Ω_n. The energy level structure of the coupled electron-nuclear system is shown in Fig. 5.2 along with the coupling strengths for $n \leq 1$: since $\Omega_{n+1} = \eta_n\Omega_n$ where $\eta_n = \sqrt{n+1}[1-\mathcal{O}(n/N)]$, one can note the analogy with the Jaynes-Cummings model [135] of quantum optics (see following chapter). We use the nonlinearity of such a JC-type two-level system coupled to a nearly-bosonic mode to effect elementary quantum gates.

Quantum information stored in the $n = 0, 1$ manifold can be mapped reliably from nuclear states to the electron spin and back [42] via a generalized rotation

$$R_{en}^{xy}(\pi/2, 0)(\alpha|0\rangle + \beta|1\rangle)|\downarrow\rangle = |0\rangle(\alpha|\downarrow\rangle + i\beta|\uparrow\rangle), \tag{5.3}$$

where $R_{en}^{xy}(\theta,\phi) = e^{i\phi S^z}e^{-i\theta H/(\Omega_1)}e^{-i\phi S^z}$. The transfer of quantum information from the nuclear ensemble to the electron spin allows for fast single qubit operations to be performed: after a $|\downarrow\rangle$ electron is injected into the dot, the quantum information is transferred to the electron spin, and then the operation is performed on the electron. Finally, the quantum information is mapped back to the nuclear ensemble. A z-axis rotation can be accomplished by waiting in a static magnetic field or through a laser-induced spin-dependent AC Stark shift [154]. x-axis rotations can be done via ESR [13, 155] (with $\Omega_{\rm ESR} \gtrsim 1\ {\rm ns}^{-1}$) or optical Raman spin flips through a virtual trion state (with $\Omega_{\rm opt,ESR} \gtrsim 10\ {\rm ns}^{-1}$) [52]. Measurement of the ensemble nuclear spin state can be implemented by mapping the quantum information to electron spin, and carrying out an electron spin measurement either by state selective ionization

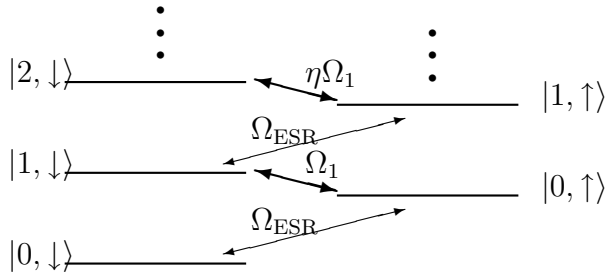

Figure 5.2: Level structure of the combined electron spin and nuclear dark state plus excited states. For $N \to \infty$, the coupling between the two excitation manifold is stronger by $\eta \to \sqrt{2}$.

followed by charge measurement with a quantum point contact [156] or by detecting fluorescence in a spin-dependent cycling transition [154, 157].

To perform a two-qubit gate between quantum dots A and A', a single electron can be used to transfer quantum information between the dots: the state of nuclear spin qubit A is mapped onto the electron, which is then moved to A', where a controlled-phase (CP) gate between the nuclear and the electronic qubit is applied using the nonlinearity of the interaction. Following Ref. [158], a two-qubit CP-gate (up to single qubit gates) is given by

$$R_{en}^{xy}(\pi/4, 0) R_{en}^{xy}(\pi/\eta, -\pi/2) R_{en}^{xy}(-\pi/4, 0). \tag{5.4}$$

In the computational basis, this corresponds to

$$\begin{pmatrix} 1 & 0 & 0 & 0 \\ 0 & e^{i\pi/\eta} & 0 & 0 \\ 0 & 0 & e^{-i\pi/\eta} & 0 \\ 0 & 0 & 0 & -1 \end{pmatrix}. \tag{5.5}$$

After this operation, the quantum information carried by the electron spin is mapped back onto the nuclear spin ensemble A. Applying a z-rotation of $-\pi/\eta$ to qubit A and one of π/η to qubit A' yields a CP gate. Note that the electron spin transport required here, e.g. through undoped nanowires or an array of quantum dots, is a relatively robust and fast means of implementing long-range two-qubit gates [159].

5.1.3 Long-range Entanglement

For distant dots, where electron spin transport between ensembles is difficult or impossible, it may be easier to generate entanglement off-line, apply local purification protocols and then use it to effect non-local gates, following

Ref. [160]. Entanglement between distant electron spins can be generated optically, using spin-flip optical Raman transitions [151], or electronically, such as through adiabatic splitting of a spin singlet in a double dot. The electron-nuclear state mapping procedure can then ensure that the distant nuclear spin ensembles are entangled. Starting with the entangled nuclear state $\frac{1}{\sqrt{2}}(|01\rangle + |10\rangle)$ (between dots A' and B', cf. Fig. 5.1), we can implement a CP gate on dots A and B (deterministically) by performing local unitaries and measurements of AA' and BB' as follows: (i) perform a $\mathrm{CNOT}_{A\to A'}$ then measure A'. (ii) Perform a CP gate $|10\rangle \to -|10\rangle$ at BB' followed by a Hadamard gate and measurement at B'. (iii) Local phase flips $|0\rangle \to -|0\rangle$ at A (B) if the measurement outcomes at B'(A') were "1" complete the CP gate between A and B.

5.2 Error Analysis

We next analyze various sources of errors due to finite polarization, inhomogeneity, nuclear spin dynamics, and electron spin decoherence.

Finite Polarization and Dark States

To understand the role of finite polarization, the specific cooling procedure must be examined. When the nuclear ensemble starts as a thermal mixture, cooling to dark states can be achieved by coupling polarized electron spins to the nuclear ensemble, see Chapter 2. Regardless of the details of cooling, the final density matrix will be a statistical mixture of dark states $|\mathcal{D}(m,\beta)\rangle$, where $A^-|\mathcal{D}(m,\beta)\rangle = 0$. m is the number of spin excitations locked in dark states ($m = 0$ is the fully polarized state) and β is the permutation group quantum number (see Section 2.1 and Ref. [104]). In practice, the cooled nuclear ensemble density matrix is a mixture of different dark states, i.e. $\rho = \sum_{m,\beta} \rho_{m,\beta} |\mathcal{D}(m,\beta)\rangle\langle\mathcal{D}(m,\beta)|$. It was shown in Ref. [42] that the "homogeneous" dark states can be mapped 1:1 to inhomogeneous ones. When homogeneous dark states $|I,-I\rangle$ are written in the single spin basis as

$$|I,-I=m-N/2,\beta\rangle = \sum_{\{j\}_m} c_{I,\beta}(\{j\})|\{j\}\rangle$$

where the set $\{j\}_m$ labels m spins that are pointing up (and the rest down), then it follows from $I^-|I,-I,\beta\rangle = 0$

$$\sum_{l\notin\{i\}_{m-1}} c_{N/2-m,\beta}(\{i\}+l) = 0 \tag{5.6}$$

for all $\{i\}_{m-1}$. Additionally, I^- is invariant under permutation so there exists a representation for dark states where every individual spin configuration is equally probable, i.e. $|c_{I,\beta}(\{i\})|^2 = |c_{I,\beta}(\{j\})|^2 = \binom{N}{N/2-I}^{-1}$. Each dark state $|I, -I = -N/2 + m, \beta\rangle$ has now its inhomogeneous counterpart given by

$$|\mathcal{D}(m,\beta)\rangle \propto \sum_{\{j\}_m} \left(\prod_{k\in\{j\}} \frac{1}{\alpha_k} \right) c_{N/2-m,\beta}(\{j\})|\{j\}\rangle, \tag{5.7}$$

as can be checked by direct calculation.

Thus the inhomogeneous counterparts have the same symmetry properties as the fully polarized state, and a manifold of excited states can be defined from a given dark state, $|n(m,\beta)\rangle \propto (A^+)^n |\mathcal{D}(m,\beta)\rangle$. Hence the above considerations for perfectly polarized nuclei map to the case when the nuclear ensembles start in any given dark state, not just the fully polarized state.

When the mixture of inhomogeneous dark states (as introduced above) is taken as the initial state for the investigation of the gate performance, as it is the case in what follows, then this is a worst case estimate. The states under consideration are generally not eigen states of the A^z-operator, and it is the variance of this operator that gives the largest error, as will be shown below. However, in Chapter 2 it was shown that in natural cooling processes the inhomogeneous Knight field plays a crucial role. For illustration: if one would consider a cooling protocol where the inhomogeneous Knight field would be suppressed by some means, then the states defined in Eq. (5.7), would be the steady states of this protocol. If one further imagines that the inhomogeneous Knight field would be switched on at some point, then these states would *not* be steady states anymore, but could be dephased first, and subsequently polarized further. As this positive effect is built-in in most conceivable cooling protocols, the error estimation based on Eq. (5.7) are to be taken as worst cases for realistic inhomogeneous situations.

As each dark state has a different $\delta_n(m,\beta), \Omega_n(m,\beta)$, interaction times and applied magnetic fields can only produce $R^{xy}_{en}(\theta,\phi)$ with the desired angle θ for some fraction of the given mixture. The inhomogeneous mixture effects can be characterized by examining the subgroups of dark states with different detunings, which lead to errors in Rabi oscillations $p \simeq (\sigma_\delta/\Omega_1)^2$, where σ_δ is the standard deviation of possible δ_1 values over the distribution $\rho_{m,\beta}$. In the homogeneous case with spin-1/2 nuclei,

$$\sigma_\delta \simeq g\sqrt{(1-P^2)}.$$

This formula follows directly from the variance of I^z in a maximally mixed state of polarization P. Note that here the polarization is $P = 2\langle I^z\rangle/N \in$

$[-1,1]$. Even at high ($P \sim 0.95$) polarizations, the effect of different detunings can be substantial ($p \sim 0.03$). This provides the strongest limit to realization of R_{en}^{xy} [1].

The inhomogeneous nature of the hyperfine coupling offers benefits in the cooling as described above, but on the other hand induces a new class of errors: The logical states of the system (the m-excitation manifolds) are no longer eigenstates of $J^z = A^z + S^z$ and of $\mathbf{A}^2$. As a consequence, there is a nonzero probability that the system moves out of the computational subspace during the gate operation. We estimate these leakage errors using the techniques developed in Chapter 4 and in Refs. [41, 42]. First we define the parameters characterizing the leakage out of the subspace. Leakage out of $|0,\downarrow\rangle$ is defined by $H_z|0,\downarrow\rangle = \omega_{0,\downarrow}|0,\downarrow\rangle + b_{0,\downarrow}|b_0,\downarrow\rangle$, with $\omega_{0,\downarrow} = \langle 0,\downarrow|H_z|0,\downarrow\rangle$, $b_{0,\downarrow}^2 = \langle H_z^2\rangle - \langle H_z\rangle^2$ and $|b_0,\downarrow\rangle = (H_z - \omega_{0,\downarrow})|0,\downarrow\rangle/b_{0,\downarrow}$. Here and in the following (as in the preceding chapter) all leakage states, like $|b_0,\downarrow\rangle$, will be defined such that they are normalized. For $n \geq 0$ we have

$$\begin{aligned}(H_{\rm ff} + H_z)|n,\uparrow\rangle &= \omega_{n,\uparrow}|n,\uparrow\rangle + \Omega_n|n+1,\downarrow\rangle + b_{n,\uparrow}|b_n,\uparrow\rangle, \\ (H_{\rm ff} + H_z)|n{+}1,\downarrow\rangle &= \omega_{n+1,\downarrow}|n{+}1,\downarrow\rangle + \Omega_n|n,\uparrow\rangle + b_{n+1,\downarrow}|b_n,\uparrow\rangle + c_{n+1,\downarrow}|c_n,c_{n,s}\rangle,\end{aligned} \tag{5.8}$$

with

$$\begin{aligned}\omega_{n,\uparrow} &= \langle n,\uparrow|H_z|n,\uparrow\rangle, \\ b_{n,\uparrow}^2 &= \langle n,\uparrow|H_z^2|n,\uparrow\rangle - \omega_{n,\uparrow}^2, \\ |b_n,\uparrow\rangle &= (H_z - \omega_{n,\uparrow})|n,\uparrow\rangle/b_{n,\uparrow}, \\ \omega_{n,\downarrow} &= \langle n,\downarrow|H_z|n,\downarrow\rangle, \\ b_{n+1,\downarrow} &= \langle b_n,\uparrow|H_{\rm ff}|n+1,\downarrow\rangle, \\ c_{n+1,\downarrow}^2 &= \langle n+1,\downarrow|(H_{\rm ff} + H_z - \omega_{n+1,\downarrow})^2|n+1,\downarrow\rangle - \Omega_n^2 - b_{n+1\downarrow}^2, \\ |c_n,c_{n,s}\rangle &= \Big((H_{\rm ff} + H_z - \omega_{n+1,\downarrow})|n+1,\downarrow\rangle - \Omega_n|n,\uparrow\rangle - b_{n+1,\downarrow}|b_n,\uparrow\rangle\Big)/c_{n+1,\downarrow}.\end{aligned}$$

The above defined coefficients lead to "cascaded" couplings between states, that can be visualized similarly as in Fig. 4.1. Note however, that $|n\rangle$ actually implicitly carries further indices m and β, reflecting the fact that in comparison with Chapter 4 we are dealing here with the more complicated situation of a dark state ensemble. The various coefficients defined in the above equations can be calculated directly using Eq. (5.7) and the results from Ref. [42]

[1] In a dark state ensemble the errors stemming from the variance in the Rabi frequencies σ_Ω is strongly suppressed in comparison to the detuning-based errors. This can be most simply seen by noting that $\Omega \approx g/2 \times \sqrt{1 - m/N}$ and thus depends also on the variance in the z-quantum number m. However, the contribution of this "unknown" parameter is suppressed here by $1/N$, relative to the detuning based errors.

(see Equation (9) and following in this article). For small leakage out of the computational states, the error scales as $(|b_{n,\uparrow}|^2 + |b_{n,\downarrow}|^2 + |c_{n,\uparrow}|^2)T^2$, where T is the gate operation time. It turns out that the resulting gate error p_{inhom} is small for $N \sim 10^5$; at high polarizations ($P > 0.95$) $p_{\text{inhom}} \lesssim 10^{-3}$. However, there is another kind of error that will scale unfavorably with particle number in the limit of high polarization: The error due to differences in Zeeman energy associated to different nuclear species. Large particle number N implies a smaller coupling, which in turn means a larger influence of Zeeman-variation induced errors during the longer gate operation time. For materials like GaAs, with gyromagnetic ratios varying greatly from species to species, this limits the effectiveness of gate operations at high magnetic field, resulting in the errors in the range of 10^{-3} as indicated in Fig. 5.3.

Nuclear spin dephasing

We now show that for the logical basis states we have chosen, there is no collective enhancement of decoherence. Starting with a single spin error, i.e. $E_j = \mathbf{n} \cdot \mathbf{I}_j$, we note that the logical states $|0\rangle, |1\rangle, |2\rangle$ are mapped to new states $|x(0)\rangle = E_j|0\rangle$ and similarly for $|x(1)\rangle, |x(2)\rangle$. These new states have, up to order $1/\sqrt{PN}$, the same properties as the original logical states as far as collective operators are concerned.

These new states transform under qubit operations as

$$\begin{aligned} A^-|x(0)\rangle &= 0 + [A^-, E_j]|0\rangle, \\ A^+|x(0)\rangle &= |x(1)\rangle + [A^+, E_j]|0\rangle, \\ A^-|x(1)\rangle &= |x(0)\rangle + [A^-, E_j]|1\rangle, \end{aligned} \tag{5.9}$$

and similarly for $|x(2)\rangle$. Each error term is bounded by $\|[A^\pm, E_j]\| \leq 1/\sqrt{N}$ (because only one term in the sum of the collective operator is "picked out" in the commutator; cf. the "benign" behavior of localized defects in Ch. 4). Therefore, after a single spin event a given logical state of a QD nuclear spin ensemble maps to a superposition of new orthogonal states, $|x(k)\rangle$, with the same logical value as the original state, up to errors over a logical operation of order $1/(\sqrt{N})^2 = 1/N$. If errors add incoherently, a single-spin decoherence mechanism acting on every spin with a rate γ will lead to an error rate for the logical states of $N\gamma/N = \gamma$.

The main mechanism for such spin decoherence is due to nuclear dipole-dipole interactions, and has a rate for a single spin of $\gamma_{DD} \sim 60\text{ms}^{-1}$, which by the above argument leads to a similar error rate for our chosen logical basis. However, active corrections can be performed with NMR pulse sequences that average the dipole-dipole Hamiltonian, such as WaHuHa, improving the

error rate to $\tau_{whh}^2 \gamma_{DD}^3$ [161, 162, 163]. After correction, dark state coherences could have lifetimes on the order of $0.1 - 1$ s for moderate cycle times τ_{whh}.

Electron Spin Manipulation Errors

The errors of manipulation of single electron spins in quantum dots via microwave or optical fields have been considered in detail elsewhere [13, 52, 155, 157], and only the relevant results are quoted here. Electron spin coherence will most likely be limited by different Overhauser shifts corresponding to different detunings, with errors going as $p \simeq (\sigma_\delta/\Omega_{\rm ESR})^2$; fast ESR ($\sim 6{\rm ns}^{-1}$) could mitigate this effect. With optical fields, even faster effective Rabi-oscillations are predicted ($\Omega_{\rm opt,ESR} \sim 50{\rm ns}^{-1}$) with errors then limited by spontaneous emission to $\sim 10^{-3}$. As for measurement, the fundamental limit will be set by relaxation of the electron spin, which has a time scale $\Gamma^{-1} \sim 0.1 - 10$ ms, based on recent measurements of the spin relaxation time [156, 164].

Transport Errors

Moving individual electron spins over short distances incurs phase errors due to uncertainty in the local nuclear field of the transport channel. The error induced by randomly oriented nuclei during transit can be estimated by the time-averaged hyperfine field the electron wave packet encounters over the whole process, $A/\sqrt{nLhl}$, where n is the density of lattice nuclei, L is the length of the channel, and hl is the transverse area of the channel.

The time scale for transfer depends upon the degree of transverse confinement, as only the ground state of the channel is to be occupied. Working in the ground state of the transverse channel means the wave packet can only have energies $|v|^2 m^*/2 \ll \hbar^2 l^2/m^*$, where m^* is the effective electron mass (the typical length scale for an harmonic oscillator is $l^{-2} \sim m\omega/\hbar$). For GaAs $m^* = 0.067 m_e$. For a 50nm wide and 10nm high channel, the maximal electron shuttling velocity is thus $\ll 30\mu{\rm m\ ns}^{-1} = 3 \times 10^4$ m/s. For a QD separation of 1μm, the expected dephasing probability due to thermal nuclei is $\simeq 5 \times 10^{-5}$ for a 3ns transfer time. Alternatively, we can take advantage of the long correlation time of the nuclear spin effective field, with either active metrology (as mentioned above) or by sending the electron spins in a decoherence free subspace [86].

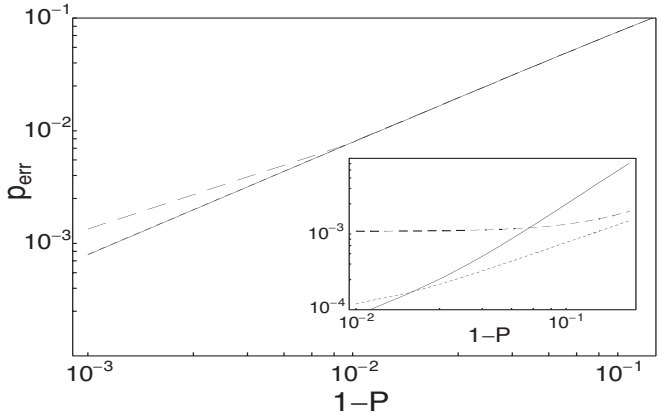

Figure 5.3: For a cooled dark state density matrix, expected error for a controlled-phase operation between electron spin and nuclear spin as a function of polarization (CdSe: solid, InAs: dotted, GaAs: dashed; in the main figure, CdSe and InAs are indistinguishable). The inset shows the effects of narrowing the nuclear distribution by a factor of 10 for different materials.

5.2.1 Quantitative Error Estimation for GaAs, InAs and CdSe

We consider three materials with demonstrated electronic and optical quantum dots (GaAs, $N = 10^5$; InAs, $N = 10^{4.6}$; CdSe, $N = 10^4$). The expected error of a two-qubit gate operation, defined as $\mathrm{tr}(U_{\mathrm{perfect}} U_{\mathrm{ideal}}^{\dagger})/4$, where U_{ideal} is given by Eq. (5.5), is plotted in Fig. 5.3. As the error is dominated by the detuning error, it is material independent, and is a few percent at 95% polarizations.

To combat these errors, a series of measurements may be made to determine the effective detuning of the system better than the thermal mixture limit σ_δ. This can be done e. g. by a measurement made with the single electron in the quantum dot, in direct analogy to single ion Ramsey interferometry in atomic clocks [165]; the distribution is then narrowed, with $\tilde{\sigma}_\delta \simeq \sigma_\delta/\sqrt{n}$, where n is the number of measurements. Note that more sophisticated and efficient measurement schemes have been tailored for the QD setup [36, 37, 38]. An improvement in the uncertainty of the mixture's detuning of a factor of 10 yields high fidelity operation, as shown in the inset to Fig. 5.3.

Smaller dots produce better results at higher polarizations due to their greater coupling strengths. The limits for GaAs are due to the large species in-

homogeneity and the incommensurate requirement of sufficient magnetic field to perform effective coherent averaging of dipole-dipole interactions. Low species inhomogeneity allows for higher magnetic field, faster WaHuHa-type correction sequences, and fewer errors in the transfer operation. This would be the case for quantum dots defined in nanotubes with isotopically enhanced ^{13}C or in CdSe quantum dots.

5.3 Conclusions

In conclusion, we have detailed a scheme for quantum information processing using dynamically defined qubits composed of collective excitations of nuclear spins in a quantum dot. For small dots with near-homogeneous Zeeman splittings, large but finite polarization (95%) is already sufficient to reach an error rate in two-qubit operations of order a few percent. Combined with the positive theoretical findings regarding nuclear spin cooling presented in Chapter 2, and rapid experimental progress in a variety of systems, the required high polarization are in reach. Our calculations indicate that the dominant source of error may be mitigated through narrowing the mixture of dark states.

Chapter 6

Quantum Optical Description of the Hyperfine Interaction

In the previous chapters we have seen how to polarize nuclear ensembles, we noted that cooled nuclear ensembles suppress electron spin decoherence and presented first examples of active usage of the nuclei. The latter is elaborated in this chapter, by considering multiple excitations of the polarized nuclear spin ensemble. Doing so, we develop an á la quantum optics theory to describe the inhomogeneous coupling of a single electron to the nuclear spin environment in a quantum dot in terms of a collection of bosonic modes interacting with a two-level system. At high polarization the electron couples predominantly to one mode, giving rise to an interaction which closely resembles the Jaynes-Cummings model of quantum optics.

During the last two decades quantum optics has succeeded in achieving an extraordinary degree of quantum control of systems at the single-quantum level [166]. This progress, illustrated by the manipulation of single atoms and photons in cavity quantum electrodynamics (QED) [131], and the storage and laser cooling of single trapped atoms [167, 168] and ions [132, 169], is largely based on sophisticated usage and control of the Jaynes-Cummings (JC) interaction [10, 131, 135]. It describes the interaction between a two level system (a qubit, for example two internal states of an atom or an ion) and a bosonic mode (corresponding to a cavity mode in the case of cavity QED, or a motional mode in the case of trapped ions). Performing the conditional gates required for quantum information processing and the production of interesting states such as Schrödinger cat and squeezed states [170] are examples of the many successful applications of the JC interaction.

Extending the results presented in the previous chapters, we consider here multiple excitations of the polarized ensemble. We show that indeed these excitations have bosonic character, and thus the electron-nuclear sys-

tem mimics the atom-light mode dynamics of the JC model. More precisely, the collective spin operators are mapped to a set of bosonic operators under the assumption that the ratio between the average number of nuclear spins flipped (with respect to a fully polarized ensemble), to the average number of nuclear spins that experience the interaction with the electron is small. At full polarization all but one bosonic modes play no role and the coupling of the electron to only one of the modes describes the situation. To first order in the perturbation series in the small parameter, the presence of the bath renormalizes the Rabi frequency and the detuning of the JC model by a factor that depends both on the number of bosonic excitations and on the shape of the electron wave function. The deviations from the ideal JC Hamiltonian still leave us with a highly useful model which is applied for the derivation of analytical formulas for the electron spin evolution, revealing Gaussian and algebraic decay for off-resonant and resonant evolution, respectively. Apart from generally opening doors for the transfer of quantum information protocols from quantum optics to the semiconductor domain our model also allows for the design of specifically tailored proposals, for which we give as an example a scheme for deterministically generating highly squeezed states [171] of the nuclear spins.

The idea of turning the nuclear spin environment into a useful resource is pursued throughout this thesis. It had previously already been introduced in remarkable recent theoretical work [41, 42], where Taylor *et al.* have shown that the interaction between the electron and the nuclear spins can be used to prepare and control the nuclear ensemble and to provide a robust, long-lived quantum memory for the information held by the electron. The performance of this quantum memory has been investigated by Song *et al.* [172] using a simple bosonic formalism that did not take into account the non-bosonic corrections of the strongly coupled mode (as we will explain later) and for explicit calculations only considered the presence of the bath modes in the homogeneous limit. In lowest order the results of this chapter reduce to those previous ones. However, we extend the concepts and put them into a more general framework, allowing for a closer connection to quantum optical quantum information processing. Given that Ref. [172] has already presented some related results on the bosonic formalism, we will put more emphasis on the novel applications and results achieved by the usage of the formalism.

This chapter is organized as follows: In Section 6.1 the spin Hamiltonian is transformed into a Hamiltonian containing the bosonic modes. A considerably simpler effective Hamiltonian is derived in Section 6.2. We will then consider in Section 6.3 the electron spin dynamics with the derived model and finally discuss our proposal for deterministically squeezing the nuclear spin state in Section 6.4.

6.1 Model

As before, we consider a single electron spin and N nuclear spins in a quantum dot in an external magnetic field B along the z-axis. We denote the electron spin operator by $\mathbf{S} = \left(S^x, S^y, S^z\right)$ and that of the ℓ-th nuclear spin by $\sigma_\ell = \left(\sigma_\ell^x, \sigma_\ell^y, \sigma_\ell^z\right)$. For simplicity we will consider spin-$\frac{1}{2}$ nuclei of one species only. We write the HF Hamiltonian as

$$H = H_{\text{ff}} + H_{\text{zz}} = \frac{g}{2}(A^+S^- + S^+A^-) + gA^z_{\text{eff}}S^z, \tag{6.1}$$

with $\left(A^+, A^-, A^z\right) = \sum_\ell g_\ell \left(\sigma_\ell^+, \sigma_\ell^-, \sigma_\ell^z\right)$ and couplings $g_\ell = \frac{|\psi(\mathbf{r}_\ell)|^2}{\sqrt{\sum_\ell |\psi(\mathbf{r}_\ell)|^4}}$, and $g = A\sqrt{\sum_\ell |\psi(\mathbf{r}_\ell)|^4}$, such that $\sum_\ell g_\ell^2 = 1$. The effective magnetic field for the electron is $A^z_{\text{eff}} = A^z + \widetilde{B}$, with $\widetilde{B} = \frac{g^*}{g}\mu_B B$.

Homogeneous case

The bosonic behavior of the collective nuclear excitations is most obvious in the case of constant couplings. The matrix elements of the operators $I^\pm$ acting on collective angular momentum state are given by the standard expressions $I^+\big|N/2, -N/2{+}n\big\rangle = \sqrt{n+1}\sqrt{1-\frac{n}{N}}\big|N/2, -N/2{+}n{+}1\big\rangle$. For small excitation number n the action of the spin operators thus corresponds to the one of bosonic creation operators acting on Fock states ($a^\dagger|n\rangle = \sqrt{n+1}|n+1\rangle$). Formally this simple observation is reflected in the well-known Holstein-Primakoff transformation [105], which maps spin operators to bosonic ones by "manually" correcting the operators such that the correct matrix elements are obtained $I^+ \to a^\dagger\sqrt{1 - a^\dagger a/N}$. Clearly, when $N \sim 10^5 - 10^6$, as in the case considered here, the second term in the square root can be neglected in comparison to unity– given low excitation number of the collective state and high polarization of the sample.

In the following we develop a systematic way of introducing bosonic operators in the case of finite polarization and inhomogeneous coupling of the electron to the nuclei. We will first identify the small parameter in our theory. Then we will address the general problem of how to describe the nuclear spin ensemble in terms of a main bosonic mode and a bath of additional bosonic modes. Eventually it is shown how to include the effect of this bath of bosonic modes as a perturbation to the JC model.

We remark here that is is possible to calculate the deviations from bosonicity working in the spin picture using methods related to the ones used in Chapters 4 and 5. This is done is Appendix D. However, the approach investigated in the next sections is more practical and therefore preferable[1].

[1] Clearly, exact mappings from spins to bosons would be a third route to follow. One

Small Parameter

Due to the lack of symmetry in the inhomogeneous case the connection between collective spin excitations and bosonic behavior is less straightforward than in the homogeneous case. A measure of the non-bosonicity of the operators is the deviation from bosonic commutation relations. For the collective spin operators

$$[A^-, A^+] = 1 - 2\sum_\ell g_\ell^2 \sigma_\ell^+ \sigma_\ell^-, \tag{6.2}$$

and thus the norm of the operator $\sum_\ell g_\ell^2 \sigma_\ell^+ \sigma_\ell^-$ quantifies this deviation. This norm is the small parameter ε that we want to identify. When it is small, bosonic operators can be introduced and the correction to them can be taken into account by introducing a set of bath operators. For a nuclear state with at most m spin flips with respect to the spin-down state

$$\Big\| \sum_\ell g_\ell^2 \sigma_\ell^+ \sigma_\ell^- \Big\|_m \leq m \max_\ell g_\ell^2 = \frac{m}{N_{\text{eff}}}, \tag{6.3}$$

where we have defined $N_{\text{eff}} = 1/\max_\ell g_\ell^2$ and $\|\cdot\|_m$ indicates the norm within the nuclear spin subspace where at most m spins are flipped. For a nuclear ensemble with $\overline{m}$ spin flips on average, we will define the parameter ε as

$$\varepsilon = \frac{\overline{m}}{N_{\text{eff}}}. \tag{6.4}$$

The parameter N_{eff} characterizes the width of the electron wave function and therefore the effective number of nuclei participating in the collective spin excitation A^+. For a homogeneous situation in which $g_\ell = 1/\sqrt{N}$, we have that $N_{\text{eff}} = N$. For a Gaussian distribution $g_\ell \propto e^{-\ell^2/(2w^2)}$, the effective number of nuclei is just proportional to the width of the Gaussian, $N_{\text{eff}} \propto w$. The parameter ε characterizes the probability with which the collective spin operator A^+ finds, when acting on the nuclear ensemble, a nucleus with its spin flipped. In the following we will assume that the parameter ε is small, so that the effective Hamiltonian describing the dynamics of the problem will be close to the JC model. Note that the more localized the electron wave function is, the smaller the number $\overline{m}$ of allowed flipped spins flips is, when ε is to remain small. (It could happen that ε is large, but still the bosonic approximation can be applicable. For example, a very localized electron might almost exclusively interact with very highly polarized spins,

could first map the spin operators to hard-core bosonic operators, and then express the latter ones in terms of (projected) standard bosonic operators. However, this leads to complicated expressions of limited use for the situation at hand.

whereas the excitations still present in the nuclear ensemble might be located at quasi-decoupled nuclei. In the general situation however, ε serves as a good conservative estimate for the deviations from bosonicity.)

From collective spin modes to bosonic modes

Given the form of Hamiltonian (6.1) we describe the spin system in terms of N collective spin operators. We naturally choose one of these modes to be represented by the operator A^+. Then we define a bath of additional spin operators of the form

$$A_k^+ = \sum_{\ell=1}^{N} g_\ell^{(k)} \sigma_\ell^+, \qquad k = 1, \ldots, N-1, \tag{6.5}$$

such that the conditions $\mathbf{g} \cdot \mathbf{g}^{(k)^*} = 0, \mathbf{g}^{(k)} \cdot \mathbf{g}^{(k')^*} = \delta_{k,k'}$ for all $k, k' = 1, \ldots, N-1$ are fulfilled. It is possible[2] to choose the bath modes (6.5) such that $\max_\ell \left|g_\ell^{(k)}\right|^2 \leq 1/N_{\text{eff}}$, so that they all have the same "size" as the main mode A^+. The algebra of these operators is given by the equations

$$\begin{aligned} \left[A^-, A_k^+\right] &= -2 \sum_\ell g_\ell g_\ell^{(k)^*} \sigma_\ell^+ \sigma_\ell^-, \\ \left[A_k^-, A_{k'}^+\right] &= \delta_{k,k'} - 2 \sum_\ell g_\ell^{(k)} g_\ell^{(k')*} \sigma_\ell^+ \sigma_\ell^-, \end{aligned} \tag{6.6}$$

together with equation (6.2). They do not satisfy bosonic commutation relations. However, the corrections to their bosonic character are all of order ε on the relevant subspace, since we have that $\| \sum_\ell g_\ell^{(k)} g_\ell^{(k')*} \sigma_\ell^+ \sigma_\ell^- \|_m \leq m \max_\ell \left\{ \left|g_\ell^{(k)}\right| \left|g_\ell^{(k')}\right| \right\} \leq \varepsilon$, $\forall k, k'$ [3].

We want to map the above spin system onto a problem of bosonic modes. Therefore we need to find a mapping $\mathcal{B}$ of the set of collective spin operators

[2] The electronic wave function can be represented, for example, as a superposition of n_F Fourier modes. For the dots and (smooth) wave functions we are considering only a small number of modes is needed to represent the electron wave function with high precision, $n_F \ll N$. Therefore any of the orthogonal modes is either a Fourier mode directly or a superposition of at most n_F Fourier modes, and it follows readily that $|g_\ell^{(k)}|^2 \leq n_F/N$ for all k, l. We have thus found the bound for all the modes. Additionally for the smooth wave functions considered (e.g. Gaussians) $g_{\max}^2 \sim n_F/N$, and thus it is sufficient to retain $g_{\max}$ as the parameter quantifying the inhomogeneity.

[3] The freedom in the choice of the orthogonal modes can not have any influence on the predicted physical phenomena. However, it would certainly be possible to choose modes that display pronounced non-bosonic behavior. The (re-)summation of all the non-bosonic effects would yield the same results as the ones obtained by our choice; the latter being preferable because it is more convenient.

$A^-, A^+, \{A_k^-, A_k^+\}$ onto a set of bosonic operators $a, a^\dagger, \{a_k, a_k^\dagger\}$, such that the spin algebra is preserved. This means that the equations

$$\begin{aligned}\left[\mathcal{B}(A_k^-), \mathcal{B}(A^+)\right] &= \mathcal{B}\left(\left[A_k^-, A^+\right]\right), \\ \left[\mathcal{B}(A_k^-), \mathcal{B}(A_{k'}^+)\right] &= \mathcal{B}\left(\left[A_k^-, A_{k'}^+\right]\right),\end{aligned} \tag{6.7}$$

have to be fulfilled for all $k, k' = 1, \ldots, N-1$; and similarly for the commutators involving z-collective operators. We write the mapping as

$$\begin{aligned}A^+ &\xrightarrow{\mathcal{B}} a^\dagger + \epsilon, \\ A_k^+ &\xrightarrow{\mathcal{B}} a_k^\dagger + \epsilon_k.\end{aligned} \tag{6.8}$$

Here, the operators ϵ, $\{\epsilon_k\}$ take into account the non-bosonic part of the spin operators. Therefore, their norms are all of order ε. They are functions of the set of bosonic operators $a, a^\dagger, \{a_k, a_k^\dagger\}$, and are implicitly defined through the set of equations (6.7).

In addition to preserving the commutation relations, the mapped operators have to reproduce the matrix elements of the original spin operators correctly. We will construct the mapping in the following such that this is true for the fully polarized case with the natural identification $|\downarrow, \downarrow, \ldots, \downarrow\rangle \to |0, 0, \ldots, 0\rangle$, where the entries in the latter ket are the occupation numbers of the modes. Any spin state can be expressed in terms of bosons, by changing from localized to delocalized spins operators, and the substitution of those by their bosonic counterparts. The corrections of these mapped operators are functions of the same "bare bosonic" operators and thus the identification of the "vacuum" states suffices to obtain well defined expressions. The resulting state is the starting point for investigations employing the bosonic Hamiltonian. The bosonic state corresponding to a mixture of dark states is constructed and studied in Section 6.2.

The mapping to first order in ε

When the electron couples homogeneously to all nuclear spins, the three operators $\left\{\frac{1}{\sqrt{N}}\sum_\ell \sigma_\ell^+, \frac{1}{\sqrt{N}}\sum_\ell \sigma_\ell^-, \frac{1}{\sqrt{N}}\sum_\ell \sigma_\ell^z\right\}$ form a closed subalgebra and can be exactly mapped to a set of N bosons

$$\begin{aligned}A^- &\longrightarrow \sqrt{1 - 2C_\mathrm{h}}\; a, \\ A^z &\longrightarrow -\frac{\sqrt{N}}{2} + \left(a^\dagger a + \sum_k a_k^\dagger a_k\right)/\sqrt{N},\end{aligned}$$

where $C_\mathrm{h} = \left(\frac{1}{2}a^\dagger a + \sum_k a_k^\dagger a_k\right)/N$.

In the general case, in which the coupling is not homogeneous, the operators $\{A^+, A^-, A^z\}$ do not form a closed subalgebra. Note though, that for the derivation of a practical and useful mapping onto a bosonic problem mimicking the dynamics of the spin Hamiltonian (6.1) it is not necessary that the complete algebra of nuclear spin operators is preserved by the mapping. The Hamiltonian (6.1) only contains certain superpositions of the collective spin operators. Therefore it is sufficient to formulate a bosonic description that preserves the algebra generated by this set of operators. Having in mind the time evolution of the density operator written as a combination of nested commutators, one can imagine the coupling of the "bath modes" as a cascaded system, in which the bath only contributes in less important higher orders.

Thus we now find bosonic equivalents of $\{A^+, A^-, A^z\}$. This generally is complicated– as one can readily see considering the exact hardcore boson mapping. In the limit of small ε, however, we find a significantly simpler mapping: Considering

$$[A^-, A^+] = 1 - 2D, \tag{6.9}$$

with

$$\begin{aligned} D &= \gamma_4 A^+ A^- + \big[A^+ \sum_{k=1}^{N-1} \beta_k^{(3)} A_k^- + \text{H.c.}\big] + \sum_{k,k'=1}^{N-1} \alpha_{k,k'}^{(2)} A_k^+ A_{k'}^-, \\ \gamma_p &= \sum_{\ell=1}^{N} g_\ell^p, \\ \beta_k^{(p)} = \sum_{\ell=1}^{N} g_\ell^p g_\ell^{(k)*}, &\qquad \alpha_{k,k'}^{(p)} = \sum_{\ell=1}^{N} g_\ell^p g_\ell^{(k)} g_\ell^{(k')*}, \end{aligned} \tag{6.10}$$

we know that $\|D\|_m \sim \varepsilon$ and thus we neglect second order corrections to that term, arriving at the bosonic expression $D \to d = \gamma_4 a^\dagger a + (a^\dagger b + b^\dagger a) + \sum_{k,k'=1}^{N-1} \alpha_{k,k'}^{(2)} a_k^\dagger a_{k'}$. From this now we determine the relevant correction to the mapped bosonic raising and lowering operators which obey the commutation relation Eq. (6.9),

$$\begin{aligned} &D \longrightarrow d \\ &A^- \longrightarrow \big(1 - C\big) a, \\ &C = \frac{\gamma_4}{2} a^\dagger a + \frac{3}{2}\big(a^\dagger b + b^\dagger a\big) + \sum_{k,k'=1}^{N-1} \alpha_{k,k'}^{(2)} a_k^\dagger a_{k'}, \end{aligned} \tag{6.11}$$

where $b^\dagger = \sum_{k=1}^{N-1} \beta_k^{(3)} a_k^\dagger$. The parameter γ_x will be repeatedly used in the

following, thus it is noteworthy that

$$N^{1-x/2} \leq \gamma_x \leq N_{\text{eff}}^{1-x/2}.$$

Furthermore, the operator $A^z = -\gamma_1/2 + \gamma_3 A^+A^- + \left[A^- \sum_{k=1}^{N-1} \beta'_k A_k^+ + \text{H.c.}\right] + \sum_{k,k'=1}^{N-1} \alpha'_{k,k'} A_k^+ A_{k'}^-$ is in lowest order in ε mapped onto

$$C_z = -\frac{\gamma_1}{2} + \frac{\gamma_3}{2} a^\dagger a + \left(a^\dagger c + c^\dagger a\right) + \sum_{k,k'=1}^{N-1} \alpha_{k,k'}^{(1)} a_k^\dagger a_{k'}, \tag{6.12}$$

with $c^\dagger = \sum_{k=1}^{N-1} \beta_k^{(2)} a_k^\dagger$ and one finds that with this choice the commutations relations of the boson operators $\{A^\pm, A^z\}$ reproduce the ones for the spins to the desired order.

Inserting the derived bosonic expressions into the Hamiltonian yields

$$H_b = g/2 \left[a^\dagger \big(1 - C\big) S^- + \text{H.c.}\right] + g \left(C_z + \widetilde{B}\right) S^z. \tag{6.13}$$

This Hamiltonian represents the interaction of a two level system with a collection of bosonic modes. It contains to zeroth order the JC-like interaction and both correcting operators C and C_z consist of three different contributions: A term proportional to the number of bosons in the main mode, a, a coupling of the main bosonic mode to a superposition of bath modes (b and c), and a coupling among the different modes in the bath, a_k. As mentioned in the beginning of this chapter, Song *et al.* have used a bosonic description of the HF interaction to study the performance of a quantum memory [172]. Comparing Eq. (42) of this reference with the previous equation we see that our formalism indeed reduces in lowest order to their result. In the next section it is shown how the derived bosonic expression can be considerably simplified for the situation of our interest, but at the same time keeping the most relevant effects of the derived correction terms.

6.2 Effective Bosonic Hamiltonian

The fact that the operators C and C_z that appear in the bosonic Hamiltonian (6.13) have non-diagonal terms in which the different modes in the bath couple with each other and with the main mode, makes it difficult to evaluate the time evolution of the whole system exactly. However, we are not interested in studying the evolved state of the whole system, but only in the valuable information about the electron and the main bosonic mode. We show in the present section that the evolved state of this reduced system can be easily calculated.

The initial state

Let us consider an initial bosonic mixed state of the form

$$\rho(0) = |\sigma_e n_0\rangle\langle\sigma_e n_0| \otimes \rho_B, \tag{6.14}$$

where the electron is in the pure spin state $|\sigma_e\rangle$, we have n_0 excitations in the main mode a, and the bath is in the thermal state $((1-e^{-\lambda})e^{-\lambda n})^{\otimes N-1}$. The parameter λ plays the role of an effective temperature and it is related to the mean number of bosons in the bath, $\overline{m}$, by the equation $\overline{m}/N = 1/(e^{\lambda}-1)$.

For later convenience we rewrite the thermal bath state as

$$\rho_B = \sum_m p(m)\rho_m, \tag{6.15}$$

with $p(m) = (1-e^{-\lambda})^{N-1}e^{-\lambda m}$, and $\rho_m = \sum_\beta \big|\sum_k n_k^{(\beta)} = m\big\rangle\big\langle \sum_k n_k^{(\beta)} = m\big|$, where the states $\big|\sum_k n_k^{(\beta)} = m\big\rangle = \prod_k \frac{(a_k^\dagger)^{n_k^{(\beta)}}}{\sqrt{n_k^{(\beta)}!}}|0\rangle$ represent all possible ways of distributing m bosons over the $N-1$ bath modes, labeled by the index β. Note that with the state of the bath given by (6.15), and $n_0 = 0$, the initial state $\rho(0)$ is a mixture of states with zero excitations in the main bosonic mode a and thus all the states in the mixture are dark states for the given couplings, since we have

$$a\big|0\big\rangle\big|\sum_k n_k^{(\beta)} = m\big\rangle = 0.$$

The bosonic bath state above is useful to represent typical steady states of the nuclear spin ensemble after realistic cooling procedures, which themselves rely on the hyperfine interaction, as explained in Chapters 2 and 3. For instance, by cycling spin polarization through the quantum dot the nuclei are driven into a mixture of dark states $\rho_s = \sum_m p(m)\sum_{\beta_s}|D(m,\beta_s)\rangle\langle D(m,\beta_s)|$, which has the same form as (6.15). The dark states are defined by

$$A^-|D(m,\beta_s)\rangle = 0, \tag{6.16}$$

the quantum number m is the number of spin flips with respect to the fully polarized state,

$$\sum_\ell \sigma_\ell^z|D(m,\beta_s)\rangle = N/2 - m, \tag{6.17}$$

and β_s is an additional quantum number that labels dark states with the same m. Both of these characteristic features Eqs. (6.16) and (6.17) of the spin states are reflected in the initial bosonic state (6.14)

The effective Hamiltonian: direct sum of renormalized JC models

We want to study the dynamics of the initial state given in Eq. (6.14) under the Hamiltonian (6.13). We are interested in the reduced density matrix of the system formed by the electron and the main mode, $\sigma(t) = \mathrm{tr}_B \rho(t)$, where tr_B denotes the trace over the $N-1$ bath modes. Calculations to second order in perturbation theory show that, to first order in $\varepsilon = \overline{m}/N_{\mathrm{eff}}$, the same dynamics is generated by the full bosonic Hamiltonian (6.13) and the simplified Hamiltonian

$$H_b^{(0)} = \frac{g}{2}\left[\left(1 - C^{(0)}\right) a S^+ + \mathrm{H.c.}\right] + g\left(C_z^{(0)} + \widetilde{B}\right) S^z, \tag{6.18}$$

where

$$C^{(0)} = \frac{\gamma_4}{2} a^\dagger a + \frac{1-\gamma_4}{N} \sum_k a_k^\dagger a_k,$$
$$C_z^{(0)} = -\frac{\gamma_1}{2} + \gamma_3 a^\dagger a + \frac{\gamma_1}{N} \sum_k a_k^\dagger a_k.$$

The proof of this is given in Appendix E, where also the importance of the shape of the electronic wave function is analyzed in detail. We note that this result states, that the off-diagonal terms of the operators (6.11) and (6.12), which describe processes in which a boson is transferred from the bath to the main mode or between different modes in the bath, are, to first order in ε (and under the additional conditions on the electron wave function specified in Appendix E), not relevant for the dynamics of the reduced density matrix. Still, the operators C and C_z clearly lead to a bath-dependent system evolution: Writing the bosonic Hilbert space as a direct sum of subspaces of well defined number of excitations in the bath $\sum_k a_k^\dagger a_k = m$ and in the main mode $a^\dagger a = n_0$, the effective Hamiltonian (6.18) can be written as a direct sum of JC-like Hamiltonians

$$H_b^{(0)} = \frac{g}{2} \bigoplus_{n_0,m} \begin{pmatrix} \Delta_{n_0,m} & \Omega_{n_0,m} \\ \Omega_{n_0,m} & -\Delta_{n_0,m} \end{pmatrix}_{|n_0\uparrow\rangle, |n_0+1\downarrow\rangle}, \tag{6.19}$$

with the parameter dependent generalized Rabi frequency

$$\Omega_{n_0,m} = \sqrt{n_0+1}\left[1 - \frac{\gamma_4}{2} n_0 - \frac{1-\gamma_4}{N} m\right], \tag{6.20}$$

and the detuning

$$\Delta_{n_0,m} = \left[\gamma_3\left(n_0 + \frac{1}{2}\right) + \frac{\gamma_1}{N} m + \widetilde{B}\right]. \tag{6.21}$$

This is the main result of this chapter. It establishes that for each doublet $\{|n_0\uparrow\rangle, |n_0+1\downarrow\rangle\}$ the dynamics is approximately JC with a Rabi frequency and a detuning that depend on the number of excitations in the bath. The dependence on the inhomogeneity of the wave function is implicit both in the parameter g and in the coefficients γ_p.

Apart from opening doors for the transfer of knowledge from quantum optics, this expression can be used to get approximate analytic formulas for the electron spin dynamics in cases where typical expansions in the external magnetic field are not applicable, as we will show in the next section.

6.3 Study of Electron Spin Decay with the Bosonic Formalism

Longitudinal Dynamics

For concreteness we consider the electronic initial state $|\sigma_e\rangle = |\uparrow\rangle$ and the bath of bosonic modes is in a thermal state, cf. Eq. (6.15), and find

$$\begin{aligned} 2\langle S^z(t)\rangle &= \sum_m p(m)\left(\cos^2\frac{g}{2}\widetilde{\Omega}_{n_0,m}t \;+\frac{\Delta^2_{n_0,m}-\Omega^2_{n_0,m}}{\widetilde{\Omega}^2_{n_0,m}}\sin^2\frac{g}{2}\widetilde{\Omega}_{n_0,m}t\right)\\ &= \sum_m p(m)\left(\frac{x_{n_0,m}}{1+x_{n_0,m}}+\frac{\cos g\widetilde{\Omega}_{n_0,m}t}{1+x_{n_0,m}}\right), \end{aligned} \tag{6.22}$$

where we used the generalized Rabi frequency $\widetilde{\Omega}^2_{n_0,m} = \Omega^2_{n_0,m} + \Delta^2_{n_0,m}$ and $x_{n_0,m} = \Delta^2_{n_0,m}/\Omega^2_{n_0,m}$. The latter parameter quantifies how resonant the evolution is; for $x_{n_0,m} \gg 1$ spin flips of the electron are suppressed due to energy mismatch, whereas for $x_{n_0,m} \ll 1$ spin exchange dominates. We have calculated the above expression numerically and plotted it in Figs. 6.1 and 6.2 for various situations. In Fig. 6.1 we plot $\langle S^z(t)\rangle$ as a function of time and the effective magnetic field

$$B_{\text{eff}} = \langle A^z_{\text{eff}}\rangle = \widetilde{B} - \frac{\gamma_1}{2} + \frac{\gamma_1\overline{m}}{N}. \tag{6.23}$$

We can clearly see the pronounced transition from the far-off-resonance regime with large B_{eff}, where the Rabi oscillations are suppressed, to the resonant regime with $B_{\text{eff}} = 0$, where long-lived oscillations occur. However, also in the resonant regime a decay of the oscillations with time is observed. Our model provides a simple intuitive understanding of that behavior: The evolution of the system is given by an average over different JC evolutions with different generalized Rabi frequencies (corresponding to different numbers m

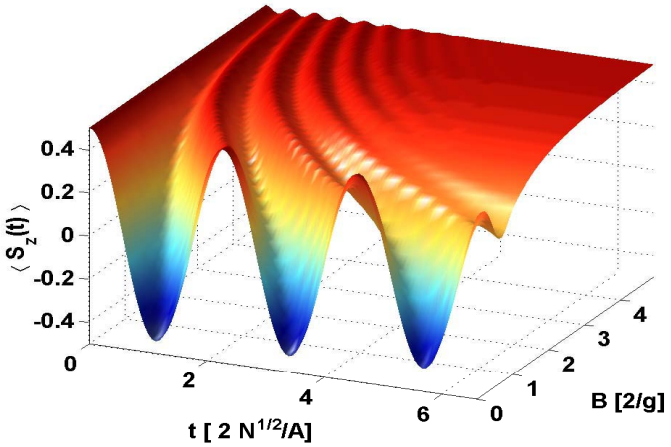

Figure 6.1: Evolution of the z-component of the electron spin, $\langle S^z(t)\rangle$, as a function of time and effective magnetic field B_{eff}. The system is initially in the state (6.14) with $\sigma_e = \uparrow$, $n_0 = 0$, $\overline{m}/N = 0.1$, and $N = 10^5$. We consider a Gaussian electronic wave function, $\psi(\mathbf{r}) \propto \exp(-r^2/w^2)$, with $w = N/4$.

of excitations in the bath). This is a clear cause of dephasing. Additionally, for some subspaces of the mixed initial state, characterized by the number of excitations m, the corresponding JC model has a substantial detuning, which results in a reduced contrast of the oscillations.

To better capture the physics underlying the evolution of the z-component of the electron spin, let us consider the limiting cases of far-off-resonant and resonant effective magnetic fields, for which approximate analytic expressions can be derived. To simplify the analytical calculations we take into account that the probabilities $p(m)$ are, due to the central limit theorem, approximated by

$$p(m) \cong \frac{1}{\sqrt{2\pi}\sigma} e^{-(m-\overline{m})^2/(2\sigma^2)},$$

where the width of the probability distribution is given by $\sigma = \sqrt{\overline{m}\left(1+\frac{\overline{m}}{N}\right)}$.

Resonance– Taking the continuum limit and using the resonance condition $x_{n_0,m} \ll 1$, the Gaussian integral (6.22) is approximated by

$$\langle 2S^z(t)\rangle \approx \frac{\cos\left(\frac{g}{2}\overline{\Omega}t + \frac{1}{2}\nu(t)\right)}{\left[1+\left(\frac{g}{2}\Gamma_r t\right)^2\right]^{1/4}} + \frac{\Gamma_r}{2\overline{\Omega}}\left(1 - \frac{\cos\left(\frac{g}{2}\overline{\Omega}t + \frac{3}{2}\nu(t)\right)}{\left[1+\left(\frac{g}{2}\Gamma_r t\right)^2\right]^{3/4}}\right), \tag{6.24}$$

where

$$\overline{\Omega} = \sum_m p(m)\Omega_{n_0,m} = \sqrt{n_0+1}\left(1 - \frac{\gamma_4 n_0}{2} - \frac{\overline{m}}{N}\right), \tag{6.25}$$

is the Rabi frequency averaged over all possible number of excitations in the bath, and we have defined

$$\Gamma_r = 2\frac{\Gamma}{\overline{\Omega}},$$
$$\Gamma = \left(\frac{\gamma_1\sigma}{N}\right)^2,$$
$$\nu(t) = \arctan(g\Gamma_r t/2).$$

We have thus found that the longitudinal resonant dynamics is governed by a sum of two algebraic decays. The second term in Eq. (6.24) falls off faster in time than the first and additionally it is suppressed with the prefactor $\Gamma_r/\overline{\Omega}$ which vanishes for large polarization. Thus $\langle S_z(t)\rangle$ decays predominantly algebraically with $1/\sqrt{t}$.

The parameter Γ characterizes the number of Rabi oscillations that the electron spin performs before it decays,

$$N_{\text{osc}} = \frac{T_{\text{decay}}}{T_{\text{Rabi}}} \sim \frac{g}{g\Gamma} \sim \frac{1}{\overline{m}/N},$$

where for the last step in the above equation we used the scaling behavior of the γ_x. In the limit of a fully polarized system $\bar{m} \to 0$ and $N_{\text{osc}} \to \infty$. Also $\Gamma, \Gamma_r \to 0$ and the longitudinal dynamics reduce to a single undamped oscillation. It has been noted [32, 65] that in the very special and exactly solvable case of full polarization, there are indeed undamped oscillations, with small corrections $\mathcal{O}(1/N)$, which (consistently) do not appear in the above formula due to the various approximations that led to it. The strength of our approach is the validity and practicability for non-perfect polarization.

The average frequency of the oscillations $\overline{\Omega}$ decreases, for a given electron wave function, as the degree of polarization of the nuclei decreases (see Eq. (6.25) and Fig. 6.2). On the other hand, for a given polarization, the average frequency of the oscillations increases as the size of the electronic wave function decreases (Fig. 6.2). This can be seen by noticing that the coupling constant g decreases with N_{eff}.

Off-Resonance– Evaluating the integral (6.22) under the condition $x_{n_0,m} \gg 1$ yields

$$\langle 2S^z(t)\rangle \approx 1 - 2\frac{\overline{\Omega}^2}{B_{\text{eff}}^2}\left(1 - e^{-\frac{1}{2}(g\Gamma t)^2}\cos(gB_{\text{eff}}t)\right).$$

One can clearly see that with increasing magnetic field the electron spin becomes less likely to leave its initial state: The flip-flop part of the Hamiltonian is suppressed with B_{eff}^2. Gaussian decay in this situation has been found in previous studies, see e.g. Ref. [66, 67].

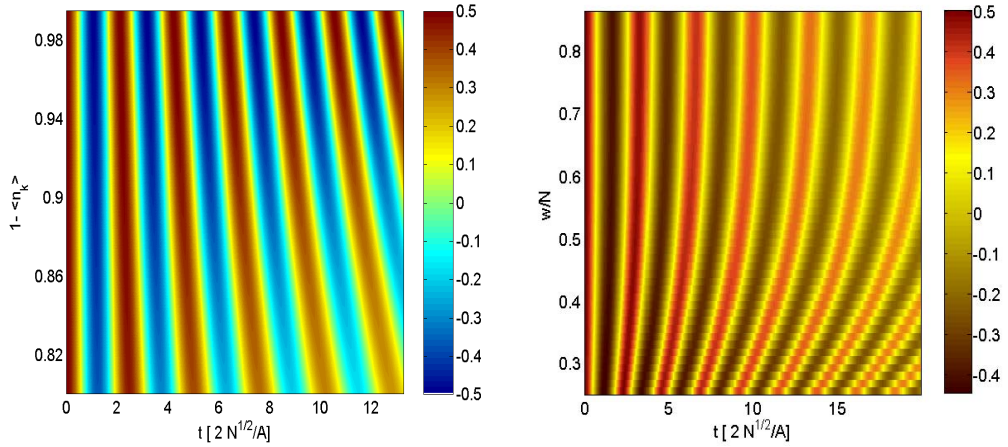

Figure 6.2: Color coded resonant evolution of the z-component of the electron spin, $\langle S^z(t)\rangle$, as a function of time and polarization (left plot) and inhomogeneity (right plot) of the electron wave function. For the left plot $w = N/4$ and the remaining parameters are as in Fig. 6.1.

Transversal Dynamics

Consider now an electron which is initially in the spin state $|\sigma_e\rangle = \frac{1}{\sqrt{2}}(|\uparrow\rangle + |\downarrow\rangle)$ and the main bosonic mode containing one excitation, $n_0 = 1$. We have calculated $\mathrm{Re}\big(\langle S^+(t)\rangle\big)$ and plotted the result in Fig. 6.3. In the off-resonant regime we observe a decay of this quantity, which is approximately Gaussian. The situation gets interesting in the resonant regime, in which oscillations occur with a beating of two different frequencies. Our formalism provides a simple explanation for this remarkable behavior.

In order to get an intuitive understanding of the beating, let us for a moment consider a well defined number m of excitations in the bath, and $n_0 = 1$ excitations in the main mode. For that case the evolved state of the reduced system is

$$|\phi(t)\rangle \propto \alpha_1(t)|1,\uparrow\rangle + \beta_2(t)|2,\downarrow\rangle + \alpha_0^*(t)|1,\downarrow\rangle + \beta_0(t)|0,\uparrow\rangle,$$

with $\alpha_{n_0}(t) = \cos\frac{g}{2}\widetilde{\Omega}_{n_0,m}t + i\frac{\Delta_{n_0,m}}{\widetilde{\Omega}_{n_0,m}}\sin\frac{g}{2}\widetilde{\Omega}_{n_0,m}t$, $\beta_{n_0}(t) = -i\frac{\Omega_{n_0,m}}{\widetilde{\Omega}_{n_0,m}}\sin\frac{g}{2}\widetilde{\Omega}_{n_0,m}t$. Thus, the reduced system evolves into two different JC doublets $\{|1,\uparrow\rangle, |2,\downarrow\rangle\}$ and $\{|1,\downarrow\rangle, |0,\uparrow\rangle\}$, which give rise to two different frequencies. In the resonant regime, in which $x_{n_0,m} \ll 1$, we have

$$\langle S^+(t)\rangle \approx \cos\left(\frac{g}{2}\Omega_{0,m}t\right)\cos\left(\frac{g}{2}\Omega_{1,m}t\right), \tag{6.26}$$

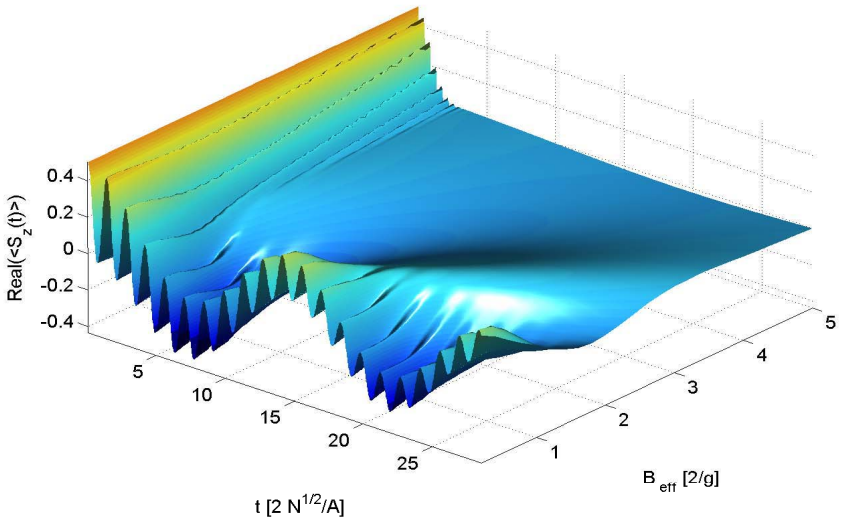

Figure 6.3: Evolution of the in-plane component of the electron spin, $\mathrm{Re}(\langle S^+(t)\rangle)$, as a function of time and effective magnetic field, B_{eff}. The electron is initially in the spin state $|\sigma_e\rangle = \frac{1}{\sqrt{2}}(|\uparrow\rangle + |\downarrow\rangle)$, $n_0 = 1$, $N = 10^4$. Other parameters are as in Fig. 6.1.

which clearly reflects the beating observed in Fig. 6.3.

In order to take into account the different possible excitation numbers in the mixture of bath states (6.14), again an integral over a Gaussian probability distribution is evaluated (under the resonance condition $x_{n_0,m} \ll 1$)

$$\mathrm{Re}\big(\langle S^+(t)\rangle\big) \approx \frac{\cos\left(\frac{g}{2}\Omega_- t + \widetilde{\nu}_-(t)\right)}{4\left(1+\frac{g^2}{4}\Gamma^4 t^2\left(\bar{\Omega}_{n_0}^{-1} - \bar{\Omega}_{n_0-1}^{-1}\right)^2\right)^{1/4}} + \\ + \frac{\cos\left(\frac{g}{2}\Omega_+ t + \tilde{\nu}_+(t)\right)}{4\left(1+\frac{g^2}{4}\Gamma^4 t^2\left(\bar{\Omega}_{n_0}^{-1} + \bar{\Omega}_{n_0-1}^{-1}\right)^2\right)^{1/4}}, \tag{6.27}$$

with

$$\begin{aligned} \Omega_\pm &= \bar{\Omega}_{n_0} \pm \bar{\Omega}_{n_0-1}, \\ \bar{\Omega}_{n_0} &= \sqrt{n_0+1}\left(1 - \frac{\overline{m}}{N} - \gamma_4\frac{n_0}{N}\right), \\ \widetilde{\nu}_\pm(t) &= \frac{1}{2}\arctan\left(g\Gamma^2 t/2\left(\bar{\Omega}_{n_0}^{-1} \pm \bar{\Omega}_{n_0-1}^{-1}\right)\right). \end{aligned} \tag{6.28}$$

As for the longitudinal dynamics, the transversal components are governed by two algebraic decays. However, in Eq. (6.27) the two terms are

equally important and their interplay can lead to interesting deviations from the monotonic decrease in the amplitude of the oscillation.

Noting that the functions $\tilde{\nu}_{\pm}(t)$ in the arguments of the cosines are only slight phase shifts, and that the denominators of the two terms in (6.27) are close to one for the first few Rabi periods in the case we consider ($\Gamma < \bar{m}/N \ll 1$), straightforward application a trigonometric identity makes it obvious that Eq. (6.27) captures both the beating of the two frequencies $\big(\cos(g\Omega_- t/2)+\cos(g\Omega_+ t/2) = 2\cos(g\bar{\Omega}_{n_0} t/2)\cos(g\bar{\Omega}_{n_0-1} t/2)\big)$ and the decay due to the mixture of bath states.

6.4 Squeezing

In the previous section we have seen that the bosonic description gives intuitive insight into the electron-nuclear spin dynamics in a QD, and allows for the calculation of electron spin dynamics in the resonant case at high polarization. In the present section we employ the bosonic formalism to design a novel scheme to squeeze the nuclear spins.

The reduction of the variance of the collective nuclear spin operators can enhance the electron spin coherence time. Several measurement schemes have been proposed for achieving this goal [36, 37, 38]. Here we consider nuclear ensembles polarized along the z-direction and we devise a scheme that allows to deterministically squeeze the state in the x- or y-direction.

To this end we propose to generate an effective Hamiltonian whose ground state is squeezed and cool the nuclear spins to that ground state. The effective Hamiltonian emerges from an iteration of resonant HF evolution and fast electron spin rotations. The cooling works essentially in the same way as the basic polarization schemes discussed in the literature, cf. the first chapters of this thesis. Using realistic values for the relevant parameters we find that squeezing of 90 %, or 10 dB, is possible. Such strongly squeezed states are interesting not only for tuning the electron spin dynamics, but in the more general context of high precision measurements [173].

Model– Consider the hyperfine evolution for a time $\nu\tau/M$, where ν is a real number, τ a time interval, and M a positive integer. When this evolution is sandwiched by two $\pi/2$-rotations of the electron spin around the x-axis the time evolution operator becomes

$$\begin{aligned} U' &= \exp\left(i\frac{\pi}{2}\sigma^x\right)\exp\left(-iH\nu\tau/M\right)\exp\left(i\frac{\pi}{2}\sigma^x\right) \\ &= -\exp\left[-ig\nu\tau/M\left(A^+\sigma^+ + A^-\sigma^- - A^z\sigma^z\right)\right] \\ &= -\exp\left[-iH'\nu\tau/M\right]. \end{aligned} \tag{6.29}$$

The rotations around the x-axis can be performed according to any of the proposals for single qubit gates, see e.g. Sec. 5.1.1 and references therein.

Alternating M times between the regular HF evolution for a time $\mu\tau/M$ and the "anti-HF" evolution given by U' generates up to an irrelevant phase

$$\begin{aligned} U_{\text{eff}} &= \left(\exp\left[-iH'_{\text{HF}}\nu\tau/M\right]\exp\left[-iH_{\text{HF}}\mu\tau/M\right]\right)^M \\ &\approx \exp\left[-ig\tau\left(\tilde{A}^-\sigma^+ + \tilde{A}^+\sigma^-\right)\right], \end{aligned} \tag{6.30}$$

where $\tilde{A}^- = \mu A^- + \nu A^+$ and $\tilde{A}^+ = (\tilde{A}^-)^\dagger$. The approximate equality becomes exact in the limit of $M \to \infty$ (Trotter-formula [174, 175]). Note that the z-part of the interaction cancels identically. In order to preserve the angular momentum algebra for the tilded collective operators in the homogeneous case, we impose that $\mu^2 - \nu^2 = 1$. Hence μ, ν can be parameterized by a single quantity ξ, such that $\mu = \cosh\xi$ and $\nu = \pm\sinh\xi$. The sign of ν can be controlled by the rotations that are applied between the HF evolutions: Replacing the x-rotations described above with y-rotations leads to a minus sign for the parameter ν. This freedom is important for the choice of the quadrature operator that is to be squeezed[4]. We will see later that the x- and y-variances are $\propto (\mu \mp \nu)^2$, respectively. Thus changing the sign of ν changes the squeezed quadrature. In the following we focus for clarity on $\nu = +\sinh\xi$, i.e. squeezing of the x-component.

The steady states of the cooling process for $\tilde{A}$-modes are given by

$$\left(\mu A^- + \nu A^+\right)|\psi_s\rangle = 0. \tag{6.31}$$

These are the states of our interest, whose properties we discuss in the following.

Squeezing in the bosonic limit– For clarity we first consider the case of ideal bosonic operators which is a good approximation for a very highly polarized initial nuclear spin state, i.e. $A^+ \to a^\dagger$. The transformed bosonic operators is $\tilde{a} = \mu a + \nu a^\dagger$, which is a canonical transformation, i.e. $[\tilde{a}, \tilde{a}^\dagger] = 1$, given $\mu^2 - \nu^2 = 1$. The time evolution operator in Eq. (6.30) thus describes a JC-like interaction of the electron and the *tilded* bosonic mode.

To see that the vacuum of the transformed bosonic operator $\tilde{a}$ is a squeezed state, note that $\tilde{a} = UaU^\dagger$ with $U = S(\xi) = \exp\left[1/2\left(\xi^* a^2 - \xi a^{\dagger 2}\right)\right]$ being the squeezing operator. Therefore $|\tilde{0}\rangle = S(\xi)|0\rangle$ implies $\tilde{a}|\tilde{0}\rangle = 0$, which shows that the squeezed vacuum $S(\xi)|0\rangle$ is really annihilated by $\tilde{a}$. The

[4] When y-rotations are used, the z-component of the HF interaction does not cancel in the effective Hamiltonian. This does not mean that the scheme we present has to be modified, but will lead to larger influences of the bath modes.

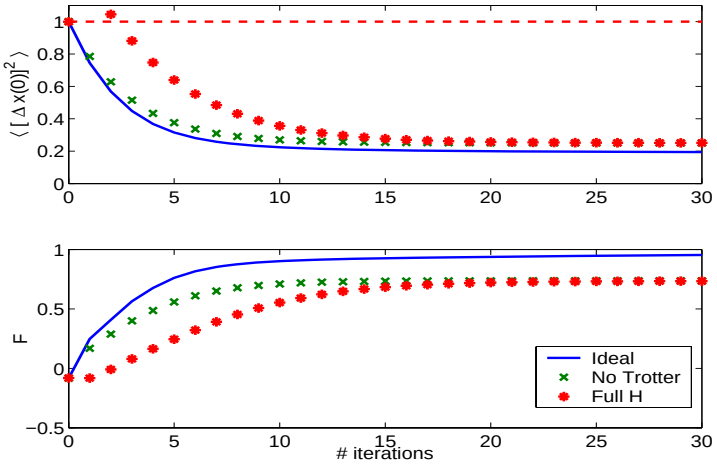

Figure 6.4: Upper plot: squeezing of the quadrature $x(0)$ below the standard quantum limit (dashed line). Lower plot: the fidelity F quantifying closeness to ideal squeezed vacuum state $S(\xi)|0\rangle$. $\mu = \sqrt{2}$ and $\nu = 1$ for both plots. A resonance situation with an initial nuclear state being a mixture of dark states with $\bar{m}/N = 0.1$, $N = 10^4$ is considered, and the width of the Gaussian electron wave function is $N/4$.

variance $\mathrm{Var}(O) = \langle(\Delta O)^2\rangle = \langle O^2\rangle - \langle O\rangle^2$ of the quadrature operators $x(\varphi) = ae^{i\varphi} + a^\dagger e^{-i\varphi}$, is for these states given by

$$\begin{aligned} \langle 0|S(\xi)^\dagger(\Delta x(0))^2 S(\xi)|0\rangle &= |\mu - \nu|^2 = e^{-2\xi}, \\ \langle 0|S(\xi)^\dagger(\Delta x(\pi/2))^2 S(\xi)|0\rangle &= |\mu + \nu|^2 = e^{+2\xi}. \end{aligned} \tag{6.32}$$

Numerical results– We now model the temporal evolution during the cooling process in more detail in order to take into account the corrections to the ideal bosonic model and the finite number M of interactions. We simulated the squeezing procedure first for fixed interaction time $g\tau = \pi/4$ and squeezing parameters $\mu = \sqrt{2}$, $\nu = 1$. The latter fixes the amount of squeezing achievable, by Eq. (6.32), but allows for the illustration of our scheme. Later we estimate how large the squeezing can be. The upper plot of Fig. 6.4 shows the evolution of the variance $\langle(\Delta x(0))^2\rangle$ for one such cooling process. When the Trotter-formula is not used (crosses and stars) the single qubit rotations are taken to be 100 times faster than the timescale for the Rabi-Oscillations g^{-1}. The time interval $g\tau$ is split into $M = 20$ pieces[5]. In both plots the solid line stands for the results in the case of an ideal bosonic Hamiltonian (no

[5]If single qubit rotations were severely limited in their speed, then M could not be increased infinitely, because otherwise in the outlined scheme the evolution due to H_0

bath) and under the assumption of the validity of the Trotter-formula, the crosses still assume an ideal Hamiltonian, but do no use the Trotter-formula and the stars take into account the influence of the bath additionally.

It is clearly shown in Fig. 6.4 that considerable squeezing below the standard quantum limit $\sqrt{1/2|\langle[x(0), x(-\pi/2)]\rangle|} = 1$ is achieved. The numerical plots confirm that the procedure does not crucially depend on the simplified situation we considered for the analytical arguments in the previous paragraphs: Even when a rather moderate polarization of 90% is assumed (same thermal state of the bath as has been used before, the main mode is in state $|0\rangle$), and the whole Hamiltonian $H_b^{(0)}$ from Eq. (6.19) is used, we find a reduction of the noise by more than a factor of 4, which is close to the ideal value for the parameters μ, ν considered in this example. The upper plot of Fig. 6.4 indicates that the imperfections in the amount of squeezing obtained are mainly due to the non-applicability of the Trotter formula (see also figure caption).

In the lower plot of Fig. 6.4 we show the fidelity

$$F = 1 - D(\rho_j, |\tilde{0}\rangle\langle\tilde{0}|), \tag{6.33}$$

where $D(\sigma, \rho) = \mathrm{tr}|\sigma - \rho|$ is the trace distance between σ and ρ [4], $|O| = \sqrt{O^\dagger O}$ and ρ_j the state of the nuclei after the removal of the jth electron. The fidelity F in all considered situations clearly shows that our scheme is driving the system towards the squeezed vacuum state. As the resulting state of our cooling procedure approximates the squeezed vacuum state very well, we find accordingly that the squeezing obtained approaches the theoretical ideal value $\langle(\Delta x(0))^2\rangle = 1 + 2(1 - \sqrt{2}) \approx 0.17$.

However, in the presented data even in the case of the ideal Hamiltonian and the assumption of the validity of the Trotter-formula, a fidelity of only $F = 0.95$ has been found. This is largely due to the fixed effective interaction time $g\tau = \pi/4$ chosen initially. For the data presented in the upper plot of Fig. 6.5, we made a more careful choice of interactions times. All $k_e(= 30)$ electrons that are passed through the dot have an individual interaction time

$$\tau_m = \pi/(g\sqrt{2(k_e - m + 1)}). \tag{6.34}$$

The mth electron will by this choice of interaction times transfer all excitations from $|\tilde{m}\rangle$ to $|\tilde{m} - 1\rangle$, starting from the state $|K_e\rangle$, because this time is exactly matched to a $\pi/2$ rotation for the Rabi frequency of for the transition from $\tilde{m}$ to $\tilde{m} - 1$. Thus the successive interaction with all K_e electrons will "sweep" all excitations to the ground state $|\tilde{0}\rangle = S(\xi)|0\rangle$ of the transformed

during the pulses is contributing more than the actual evolution in between them, which seriously harms the scheme.

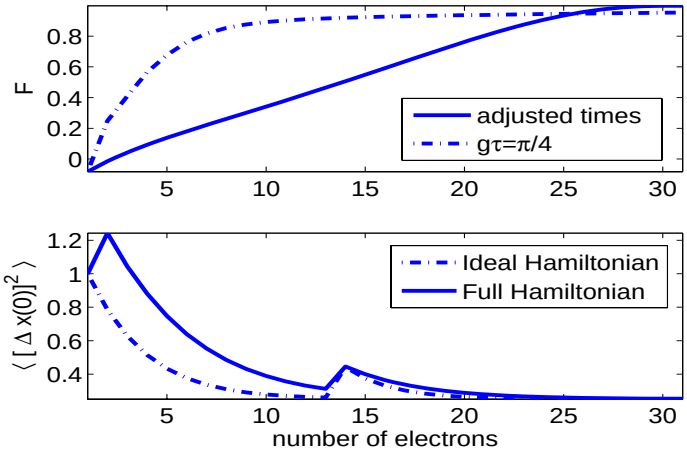

Figure 6.5: Upper plot: By choosing the interaction times more carefully (see text for details), the pure squeezed state $S(\xi)|0\rangle$ is approximated to a promille-precision (cf. Eq. (6.33)). Lower plot: At iteration 14 a wrongly polarized electron is injected. The resulting squeezing remains unaffected. All non-mentioned parameters are as for previous figure.

operator $\tilde{a}$. Note that as the initial state $|0\rangle$ only has very little occupation of states with a high number of excitations in the tilded basis, and consequently only a small number of electrons ~ 6 is sufficient to achieve a high fidelity.

The evolution of the fidelity F for such a cooling process is shown in the upper plot of Fig. 6.5 and one clearly sees the advantage over the naive choice of a fixed interaction time. The final fidelity is on the order of $1 - 10^{-3}$.

Finally we have qualitatively confirmed that the squeezing process is stable against the injection of wrongly polarized electrons, for which we give as an example the data presented in the lower plot of Fig. 6.5.

Squeezing in the homogeneous limit– Before going into a discussion of the influence of imperfections on our scheme, we verify the bosonic results by comparison with a homogeneous spin system. Squeezing of the collective nuclear spin is manifested in the variances of the x- and y-components of the total spin $I^\mu = 1/\sqrt{N}\sum_i I_i^\mu$ $(\mu = \pm, z)$. The calculation of the variances of these operators in the states defined by Eq. (6.31) is straightforward in the case of homogeneous coupling constants

$$\begin{aligned}\langle(\Delta I_x)^2\rangle_{\psi_s} &= -\frac{\mu-\nu}{\mu+\nu}\frac{2\langle I_z\rangle}{\sqrt{N}} = -e^{-2\xi}\frac{2\langle I_z\rangle}{\sqrt{N}},\\ \langle(\Delta I_y)^2\rangle_{\psi_s} &= -\frac{\mu+\nu}{\mu-\nu}\frac{2\langle I_z\rangle}{\sqrt{N}} = -e^{+2\xi}\frac{2\langle I_z\rangle}{\sqrt{N}},\end{aligned} \tag{6.35}$$

where we used the equation $\left(I_x e^{-\xi} + iI_y e^{+\xi}\right)|\psi_0\rangle = 0$. The states defined in Eq. (6.31) are thus minimal uncertainty states [171, 176]. Note that $\mathrm{Var}(A^{x,y}) \geq 0$, thus (6.35) implies that for $\langle I^z\rangle > 0$ there are no states satisfying Eq. (6.31) for $|\mu| > |\nu|$.

Comparing Eqs. (6.35) with the ones for the inhomogeneous system at high polarization in the bosonic description (6.32), one sees that the achieved squeezing depends in both situations in the same way on the parameter ξ. In the case of the spins it has an additional factor of $-2\langle I_z\rangle/\sqrt{N}$, which sets the standard quantum limit. At high polarization this factor approaches 1, thus converging to the bosonic prediction. While the spin description coincides with the bosonic one for homogeneous coupling constants, one of the major strengths of the bosonic formalism is the validity also for inhomogeneous couplings.

Experimental feasibility and maximal squeezing– The requirements regarding the control of the system are rather moderate: One needs to move electrons into and out of the dot on timescales of typical resonant hyperfine Rabi-oscillation, i.e. ns. As we have seen above these times do not need to be very precisely determined. Furthermore the single electron spin rotations need to be done fast in comparison to the timescale of the hyperfine flips.

In order to achieve as much squeezing as possible, ξ should be made as large as possible. This is turn means that μ and ν should be increased. Constraints are set by the facts that the electron spin rotations have to be carried out on a time scale t_{sq} fast compared to the electron hyperfine interaction timescale g^{-1} and the Trotter formula is valid only when $g\mu\tau/M \ll 1$. These technical constraints $gt_{sq} < (\mu,\nu)/M < 1$ can be readily fulfilled given that in optical setups $gt_{sq} \sim 10^{-3}$ without limiting the size of the squeezing parameter [52, 177]. In lateral dots the single qubit gates experimentally demonstrated so far, are on the $\sqrt{N}/A$-timescale [25], but there is much room for experimental optimization and furthermore one might use double-dot setups, where single qubit gates are conveniently mediated by exchange, again fulfilling the requirements given above [23, 29, 87]. The final limitation is set by the dynamics of nuclear spin system beyond the hyperfine interaction. At a fundamental level this decoherence time t_{nuc} is most likely set by dipolar interactions between the nuclei. Furthermore, in the discussion so far we have also neglected nuclear Zeeman energies, which show strong interspecies variation, and thus have to be included in our error analysis.

We consider in the following paragraph the effect on the squeezing procedure by one general local error σ^r $(r = x, y, z)$ at site l, $|\psi_s\rangle \to \sigma_l^r |\psi_s\rangle =: |\tilde{\psi}_s\rangle$ and show that the effect of such a local error scales with $1/N$ and shows no

strong increase with the squeezing. Using $\sigma^r\sigma^q\sigma^r = (-1)^{q\neq r}\sigma^q$ we have

$$\begin{aligned}\langle A^q\rangle_{\tilde{\psi}_s} &= \langle (A^q - g_l(\sigma_l^q + \sigma_l^r\sigma_l^q\sigma_l^r))\rangle_{\psi_s} = \langle (A^q - 2(1-\delta_{qr})g_l\sigma_l^q)\rangle_{\psi_s} \\ &= -2(1-\delta_{qr})g_l\langle\sigma_l^q\rangle_{\psi_s}.\end{aligned}$$

Using $\sigma_l^r(A^q)^2\sigma_l^r = (\sigma_l^r A^q\sigma_l^r)^2 = (A^q - 2(1-\delta_{qr})g_l\sigma_l^q)^2$ to compute $\langle (A^q)^2\rangle_{\tilde{\psi}_s}$ yields $\langle (A^q)^2\rangle_{\tilde{\psi}_s} = \langle (A^q)^2\rangle_{\psi_s} + (1-\delta_{qr})\left[4g_l^2 - 2g_l\langle (A^q\sigma_l^q + \sigma_l^q A^q)\rangle_{\psi_s}\right]$, and thus (with $\langle A^q\rangle_{\tilde{\psi}_s}$ from above) for the variance after an error σ^r,

$$\mathrm{Var}_{\tilde{\psi}_s}(A^q) = \mathrm{Var}_{\psi_s}(A^q) + (1-\delta_{qr})4g_l^2\left[1 - \langle\sigma_l^q\rangle^2 - \frac{1}{2g_l}\langle A^q\sigma_l^q + \sigma_l^q A^q\rangle\right].$$

The latter expectation values are calculated by writing the A^q in terms of tilded operators, e.g. $A^x = (\mu-\nu)(\tilde{A}^- + \tilde{A}^+)$, and then use the property $\tilde{A}^-|\psi_s\rangle = 0$. Proceeding in a similar fashion for the y-components yields

$$\begin{aligned}\mathrm{Var}_{\tilde{\psi}_s}(A^x) &= \mathrm{Var}_{\psi_s}(A^x) + 4g_l^2(1-\delta_{xr})\left[1 - \langle\sigma_l^x\rangle^2 - (\mu-\nu)^2\langle\sigma_l^z\rangle\right], \\ \mathrm{Var}_{\tilde{\psi}_s}(A^y) &= \mathrm{Var}_{\psi_s}(A^y) + 4g_l^2(1-\delta_{yr})\left[1 - \langle\sigma_l^y\rangle^2 + (\mu+\nu)^2\langle\sigma_l^z\rangle\right].\end{aligned}$$

Thus the effect of local errors on the variances scales with $g_l^2 \sim 1/N$, i.e. the local error rate is not scaled up by the number N of participating nuclei. Note that small $\mathrm{Var}(A^x) \sim (\mu-\nu)^2$ implies an error contribution scaling in the same way in μ, ν. In practice, one needs to average over all possible ways an error could occur. As seen from the above equation each of these term involves the unperturbed variance and an error term. The first term can thus be "pulled out" in the average, and the average over the error terms does not change the scaling with particle number. For the simulation of one Rabi period of the electron and the transformed nuclear degree of freedom, one has to fulfill $(\mu+\nu)g\tau \sim (\mu+\nu) \ll gt_{nuc}$. With the nuclear spin diffusion time typically many orders of magnitude ($\sim$5) longer than the Rabi period g^{-1} and roughly $k_e = 10$ electrons necessary for the squeezing procedure, this type of nuclear decoherence does not give strong constraints on the achievable entanglement. However, the spread of nuclear Zeeman energies is typically ~ 20 neV for the large magnetic fields required for resonant electron-nuclear HF flips. This yields $k_e(\mu+\nu) \ll 20$, which shows that squeezing is possible, but the amount of squeezing will be limited to below 10 dB. Note however, that resonant HF flips can be ensured by *effective* magnetic fields, that yield tenfold smaller nuclear Zeeman energies and thus dramatically improved squeezing. Ways to achieve these include ac-stark shifts in optical dots [178] and voltage bias in lateral double dots [23, 29, 49].

6.5 Conclusions

We have shown that the electron-nuclear hyperfine spin dynamics in QDs can be described by an effective Jaynes-Cummings(-like) model. It turned out that generally one has to consider several bath modes, but in the limit of high polarization or, in the language of this chapter, small ε, the single mode approximation becomes useful. With these results new avenues open up for the study and usage of HF interactions in QDs and allow for a closer connection to the vast QIP literature in quantum optics. As illustration for the usefulness of our approach, we have presented results on the electron spin evolution in the resonant regime, which is out of reach of traditional approaches employing a perturbation expansion in the external magnetic field. Furthermore we have designed a new way of achieving highly squeezed collective nuclear spin states.

Chapter 7

Entanglement Creation

The quest to realize quantum information processing (QIP) has motivated an impressive race to implement high precision preparation and manipulation of isolated two-level quantum systems (qubits) in a wide variety of physical settings [179]. A hallmark achievement for each such approach is the generation of quantum entanglement through controlled interaction between two or more qubits. Since switchable direct interactions between qubits often entail additional decoherence mechanisms, many QIP proposals rely on interactions *mediated* by an additional quantum system [12, 19, 52]. As a rule this mediator (just as the qubits themselves) needs to be prepared in a pure state to achieve high-fidelity quantum operations and it may look futile to use a high-entropy mesoscopic spin bath for this task. In contrast to these expectations, we show here that high-fidelity entanglement generation can be realized even if the qubits can only interact with an arbitrarily mixed spin bath, provided that this interaction can be switched on and off, single-qubit unitaries are available, and the bath has slow internal dynamics. This is motivated by and will be illustrated through the example of electron-spin qubits in quantum dots (QDs) [13], where the ensemble of lattice nuclear spins represents a strongly coupled but slowly evolving spin bath.

Before introducing this system, it is interesting to note, that entanglement via a small, moderately mixed system has been shown to be possible, e.g., for trapped ions [180, 181, 182, 183]. On the other hand, entanglement generation via a bath has been predicted before, but these studies focused on short time transient effects [184], provided proofs of principle [185, 186], or required a highly structured environment [187]. In contrast, we present an experimentally realizable high-fidelity scheme, which works even for infinite bath temperature. These results shed new light on the possibility to use baths as resources.

Nuclear spins in quantum dots have received much theoretical [59, 65,

70, 107, 188, 189] and experimental [23, 30] attention in the QIP context as the main source of electron-spin decoherence through the strong hyperfine coupling. It has also been noted that their slow internal dynamics and long decoherence time [62, 63] make the ensemble of nuclear spins useful as a quantum memory [42] or for quantum computation (Chapter 5). These applications, however, require careful and yet unachieved preparation of the nuclear system (Chapters 2 and 3). What we show here is, that the unprepared, highly or even maximally mixed (nuclear) system is able to mediate coherent interaction between electrons and thereby allows the generation of highly entangled states of many (electron spin) qubits without any electron-electron interaction.

We consider in this chapter a QD in the single-electron regime and assume the availability of single-electron state preparation and measurement as well as the controlled shuttling of prepared electrons into and out of the QD. Additionally required is control of the detuning (e.g., by a magnetic or electric field), which switches the hyperfine (HF) interaction between resonant and off-resonant regimes. We first in Section 7.1 show how sequential interaction of three electrons with the nuclear bath can generate a maximally entangled pair of electron spins. More generally, the class of states that can be generated via the spin bath is characterized in terms of matrix product states (Section 7.1.2). In Section 7.2 we show that imperfect electron spin operations, inhomogeneous couplings between electron and nuclei and modifications to the ideal static spin bath still allow for the scheme to be realized. In situations where spin-orbit coupling is large, our scheme can be an interesting alternative to the standard exchange based setups, because it does not involve occupation of any higher orbital levels [190, 191]. An independent iterative entanglement generation scheme (in contrast to the sequential one) is presented in Sec. 7.3. It allows for high fidelity generation of Bell pairs in the same infinite temperature situation, with the difference that an adiabatic, instead of a fast, magnetic pulse changing from resonant to off-resonant conditions is used. Its performance is quantified numerically and shown to be very good. The question whether electrons and nuclei become entangled during the HF interaction is addressed in Sec. 7.4, where we show that this entanglement is very weak indeed. That makes the high fidelity entanglement between the electrons more surprising (note Ref. [185] though). The chapter, and this thesis, closes with some concluding remarks in Section 7.5.

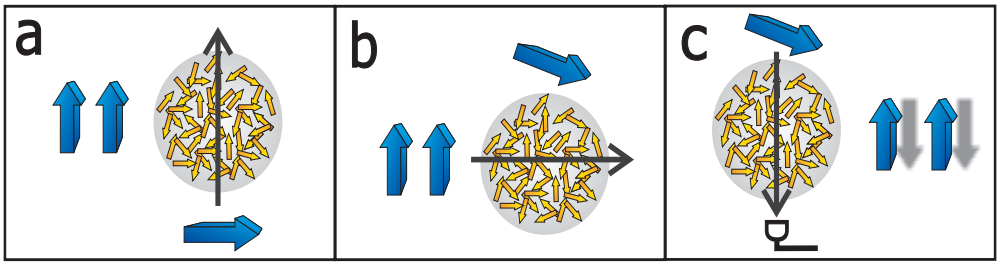

Figure 7.1: (Color online) Sketch of the protocol. (a) The z-polarized "control electron" interacts resonantly with the nuclear spin bath. (b) A sequence of x-polarized electrons interacts off-resonantly with the bath. (c) The control electron interacts resonantly again and is then measured in the z-basis. Result $\downarrow$ projects the other electrons to a GHZ state.

7.1 Entanglement Generation

We consider (again) each electron coupled via the uniform Heisenberg interaction to the bath of N nuclear spins and to an external magnetic field B_z

$$H = \frac{A}{2N}\left(I^+S^- + S^+I^-\right) + \frac{A}{N}I^zS^z + g^*\mu_B B_z S^z. \tag{7.1}$$

$\mathbf{S}$ is the spin operator for the electron and $I^\mu = \sum_i I_i^\mu$ are the three components of the collective nuclear spin operators ($\mu = \pm, z$ and $[I^+, I^z] = -I^+$, $[I^+, I^-] = 2I^z$). g^* is the electron g-factor and μ_B the Bohr magneton. We consider spin-1/2 nuclei, neglect bath dynamics, the bath spins' Zeeman energies, and inhomogeneities in the Heisenberg couplings for now, and discuss the validity of these approximations in Sec. 7.2.

We use the Dicke basis $\{|I, m, \beta\rangle\}$, where $I(I+1)$ is the eigenvalue of the collective angular momentum operator $\mathbf{I}^2$, and the eigenvalue of I^z is given by m. β is the permutation quantum number [104]. The initial state of the spin bath in the following is the identity

$$\rho_{\text{bath}} = \frac{1}{2^N}\sum_{I,m,\beta} |I, m, \beta\rangle \langle I, m, \beta| = \mathbb{1}_{2^N}/2^N. \tag{7.2}$$

In the following we omit β, because its only effect is to give a weight $D(I)$ to the (I, m)-subspace[1]. This situation of a completely unknown bath state is, e.g., a suitable description for GaAs QDs even at temperatures as low as 100 mK [23, 30]. For the rest of this chapter, time will be given in units of N/A.

[1] Considering small imperfections, β does become important, as discussed and explained in Sec. 7.2.

7.1.1 Two Qubit Entanglement

The first electron spin (which we also refer to as ancilla electron) is prepared in the state $|\uparrow\rangle$ and interacts *resonantly* for a time t_1 with the nuclear spin bath. Working in an interaction picture with $H_0 = -1/4$ gives the evolved state for each of the terms in the above mixture

$$U|I,m,\uparrow\rangle = c_{Im}(t_1)|I,m,\uparrow\rangle + s_{Im}(t_1)|I,m+1,\downarrow\rangle, \tag{7.3}$$

with $U = e^{-iHt_1}$ and

$$c_{Im}(t_1) = \cos\left(\frac{(1+2I)t_1}{4}\right) - i\frac{1+2m}{1+2I}\sin\left(\frac{(1+2I)t_1}{4}\right),$$
$$s_{Im}(t_1) = \frac{-2i\sqrt{(I-m)(1+I+m)}}{1+2I}\sin\left(\frac{(1+2I)t_1}{4}\right).$$

Then the next electron spin, initial state $|+\rangle = 1/\sqrt{2}(|\uparrow\rangle + |\downarrow\rangle)$, interacts for a time t_2 *off-resonantly* (e.g., in the presence of a large B_z) with the spin bath. For $g^*\mu_B B_z \gg A/\sqrt{N}$, the flip-flop part of the Hamiltonian can be approximately neglected [67], yielding

$$V(t_2)|m,+\rangle = \frac{1}{\sqrt{2}}|m\rangle\big(e^{-i(\tilde{B}+m)t_2/2}|\uparrow\rangle + e^{+i(\tilde{B}+m)t_2/2}|\downarrow\rangle\big),$$

where $\tilde{B} = g^*\mu_B B_z N/A$ and the index I has been omitted for brevity. Remarkably, by choosing the interaction time $t_2 = \pi$, the state of the electron is transformed to

$$(-i)^m\,|(-)^m\rangle\,,$$

i.e. for even $m = 2k$ to $(-1)^k|+\rangle$ and for odd $m = 2k+1$ to $-i(-1)^k|-\rangle$. For convenience we assume $\tilde{B}t_2/2 = 2\pi\ell$, $\ell \in \mathbb{N}$, which is adjusted by the "free" parameter of the large field.

With the third electron, also in $|+\rangle$ initially and the same interaction, the state becomes

$$\pm c_{Im}(t_1)|I,m,\uparrow\rangle|\pm\pm\rangle \mp s_{Im}(t_1)|I,m+1,\downarrow\rangle|\mp\mp\rangle, \tag{7.4}$$

with upper (lower) signs referring to even (odd) m.

In the final step, the ancilla electron interacts resonantly with the nuclei again [cf. Eq. (7.3)], giving

$$\begin{aligned}&\pm c_{Im}(t_1)\big|\pm\pm\big\rangle\big[c_{Im}(t_1)|m,\uparrow\rangle + s_{Im}(t_1)|m+1,\downarrow\rangle\big]\\ &\mp s_{Im}(t_1)\big|\mp\mp\big\rangle\big[c^*_{Im}(t_1)|m+1,\downarrow\rangle + s_{Im}(t_1)|m,\uparrow\rangle\big],\end{aligned} \tag{7.5}$$

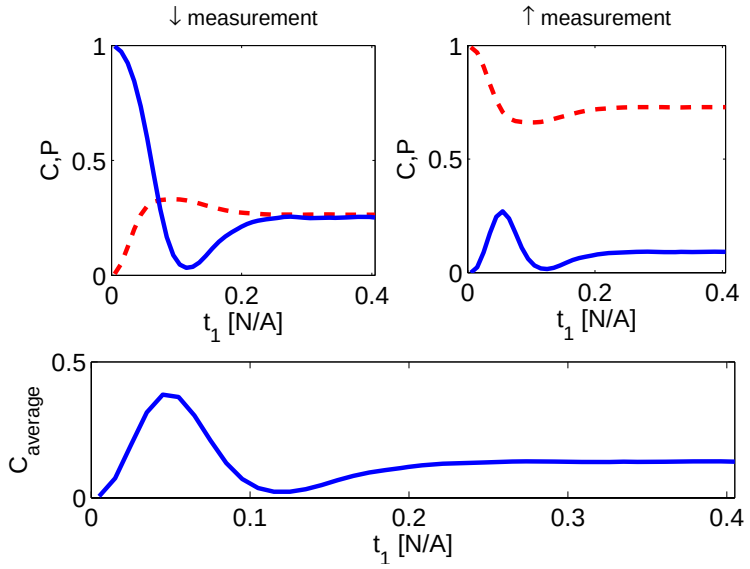

Figure 7.2: (Color online) Creation of 2-qubit entanglement for $N = 10^3$ bath particles. Solid, blue lines show the concurrence C [192] after a spin up and down measurement, respectively (upper plots), and the average concurrence (lower plot). Dashed, red lines show the probability P for a spin up or down measurement.

for even/odd m and is eventually measured projectively in the z-basis. If the measurement outcome is $\downarrow$ it is clear from Eq. (7.5) that in each subspace the second and third electrons are in the maximally entangled state

$$|m+1\rangle\big(|++\rangle - e^{\pm i\phi_m}|--\rangle\big)/\sqrt{2},$$

where the phase $\phi_m = 2\arg(c_{Im})$ depends on the quantum numbers I and m, leading to a washing out of the entanglement when the average over the different subspaces is taken. However, for short times ($(2I+1)t_1 \ll 1$ for typical values of $I \sim \sqrt{N}$) this phase tends to zero and near ideal entanglement is created, albeit at the price of a lower success probability, see Fig. 7.1. In this figure we present the concurrence [192] as a measure of entanglement; it is defined as

$$C(\rho) = \max\{0, r_1 - r_2 - r_3 - r_4\},$$

where the r_i are the square roots of the eigenvalues of $\rho\tilde{\rho}$ in descending order. Here $\tilde{\rho}$ is $\tilde{\rho} = (\sigma_y \otimes \sigma_y)\rho^*(\sigma_y \otimes \sigma_y)$ with the complex conjugation taken in the standard basis.

In the long time limit, the probability for a, say, $\downarrow$ measurement becomes constant. The reason for not showing oscillations- as one might have

suspected from inspection of Eq. (7.5)- lies in the subspace dependent Rabi-like frequencies which create a "dynamic equilibrium" leading to an approximately constant final measurement probability[2]. This has been similarly noted for the uninterrupted evolution of a single electron by a simple semi-classical theory, see e.g. Ref. [66]. Also the amount of created entanglement stays constant and finite in the quasi steady state ($C_{qss} \approx 0.15$ in the example of Fig. 7.2), showing that the subspace-dependent phases discussed in the previous paragraph are not fully random.

In the limit of small particle number, $N \to 1$, boundary effects decrease the performance (in particular: the success probability) of the entanglement protocol: The state $|I, I\rangle$ does not interact with the first electron; an unwanted effect that becomes more relevant for smaller particle numbers.

7.1.2 Multipartite Entanglement

The presented scheme generalizes in a straightforward manner to multipartite entanglement creation. Following the same protocol using n electrons with arbitrary initial states $|\psi_1\rangle, \ldots, |\psi_n\rangle$, the final state becomes

$$|\Psi_n\rangle = 1/\sqrt{2}\left(\mathbb{1} + [(-1)^{m+1} i\sigma_z]^{\otimes n}\right)|\psi_1, \ldots, \psi_n\rangle, \tag{7.6}$$

where the matrices are given in the standard z-basis and we assumed the short time limit $t_1 \to 0$ for clarity. If $|\psi_k\rangle = |+\rangle$ for all k, this is a n-partite GHZ state. The m-dependent relative phase in the above equation restricts to generation of GHZ-states with even particle number.

When multiple resonant interactions with the ancilla and varying interaction times are allowed, a larger class of states becomes accessible. To see which states can be prepared in principle, we exploit the similarity of our setup to the sequential entanglement generation scheme analyzed in Ref. [193]. There it was shown, that all the matrix product states (MPS) of bond dimension d can be prepared if a string of qubits interacts sequentially with a d-dimensional ancilla system and *arbitrary unitaries* can be performed on ancilla and qubit in every step.

To apply this result to the present case, ancilla electron and nuclear spin system together represent the control qubit: an effective $d = 2$ system with Hilbert space spanned for given (I, m) by $\{|I, m, \uparrow\rangle, |I, m+1, \downarrow\rangle\}$. To see that arbitrary unitaries are possible, note that x-rotations of the control qubit are caused by resonant interaction, while a static B_z-field causes z-rotations. From these, all single qubit gates on the control qubit can be

[2]The finite number of frequencies implies a "revival" at long timescales (out of the region of our interest).

constructed. The off-resonant interaction considered before performs essentially a CNOT gate between the passing and the control qubit. In the CNOT gate the "control qubit" is the control and the passing electron the target, in the $|\uparrow,\downarrow\rangle$ and $|\pm\rangle$ basis, respectively. Combined with single-qubit gates (on the passing electron), this seems to be enough to allow for arbitrary transformations on the coupled control-target system. However, the situation is more complicated since the effective gate performed by the off-resonant interaction *differs* for even and odd parity of the control qubit, namely $V(\pi) = e^{(-1)^m i\frac{\pi}{4}\sigma_z}\sigma_{x,1}^m CNOT_{1\to 2}\sigma_{x,1}^m$, i.e., there is not only, as seen before, a parity-dependent phase but whether logical-0 or logical-1 controls the bit-flip in the passing qubit also depends on the parity of m. One way to remove this m-dependence and enable the generation of arbitrary states is to perform an "I^z parity measurement" by sending an electron $|+\rangle$ into the dot, and then measure it in the $|\pm\rangle$ basis after off-resonant interaction for a time π. Depending on the outcome, either the odd or the even states are projected out. Remarkably, gaining this single bit of information about the 2^N-dimensional bath then allows us to remove all m-dependence and perform clean CNOT-gates. Hence *arbitrary* two-qubit gates can be performed, which implies that all MPS with two dimensional bonds can be sequentially created [193].

Direct resonant interactions lead to very low fidelity x-rotations due to averaging over the different subspaces, indicating that prior measurement [38, 37, 36] or cooling [74] of the spin bath might be necessary. More sophisticated control schemes, however, allow for near unit fidelity single qubit rotations with no prior preparation: In Ref. [194] is was proven that high fidelity arbitrary single qubit gates can be effected by a Hamiltonian $H = \delta\sigma_z + \Omega(\sigma_x\cos\phi + \sigma_y\sin\phi)$, when only the parameter ϕ can be controlled precisely. For δ and Ω it is sufficient to know that they are non-zero for some value of a controllable external parameter and zero for another. In our situation we have the three Hamiltonians

$$
\begin{aligned}
H_1 &= \Delta\sigma_z = B\mu_I\sigma_z/2 \quad \text{nuclear Zeeman} \\
H_2 &= \frac{A}{2N}[(m+1/2)\sigma_z + \xi_{I,m}\sigma_x] \quad \text{resonant HF} \\
H_3 &= \frac{A}{2N}[\pm(\tilde{B}+m+1/2) + \tilde{B}\mu_I/(\mu_B g^*)]\sigma_z \quad \text{off}-\text{resonant HF}
\end{aligned}
$$

at hand. The Pauli matrices are acting on the control qubit, μ_I is the nuclear magnetic moment and $\xi_{I,m} = \sqrt{I(I+1) - m(m+1)}$. The plus and minus signs for H_3 can be effected through spin flips of the passing electron (recall that $\sigma_x e^{iHt}\sigma_x = e^{i\sigma_x H\sigma_x t}$ and $\sigma_x\sigma_z\sigma_x = -\sigma_z$). These Hamiltonians can be

switched on and off (adiabatically [3]) at will. Appropriate iterations of evolutions can lead to effective Hamiltonians of weighted sums and commutators of $H_{1,2,3}$. In particular, the subspace independence of the parameter $\Delta \propto B$ allows for generation of any weighted sum of σ_x and σ_y with the weights being (I, m)-independent, thus making the results of Ref. [194] applicable. We have thus shown that while naive use of resonant interactions will lead to poor gate fidelities for the control qubit, enhanced control schemes still allow for full access to high fidelity rotations. Hence, in principle, the interactions outlined above are sufficient to prepare all $d = 2$-MPS with high fidelity and, if the passing electrons can be brought into interaction with the ancilla again at any time, universal quantum computation on an electron-spin quantum register can be performed, with all interactions mediated by the highly mixed spin bath.

We finally note that for the generation of particular multipartite entangled states it might be more favorable to enlarge the set of allowed operations, than to aim for situations where all MPS-2 can be created. The n-partite W-state is such an example: a first ancilla interacts off resonantly for a time π and is subsequently measured in the $\pm$ basis, and thereby the state of the nuclei is projected to either even or odd values of m, respectively. The next n spins interact resonantly for short times Δt with the bath leading to first order in Δt to the state

$$|m, \uparrow, \ldots, \uparrow\rangle + i\Delta t |m+1\rangle \sum_{i=1}^{n} |\downarrow, \ldots, \downarrow, \uparrow_i, \downarrow, \ldots, \downarrow\rangle.$$

Now a second ancilla measures the parity of the state in the same way as the first one did previously. If the measurement outcomes coincide, the scheme has failed, if not, the W-state is successfully created. Note that the corrections to the state come only in $\mathcal{O}((\Delta t)^3)$. The roles of resonant and off resonant interactions are thus somewhat reversed for W- and GHZ-states, but both can be generated (probabilistically) via the mixed spin bath with simple and straightforward protocols.

7.2 Realization with Quantum Dots

We discuss now various couplings that have been neglected in the idealized Hamiltonian Eq. (7.1) but are present in the QD setup. We are concerned here only with their effects on the basic entanglement generation scheme. It

[3] We assume here perfect storage of the ancilla electron in a "protected" region free of HF interactions. HF Hamiltonians can then be switched adiabatically by shifting the electron wave function slowly from the protected region to the spin bath.

is clear that the scheme can only work as long as it is fast compared to the electron T_2 time, since the coherence of the ancilla electron must be preserved. We see below that neither nuclear dynamics nor inhomogeneity place more stringent conditions on our scheme.

Inhomogeneity– The HF Hamiltonian in QDs has a slightly different form from the one in Eq. (7.1), because the collective bath operators have a spatial dependence $I^\mu = \sum_i \alpha_i I_i^\mu$, $\mu = \pm, z$. The coupling constants α_i are $\propto \mu_{I,i}|\psi_e(r_i)|^2$, with $|\psi_e(r_i)|^2$ being the probability of finding the electron at location r_i. We focus our analysis on short resonant interaction times $\Delta t_1 \ll \sqrt{N}/A$. The state after the above protocol conditioned on a $\downarrow$ measurement is proportional to

$$\sum_{\psi,\psi'} \langle\psi'|A^+ e^{i(\sigma_1^z+\sigma_2^z)A^z t_2} + e^{i(\sigma_1^z+\sigma_2^z)A^z t_2} A^+|\psi\rangle |++\rangle \times \text{H.c.},$$

where the Pauli matrices act on the off-resonant electrons. Evaluating the matrix elements and introducing the normalization we get

$$\rho(t_2) = \frac{1}{\mathcal{N}(t_2)} \sum_j \alpha_j^2 \sum_{\substack{i_1,\ldots,i_N=\pm 1/2 \\ i_j=-1/2}} (|+_0\, +_0\rangle + |-_j\, -_j\rangle) \times \text{H.c.}, \tag{7.7}$$

with the states

$$\begin{aligned} |+_0\,(t_2)\rangle &= e^{i\omega_0 t_2/2}|\uparrow\rangle + e^{-i\omega_0 t_2/2}|\downarrow\rangle, \\ |-_j\,(t_2)\rangle &= e^{i\omega_j t_2/2}|\uparrow\rangle + e^{-i\omega_j t_2/2}|\downarrow\rangle, \end{aligned}$$

the frequencies $\omega_0 = \omega_0(\{i\}) = \sum_\ell \alpha_\ell i_\ell$ and $\omega_j = \omega_0 + \alpha_j$ and the normalization

$$\mathcal{N}(t_2) = 4\sum_j \alpha_j^2[3 + \cos(\alpha_j t_2)].$$

The time dependence of the states has been omitted for brevity in the above formula. Straightforwardly one now determines the overlap F with the desired maximally entangled state $\langle\phi_-|\rho(t_2)|\phi_-\rangle$

$$F(t_2) = 2\sum \alpha_j^2 \Big/ \sum_j \alpha_j^2(3 + \cos(\alpha_j t_2)). \tag{7.8}$$

This expression readily gives the fidelity for arbitrary particle numbers and arbitrary distributions of coupling constants. For $N \gg 1$, the obtained entanglement is independent of particle number, and for the relevant situation of Gaussian coupling $F = 0.90, 0.83, 0.78$ for 1D, 2D and 3D, respectively. Including the difference in magnetic moments for Ga and As [^{75}As: $\mu_{I,\text{As}} = 1.44$,

^{69}Ga: $\mu_{I,\mathrm{Ga},1} = 2.02$ (60%) and ^{71}Ga: $\mu_{I,\mathrm{Ga},2} = 2.56$ (40%)] these values become $F = 0.83, 0.78, 0.74$, indicating that our scheme can tolerate realistic inhomogeneities.

For small inhomogeneity (as measured e.g. by the variance in the coupling constants) we find the optimal time $t_2^{\mathrm{opt}} = \pi\gamma_3/\gamma_4$, with $\gamma_x = \sum_j \alpha_j^x$. The corresponding fidelity is $F = 1 - \frac{\pi^2}{2}[1 - \gamma_3^2/(\gamma_2\gamma_4)]$.

Nuclear Zeeman energies– Considering one homogeneously coupled species of nuclear spins, the state of Eq. (7.4) will have an additional m-dependent phase. In each invariant subspace this produces an overall phase $\propto B_z t_2 m$, and a relative phase $\propto B_z t_2$ between the two parts of the superposition. This might not seem harmful, but due to the parity effect, the *sign* of the phase depends on the parity of m. Since this phase is of order π it could spoil the protocol. However, by simply waiting for a time t_p after each of the n electrons has passed the total relevant phase becomes $(-1)^m n B_z(t_2 + t_p)$ and with $t_p + t_2$ an integer multiple of π/B_z is again m independent. For systems with strongly varying nuclear magnetic moments, one can empty the QD and reverse the magnetic field, which causes complete cancellation of the undesired phase.

Bath dynamics– The major internal dynamics of nuclear spins in QDs stems from the indirect hyperfine mediated interaction, and the direct dipolar interaction [70, 189]. Both mechanisms lead to bi-local errors that contain spin flip terms $\propto (\Gamma_d^{kl} + \Gamma_i^{kl}) I_k^+ I_l^-$ and phase changing zz-terms $\propto \Gamma_d^{kl} I_k^z I_l^z$. The transition rates for direct and indirect interactions are Γ_{dd}/r_{kl}^3 and $\alpha_i\alpha_j/\Omega_e$, respectively, where Ω_e is the electron Zeeman splitting and $r_{kl} = |\mathbf{r}_k - \mathbf{r}_l|$.

The dephasing terms $\propto I_i^z I_j^z$ lead to a relative phase between the terms in Eq. (7.7), similar to the nuclear Zeeman energies. The energy difference, i.e. the Zeeman splitting of a single nuclear spin in the field of its neighbors, in a mean field treatment, is a few times Γ_{dd} [74]. Thus our scheme requires $t_2\Gamma_{dd}/r_0^3 = N\Gamma_{dd}/(r_0^3 A) \ll 1$; given $r_0^3/\Gamma_{dd} \approx 0.1$ms [59] for nearest neighbors, and $A^{-1} \approx 40$ ps, this is readily fulfilled even for large dots.

We have seen above that for each term in the mixed state, the qubits rotate in the equatorial plane of the Bloch sphere with frequencies α_j when the jth nuclear spin has been flipped. If this particular spin is involved in a spin flip due to bath dynamics, the resulting rotation with "wrong" frequency spoils the entanglement. The errors in the rotation angle for the term containing the flip of the jth spin are $\epsilon_{d,i}^j = \sqrt{\sum_k (\Gamma_{d,i}^{kj} t)^2 (\alpha_j - \alpha_k)^2 (t_2^{\mathrm{opt}})^2}$, and the final overall errors $\sum_j \alpha_j^2 \epsilon_{d,i}^j / \sum_j \alpha_j^2$. We evaluate the above sums in the continuum limit for Gaussian couplings and get for the indirect flips a total error $\delta_i \pi^2 A \gamma_3^2/(\gamma_4^2 \Omega)$, where δ_i is determined by the integrals over the cou-

pling constants. Taking $A/\Omega < 1$ for the large (> 1 T) fields that we require, we find errors 2.4%, 2.0%, and 1.5% for 1D, 2D, and 3D, respectively, for $N = 10^4$ (we define N here as the number of nuclei within the $1/(2e)$-width of the Gaussian). For the direct nuclear dipole-dipole transitions the error is of size $\delta_d \pi^2 \gamma_3^2 \Gamma_{dd}/(A r_0^3 \gamma_4^2)$, where numerical evaluation of the "dipolar integrals" δ_d yields $0.01\%, 0.8\%, 5\%$ for the same situation as above. This overall error is thus on the order of a few percent for realistic situations.

Storage– We implicitly assumed the possibility of storing the electrons protected from any bath. In QD structures this could be achieved by shuttling the electrons to a nuclear spin-free region or employing dynamical decoupling schemes, see e.g. [70]. The required storage times of a few tens of μs should be readily achieved.

Imperfect Electronic Operations– A finite probability that an up-electron is wrongly detected as a down electron (or vice versa), degrades the final entanglement. However, as only one electron needs to be measured, the effect is no worse for the n-partite GHZ-state than for the Bell state $|\Phi^+\rangle$. The same goes for variations in the resonant interaction time t_1. In contrast, errors in the electron preparation and variations in the off-resonant interaction time t_2, since they affect each of the n electrons lead to a fidelity reduction that scales exponentially with n. Variations in t_2 must be such that $\tilde{B}\delta t_2 \ll 1$ with $\tilde{B} \gg A/\sqrt{N}$, which makes this the most stringent, but still realistic [86, 110], requirement for electron timing.

Fidelity of the control qubit rotations– As discussed in Sec. 7.1.2 the resonant interaction of the ancilla electron and the spin bath can be viewed as a x-rotation of the control qubit in the sequential generation scheme. In the ideal case the rotation would be $U = -i\sigma^x$, cf. Eq. (7.3). The difference between the actual and the ideal unitary operation [195] for each I and m is quantified as

$$\mathcal{D}_{Im}(t) = \left\| -i\sigma^x - \begin{pmatrix} c_{Im}(t) & s_{Im}(t) \\ s_{Im}(t) & c^*_{Im}(t) \end{pmatrix} \right\|,$$

where $\|A\| = \sqrt{\mathrm{tr} A^\dagger A}$ is the Frobenius norm. We find

$$\mathcal{D}_{Im}(t) = \sqrt{1 - \frac{2\sqrt{(I-m)(I+m+1)}}{1+2I} \sin((1+2I)t/4)}.$$

We define the fidelity $F(t) \in [0, 1]$

$$F(t) = 1 - \overline{\mathcal{D}}(t)/\sqrt{8},$$

with $\overline{\mathcal{D}}(t) = \sum_{Im} D(I)\mathcal{D}_{Im}(t)$ being the relevant average distance for a mixed state.

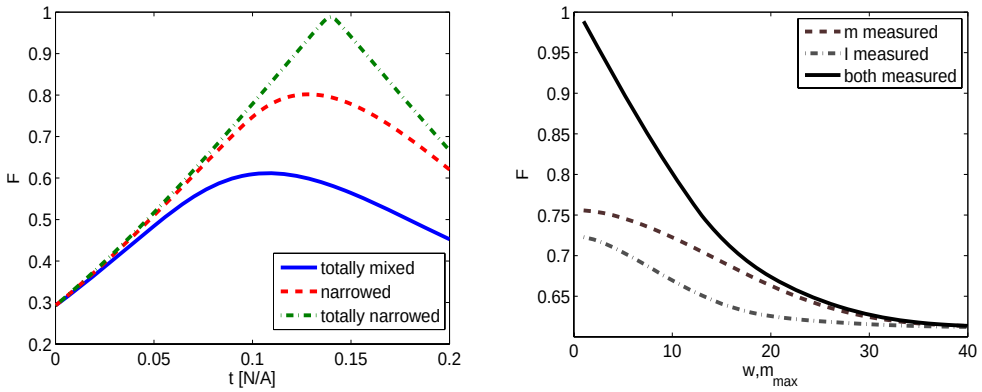

Figure 7.3: (Color online) Influence of a nuclear spin state measurement on the fidelity of the control qubit operations for $N = 10^3$. Left plot: The fidelity F as a function of time for the completely mixed state (blue solid line), a partially narrowed spin distribution (red dashed line, $m_{\max} = 9$ and $w = 9$), and a fully narrowed distribution (green dashed-dotted line). Right plot: Fidelity as a function of the measurement parameters $m_{\max}$ and w, for individual measurements of I and m (non-solid lines) and simultaneous ones (solid line).

The optimal fidelity for the completely mixed state is $F(t_{\text{opt}}) \approx 0.62$, which is rather low -as expected- and thus leads us to the study of the effect of nuclear state measurements [36, 37, 38] on the control qubit operations. For simplicity we consider I and m distributions after the measurement which are described by the original (pre-measurement) ones, but are "cut" at the edges, i.e. $p(I, m) = 0$ if $I \notin [\bar{I}-w, \bar{I}+w]$ or if $m \notin [-\min(I, m_{\max}), +\min(I, m_{\max})]$. The parameters describing how well total angular momentum and its z projection have been measured are thus w and $m_{\max}$, respectively.

In Fig. 7.3 we present the time evolution of the fidelity for different nuclear spin (I-,m-) distributions (left plot). Clearly, for the fully narrowed distribution ideal operations are possible. Exemplary we present the fidelity for a distribution which has been narrowed down by approximately 1/2 (for $N = 10^3$ spins, we take $m_{\max} = 9$ and $w = 9$), which yields a fidelity of 80%. Furthermore the dependence of the fidelity on the measurement parameters $m_{\max}$ and w is studied (right plot). It turns out that the measurement of either z-projection or total angular momentum does not yield a significant increase in the fidelity (it stays below 80%), but only the simultaneous measurement yields the desired high fidelities.

In this paragraph we have quantified the influence of generic nuclear spin measurements on the fidelity of the control qubit rotations. The rather high

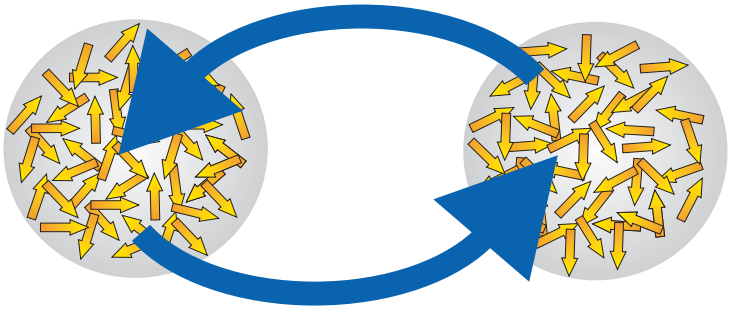

Figure 7.4: (Color online) Sketch of the iterative protocol. Two (electron-) spins-1/2 interact sequentially multiple times with two spin baths for short times in the presence of an adiabatically changed magnetic field.

accuracy needed both for the z-component and the total angular momentum indicates that the control theoretic ideas outlined in Sec. 7.1.2 and Ref. [194] are likely the more promising route. The combination of cooling techniques as outlined in Chapters 2 and 3 with measurements as outlined above would be another interesting option, that likely leads to further increase of the performance of the scheme. (Note that the last paragraph discussing the fidelity of rotations is relevant only for the involved setup aiming for arbitrary rotations; for the GHZ-generation the requirements are much more modest.)

7.3 Iterative Scheme

We consider two (electron-)spins that interact with two spin baths iteratively (the situation can be envisioned as a circular two-electron current running through two quantum dots, see Fig. 7.4). The two spins are first prepared in the product state $|\uparrow\downarrow\rangle$ at high magnetic field B_z. Adiabatically lowering and raising the field induces a phase for the triplet, but not the singlet component of the two-spin state. The phase can be chosen ($\theta = \pi/2$) to yield a maximally entangled state. Note that the electron envelope wave functions are not overlapping during the whole course of the entanglement generation protocol, and thus the Pauli principle plays no direct role and possibly harmful occupation of higher lying orbitals is avoided.

We assume that the interaction of each electron with each bath is short compared to the typical hyperfine interaction timescale $t_{\rm int} \ll \sqrt{N}/A$, and decoherence effects occurring during the electron shuttle can be neglected.

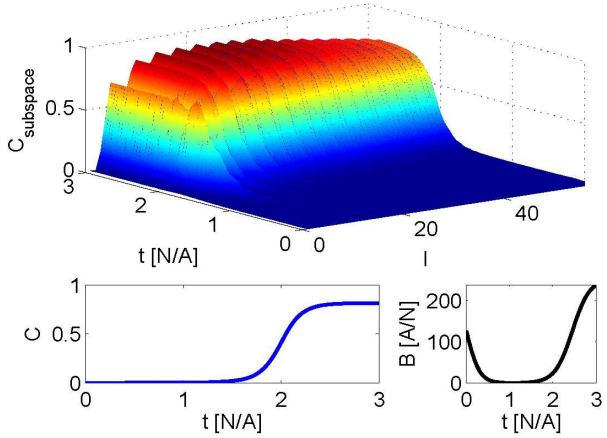

Figure 7.5: (Color online) Entanglement generation with the iterative protocol for $N = 10^3$ particles. The upper plot shows that the adiabatic sweep generates a high amount of entanglement (approximately) independent of the subspace of total angular momentum of the bath state (within each I-subspace a mixture over all allowed z-eigenstates was considered). The lower left plot shows the development of the total concurrence C during the particular field sweep depicted in the lower right plot.

In this case a Trotter expansion leads to the effective Hamiltonian

$$\begin{aligned} H =& \frac{A}{N}(\mathbf{S_1} + \mathbf{S_2}) \cdot (\mathbf{I_1} + \mathbf{I_2}) + 2g^*\mu_B(S_1^z + S_2^z)B_z, \\ =& \frac{A}{N}\mathbf{S}_{\text{tot}} \cdot \mathbf{I}_{\text{tot}} + S_{\text{tot}}^z \tilde{B}, \end{aligned} \tag{7.9}$$

where indices 1 and 2 refer to the respective spin-1/2 particle or bath and we defined the total spin operators. The dynamics of the effective spin-1 coupled to the bath has (similarly to the single particle case discussed in Sec.7.1.1) simple block diagonal form, $\{|I, m+1\rangle|T_-\rangle, |I, m\rangle|T_0\rangle, |I, m-1\rangle|T_+\rangle\}$ constituting the invariant subspaces. Here the $T_{\pm,0}$ denote the usual spin triplet states. The two-spin singlet $|S\rangle = 1/\sqrt{2}(|\uparrow\downarrow\rangle - |\downarrow\uparrow\rangle)$ is completely decoupled from the dynamics.

We consider an initially prepared unentangled spin state $|\uparrow\downarrow\rangle \propto |T_0\rangle + |S\rangle$, and a large magnetic field B_z, such that this state is an eigenstate of the system. Lowering and subsequently raising the magnetic field adiabatically leaves the system in an eigenstate, but the T_0 and the S states acquire different adiabatic phases. For the decoupled singlet this phase is zero for all interaction times and external fields. For arbitrary magnetic fields, the phase

of the (adiabatic) triplet depends on the quantum numbers I and m of the bath. However, at zero field, the eigenvalue of the adiabatic T_0 eigenstate (i.e. the one the triplet evolves into during a magnetic field sweep from high field to zero field) is independent of both quantum numbers[4]. Thus by scanning fast over the region with the subspace-dependent adiabatic phases of the T_0 state and remaining long in the $B = 0$-phase an approximately I, m-independent phase is imprinted in the two-electron state

$$\left(e^{i\int dB\,\theta(B,I,m)}|T_0\rangle + |S\rangle\right)|I,m\rangle \approx \left(e^{i\theta}|T_0\rangle + |S\rangle\right)|I,m\rangle,$$

and choosing $\theta = \pi/2$ generates a maximally entangled state.

We have simulated this process numerically without making the assumption of the Trotter formula, and taking a specific functional form of the adiabatic magnetic field sweep (a tanh-profile in the data presented) and verified the generation of strong electron entanglement. In Fig. 7.5 one can clearly seen that the acquired phase is for realistic parameters nearly independent from the two bath-quantum numbers, and high-fidelity entanglement generation is possible[5].

The estimations for the constraints due to nuclear spin dynamics influencing the entanglement generation with the iterative scheme are analogous as for the sequential one, discussed in Sec. 7.2. The nuclear Zeeman energies do not play a significant role, as is readily seen be considering the dynamics in each invariant subspace: The Zeeman energy acts as a small (because $\mu_N \sim 10^{-3}\mu_B$) diagonal term (a detuning), that has negligible influence on the eigenvalues– as we have successfully verified numerically. Estimating the effect of inhomogeneities is less straightforward in comparison to the sequential scheme; we have simulated the process for small particle numbers (8), and found that the created Bell pairs contained about 10% less entanglement for inhomogeneous (Gaussian) couplings in comparison to the homogeneous case.

In Fig. 7.6 we present explicitly the exact numerical data comparing the amount of generated entanglement for different levels of inhomogeneities. The coupling constants were chosen Gaussian, with the width ω characterizing the inhomogeneity. First we observe that the overall entanglement is

[4]This is straightforwardly seen by writing the Hamiltonian in the invariant subspaces and calculating the eigenvalues. The underlying reason for the non-zero, but I, m-independent eigenvalue is the approximate symmetry of the coupling of T_0 to T_+ and T_-. The small *difference* in the coupling constants is independent of the invariant subspace under consideration.

[5]Note that we have not performed optimization (different pulse shapes, rise/fall times, ...) of the field sweep; indicating that the proposed procedure is robust and that careful tuning of parameter very likely allows for even higher entanglement.

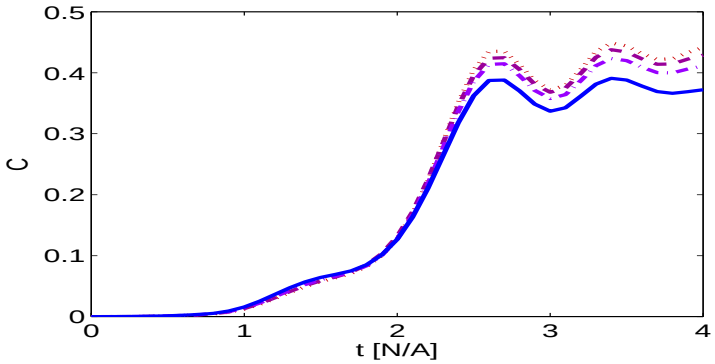

Figure 7.6: (Color online) Exact numerical study of the influence of inhomogeneities in the iterative entanglement protocol for $N = 8$ nuclear spins. The dotted line is for $\omega = 10$ (homogeneous limit, dashed: $\omega = 6$, dashed-dotted: $\omega = 5$, and the solid line stands for $\omega = 4$.

also for the case of homogeneous coupling constants lower than it was for the previously studied case of 1000 bath spins. However, as our protocol suffers from "boundary effects" in the different I-subspaces as mentioned earlier it is rather remarkable that for particle numbers as small as 8, a concurrence of nearly 1/2 is attained. Second, the data shows that the reduction of the obtained entanglement due to inhomogeneous coupling is very small (on the order of 10% for rather inhomogeneous situations $\omega = 4$).

7.4 Electron-Nuclear Entanglement

In the following subsection we investigate whether not only several electron spins can become entangled *via* the nuclei, but whether the electron and the nuclear spin ensemble might also get entangled during their interaction. Is is straightforwardly seen that the interaction will lead to some entanglement, so the more interesting question we answer is, *how much* entanglement is generated by using the negativity as a measure. Before doing so we try to get an intuition for the kind of quantum correlations we are dealing with. A certain state $|I, m, \uparrow\rangle$ evolves (approximately and ideally) to $1/\sqrt{2}(|I, m, \uparrow\rangle + i|I, m+1, \downarrow\rangle)$. This state is maximally entangled for $I = 1/2$. Now one might be tempted to think that if one could achieve this evolution approximately for all I and m then the final state would be highly entangled (as it is a mixture over many of these supposedly highly entangled states). However, this is not the case. Intuitively this can be understood by noting that for $I = 1/2$ a potential measurement of the electron would yield

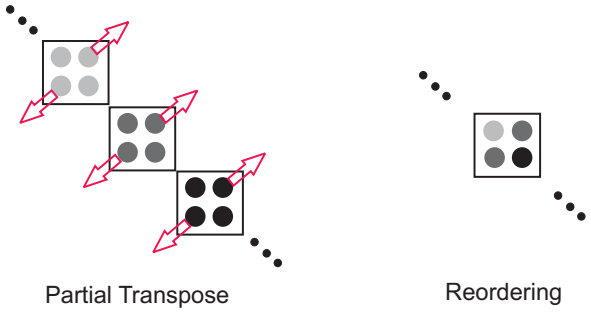

Figure 7.7: (Color online) Schematic representation of the two main steps in the calculation of the negativity of the coupled electron nuclear spin state. The sketched matrix is given in the $\{|I, m, \uparrow\rangle, |I, m+1, \downarrow\rangle\}$-basis for each I present in the mixture.

full information about the nuclear state. But for a large and completely mixed state, the information about the nuclei obtained through an electron measurement becomes negligible (in a manner of speaking because any of the two measurement outcomes is "connected" with (m)any different nuclear spin configuration(s)).

In the following we use the *negativity* for quantification of the entanglement between electron and nuclei. To this end we define the partial transposition of a bipartite quantum state ρ_{AB}. If we express ρ_{AB} in an orthonormal product basis,

$$\rho_{AB} = \sum_{i,j} \sum_{k,l} \langle i,k|\, \rho\, |j,l\rangle \;\; |i\rangle_A \langle j| \otimes |k\rangle_B \langle l|\,,$$

then the partial transpose with respect to system A is given by

$$\rho^{T_A} = \sum_{i,j} \sum_{k,l} \langle i,k|\, \rho\, |j,l\rangle \;\; |j\rangle_A \langle i| \otimes |k\rangle_B \langle l|\,.$$

Important properties of the partial transposition of ρ_{AB} are that its spectrum is independent of both the choice of the local basis and on whether the partial transposition has been taken with respect to subsystem A or B. The positivity of the partial transpose of a state is a necessary condition for separability [196, 197, 198].

The negativity $\mathcal{N}$ of a state ρ is defined as

$$\mathcal{N}(\rho) = ||\rho^{T_A}||_1 - 1, \tag{7.10}$$

where $||A||_1 = \mathrm{tr}|A| = \mathrm{tr}\sqrt{A^\dagger A}$ is the trace norm, given by the sum of the singular values of A. It is known that the negativity is an entanglement

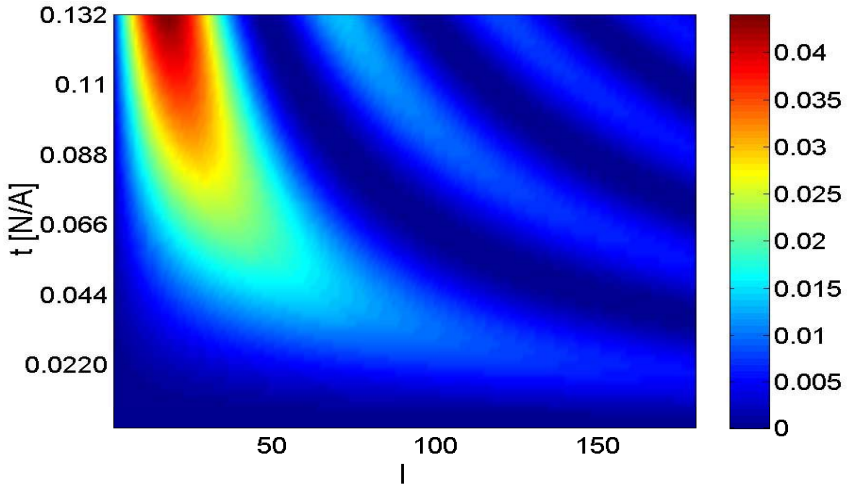

Figure 7.8: (Color online) Entanglement between electron and $N = 10^4$ nuclear spins during resonant interaction as quantified by the negativity $\mathcal{N}$ in the various relevant subspaces I. The entanglement generally is low as explained in the main text (maximal entanglement would correspond to $\mathcal{N} = 1$ for each of the subspaces).

monotone [199][6]. Since (partial) transposition preserves the trace, we have that $\mathcal{N}(\rho)$ is given by two times the sum of the moduli of the negative eigenvalues of ρ^{T_A}. It is the negativity that we will use in the following to quantify electron-nuclear spin entanglement.

The electron-nuclear dynamics leads to a block diagonal density matrix for all times, which is composed of small 2×2-blocks containing the only non-zero off-diagonal elements. The partial transpose with respect to the electron system is thus easily visualized as sketched on the left of Fig. 7.7. The eigenvalues λ (parameterized by I, m, t) of the partial transpose are readily seen to be defined by

$$(s_{m-1}^2 - \lambda)(c_{m+1}^2 - \lambda) - (c_m s_m)^2 = 0,$$

where the $I-$ and time-dependence has been omitted for brevity. Negative eigenvalues exist when

$$n_e = s_{m-1}^2 c_{m+1}^2 - s_m^2 c_m^2 > 0.$$

[6]Note though, that for systems larger than 2×3 the negativity suffers from vanishing for some (so called *bound*-)entangled states [200] and thus zero negativity does not always imply that the state at hand is unentangled.

As can be seen from Eq. (7.3) and following, the difference between the coefficients c, s for "neighboring" m-values is small. Thus n_e stays small indicating both low entanglement and negativity[7].

We have numerically computed the negativity for $N = 10^4$ nuclear spins in the homogeneous situation, with the results summarized in Fig. 7.8. The data confirms the expectation that only a very small amount of entanglement is created. This holds true even within a given I-subspace, so even if the total angular momentum could be measured, the the electron-nuclear entanglement stays low (in each subspace a mixture of all possible z-projections was used of course). Note also that the correlations are decreasing for increasing particle number, as then an electron spin measurement yields less information about the nuclear spin state.

To summarize the last paragraphs, we can put on record that the infinite temperature mesoscopic spin bath does not become significantly entangled with the electron spin through the Fermi contact hyperfine interaction. However, it *can* be used to mediate strong entanglement between electrons, as seen in the previous sections[8].

7.5 Conclusions

Generation of entanglement between electron spins is an important milestone and building-block for solid state QIP and has received a large amount of attention, see e.g. [202, 203, 204, 205] and Chapter V in the review [11], and references therein. Most, and also the most promising, proposals rely on the exchange interaction. However, it has been pointed out that charge fluctuations will seriously effect any electron spin manipulation based on exchange [190], and subsequently new electron entanglers [206] and quantum computation schemes have been proposed [87]. Our proposal is resistant against charge noise, in the sense that no higher orbitals are occupied. Furthermore, our proposal has the advantage that is generically suitable for the creation of multipartite entanglement. Note also, that when electrons can be prepared in two directions, then our protocol does not require any single qubit gates for the creation of n-partite GHZ states.

We studied a situation where *nothing* is known about the state of a spin bath. Remarkably, this maximal ignorance still allows for the generation of high fidelity multipartite entanglement via the bath. When only one bit of information is extracted from the spin bath, arbitrary gates between the bath

[7] Similar considerations have been carried out for slightly less complex JC-system with a thermal bosonic field [201].

[8] Cubitt *et al.* [185] have studied in a more formal context the creation of entanglement via mixed systems and found that generally "the messenger needs not be entangled".

and the qubits are possible, and all matrix product states with 2D bonds can be sequentially created. These gates can be achieved by application of ideas from control theory and adiabatic passage [194]. The explicit protocols we presented can be realized in quantum dot setups, where entanglement could be created on a timescale of a few μs (in typical GaAs dots). Despite being a somewhat slow mechanism, it could prove superior to exchange based schemes in situations where charge fluctuations are large and is genuinely suitable for multipartite entanglement generation.

Future studies of various experimental setups [20, 131] could shed new light on and explore further our observation that it is (sometimes) not necessary to know *with what* you interact, as long as you know *how*.

Appendix A

Polarization with Static External Magnetic Field

In this appendix we consider the cooling protocol as introduced in Section 2.1 and derive a more general master equation, which does not require the assumption that the external magnetic field is adjusted continuously during the polarization process. This has the advantage of a minimum of experimental control necessary, but the drawback of a reduced cooling rate.

Consider again the hyperfine Hamiltonian

$$H = H_{\text{ff}} + g(g^*\mu_B g^{-1} B_{\text{ext}} + \langle A^z \rangle) S_z + g\left(A^z - \langle A^z \rangle\right) S_z.$$

We now go to an interaction picture with respect to the effective magnetic field so that the Hamiltonian becomes

$$H_I = e^{iH_0 t} H_1 e^{-iH_0 t},$$

with $H_1 = H_{\text{ff}} + g\left(A^z - \langle A^z \rangle\right) S_z$ and $H_0 = g(g^*\mu_B g^{-1} B_{\text{ext}} + \langle A^z \rangle) S_z$. Now using $e^A B e^{-A} = \sum_{m=0}^{\infty} \frac{1}{m!} B_m$ (with $B_m = [A, B]_m := [A, [A, \ldots [A, B]]]$) we have that

$$\begin{aligned} A^- S_+ &\to A^- S_+ e^{i\omega t}, \\ A^+ S_- &\to A^+ S_- e^{-i\omega t}, \end{aligned} \tag{A.1}$$

with $\omega = g(g^*\mu_B g^{-1} B_{\text{ext}} + \langle A^z \rangle)$. The procedure allows us to study large effective magnetic fields, without compromising the validity of the expansion of the time evolution operator. As before, the time evolution operator in the rotating frame is expanded to second order in a Dyson series, which is a valid approach as also the z-terms in H_I are of the required smallness. Note further that the change of $\langle A^z \rangle$ during a timestep Δt is very small, thus not compromising our approach. The terms of the z-interaction have the same

form in the rotating frame as in the Schrödinger picture. The polarizing terms lead to the following expression for the evolved state

$$\int_0^{\Delta t} dt_1 \int_0^{t_1} dt_2 \Big(f(t_1,t_2) A^+ A^- \rho_0 + \rho_0 f(t_1,t_2)^* A^+ A^- - 2\mathrm{Re}(f(t_1,t_2)) A^- \rho_0 A^+ \Big),$$

with $f(t_1,t_2) = \exp(i\omega(t_2-t_1))$. The integrals are readily evaluated

$$\int_0^{\Delta t} dt_1 \int_0^{t_1} dt_2 f(t_1,t_2) = \frac{1 - e^{i\Delta t\omega} + i\Delta t\omega}{\omega^2} =: F, \tag{A.2}$$

and therefore the full Liouvillian becomes

$$\mathcal{L}\rho\Delta t = \mathcal{L}_z\rho - \frac{g^2}{4}\Big(\mathrm{Re}(F)\big(A^+A^-\rho + \rho A^+A^- - 2A^-\rho A^+\big) + i\mathrm{Im}(F)\,\big[A^+A^-,\rho\big]\Big). \tag{A.3}$$

The limiting behavior of the variable F for very small and very large effective magnetic field is easily seen to be correct: In the case of vanishing effective magnetic field the dynamics in the rotating frame should coincide with the treatment including the field adjustments presented earlier. This is the case as

$$\omega \to 0 \Rightarrow F \to (\Delta t)^2/2,$$

which follows directly from expansion of the exponential in Eq. (A.2). For a strong effective magnetic field

$$\omega \to \infty \Rightarrow F \to 0,$$

and thus the polarizing terms in the Liouvillian of Eq. (A.3) tend to zero: The polarization of the nuclear spin system becomes quenched, because hyperfine flips are "infinitely" detuned.

Generally the Liouvillian from Eq. (A.3) gives rise to a nuclear spin polarization rate, that is itself dependent on the polarization (that has already been dynamically generated), because $\omega \propto f(\langle A^z \rangle)$. This situation has been discussed for *incoherent* processes already in the 1970s, see e.g. Refs [84, 207]. It was also the subject of a number of recent remarkable optical spin cooling experiments in QDs, which studied pronounced effects of this nonlinearity such as, for example, hysteresis. However, recent experimental data did not show full agreement with the incoherent theory [102], so that a detailed study of coherent effects in optical nuclear spin polarization procedures with the formalism developed here is an interesting future research project.

Appendix B

Bosonic Mode Picture of the Cooling Process

We develop here a "mode picture" of the cooling process that provides handy qualitative intuition for dark state effects in spin cooling[1]. In the following we will denote with "mode" $A_k^- = \sum_i g_i^{(k)} I_i^-$ ($b_k = \sum_i g_i^{(k)} a_i$) with $\mathbf{g}^{(k')} \cdot \mathbf{g}^{(k)} = \delta_{k,k'}$.

Strength of the mode-mixing A^z-term

The importance of the inhomogeneous Knight shifts induced by the z-part of the HF interaction was emphasized in Chapter 2. We will show here, that the inhomogeneous Knight shifts lead to mode mixing in the bosonic picture. In the bosonic approximation the interesting (non-constant) part of the z-interaction is ($\gamma_x = \sum_i g_i^x$)

$$\begin{aligned} A^z &= \sum_i g_i a_i^\dagger a_i = \sum_i g_i \sum_{k_1,k_2} g_i^{k_1 *} g_i^{k_2} b_{k_1}^\dagger b_{k_2} \\ &= \gamma_3 b_0^\dagger b_0 + \Big(b_0^\dagger \sum_{k\neq 0,i} g_i^2 g_i^k b_k + \text{H.c.} \Big) + \sum_{k_1,k_2\neq 0,i} g_i g_i^{k_1 *} g_i^{k_2} b_{k_1}^\dagger b_{k_2}. \end{aligned} \tag{B.1}$$

Recall that the polarizing terms in the master equation couple only to the mode b_0. The above z-term on the other hand couples the mode b_0 to other modes, which can be seen clearly when the above equation is rewritten as

$$A^z = \gamma_3 b_0^\dagger b_0 + b_0^\dagger \tilde{c} + b_0 \tilde{c}^\dagger + \ldots,$$

with $\tilde{c} = \sum_i g_i^2 a_i - \gamma_3 b_0$ such that the operator $\tilde{c}$ commutes with b_0, $[b_0, \tilde{c}^\dagger] = 0$, i.e. describes an orthogonal mode of the system. Normalizing the operator

[1] In Chapter 6 the bosonic description will be investigated in a more general context.

gives the proper commutation relations for a bosonic mode

$$\tilde{c} \to c = \frac{1}{\sqrt{\gamma_4 - \gamma_3^2}} \tilde{c} \Rightarrow [c, c^\dagger] = 1. \tag{B.2}$$

Even though the polarization terms in the master equation only cool the mode b_0, the inhomogeneous Knight field transfers excitations from the c-mode to the b_0 mode and thereby also the c mode is cooled. The efficiency of the Knight field induced cooling depends on the shape of the electron wave function. The above normalization is not well-defined for homogeneous coupling constants (where $\gamma_4 - \gamma_3^2 = 0$), which reflects the fact that in this situation there is no coupling to other modes.

The mode c is again coupled to another mode through the z-interaction and so on. This leads to a cascade of modes, each coupled to the next through the inhomogeneous Knight shifts. This cascade of coupled modes serves as a "conveyor-belt" that delivers excitations to the b_0 mode, where the excitations are then removed. In addition to this combination of mixing and cooling, there are the "completely uncooled" modes. These modes are mixed, but they are not strongly mixed with the cooled mode, cf. the last term in Eq. (B.1). This intuition is put into graphical form in Fig. B.1, in which we label the mode b_0 as "no. 1". (The yellowish/light grey small oval is to depict a second mode that is actively cooled in a later state of the cooling protocol, as will be explained in more detail later.)

We now evaluate a figure of merit for the strength of the mode mixing relative to the polarization rate, characterizing the mixing by the coupling to mode c,

$$\frac{\Gamma_{\text{mix}}}{\Gamma_{\text{pol}}} = \frac{g\sqrt{\gamma_4 - \gamma_3^2}}{g^2(\Delta t)\bar{g}^2} \sim \mathcal{O}\left(\frac{\sqrt{N}}{0.1}\right),$$

where a mean coupling strength of $\bar{g} = \sum_i g_i/N$ was used and the given scaling behavior is true when the electron wave function is such that the difference between the two numbers γ_3^2, γ_4 is of the same order as the numbers themselves, namely $1/N$. The latter holds for the Gaussian wave function we have studied so far.

We now give some concrete examples for the relative strength of polarizing and mixing dynamics for Gaussians of width $N/4$

$$\frac{\Gamma_{\text{mix}}}{\Gamma_{\text{pol}}} \approx \begin{cases} 182 & (\text{N}{=}10^3,\ 1\text{D}), \\ 625 & (\text{N}{=}10^3,\ 2\text{D}), \\ 1798 & (\text{N}{=}10^3,\ 3\text{D}), \\ 1951 & (\text{N}{=}10^4,\ 2\text{D}). \end{cases} \tag{B.3}$$

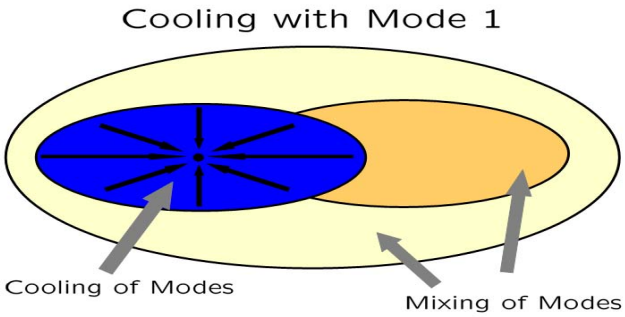

Figure B.1: Schematic graphical representation of the cooling procedure in the bosonic mode picture. Only mode no.1 (black dot within the blue/dark grey oval) is cooled "directly", but a larger number is cooled via the inhomogeneous Knight field (left oval). Nevertheless there are remaining modes which can not be cooled (yellowish/light grey areas).

These considerations show that the mixing dynamics can be strong enough to deliver coolable excitations at a rate that allows the cooling process to proceed with its optimal speed.

Note however, that even in situations where the mixing rate is large, there can be excitations that are not transferred to the coolable region in mode space (yellowish/light grey areas in Fig. B.1). (The mixing rate we used above was determined by the mode c alone.) This is particularly true in systems, where many spins have very similar coupling constants and do not experience strong inhomogeneities of the Knight field. So even though the above equations show that with increasing dimension the ratio of the two rates becomes larger in otherwise analogous situations, in higher dimensions there are more dark states, and thus cooling in a certain mode leads to lower total polarization. In Fig. B.1 this corresponds to a larger yellowish/light grey area. The interplay between fast cooling of a few modes and inaccessibility of other modes can be very well illustrated by studying the performance of the cooling procedure in different dimensions. This is not a purely academic exercise because quasi-2D and real 3D confinement potentials do occur in experiments; the arising effects are explored in Appendix C. A successful cooling scheme has to take into account both aforementioned effects: Efficient mode mixing and good covering of the mode space. We demonstrate in Section 2.2.4 that our enhanced cooling protocols involving a few mode changes satisfy these requirements.

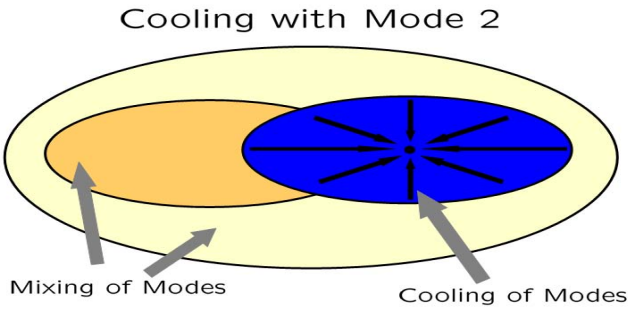

Figure B.2: Schematic graphical representation of the cooling procedure in the bosonic mode picture (continued). Mode no.2 is cooled in a way similar to mode no.1, see Fig. B.1. In addition it is important to note that the uncooled modes (yellowish/light grey areas) get mixed, leading to a repopulation of excitations coolable with mode no.1.

Breaking up Dark States in the Bosonic Picture

We want to develop an intuitive understanding of the phenomena that occur when the b_0 mode is changed during the cooling process, i.e. the shape of the electron wave function is changed. The cooling behavior for a mode 2 is very similar to the cooling behavior in the first mode: A range of modes is cooled through the combination of inhomogeneous Knight shifts and polarization dynamics, see Fig. B.2. However, it is important to note that also the uncooled modes are mixed in the polarization process (Figs. B.1 and B.2).

We analyze now what the effect of this mode mixing of the uncooled modes is in a sequence of mode changes $1 \rightarrow 2 \rightarrow 1$. The collection of modes coupled considerably through the z-interaction is cooled in the first step of the sequence. We assume that the cooling procedure in this first step runs long enough to achieve a (quasi-) steady state, i.e. at the end of the first step in the sequence the cooling rate slows down, approaching zero. Then the cooling rate increases rapidly when mode 2 is employed in the second step of the sequence, because it has access to a different collection of modes that it can cool. Again, after a some time a (quasi-)steady state with a negligible cooling rate will be reached. The third step of the cooling sequence returns to mode 1. This is the mode that reached a steady state during the first part of the sequence, so one might doubt that going back to this mode yields any further cooling. However, in addition to the cooling dynamics there is always mode mixing in the uncooled modes. In particular when mode 2 is cooled (in the second step of the three-step sequence considered here), there will be transfer of excitation into the modes which are coolable by mode 1.

Appendix C

Role of Dimensionality in Nuclear Spin Cooling

The study of the influence of the dimensionality of a QD on the performance of the cooling protocol (Chapter 2) is interesting both because 2D and 3D situations have been experimentally realized, and a change in dimension illustrates nicely the interplay between cooling potential in a given mode and cooling speed (Appendix B).

Cooling in 1D

For Gaussian couplings in 1D one expects that in the center of wave function the blocking of cooling due to dark states should be most severe, because there the slope of the wave function is zero. Going outwards the (absolute value of the) first derivative is reaching a maximum, and then tends to zero again. In the center of the dot there will thus be a competition between the largest cooling rate (due to the large electron population probability) and destructive quantum interference quenching the cooling dynamics. In the region of the maximal derivative of the electron wave function one expects of lower cooling rate, but less dark-state-blocking. The outer region of the dot remains largely uncooled because of the low polarization rate.

In Fig. C.1 we study the 1D situation for the "Spin" and bosonic approximation numerically. The polarization distribution in the QD shows the expected features: The polarization in the center of the dot is quantum blocked, the inhomogeneous Knight field on the slopes of the wave function lifts this blockade and the outer parts are cooled inefficiently because of the small probability for the electron to be in this region.

Cooling rate and final polarization are smaller in the bosonic approximation, see Sec. 2.2.2, but the qualitative agreement between approaches (*ii*) and (*v*) remains.

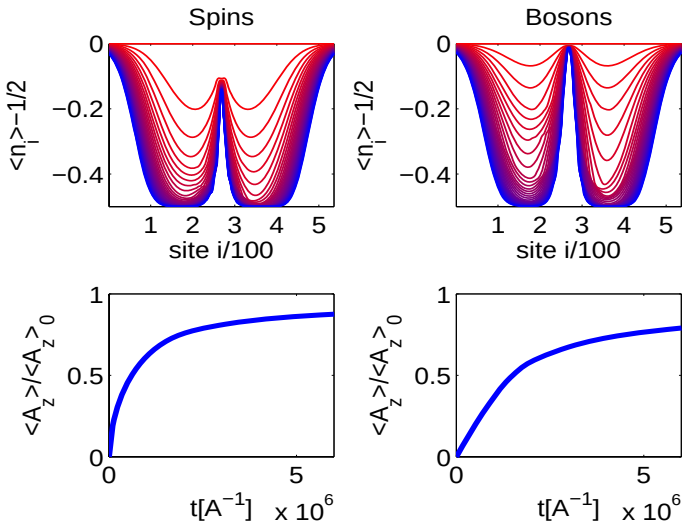

Figure C.1: Spin population at the different lattice sites (top) and total polarization (bottom) for the (ii)-bosonic approximation scheme (left) and the (v)-"spin" approximation scheme (right). The couplings are a 1D Gaussian shifted by 1/3 from the center.

Cooling a larger area in 1D

To overcome the quantum blockade in the center of the dot, shifts of the electronic density distribution can be used- as discussed previously. One question that has not been addressed so far is whether one can shift the electron over larger distances and thereby not only approach the minimal value of $\langle A^z \rangle$, but also the ground state of the nuclear spins system, i.e. minimize $\langle I^z \rangle$. Without pursuing this question in detail, we present an exemplary simulation in Fig. C.2: One starts there with a Gaussian wave function at a certain location and then shifts it over a range of nuclear spin sites (in the presented data this range is about $5\times$ the initial extent of the wave function).

The distribution of the spin polarization in Fig. C.2 displays some features familiar from the previous paragraph: initially (left side) in the center of the wave function one can not cool. Then as one moves along with shifting the wave function these limits are overcome, in particular in the region which was dark for the first wave function (around site $i = 30$). Indeed, as one can see in the polarization spin distribution in Fig. C.2, by shifting the electron wave function one can cool large areas of nuclei- without considerable limitations through dark states.

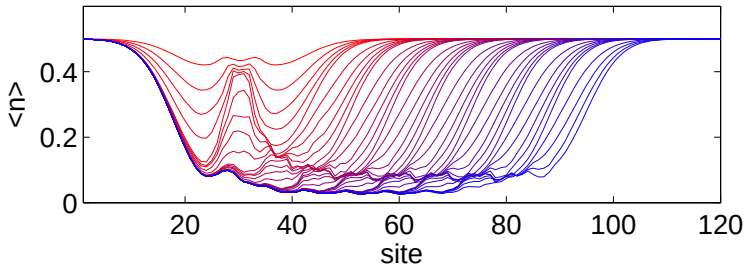

Figure C.2: Polarization dynamics with coupling constants shifted in 8 steps from left to right. The couplings are again drawn from a 1D Gaussian with width $w = N/8$.

2D and 3D

In this subsection we study the influence of the dimensionality of the Gaussian electron wave function on the cooling rate and the final polarization. This is of practical importance because the electron profile can be engineered from real 3D situation to (quasi-)2D situations.

As we do not consider dipolar interactions, or any other geometry dependent interactions explicitly, the coupling constants can be thought of as a 1D distribution in all dimensions (with the actual value of course obtained by rearranging the values of the Gaussian from different dimensions). We compare here the wave functions that couple the same total number of nuclei, e.g. $N_1 = 512$ spin on a line with 1D Gaussian couplings and $8 \times 8 \times 8 = N_3^3$ spins for a 3D cube (with the width $w = N_3/4$ in each direction).

In higher dimensions the most strongly coupled spins have larger coupling constants than the corresponding ones in smaller dimensions. Additionally, as shown in Appendix B for the bosonic description, the coupling of the b_0-mode to the mode c by the z-term is larger for higher dimensions. Thus, it is to be expected that the initial cooling rate should increase with increasing dimension. This is confirmed numerically as shown in Fig. C.3.

After this initial boost, the cooling starts to slow down faster and saturates at smaller final polarization for higher dimensions. The latter is due to the higher amount of symmetry: Whereas in 1D one has two *points* with the "same" coupling constants, in 3D one has *shells* of spins that are very similarly coupled.

We remark that by comparing the two plots in Fig. C.3 one confirms that the "spin"- and bosonic-approach give consistent results again. Note that the differences in the final polarization predicted by the two descriptions increase with increasing dimensionality. This is to be expected, because, as mentioned

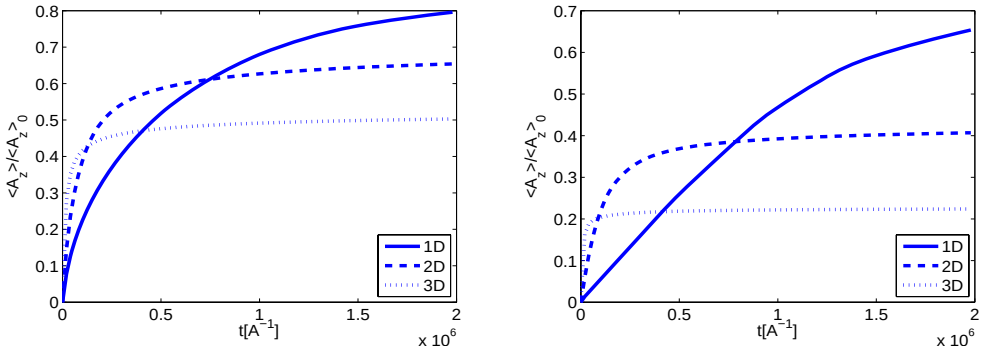

Figure C.3: Comparison of the cooling dynamics for 1D, 2D and 3D with Gaussian couplings. In each case $N = 512$ spins are coupled. For the simulation the (v)-"spin" scheme (left plot) and the (ii)-Boson scheme (right plot) have been used.

earlier, in higher dimension there will be more spins with the "same" coupling constant. On each of these shells the bosonic description will suffer an error of $\sqrt{n_{\text{shell}}}$, i.e. the smaller the number of spins in the shells, the better the bosonic description of the final polarization.

Appendix D

Matrix-Element Approach to the Bosonic Approximation

In this appendix we present an alternative approach to verify the bosonic description of the HF problem at high polarizations. The method outlined here is in close connection to the methods in Chapters 4 and 5, thereby emphasizing their usefulness beyond the examples given in these chapters. In particular, they allow for explicit microscopic calculation of the range of validity of the most simple and ideal bosonic approximation. However, the calculations are slightly cumbersome, underlining the practicality and importance of the more natural and general formalism presented in Chapter 6, which allows to incorporate the first order corrections to the ideal JC model into the effective Hamiltonian, thus ensuring validity over a larger range of parameters.

Recalling the microscopic description of the dark states as given in Section 5.2 and Ref. [42], we write the dark states as

$$|\mathcal{D}(m,\beta)\rangle = \frac{1}{\sqrt{\mathcal{N}}} \sum_{\{j\}_m} \left(\prod_{k\in\{j\}} \frac{1}{g_k} \right) c_{N/2-m,\beta}(\{j\})|\{j\}\rangle,$$
$$\mathcal{N} = \binom{N}{m}^{-1} \sum_{\{j\}_m} \prod_{k\in\{j\}} g_k^{-2}, \tag{D.1}$$

with $|c_{N/2-m,\beta}(\{j\})|^2 = \binom{N}{m}^{-1}$, and the properties of the $c_{N/2-m,\beta}(\{j\})$ specified by Eq. (5.6). In the following we will use the shorthand notation $c_m(\{j\})$ for $c_{N/2-m,\beta}(\{j\})$. We define the ladder of excited states starting from the inhomogeneous dark states $|n\rangle = (A^+)^n|0\rangle/\sqrt{n!}$, with $|\,0\rangle = |D(m)\rangle$, and

$$A^-|n\rangle = \sqrt{n}\Omega_n|n-1\rangle + \chi_n|O_{n-1}\rangle,$$

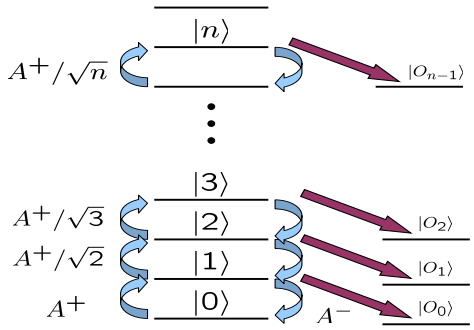

Figure D.1: Level scheme of the approximate Jaynes-Cummings dynamics.

with $\Omega_n = \langle n-1|A^-|n\rangle/\sqrt{n} = \langle n|n\rangle$, $\chi_n = \sqrt{\langle n|A^+A^-|n\rangle - 2n\Omega_n^2 + n\Omega_n^2\Omega_{n-1}}$ and $|O_{n-1}\rangle = (A^-|n\rangle - \sqrt{n}\Omega_n|n-1\rangle)/\chi_n$ such that $\langle O_{n-1}|n-1\rangle = 0$ and $|O_n\rangle$ is normalized. Note that here we have defined the parameter Ω_n slightly different from the convention used in Section 5.2, in order to underline the bosonic behavior of the collective nuclear spin mode. In the convention here, Ω_n for high polarizations has a value close to 1, with the deviations from unity quantifying the degree of non-bosonicity. Obviously the JC approximation for the collective raising and lowering operators will be good as long as $\Omega_n \approx 1$ and $\chi_n/(\sqrt{n}\Omega_n) \ll 1$, which are exactly the properties that we are going to quantify in the following as a function of the number of excitations n and the polarization of the dark state given through m.

We proceed by calculating

$$\begin{aligned}\Omega_n &= \langle D(m,\beta)|\frac{\left(\sum_i g_i\sigma_i^-\right)^n}{\sqrt{n!}}\frac{\left(\sum_i g_i\sigma_i^+\right)^n}{\sqrt{n!}}|D(m,\beta)\rangle \\ &= \frac{1}{n!\mathcal{N}}\sum_{i_1,\ldots,i_n,j_1,\ldots,j_n} g_{i_1}\cdots g_{i_n}g_{j_1}\cdots g_{j_n}\times \\ &\qquad \times\sum_{\{k\},\{l\}} c_m(\{k\})c_m(\{l\})\prod_{k\in\{k\},\,l\in\{l\}}\frac{1}{g_kg_l}\langle\{k\}|\sigma_{i_1}^-\cdots\sigma_{i_n}^-\sigma_{j_1}^+\cdots\sigma_{j_n}^+|\{l\}\rangle/\mathcal{N},\end{aligned}$$

which is generally a complicated expression. We devise here a systematic expansion, by exploiting the dark state properties: When a collective annihilation operator is acting on spins that have not been part of a collective excitation in the case of a fully polarized system, this, of course, does not give a contribution to the matrix element. For a dark state, this property is approximately preserved; collective spin operators A^- annihilating spin excitations that have *not* been created by A^+ operators (but were present in the

dark state) only give a small contribution. This yields a natural expansion of the above matrix element in the limit of high polarization. More specifically, the first and largest contribution is calculated by matching all i-indices in the above expression with the j-indices. There are $n!$ ways of doing this, thus yielding

$$\Omega_n^{(1)} = \frac{1}{\mathcal{N}} \sum_{\{l\}} \Pi_{l\in\{l\}} g_l^{-2} |c_m(\{l\})|^2 \sum_{i_1\neq i_2\cdots i_n\,;\, i_x\notin\{l\}} g_{i_1}^2 \cdots g_{i_n}^2 = \sum_{i_1\neq i_2\cdots i_n\,;\, i_x\notin\{l\}} g_{i_1}^2 \cdots g_{i_n}^2.$$

Using the notation $g_{\max}^2 = N_{\text{eff}}^{-1} (\ll 1)$, one extracts straightforwardly the bound

$$\Omega_n^{(1)} \geq 1 - \frac{1}{N_{\text{eff}}} \left(nm + \binom{n}{2} \right).$$

The contribution where one of the collective spin annihilation operators is not acting on the spins that have been acted upon previously by the collective spin up operators is

$$\begin{aligned} |\Omega_n^{(2)}| = \Bigg| \frac{1}{\mathcal{N}} \sum_{\{l\}} \Pi_{l\in\{l\}} g_l^{-2} \sum_{i_1\neq i_2\cdots\neq i_{n-1}\,;\, i_x\notin\{l\}} g_{i_1}^2 \cdots g_{i_{n-1}}^2 \times \\ \times \sum_{i\in\{l\}} g_i^2 \sum_{j\notin\{l\}+i_1+\cdots+i_{n-1}} c_m(\{l\}-i+j) c_m(\{l\}) \Bigg|, \\ \leq \left| \frac{1}{\mathcal{N}} \sum_{\{l\}} \Pi_{l\in\{l\}} g_l^{-2} \sum_{i_1\neq i_2\cdots\neq i_{n-1}\,;\, i_x\notin\{l\}} g_{i_1}^2 \cdots g_{i_{n-1}}^2 \sum_{i\in\{l\}} g_i^2 n \binom{N}{m}^{-1} \right| \leq \frac{nm}{N_{\text{eff}}}. \end{aligned}$$

In obtaining the above inequality, the dark state property from Eq. (5.6) has been used. Continuing in the same fashion shows that the kth order terms, $|\Omega_n^{(k)}|$, scale as $(nm/N_{\text{eff}})^k$ and consequently can be consistently neglected, showing that

$$|\Omega_n| \geq 1 - \frac{1}{N_{\text{eff}}} \left(2nm + \binom{n}{2} \right) =: 1 - \epsilon_{n,m}. \tag{D.2}$$

After rewriting

$$\chi_n^2 = \langle n+1|n+1\rangle (n+1) + \langle n| \sum_i g_i^2 \sigma_i^z |n\rangle - 2n\Omega_n^2 + n\Omega_n^2 \Omega_{n-1}, \tag{D.3}$$

this quantity is calculated in an analogous way (using $\Omega_{n+1} < \Omega_n$, and $\langle n| \sum_i g_i^2 \sigma_i^z |n\rangle = -\Omega_n + 2\sum_i g_i^2 \langle n|\sigma_i^+ \sigma_i^-|n\rangle$), with the result ($n \geq 0$)

$$\frac{\chi_n}{\sqrt{n}\Omega_n} \leq \sqrt{\frac{2m(1+1/n)+n+2}{N_{\text{eff}}}}. \tag{D.4}$$

Thus, we have explicitly verified the closeness of the spin system to the most simple bosonic description (as long as $\epsilon_{n,m}$ and $(m+n)/N_{\text{eff}}$ remain small).

Discussion and Comparison

The validity of the derived equations can be checked by taking the homogeneous limit, where exact expressions for Ω_n and χ_n can be readily obtained. From

$$I^+|I,-I+n\rangle = \sqrt{n+1}\sqrt{N}\sqrt{1-\frac{2m+n}{N}}|I,-I+n+1\rangle,$$

with $I = N/2 - m$ we determine the homogeneous expression with no prior approximations

$$\begin{aligned}\Omega_n &= \frac{1}{\sqrt{n!n!}}\langle 0|(I^-/\sqrt{N})^n(I^+/\sqrt{N})^n|0\rangle \\ &\approx \left[\prod_{k=1}^{n}\left(1-\frac{2m+k}{2N}\right)\right]^2 \approx 1-\frac{1}{N}\left(2nm+\binom{n}{2}\right),\end{aligned}$$

which indeed coincides with the approximated expression we have derived in this appendix (homogeneous version of Eq. (D.2)). Similarly, the effective bosonic theory developed in Chapter 6 yields a corresponding matrix element Ω_n, as can be seen from Eq. (6.18).

Note that generally the derived bounds Eqs. (D.2) and (D.4) will tend to be unnecessarily restrictive: In Chapter 6, we show that the first order corrections to the JC model can be incorporated into the effective Hamiltonian. This has the advantage of still yielding a model close to JC, but at the same time widening the range of applicability.

Appendix E

Derivation of the Effective Bosonic Hamiltonian

With the definitions from Section 6.2, we write the Hamiltonian Eq. (6.13) in the form $H_b = H_b^{(0)} + V_{\rm ff} + V_{\rm zz}$, where

$$\begin{aligned} V_{\rm ff} &= g/2\big[a^\dagger(C - C^{(0)})S^- + \text{H.c.}\big] \\ V_{\rm zz} &= g\big(C_z - C_z^{(0)}\big)S^z, \end{aligned} \tag{E.1}$$

and treat $V_{\rm ff}$ and $V_{\rm zz}$ in time dependent perturbation theory. We will show both contributions are higher order in the small parameter ε.

The evolved density matrix at time t is expanded as

$$\rho(t) = \rho^{(0)}(t) + \delta\rho^{(1)}(t) + \delta\rho^{(2)}(t) + \dots,$$

with $\rho^{(0)}(t) = U_0(t)\rho(0)U_0^\dagger(t)$, and $U_0(t) = e^{-iH_b^{(0)}t}$, and $\delta\rho^{(1)}(t)$ and $\delta\rho^{(2)}(t)$ are the first order and second order perturbation theory contributions coming from the Hamiltonians (E.1)

$$\begin{aligned} \delta\rho^{(1)}(t) &= \delta\rho^{(1)}_{V_{\rm ff}}(t) + \delta\rho^{(1)}_{V_{\rm zz}}(t), \\ \delta\rho^{(2)}(t) &= \delta\rho^{(2)}_{V_{\rm ff},V_{\rm ff}}(t) + \delta\rho^{(2)}_{V_{\rm zz},V_{\rm zz}}(t) + \delta\rho^{(2)}_{V_{\rm zz},V_{\rm ff}}(t) + \delta\rho^{(2)}_{V_{\rm ff},V_{\rm zz}}(t), \end{aligned} \tag{E.2}$$

with

$$\begin{aligned} i\delta\rho^{(1)}_V(t) =& U_0(t)\int_0^t dt' \left[U_0^\dagger(t')VU_0(t'), \rho(0)\right] U_0^\dagger(t), \\ i\delta\rho^{(2)}_{V,V'}(t) =& U_0(t)\int_0^t dt' \left[U_0^\dagger(t')VU_0(t'), \delta\rho^{(1)}_{V'}(t')\right] U_0^\dagger(t). \end{aligned}$$

We will show that the norm of the reduced density operators $\mathrm{tr}_B\delta\rho^{(1)}(t)$ and $\mathrm{tr}_B\delta\rho^{(2)}(t)$ are both higher order in the expansion parameter ε. We make use

of the fact that we can estimate the contributions of two operators V and V' in the form

$$\mathrm{tr}_B\left(\delta\rho_V^{(1)}(t)\right) \sim \mathrm{tr}_B\left(V\rho_B,\right)$$
$$\mathrm{tr}_B\left(\delta\rho_{V,V'}^{(2)}(t)\right) \sim \mathrm{tr}_B\left(VV'\rho_B\right).$$

1) *First order perturbation terms.* Consider first the term V_{ff}. We have that $\mathrm{tr}_B\left(V_{\mathrm{ff}}\rho_B\right) \propto \mathrm{tr}_B\left(\left(C - C^{(0)}\right)\rho_B\right)$, where

$$C - C^{(0)} = C_1 + C_2 + C_3, \tag{E.3}$$

with

$$\begin{aligned} C_1 &= \sum_k \big(\alpha_{k,k}^{(2)} - \frac{1-\gamma_4}{N}\big) a_k^\dagger a_k, \\ C_2 &= \frac{3}{2}\big(a^\dagger \sum_k \beta_k^{(3)} a_k + \mathrm{H.c.}\big), \\ C_3 &= \sum_{k\neq k'} \alpha_{k,k'}^{(2)} a_k^\dagger a_{k'}. \end{aligned}$$

Since ρ_B is a diagonal operator in the bath it follows $\mathrm{tr}_B\left(\rho_B C_2\right) = \mathrm{tr}_B\left(\rho_B C_3\right) = 0$. On the other hand, as ρ_B is of the form (6.15) $\mathrm{tr}_B\left(\rho_B C_1\right) = \frac{\overline{m}}{N}\big(\sum_k \alpha_{k,k}^{(2)} - (1-\gamma_4)\big)$. From $\sum_k \alpha_{k,k}^{(2)} = 1-\gamma_4$ we obtain $\mathrm{tr}_B\left(\rho_B C_1\right) = 0$.

Consider the next term V_{zz}. We have that $\mathrm{tr}_B\left(V_{\mathrm{zz}}\rho_B\right) \propto \mathrm{tr}_B\big(\big(C_{\mathrm{z}} - C_{\mathrm{z}}^{(0)}\big)\rho_B\big)$, where

$$C_{\mathrm{z}} - C_{\mathrm{z}}^{(0)} = C_1^{\mathrm{z}} + C_2^{\mathrm{z}} + C_3^{\mathrm{z}}, \tag{E.4}$$

with

$$\begin{aligned} C_1^{\mathrm{z}} &= \sum_k \big(\alpha_{k,k}^{(1)} - \frac{\gamma_1}{N}\big) a_k^\dagger a_k, \\ C_2^{\mathrm{z}} &= \big(a^\dagger \sum_k \beta_k^{(2)} a_k + \mathrm{H.c.}\big), \\ C_3^{\mathrm{z}} &= \sum_{k\neq k'} \alpha_{k,k'}^{(1)} a_k^\dagger a_{k'}. \end{aligned}$$

The operator (E.4) has the same form of the operator (E.3) if we substitute $\alpha_{k,k'}^{(2)}$ by $\alpha_{k,k'}^{(1)}$ and $\beta_k^{(3)}$ by $\beta_k^{(2)}$. In the same way that for the V_{ff} case discussed above we obtain $\mathrm{tr}_B\left(\rho_B C_2^{\mathrm{z}}\right) = \mathrm{tr}_B\left(\rho_B C_3^{\mathrm{z}}\right) = 0$. Since also $\sum_k \alpha_{k,k}^{(1)} = \gamma_1$, it follows that $\mathrm{tr}_B\left(\rho_B C_3^{\mathrm{z}}\right) = 0$. Thus, all first order perturbation terms are zero.

2) *Second order perturbation terms.* We will proof that the norms of the reduced operators $\mathrm{tr}_B\left(\delta\rho^{(2)}_{V_{\mathrm{ff}},V_{\mathrm{ff}}}(t)\right)$, $\mathrm{tr}_B\left(\delta\rho^{(2)}_{V_{\mathrm{zz}},V_{\mathrm{zz}}}(t)\right)$, and $\mathrm{tr}_B\left(\delta\rho^{(2)}_{V_{\mathrm{zz}},V_{\mathrm{ff}}}(t)\right)$, are higher order in ε.

Consider first the term $\mathrm{tr}_B\left(\delta\rho^{(2)}_{V_{\mathrm{ff}},V_{\mathrm{ff}}}(t)\right)$, which is proportional to $V^{(2)} = \mathrm{tr}_B\left(\rho_B\left(C-C^{(0)}\right)^2\right)$. Since ρ_B is a diagonal operator

$$V^{(2)} = \mathrm{tr}_B(\rho_B C_1^2) + \mathrm{tr}_B(\rho_B C_2^2) + \mathrm{tr}_B(\rho_B C_3^2). \tag{E.5}$$

Taking into account the form of ρ_B we obtain that

$$\mathrm{tr}_B\left(\rho_B C_1^2\right) + \mathrm{tr}_B\left(\rho_B C_3^2\right) = \frac{\overline{m}}{N}\left(\frac{\overline{m}}{N}+1\right)\delta,$$

$\delta = \gamma_4 + \gamma_4^2 - 2\gamma_6 - \frac{(1-\gamma_4)^2}{N-1}$. Since $\gamma_p = \sum_\ell g_\ell^p \leq N/N_{\mathrm{eff}}^{p/2}$ it follows

$$\mathrm{tr}_B\left(\rho_B C_1^2\right) + \mathrm{tr}_B\left(\rho_B C_3^2\right) \leq \frac{\overline{m}}{N_{\mathrm{eff}}^2} = \frac{\varepsilon}{N_{\mathrm{eff}}}. \tag{E.6}$$

On the other hand

$$\mathrm{tr}_B\left(\rho_B C_2^2\right) = \frac{\overline{m}}{N}\delta_2\left(1+2a^\dagger a\right) + \delta_2 a^\dagger a,$$

with $\delta_2 = \gamma_6 - \gamma_4^2$, so that

$$\|\mathrm{tr}_B\left(\rho_B C_2^2\right)\|_m \leq (1+2n)\frac{\overline{m}}{N_{\mathrm{eff}}^3} + \frac{nN}{N_{\mathrm{eff}}^3} \leq \frac{\varepsilon}{N_{\mathrm{eff}}}. \tag{E.7}$$

This shows that the term $\mathrm{tr}_B\left(\delta\rho^{(2)}_{V_{\mathrm{ff}},V_{\mathrm{ff}}}(t)\right)$ is higher order in ε.

Proceeding in the same way the norms of the reduced operators $\mathrm{tr}_B\left(\delta\rho^{(2)}_{V_{\mathrm{zz}},V_{\mathrm{zz}}}(t)\right)$, and $\mathrm{tr}_B\left(\delta\rho^{(2)}_{V_{\mathrm{zz}},V_{\mathrm{ff}}}(t)\right)$ are calculated. The largest contribution from these terms is $\mathrm{tr}_B\left(\delta\rho^{(2)}_{V_{\mathrm{zz}},V_{\mathrm{zz}}}(t)\right) \leq \mathcal{O}(\varepsilon\sum_\ell (g_\ell-\bar{g})^2)$, with $\bar{g} = \sum_\ell g_\ell$. We have verified that for reasonable Gaussian wave functions, in particular the ones we are considering for explicit calculation in Chapter 6, that this contribution is smaller than ε^2. We remark however, that this shows that smallness of the parameter ε has to be accompanied by a small variance of the electron envelope wave function in order for the bosonic approximation to be good in the situation we are considering here.

Bibliography

[1] R. Feynman, J. Theoret. Phys. **21**, 467 (1982).

[2] D. Deutsch, Proc. Roy. Soc. A **400**, 96 (1985).

[3] P. Shor, 35th Annual Symposium on Foundations of Computer Science, 124 (1994).

[4] M. A. Nielsen and I. L. Chuang, *Quantum Computation and Quantum Information* (Cambridge University Press, Cambridge, 2000).

[5] C. H. Bennett and G. Brassard, in *Proc. IEEE International Conference on Computers, Systems, and Signal Processing, Bangalore, India* (IEEE Press, New York, 1984), p. 175.

[6] S. Groeblacher, T. Paterek, R. Kaltenbaek, C. Brukner, M. Zukowsk, M. Aspelmeyer, and A. Zeilinger, Nature **446**, 871 (2007).

[7] S. Seidelin, J. Chiaverini, R. Reichle, J. J. Bollinger, D. Leibfried, J. Britton, J. H. Wesenberg, R. B. Blakestad, R. J. Epstein, D. B. Hume, W. M. Itano, J. D. Jost, C. Langer, R. Ozeri, N. Shiga, and D. J. Wineland, Phys. Rev. Lett. **96**, 253003 (2006).

[8] D. Stick, W. K. Hensinger, S. Olmschenk, M. J. Madsen, K. Schwab, and C. Monroe, Nature Physics **2**, 36 (2006).

[9] http://www.idquantique.com/, (company webpage) .

[10] D. Bouwmeester, A. Ekert, and A. Zeilinger, *The Physics of Quantum Information: Quantum Cryptography, Quantum Teleportation, Quantum Computation* (Springer, Berlin, 2000).

[11] G. Burkard, in *Handbook of Theoretical and Computational Nanotechnology*, edited by M. Rieth and W. Schommers (Wiley, Weinheim, 2005), Chap. Theory of solid state quantum information processing.

[12] J. I. Cirac and P. Zoller, Phys. Rev. Lett. **74**, 4091 (1995).

[13] D. Loss and D. P. DiVincenzo, Phys. Rev. A **57**, 120 (1998).

[14] Y. Makhlin, G. Schön, and A. Shnirman, Rev. Mod. Phys. **73**, 357 (2001).

[15] L. M. K. Vandersypen and I. L. Chuang, Rev. Mod. Phys. **76**, 1037 (2004).

[16] D. G. Cory, A. F. Fahmy, and T. F. Havel, Proc. Nat. Acad. Sci. USA **94**, 1634 (1997).

[17] N. Gershenfeld and I. Chuang, Science **275**, 350 (1997).

[18] S. L. Braunstein, C. M. Caves, R. Jozsa, N. Linden, S. Popescu, and R. Schack, Phys. Rev. Lett. **83**, 1054 (1999).

[19] B. E. Kane, Nature **393**, 133 (1998).

[20] A. J. Skinner, M. E. Davenport, and B. E. Kane, Phys. Rev. Lett. **90**, 087901 (2003).

[21] B. Koiller, X. Hu, and S. Das Sarma, Phys. Rev. Lett. **88**, 027903 (2001).

[22] D. P. DiVincenzo, Fort. Phys. **48**, 771 (2000).

[23] J. R. Petta, A. C. Johnson, J. M. Taylor, E. A. Laird, A. Yacoby, M. D. Lukin, C. M. Marcus, M. P. Hanson, and A. C. Gossard, Science **309**, 2180 (2005).

[24] J. M. Elzerman, R. Hanson, L. H. Willems van Beveren, B. Witkamp, L. M. K. Vandersypen, and L. P. Kouwenhoven, Nature **430**, 431 (2004).

[25] F. H. L. Koppens, C. Buizert, K. J. Tielrooij, I. T. Vink, K. C. Nowack, T. Meunier, L. P. Kouwenhoven, and L. M. K. Vandersypen, Nature **442**, 766 (2006).

[26] E. A. Laird, J. R. Petta, A. C. Johnson, C. M. Marcus, A. Yacoby, M. P. Hanson, and A. C. Gossard, Phys. Rev. Lett. **97**, 056801 (2006).

[27] M. Kroutvar, Y. Ducommun, D. Heiss, M. Bichler, G. A. Dieter Schuh, and J. J. Finley, Nature **432**, 81 (2004).

[28] R. Hanson, L. H. Willems van Beveren, I. T. Vink, J. M. Elzerman, W. J. M. Naber, F. H. L. Koppens, L. P. Kouwenhoven, and L. M. K. Vandersypen, Phys. Rev. Lett. **94**, 196802 (2005).

[29] A. C. Johnson, J. R. Petta, J. M. Taylor, A. Yacoby, M. D. Lukin, C. M. Marcus, M. P. Hanson, and A. C. Gossard, Nature **435**, 925 (2005).

[30] F. H. L. Koppens, J. A. Folk, J. M. Elzerman, R. Hanson, L. H. Willems van Beveren, I. T. Vink, H.-P. Tranitz, W. Wegscheider, L. P. Kouwenhoven, and L. M. K. Vandersypen, Science **309**, 1346 (2005).

[31] G. Burkard, D. Loss, and D. P. DiVincenzo, Phys. Rev. B **59**, 2070 (1999).

[32] A. V. Khaetskii, D. Loss, and L. Glazman, Phys. Rev. B **67**, 195329 (2003).

[33] S. I. Erlingsson, Y. V. Nazarov, and V. I. Fal'ko, Phys. Rev. B **64**, 195306 (2001).

[34] W. Zhang, V. V. Dobrovitski, L. F. Santos, L. Viola, and B. N. Harmon, Phys. Rev. B **75**, 201302 (2007).

[35] W. M. Witzel and S. Das Sarma, Phys. Rev. B **76**, 045218 (2007).

[36] G. Giedke, J. M. Taylor, D. D'Alessandro, M. D. Lukin, and A. Imamoğlu, Phys. Rev. A **74**, 032316 (2006).

[37] D. Stepanenko, G. Burkard, G. Giedke, and A. Imamoğlu, Phys. Rev. Lett. **96**, 136401 (2006).

[38] D. Klauser, W. A. Coish, and D. Loss, Phys. Rev. B **73**, 205302 (2006).

[39] L.-M. Duan, J. I. Cirac, P. Zoller, and E. S. Polzik, Phys. Rev. Lett. **85**, 5643 (2000).

[40] J. F. Sherson, H. Krauter, R. K. Olsson, B. Julsgaard, K. Hammerer, I. Cirac, and E. S. Polzik, Nature **443**, 557 (2006).

[41] J. M. Taylor, C. M. Marcus, and M. D. Lukin, Phys. Rev. Lett. **90**, 206803 (2003).

[42] J. M. Taylor, A. Imamoğlu, and M. D. Lukin, Phys. Rev. Lett. **91**, 246802 (2003).

[43] *Single Quantum Dots*, edited by P. Michler (Springer, Berlin, 2003).

[44] L. Kouwenhoven, C. Marcus, P. McEuen, S. Tarucha, R. Westervelt, and N. Wingreen, in *Mesoscopic electron transport*, edited by L. L. Sohn, L. P. Kouwenhoven, and G. Schon (Kluwer Academic Publishers, Dordrecht, Boston, 1997), Chap. Electron transport in quantum dots. Proceedings of the NATO Advanced Study Institute on Mesoscopic Electron Transport.

[45] S. M. Reimann and M. Manninen, Rev. Mod. Phys. **74**, 1283 (2002).

[46] L. P. Kouwenhoven, D. G. Austing, and S. Tarucha, Rep. Prog. Phys. **64**, 701 (2001).

[47] S. Tarucha, D. G. Austing, T. Honda, R. J. van der Hage, and L. P. Kouwenhoven, Phys. Rev. Lett. **77**, 3613 (1996).

[48] H. Haug and S. W. Koch, *Quantum Theory of the Optical and Electronic Properties of Semiconductors*, 3rd ed. (World Scientific, Singapore, 1994).

[49] R. Hanson, L. P. Kouwenhoven, J. R. Petta, S. Tarucha, and L. M. K. Vandersypen, Rev. Mod. Phys. **79**, 1217 (2007).

[50] D. Schroer, A. D. Greentree, L. Gaudreau, K. Eberl, L. C. L. Hollenberg, J. P. Kotthaus, and S. Ludwig, Phys. Rev. B **76**, 075306 (2007).

[51] T. Hayashi, T. Fujisawa, H.-D. Cheong, Y.-H. Jeong, and Y. Hirayama, Phys. Rev. Lett. **91**, 226804 (2003).

[52] A. Imamoğlu, D. D. Awschalom, G. Burkard, D. P. DiVincenzo, D. Loss, M. Sherwin, and A. Small, Phys. Rev. Lett. **83**, 4204 (1999).

[53] D. P. DiVincenzo, D. Bacon, J. Kempe, G. Burkard, and K. B. Whaley, Nature **408**, 339 (2000).

[54] M. Anderlini, P. J. Lee, B. L. Brown, J. Sebby-Strabley, W. D. Phillips, and J. V. Porto, Nature **448**, 452 (2007).

[55] A. V. Khaetskii and Y. V. Nazarov, Phys. Rev. B **61**, 12639 (2000).

[56] A. V. Khaetskii and Y. V. Nazarov, Phys. Rev. B **64**, 125316 (2001).

[57] V. N. Golovach, A. Khaetskii, and D. Loss, Phys. Rev. Lett. **93**, 016601 (2004).

[58] E. Fermi, Z. Phys. **60**, 320 (1930).

[59] J. Schliemann, A. Khaetskii, and D. Loss, J. Phys: Cond. Mat. **15**, R1809 (2003).

[60] Y. Hu, H. H. O. Churchill, D. J. Reilly, J. Xiang, C. M. Lieber, and C. M. Marcus, Nature Nanotechnology **2**, 622 (2007).

[61] V. Cerletti, W. A. Coish, O. Gywat, and D. Loss, Nanotech. **16**, R27 (2005).

[62] D. Paget, G. Lampel, B. Sapoval, and V. I. Safarov, Phys. Rev. B **15**, 5780 (1977).

[63] T. Ota, G. Yusa, N. Kumada, S. Miyashita, T. Fujisawa, and Y. Hirayama, arXiv:0710.3487v1 (2007).

[64] A. M. Stoneham, *Theory of Defects on Solids* (Oxford Classic Texts in the Physical Sciences, Oxford, 1975).

[65] A. V. Khaetskii, D. Loss, and L. Glazman, Phys. Rev. Lett. **88**, 186802 (2002).

[66] I. A. Merkulov, A. L. Efros, and M. Rosen, Phys. Rev. B **65**, 205309 (2002).

[67] W. A. Coish and D. Loss, Phys. Rev. B **70**, 195340 (2004).

[68] W. M. Witzel and S. Das Sarma, arXiv:0707.1037v1 (2007).

[69] S. K. Saikin, W. Yao, and L. J. Sham, Phys. Rev. B **75**, 125314 (2007).

[70] W. M. Witzel and S. Das Sarma, Phys. Rev. B **74**, 035322 (2006).

[71] F. Jelezko, T. Gaebel, I. Popa, M. Domhan, A. Gruber, and J. Wrachtrup, Phys. Rev. Lett. **93**, 130501 (2004).

[72] L. Childress, M. V. Gurudev Dutt, J. M. Taylor, A. S. Zibrov, F. Jelezko, J. Wrachtrup, P. R. Hemmer, and M. D. Lukin, Science **314**, 281 (2006).

[73] T. Gaebel, M. Domhan, I. Popa, C. Wittmann, P. Neumann, F. Jelezko, J. R. Rabeau, N. Stavrias, A. D. Greentree, S. Prawer, J. Meijer, J. Twamley, P. R. Hemmer, and J. Wrachtrup, Nature Physics **2**, 408 (2006).

[74] H. Christ, J. I. Cirac, and G. Giedke, Phys. Rev. B **75**, 155324 (2007).

[75] C. E. Lopez, H. Christ, J. C. Retamal, and E. Solano, Phys. Rev. A **75**, 033818 (2007).

[76] J. M. Taylor, G. Giedke, H. Christ, B. Paredes, J. I. Cirac, P. Zoller, M. D. Lukin, and A. Imamoğlu, cond-mat/0407640 (2004).

[77] H. Christ, J. I. Cirac, and G. Giedke, Solid State Science (Special Issue on Solid State Quantum Information Processing) doi:10.1016/j.solidstatesciences.2007.09.027 (2007).

[78] H. Christ, J. I. Cirac, and G. Giedke, arxiv.org:07101420 (submitted to Phys. Rev. Lett.) (2007).

[79] M. Mariantoni, M. J. Storcz, F. K. Wilhelm, W. D. Oliver, A. Emmert, A. Marx, R. Gross, H. Christ, and E. Solano, arXiv.org:cond-mat/0509737 (2005).

[80] M. J. Storcz, M. Mariantoni, H. Christ, A. Emmert, A. Marx, W. D. Oliver, R. Gross, F. K. Wilhelm, and E. Solano, arXiv.org:cond-mat/0612226 (submitted to Phys. Rev. B) (2006).

[81] H. Christ, in *Mind Akademie - An den Grenzen der Wissenschaft*, edited by M. Dresler (Hirzel, Stuttgart, 2006), Chap. Quantenphysik - Vom Gespenstischen zum Praktischen, p. 15.

[82] A. W. Overhauser, Phys. Rev. **92**, 411 (1953).

[83] G. Lampel, Phys. Rev. Lett. **20**, 491 (1968).

[84] *Optical Orientation*, Vol. 8 of *Modern Problems in Condensed Matter Sciences*, edited by F. Meier and B. Zhakharchenya (North-Holland, Amsterdam, 1984).

[85] G. Salis, D. D. Awschalom, Y. Ohno, and H. Ohno, Phys. Rev. B **64**, 195304 (2001).

[86] J. M. Taylor, H.-A. Engel, W. Dür, A. Yacoby, C. M. Marcus, P. Zoller, and M. D. Lukin, Nature Physics **1**, 177 (2005).

[87] W. A. Coish and D. Loss, Phys. Rev. B **75**, 161302(R) (2007).

[88] A. S. Bracker, E. A. Stinaff, D. Gammon, M. E. Ware, J. G. Tischler, A. Shabaev, A. L. Efros, D. Park, D. Gershoni, V. L. Korenev, and I. A. Merkulov, Phys. Rev. Lett. **94**, 047402 (2005).

[89] B. Eble, O. Krebs, A. Lemaitre, K. Kowalik, A. Kudelski, P. Voisin, B. Urbaszek, X. Marie, and T. Amand, Phys. Rev. B **74**, 245306 (2006).

[90] A. Greilich, R. Oulton, S. Y. Verbin, D. Yakovlev, M. Bayer, V. Stavarache, D. Reuter, and A. Wieck, arXiv:cond-mat/0505446 (2005).

[91] C.-W. Lai, P. Maletinsky, A. Badolato, and A. Imamoğlu, Phys. Rev. Lett. **96**, 167403 (2006).

[92] A. Abragam, *Principles of Nuclear Magnetism* (Clarendon Press, Oxford, 1961).

[93] C. Deng and X. Hu, Phys. Rev. B **71**, 033307 (2005).

[94] M. S. Rudner and L. S. Levitov, Phys. Rev. Lett. **99**, 036602 (2007).

[95] A. Imamoğlu, E. Knill, L. Tian, and P. Zoller, Phys. Rev. Lett. **91**, 017402 (2003).

[96] R. Bonifacio, P. Schwendimann, and F. Haake, Phys. Rev. A **4**, 302 (1971).

[97] M. Gross and S. Haroche, Physics Reports **93**, 301 (1982).

[98] A. V. Andreev, V. I. Emelyanov, and Y. A. Ilinski, *Cooperative effects in optics: Superradiance and phase transitions* (IOP Publishing, London, 1993).

[99] K. Ono and S. Tarucha, Phys. Rev. Lett. **92**, 256803 (2004).

[100] A. K. Hüttel, J. Weber, A. W. Holleitner, D. Weinmann, K. Eberl, and R. H. Blick, Phys. Rev. B **69**, 073302 (2004).

[101] P.-F. Braun, B. Urbaszek, T. Amand, X. Marie, O. Krebs, B. Eble, A. Lemaitre, and P. Voisin, Phys. Rev. B **74**, 245306 (2006).

[102] P. Maletinsky, C. W. Lai, A. Badolato, and A. Imamoglu, Phys. Rev. B **75**, 035409 (2007).

[103] A. I. Tartakovskii, T. Wright, A. Russell, V. I. Fal'ko, A. B. Van'kov, J. Skiba-Szymanska, I. Drouzas, R. S. Kolodka, M. S. Skolnick, P. W. Fry, A. Tahraoui, H.-Y. Liu, and M. Hopkinson, Phys. Rev. Lett. **98**, 026806 (2007).

[104] F. T. Arecchi, E. Courtens, R. Gilmore, and H. Thomas, Phys. Rev. A **6**, 2211 (1972).

[105] T. Holstein and H. Primakoff, Phys. Rev. **58**, 1098 (1940).

[106] G. S. Agarwal, Phys. Rev. A **4**, 1791 (1971).

[107] S. I. Erlingsson and Y. V. Nazarov, Phys. Rev. B **70**, 205327 (2004).

[108] C. P. Slichter, *Principles of Magnetic Resonance* (Springer, Berlin, 1980).

[109] D. Paget, Phys. Rev. B **25**, 4444 (1982).

[110] M. Førre, J. P. Hansen, V. Popsueva, and A. Dubois, Phys. Rev. B **74**, 165304 (2006).

[111] S. Ludwig; M. Atatüre, private communication.

[112] I. A. Akimov, D. H. Feng, and F. Henneberger, Phys. Rev. Lett. **97**, 056602 (2006).

[113] W. A. Coish and D. Loss, Phys. Rev. B **72**, 125337 (2005).

[114] J. M. Taylor, J. R. Petta, A. C. Johnson, A. Yacoby, C. M. Marcus, and M. D. Lukin, Phys. Rev. B **76**, 035315 (2007).

[115] J. Baugh, Y. Kitamura, K. Ono, and S. Tarucha, Phys. Rev. Lett. **99**, 096804 (2007).

[116] D. Pavolini, A. Crubellier, P. Pillet, L. Cabaret, and A. Liberman, Phys. Rev. Lett. **54**, 1917 (1985).

[117] S. Ludwig, private communication, (2007).

[118] C. W. Gardiner, in *Handbook of Stochastic Methods*, edited by H. Haken (Springer, Heidelberg, 1985).

[119] S. Stenholm, Rev. Mod. Phys. **58**, 699 (1986).

[120] U. Weiss, *Quantum Dissipative Systems*, 2nd edition ed. (World Scientific Publishing Company, Singapore, 1999).

[121] A. Kuzmich and E. S. Polzik, in *Quantum Information with Continuous Variables*, edited by S. L. Braunstein and A. K. Pati (Kluwer Academic, Norwell and Dordrecht, 2003).

[122] A. Yacoby, private communication, 2007.

[123] T. Inui, Y. Tanabe, and Y. Onodera, *Group Theory and its Applications in Physics*, 2nd ed. (Springer, Berlin, 1996).

[124] P. Filipowicz, J. Javanainen, and P. Meystre, Journal of the Optical Society of America B **3**, 906 (1986).

[125] P. Meystre, G. Rempe, and H. Walther, Optics Letters **13**, 1078 (1988).

[126] H. Walther, Annalen der Physik **14**, 7 (2005).

[127] H. Walther, B. T. H. Varcoe, B.-G. Englert, and T. Becker, Reports on Progress in Physics **69**, 1325 (2006).

[128] M. Weidinger, B. T. H. Varcoe, R. Heerlein, and H. Walther, Phys. Rev. Lett. **82**, 3795 (1999).

[129] J. J. Slosser, P. Meystre, and S. L. Braunstein, Phys. Rev. Lett. **63**, 934 (1989).

[130] D. H. Feng, I. A. Akimov, and F. Henneberger, Phys. Rev. Lett. **99**, 036604 (2007).

[131] J. M. Raimond, M. Brune, and S. Haroche, Rev. Mod. Phys. **73**, 565 (2001).

[132] D. Leibfried, R. Blatt, C. Monroe, and D. Wineland, Rev. Mod. Phys. **75**, 281 (2003).

[133] A. Blais, R.-S. Huang, A. Wallraff, S. M. Girvin, and R. J. Schoelkopf, Phys. Rev. A **69**, 062320 (2004).

[134] E. Jaynes and F. Cummings, Proc. IEEE 51 **51**, 89 (1963).

[135] B. W. Shore and P. L. Knight, J. of Mod. Opt. **40**, 1195 (1993).

[136] R. H. Dicke, Phys. Rev. **93**, 99 (1954).

[137] M. Tavis and F. W. Cummings, Phys. Rev. **170**, 379 (1968).

[138] M. Orszag, R. Ramírez, J. C. Retamal, and C. Saavedra, Phys. Rev. A **49**, 2933 (1994).

[139] J. C. Retamal, C. Saavedra, A. B. Klimov, and S. M. Chumakov, Phys. Rev. A **55**, 2413 (1997).

[140] A. Retzker, E. Solano, and B. Reznik, Phys. Rev. A **75**, 022312 (2007).

[141] S. A. Wolf, D. D. Awschalom, R. A. Buhrman, J. M. Daughton, S. von Molnár, M. L. Roukes, A. Y. Chtchelkanova, and D. M. Treger, Science **294**, 1488 (2001).

[142] I. D. V. V. Privman and G. Kventsel, Phys. Lett. A **239**, 141 (1998).

[143] J. Levy, Phys. Rev. A **64**, 052306 (2001).

[144] T. D. Ladd, J. R. Goldman, F. Yamaguchi, Y. Yamamoto, E. Abe, and K. M. Itoh, Phys. Rev. Lett. **89**, 017901 (2002).

[145] P. Meystre and M. S. Zubairy, Physics Letters A **89**, 390 (1982).

[146] J. R. Kukliński and J. L. Madajczyk, Phys. Rev. A **37**, 3175 (1988).

[147] P. Rungta, V. Bužek, C. M. Caves, M. Hillery, and G. J. Milburn, Phys. Rev. A **64**, 042315 (2001).

[148] C. Deng and X. Hu, IEEE Trans. Nanotechnology **4**, (2005).

[149] R. Schack and C. M. Caves, Phys. Rev. A **60**, 4354 (1999).

[150] M. T. Björk, B. J. Ohlsson, T. Sass, A. I. Persson, C. Thelander, M. H. Magnusson, K. Deppert, L. R. Wallenberg, and L. Samuelson, Appl. Phys. Lett. **80**, 1058 (2002).

[151] C. Cabrillo, J. I. Cirac, P. Garcia-Fernandez, and P. Zoller, Phys. Rev. A **59**, 1025 (1999).

[152] J. Levy, Phys. Rev. Lett. **89**, 147902 (2002).

[153] M. Atatüre, J. Dreiser, A. Badolato, A. Högele, K. Karrai, and A. Imamoğlu, Science **312**, 551 (2006).

[154] A. Imamoğlu, Fort. Phys. **48**, 987 (2000).

[155] L. M. K. Vandersypen, R. Hanson, L. H. Willems van Beveren, J. M. Elzerman, J. S. Greidanus, S. D. Franceschi, and L. P. Kouwenhoven, *Quantum Computing and Quantum Bits in Mesoscopic Systems* (Kluwer Academic Plenum Publishers, Norwell and Dordrecht, 2002).

[156] R. Hanson, B. Witkamp, L. M. K. Vandersypen, L. H. Willems van Beveren, J. M. Elzerman, and L. P. Kouwenhoven, Phys. Rev. Lett. **91**, 196802 (2003).

[157] O. Gywat, H.-A. Engel, D. Loss, R. J. Epstein, F. Mendoza, and D. D. Awschalom, Phys. Rev. B **69**, 205303 (2003).

[158] A. M. Childs and I. L. Chuang, Phys. Rev. A **63**, 012306 (2000).

[159] Y. Ono, A. Fujiwara, K. Nishiguchi, H. Inokawa, and Y. Takahashi, Journal of Applied Physics **97**, 031101 (2005).

[160] J. I. Cirac, W. Dür, B. Kraus, and M. Lewenstein, Phys. Rev. Lett. **86**, 544 (2001).

[161] J. S. Waugh, L. Huber, and U. Haeberlen, Phys. Rev. Lett. **20**, 180 (1968).

[162] J. S. Waugh, C. H. Wang, L. M. Huber, and R. L. Vold, J. Phys. Chem. **48**, 662 (1968).

[163] M. Mehring, *High Resolution NMR Spectroscopy in Solids* (Springer, Berlin, 1976).

[164] T. Fujisawa, Y. Tokura, and Y. Hirayama, Phys. Rev. B **63**, 081304(R) (2001).

[165] S. A. Diddams, T. Udem, J. C. Bergquist, E. A. Curtis, R. E. Drullinger, L. Hollberg, W. M. Itano, W. D. Lee, C. W. Oates, K. R. Vogel, and D. J. Wineland, Science **293**, 825 (2001).

[166] J. I. Cirac and P. Zoller, Physics Today **38**, (2004).

[167] S. Nussmann, M. Hijlkema, B. Weber, F. Rohde, G. Rempe, and A. Kuhn, Phys. Rev. Lett. **95**, 173602 (2005).

[168] A. Boca, R. Miller, K. M. Birnbaum, A. D. Boozer, J. McKeever, and H. J. Kimble, Phys. Rev. Lett. **93**, 233603 (2004).

[169] R. Reichle, D. Leibfried, E. Knill, J. Britton, R. B. Blakestad, J. D. Jost, C. Langer, R. Ozeri, S. Seidelin, and D. J. Wineland, Nature **443**, 838 (2006).

[170] M. Brune, E. Hagley, J. Dreyer, X. Maytre, A. Maal, C. Wunderlich, J. M. Raimond, and S. Haroche, Phys. Rev. Lett. **77**, 4887 (1996).

[171] M. Kitagawa and M. Ueda, Phys. Rev. A **47**, 5138 (1993).

[172] Z. Song, P. Zhang, T. Shi, and C.-P. Sun, Phys. Rev. B **71**, 205314 (2005).

[173] *Quantum Squeezing*, edited by P. Drummond and Z. Ficek (Springer, Berlin, 2004).

[174] M. Suzuki, Phys. Lett. A **6**, 319 (1990).

[175] M. Suzuki, J.Math.Phys. **32**, 400 (1991).

[176] G. S. Agarwal and R. R. Puri, Phys. Rev. A **41**, 3782 (1990).

[177] P. Chen, C. Piermarocchi, L. J. Sham, D. Gammon, and D. G. Steel, Phys. Rev. B **69**, 075320 (2004).

[178] G. Jundt, private communication (2007).

[179] P. Zoller et al., Eur. Phys. J. D **36**, 203 (2005).

[180] J. F. Poyatos, J. I. Cirac, and P. Zoller, Phys. Rev. Lett. **81**, 1322 (1998).

[181] K. Mølmer and A. Sørensen, Phys. Rev. Lett. **82**, 1835 (1999).

[182] S. Schneider, D. F. James, and G. J. Milburn, (1998).

[183] J. J. García-Ripoll, P. Zoller, and J. I. Cirac, Phys. Rev. Lett. **91**, 157901 (2003).

[184] D. Braun, Phys. Rev. Lett. **89**, 277901 (2002).

[185] T. S. Cubitt, F. Verstraete, W. Dür, and J. I. Cirac, Phys. Rev. Lett. **91**, 037902 (2003).

[186] F. Benatti, R. Floreanini, and M. Piani, Phys. Rev. Lett. **91**, 070402 (2003).

[187] M. S. Kim, J. Lee, D. Ahn, and P. L. Knight, Phys. Rev. A **65**, 040101 (2002).

[188] C. Deng and X. Hu, Phys. Rev. B **73**, 241303(R) (2006).

[189] W. Yao, R.-B. Liu, and L. J. Sham, Phys. Rev. Lett. **95**, 030504 (2005).

[190] X. Hu and S. D. Sarma, Phys. Rev. Lett. **96**, 100501 (2006).

[191] W. A. Coish and D. Loss, Phys. Rev. B **75**, 161302(R) (2007).

[192] W. K. Wootters, Phys. Rev. Lett. **80**, 2245 (1998).

[193] C. Schön, E. Solano, F. Verstraete, J. I. Cirac, and M. M. Wolf, Phys. Rev. Lett. **95**, 110503 (2005).

[194] J. J. García-Ripoll and J. I. Cirac, Phys. Rev. Lett. **90**, 127902 (2003).

[195] A. Gilchrist, N. K. Langford, and M. A. Nielsen, Phys. Rev. A **71**, 062310 (2005).

[196] A. Peres, Phys. Rev. Lett. **77**, 1413 (1996).

[197] P. Horodecki, Phys. Lett. A **232**, 333 (1997).

[198] M. B. Plenio and S. Virmani, Quant. Inf. Comp. **7**, 1 (2007).

[199] G. Vidal and R. F. Werner, Phys. Rev. A **65**, 032314 (2002).

[200] M. Horodecki, P. Horodecki, and R. Horodecki, Phys. Rev. Lett. **80**, 5239 (1998).

[201] S. Bose, I. Fuentes-Guridi, P. L. Knight, and V. Vedral, Phys. Rev. Lett. **87**, 050401 (2001).

[202] X. Hu and S. Das Sarma, Phys. Rev. B **69**, 115312 (2004).

[203] D. S. Saraga and D. Loss, Phys. Rev. Lett. **90**, 166803 (2003).

[204] P. Recher and D. Loss, Phys. Rev. Lett. **91**, 267003 (2003).

[205] K. L. Hur, P. Recher, E. Dupont, and D. Loss, Phys. Rev. Lett. **96**, 106803 (2006).

[206] S. Legel, J. König, G. Burkard, and G. Schön, Phys. Rev. B **76**, 085335 (2007).

[207] M. I. Dyakonov and V. I. Perel, Sov. Phys JETP **36**, 995 (1973).

Acknowledgements

If I have seen a little further, it is by standing on the shoulders of giants.

This famous quotation certainly applies to the author of this work: Whatever accomplishments were presented here, I feel that my contribution was at best the "cherry on the top", and it is my great pleasure to thank the people that made this work possible.

I am very deeply grateful for the guidance and support *Ignacio Cirac* has provided me as my thesis advisor throughout the course of my Ph.D. His deep knowledge and understanding and his keen perception never cease to fascinate, and (in a positive way) humble, me. His remarkable friendliness and efficient problem-solving attitude will keep influencing me not only in physics questions. The research atmosphere he creates in his group and the possibilities he opens for visiting conferences and people, combined with his skills and expertise is all a graduate student can wish for.

Géza Giedke is the best ("postdoc"-)advisor and co-worker one can hope for. He has an incredibly wide knowledge and understanding of physics, and at the same time the patience to listen to all kinds of ideas. I learned a very great deal from him– about physics, especially quantum dots, and much more. His immense helpfulness, his work ethic, and his desire to do things right deeply impress me and will also in the future impact me very positively. Coming back to the above metaphor, he certainly was one of the giants hugely widening my perspective. I am very deeply indebted and grateful.

Belén Paredes gave me valuable advise, supported me and made very important contributions to parts of this thesis, for which I am very thankful.

Enrique Solano has been a constant source of ideas, and I gratefully acknowledge inspiring (and enjoyable) discussions with him.

I am grateful to *Atac Imamoğlu*, who shared valuable insights into the physics of nuclear spins in quantum dots with me, and very kindly invited me to visit him and his group at the ETH Zürich.

During my time as a Ph.D. student I have benefited from the work, ideas, and support from excellent collaborators: Jan Dreiser, Andi Emmert, Rudolf Gross, Carlos Lopez, Mikhail Lukin, Patrick Maletinsky, Matteo Mariantoni, Achim Marx, Will Oliver, Juan Carlos Retamal, Markus Storcz, Jake Taylor, Frank Wilhelm, and Peter Zoller.

I thank Jon Finley and Rudolf Gross very much for being on my Ph.D. examination committee.
Thanks to Géza Giedke, Tina Jurkat, Eric Kessler, and Heike Schwager who have proofread very large parts of this thesis.
The SFB 631 on "Solid State QIP" triggered many fun meetings, and lots of interesting discussions. Thanks to all participants for the good time, and in particular Frank Deppe, Dominik Heiss, Martin Kroner, Dawid Kupidura, Stefan Ludwig, and Florian Marquardt for insightful discussions.
During my time at the MPQ I had the pleasure to share the office with great people to discuss physics and much more: Markus Popp, Christian Schön, Oliver Buerschaper, and Christina Kraus (in chronological order). I thank them for the great time we had together and extend this gratitude to all of Ignacio's theory group, which is a highly enjoyable and unique combination of friendliness and competence. In addition to the already mentioned, in particular Miguel Aguado, Mari-Carmen Banuls, Toby Cubitt, Maria Eckholt Perotti, Juan-Jose Garcia-Ripoll, Klemens Hammerer, Theresa Hecht, Birger Horstman, Tassilo Keilmann, Eric Kessler, Barbara Kraus, Valentin Murg, Christine Muschik, Sébastien Perseguers, Diego Porras, Tommaso Roscilde, Mikel Sanz, Roman Schmied, Norbert Schuch, Heike Schwager, Frank Verstraete, Ines de Vega, Kalle Vollbrecht, and Michael Wolf were great colleagues; maybe except when beaten at table soccer/tennis (which unfortunately for many of them happened not so rarely).
As writing a Ph.D. thesis requires many contributions and qualities, I extent my thanks to this rather diverse (uncommented and very likely very incomplete) list of people: Tina and Markus Blatt, Tim Byrnes, Gemma Fernandez, Harald Giessen, Alex Göbel, Jochen Interthal, Kathi, Helga and Dieter Jurkat; Elli and Karl Kant, Naomi Kuramoto, the physics undergrad students in Marburg: Dominik, Martina, Sebastian, Stefan, Schorsch, Willi; Verena Maier, Iris Meessen, Insa Meier, Pierre Meystre, Manu Pfeiffer, Hansi Rink, Leonie and Jens Rink, Chris Search, Hans Tietze, Shoko Utsunomiya, and Schorsch Weis.
My family has always supported me in all possible ways, not only during my time as a Ph.D. student. My parents Monika and Paul and my sister Eva listened and motivated, helped me moving, made fun visits, sent packages, and and and– this here is made possible by them. I am deeply thankful.
Tina Jurkat has supported and encouraged me, woken me up, calmed me down and cheered me up during the past years; she is a constant inspiration in my life.

Thank you!

I gratefully acknowledge funding and support by the Max-Planck-Society and Sonderforschungsbereich 631 of the DFG.